U.PORTO

DOUTORAMENTO
Ciências Biomédicas

Deciphering the impact of cancer cell's secretome and its derived-peptide VGF on breast cancer brain metastasis

Rita Carvalho

D
2025

U.PORTO

Rita Carvalho

Deciphering the impact of cancer cell's secretome and its derived-peptide VGF on breast cancer brain metastasis

D.ICBAS **2025**

Deciphering the impact of cancer cell's secretome and its derived-peptide VGF on breast cancer brain metastasis

Rita Alexandra Pereira de Carvalho

INSTITUTO DE CIÊNCIAS BIOMÉDICAS ABEL SALAZAR

Rita Alexandra Pereira de Carvalho

Deciphering the impact of cancer cell´s secretome and its derived-peptide VGF on breast cancer brain metastasis

Tese de Candidatura ao grau de Doutor em Ciências Biomédicas submetida ao Instituto de Ciências Biomédicas Abel Salazar da Universidade do Porto.

Orientador – Joana Cancela de Amorim Falcão Paredes

Categoria – Group Leader (Cancer Metastasis Group, i3S) e Professora Afiliada

Afiliação – Instituto de Investigação e Inovação em Saúde (i3S), Instituto de Patologia e Imunologia Molecular da Universidade do Porto (Ipatimup) e Faculdade de Medicina da Universidade do Porto

jparedes@i3s.up.pt

Co-orientadora – Ana Sofia Pais Ribeiro

Categoria – Investigadora Assistente

Afiliação – Instituto de Investigação e Inovação em Saúde (i3S), Instituto de Patologia e Imunologia Molecular da Universidade do Porto (Ipatimup)

aribeiro@i3s.up.pt

Declaração de Honra

Eu, Rita Alexandra Pereira de Carvalho, n.º de estudante**:** up201711147**,** declaro que a presente tese é de minha autoria e não foi utilizada previamente noutro curso ou unidade curricular, desta ou de outra instituição. As referências a outros autores (afirmações, ideias, pensamentos) respeitam escrupulosamente as regras da atribuição, e encontram-se devidamente indicadas no texto e nas referências bibliográficas, de acordo com as normas de referenciação. Tenho consciência de que a prática de plágio e auto-plágio constitui um ilícito académico.



Porto, 11/09/2024

Artigos inseridos na Tese

O artigo científico publicado no âmbito desta tese, e que serviu como base para a escrita da mesma, foi o seguinte:

1. ***Nerve growth factor inducible (VGF) is a secreted mediator for metastatic breast cancer tropism to the brain.*** **Rita Carvalho**, Liliana Santos, Inês Conde, Ricardo Leitão, Hugo RS Ferreira, Célia Gomes, Ana Paula Silva, Fernando Schmitt, Carina Carvalho-Maia, João Lobo, Carmen Jerónimo, Joana Paredes, Ana Sofia Ribeiro. J Pathol. 2024 Oct;264(2):132-147. doi: 10.1002/path.6319. Epub 2024 Jul 29.

O artigo de revisão seguinte, embora não sendo parte integrante desta dissertação, foi usado na introdução da tese:

2. ***Impact of breast cancer cells´ secretome on the brain metastatic niche remodeling.*** **Rita Carvalho**, Joana Paredes, Ana Sofia Ribeiro. Semin Cancer Biol. 2020 Feb. 60:294-301. doi: 10.1016/j.semcancer.2019.10.011. E pub 2019 Nov 9. PMID:31711993.

Dedicado à minha mãe,

“When someone you love becomes a memory,

the memory becomes a treasure.”

- The most beautiful treasure that lives in my heart.

AGRADECIMENTOS

AGRADECIMENTOS

Foram anos de muito trabalho e dedicação, os quais me proporcionaram a oportunidade de crescer tanto pessoal como profissionalmente. Sempre estive rodeada por pessoas especiais, e por essa razão, não posso deixar de expressar a minha sincera gratidão a todos que fizeram parte desta etapa tão significativa da minha vida.

- À Joana Paredes, minha orientadora, não posso deixar de expressar a minha gratidão por todas as oportunidades que me proporcionaste e por acreditares em mim ao longo de tantos anos. Cheguei ao teu grupo cheia de medos e inseguranças e, graças a ti, a maioria desses medos desapareceu, tornando-me uma pessoa mais segura e confiante. Tudo isso só foi possível porque sabes liderar e ser amiga ao mesmo tempo; compreendes que cada um de nós tem o seu próprio ritmo de crescimento. A tua dedicação e paixão pela ciência são inspiradoras. Sinto que cresci muito cientificamente, pois sempre me mostraste que com trabalho e dedicação, tudo é possível. Obrigada por tudo, querida Joana!

- À Ana Ribeiro, minha coorientadora, és sem dúvida uma grande inspiração para mim, e que sorte a minha ter tido a oportunidade de trabalhar contigo ao longo destes anos. Serei para sempre grata por ter tido uma orientadora como tu, que me permitiu progredir ao meu ritmo e me forneceu todas as ferramentas para atingir os meus objetivos. O teu entusiasmo pela ciência e a tua perseverança são fascinantes. Obrigada por todo o teu apoio, dedicação, disponibilidade, carinho, amizade e por teres cuidado tão bem de mim.

- À nossa Raquel Seruca, um obrigado nunca será suficiente! Será sempre uma inspiração para mim.

- À Inês Conde, meu pintainho, obrigada por seres uma das partes mais bonitas do meu percurso. Ao longo dos anos, fomos crescendo juntas, e quero dizer-te que tenho muito orgulho em ti e na nossa amizade. É maravilhoso perceber que ganhei uma amiga tão especial como tu. Sempre estiveste lá para me apoiar, amparaste as minhas quedas e nunca deixaste de estar presente para mim. Estarei sempre aqui para ti para te dar abraços apertados e um abanão sempre que for necessário (irmã mais velha serve para isso mesmo). Love you!

- À Babi, minha Babizinha, obrigada por tanto. Foram anos de muita partilha, inúmeras conversas e algumas lágrimas misturadas. Graças a Deus, não faltou nada. Agradeço por teres sido como uma "muleta" para mim durante tantos anos. És alguém que sem dúvida quero levar para toda a vida (apesar de não acreditares, mas não mandas em mim!!!). Por

fim, quero que saibas que tenho muito orgulho em ti e na mulher/mãe guerreira que te tornaste. Estarei sempre por perto, love you.

- Carolina Noronha, nunca esquecerei todas as nossas conversas, conselhos e o apoio. Serei eternamente grata, minha querida Carolina.

- Gostaria também de agradecer aos restantes membros do grupo Cancer Metastasis: Rita Canário, Catarina Esquível, Maria Miguel, Bruno e Cristiana. Pelos bons momentos partilhados e pelo vosso apoio ao longo desta jornada. Cada um de vocês contribuiu de forma única para tornar esta experiência significativa e enriquecedora.

Ao longo desta caminhada, perdemos alguns elementos do grupo, cuja falta se fez sentir e que estarão para sempre no meu coração: Irina, Tito, Inês Morgado e Cíntia.

- Irina, minha querida! Tenho tantas saudades tuas. Ao longo destes anos, partilhámos tanto e serei sempre incrivelmente grata por ter uma amiga tão especial como tu. Obrigada por todo o carinho, apoio e pelos momentos inesquecíveis que vivemos juntas! E nunca te esqueças que atrás de uma montanha vem um montanhão. Love you!
- Ao Titinho, quero expressar a minha imensa gratidão por seres um bom amigo e por sempre alinhares nas minhas brincadeiras. Obrigada por estares sempre presente e pelo apoio ao longo do tempo.
- À minha Inês Morgado, quero expressar um enorme obrigado por todos os momentos que partilhámos e por tantas gargalhadas que demos juntas. Tenho saudades tuas, miúda. És sem dúvida uma mulher lutadora. Quando voltares, vou negar que escrevi isto!!!

- À Joana Figueiredo, Patrícia Carneiro, Sérgia Velho, Joana Carvalho, Joana Pereira e Soraia, sou muito grata pelo vosso apoio ao longo destes anos e por serem tão queridas comigo. Vocês são incríveis e gosto muito de vocês!

- Aos restantes membros do grupo EPIC e ex-membros (incluindo o grupo da minha querida tia Céu Figueiredo), quero expressar o meu sincero agradecimento pelo constante apoio, carinho e colaboração ao longo destes anos. Sem dúvida passamos momentos incríveis.

- Joana Peixoto, Verónica Fernandes, Rui, Marcelo e Ana Pestana não podia deixar de agradecer pelas fantásticas horas de almoço e pelo vosso apoio ao longo destes anos. Gosto muito de vocês, um bocadinho menos da Verónica!

- Nuno Mendes, meu querido, não sei como te agradecer por todo o teu apoio ao longo destes anos, especialmente nos últimos meses em que tens sido incansável. Gosto muito de ti.

Aos amigos e amigas que o i3S me proporcionou, Alexandra, Alex, João e Carla, não consigo expressar o quanto são importantes na minha vida. Vocês são verdadeiros pilares, sem os quais não sei como seria enfrentar os desafios do dia a dia.
- À Alexandra, que desde o primeiro dia em que nos conhecemos, senti que iria ter um lugar especial no meu coração. Para mim, tu não és apenas uma amiga, és uma verdadeira companheira de alma. Nos momentos mais felizes e nos desafios mais árduos, a tua presença foi a luz que me guiou. Obrigada por estares sempre presente, por ouvires as minhas angústias e partilhares as minhas alegrias. A tua sabedoria e compreensão tornaram os momentos difíceis mais suportáveis e os bons momentos ainda mais especiais. Obrigada, meu anjo por tudo mesmo!
- Ao Alex, meu amigo-irmão, parece que já nos conhecemos de outra vida. Tu sempre foste o meu grande conselheiro e o parceiro de conversas sem fim. Apesar de por vezes me tirares do sério (como os irmãos fazem), quero agradecer-te do fundo do coração por seres um apoio tão incrível para mim. És verdadeiramente especial!
- Ao João, meu amigo mais reservado, agradeço-te por seres uma das pessoas mais incríveis que conheço. Obrigada por ouvires os meus desabafos, por estares lá nos momentos bons e maus, e por tantos cafés e finos que compartilhamos para descomplicar a vida.
- À Carla, minha querida amiga, partilhámos tantas conversas, fininhos e boas gargalhadas. Agradeço por estares sempre presente, tornando os momentos especiais ainda mais memoráveis. És o meu besouro favorito e estou muito grata por toda a tua amizade e apoio ao longo do tempo. És especial miúda!!!

- Aos restantes membros do grupo da Taylor Swift, especialmente à Teresa e Jo, agradeço pelos fininhos de fim de dia, pelas conversas aleatórias e pelos bons momentos partilhados. Obrigado pelo companheirismo e pela amizade!

- Às melhores amigas do mundo, Diana, Miriam, Vanessa e Sofia, agradeço do fundo do coração por serem mais do que simples amigas, mas sim abraços apertados nos momentos difíceis e a minha bússola em todas as jornadas da vida. A nossa amizade é um verdadeiro porto seguro, onde celebramos juntas as alegrias e partilhamos as tristezas. Somos mais do que meras companheiras, somos apoio incondicional, risos partilhados e lágrimas enxugadas. É reconfortante saber que posso sempre contar convosco, mesmo

nos momentos mais sombrios. Obrigada por cada gesto de carinho, por cada palavra de ânimo e por cada abraço apertado que me ajudou a erguer nos momentos de fraqueza.
E para tornar tudo ainda mais especial, vocês deram-me o presente mais bonito que a vida pode oferecer – as/os nossas/os queridas/os sobrinhas/os, a minha Luísa, o meu Afonso, o meu Manel, a minha Teresinha, o meu Nico e o meu afilhado Sebastião.

- Ao meu Décio, o meu porto-seguro! Nunca me deixaste desistir, sempre acreditaste em mim. És o meu refúgio, o abraço que reconforta e acalma. Juntos, enfrentámos as dores, as perdas, as quedas e as dificuldades, mas também celebrámos conquistas pessoais e profissionais tão bonitas. Em cada desafio, crescemos e aprendemos que o céu é o limite para os nossos sonhos. Obrigado por cuidares tão bem de mim, do nosso Marley e agora do nosso filho Francisco que deu cor as nossas vidas e tornou o nosso mundo ainda melhor. Sem ti, nada seria igual.

- Ao meu pai e ao meu irmão, expresso a minha profunda gratidão por acreditarem sempre em mim! Apesar de às vezes me darem algumas dores de cabeça, saibam que estarei sempre por perto e pronta para apoiar-vos. Existe uma estrelinha no céu que me ensinou que a família é a base de tudo. Gosto muito de vocês!

- A todos os autores das publicações, expresso o meu sincero agradecimento pela vossa valiosa contribuição e dedicação.
- A todos os pacientes que enfrentam diariamente esta doença, transmito o meu apoio, força e solidariedade, não estão sozinhos nesta luta.

À Fundação para a Ciência e Tecnologia, o meu agradecimento pela Bolsa de Doutoramento concedida (SFRH/BD/135831/2018).

- Por último, quero dedicar todo este trabalho à pessoa mais importante da minha vida, que partiu a meio desta jornada devido a esta terrível doença: a minha mãe. Se cheguei até aqui, foi sempre por ela, pois foi a minha maior fonte de inspiração para ser uma mulher guerreira e lutadora, e para nunca desistir dos meus sonhos. Mãe, o amor cura tudo, embora não da forma como tanto desejávamos um dia. Ainda sinto que é o teu amor que me tem "curado" ao longo deste tempo. Obrigada, mamã, por eu ter tido a sorte de ser tua filha, algo que tanto te orgulhavas.

A TODOS OS QUE SE CRUZARAM COMIGO E AJUDARAM A TORNAR ESTE PERCURSO MEMORÁVEL, OBRIGADA!

ABSTRACT

Abstract

Brain metastases are one of the most serious clinical problems of breast cancer progression, due to the lower survival rates and lack of effective therapies. In our study, we evaluated the impact of brain organotropic breast cancer cells' secretome in the establishment of the brain pre-metastatic niche.

Our findings revealed that the secretome of brain organotropic breast cancer cells induces disruption of the blood-brain barrier and activation of microglia, both in *in vitro* and *in vivo* models. Additionally, we also observed that this secretome alters the stability of 3D cortical spheroids, ultimately enhancing cancer cell colonization in the brain.

Further, we went to evaluate the biomarkers that could be mediating this effect. We started by isolating extracellular vesicles and evaluating their impact on *in vitro* blood-brain barrier integrity. Our results suggested that extracellular vesicles are not the primary mediators of this effect, suggesting soluble factors as the key drivers of modification in the brain microenvironment during the early stages of the metastatic cascade.

Proteomic analysis of the secretome of brain organotropic breast cancer cells revealed six peptides that were specifically dysregulated, including VGF. Remarkably, we demonstrated that VGF impacts blood-brain barrier integrity and microglial function both *in vitro* and *in vivo*, and it also contributes to the colonization of cancer cells in the brain microenvironment.

Next, we explored the expression of VGF in a human breast tumor cohort. We observed that VGF was expressed both in cancer cells and in the adjacent stroma. Importantly, we were able to demonstrate that VGF-positive tumors were statistically associated with HER2 overexpression, and triple-negative molecular subtypes, as well as with poor prognosis. Further clinical validation in a different cohort of primary tumors from metastatic breast cancer cases (with primary tumors and paired metastases) showed a statistically significant association between VGF and the propensity to metastasize to the brain, significantly impacting the prognosis of breast cancer patients with brain metastasis.

In conclusion, our study unveils the potential of the secretome of brain organotropic breast cancer cells in the formation of the brain pre-metastatic niche. Moreover, we uncovered a distinctive secretome signature of brain organotropic breast cancer cells, which pinpointed VGF, that we demonstrated as being a crucial mediator in this process. Furthermore, its specific impact as a poor prognostic predictor in breast cancer patients with brain metastasis opens new avenues to target VGF to control for brain metastatic disease progression.

RESUMO

RESUMO

As metástases cerebrais representam um dos problemas clínicos mais graves associados à progressão do cancro da mama, devido às reduzidas taxas de sobrevivência e à falta de terapias eficazes. Considerando isto, no nosso estudo procurámos desvendar as fases iniciais da cascata metastática cerebral. Para isso, fomos analisar o impacto do secretoma de células de cancro da mama com tropismo para o cérebro na formação do nicho pré-metastático cerebral. Os nossos resultados revelam que o secretoma das células de cancro da mama com tropismo para o cérebro promove a disrupção significativa da barreira hematoencefálica e a ativação de células da microglia, tanto em modelos *in vitro* como *in vivo*. Além disso, observámos que o mesmo afeta a estabilidade de esferoides de córtex cerebral 3D, promovendo a colonização cerebral pelas células tumorais.

Dado o efeito relevante do secretoma na modulação no nicho pré-metastático cerebral, procurámos identificar os fatores específicos associados a este processo. Para isso, começámos por isolar vesículas extracelulares e avaliar o seu impacto na integridade da barreira hematoencefálica *in vitro*. De facto, os nossos resultados sugerem que as vesículas extracelulares não são os principais mediadores deste efeito, sugerindo os fatores solúveis como os principais mediadores na modificação do microambiente cerebral durante as fases iniciais da cascata metastática.

Por esse motivo, fomos decifrar as proteínas secretadas por células de cancro de mama com tropismo cerebral através de análises de proteómica e identificámos seis péptidos especificamente desregulados no secretoma destas células, sendo o VGF (fator de crescimento nervoso neuroendócrino) um deles.

Os nossos resultados demonstram que o VGF é um mediador chave no processo de formação do nicho pré-metastático cerebral, dado que este não só promove a disrupção da barreira hematoencefálica e ativação de células da microglia, tanto *in vitro* como *in vivo*, como também contribui para a colonização cerebral pelas células tumorais.

Posteriormente, avaliamos a expressão de VGF numa série de tumores da mama humano. Observamos que o VGF é expresso tanto nas células tumorais como no estroma adjacente. É importante destacar que encontramos uma associação significativa entre tumores positivos para VGF e um pior prognóstico das doentes, bem como uma associação com os subtipos moleculares com sobrexpressão de HER2 e triplo-negativo. Além disso, numa validação clínica posterior utilizando uma série independente de tumores primários de cancro da mama metastático (incluindo os tumores primários e as respetivas metástases), demonstrámos uma associação significativa entre a expressão do VGF e a ocorrência de metástases cerebrais, bem como com um prognóstico desfavorável para as pacientes com cancro da mama que desenvolvem metástases cerebrais.

Em conclusão, o nosso estudo revela uma assinatura única do secretoma de células de cancro da mama com tropismo para o cérebro, destacando o VGF como um mediador crucial neste processo. Além disso, demonstramos o seu impacto específico como um fator prognóstico e preditivo para doentes com cancro da mama que desenvolveram metástases cerebrais, abrindo novas perspetivas para a utilização do VGF como alvo terapêutico para o controlo da progressão da doença metastática cerebral.

LIST OF ABBREVIATIONS

List of Abbreviations

231.Bone	MDA-MB-231.Bone
231.Brain	MDA-MB-231.Brain
231.Brain.HER2	MDA-MB-231.Brain.HER2
231.Lung	MDA-MB-231.Lung
ALCAM	Activated Leukocyte Cell Adhesion Molecule
Ang-2	Angiopoietin-2
BBB	Blood-Brain Barrier
BC	Breast Cancer
BCRP	Breast Cancer Resistance Protein
bFGF	Basic Fibroblast Growth Factor
BMDCs	Bone Marrow-Derived cells
BMP2	Bone Morphogenetic Protein 2
BrMS	Brain Metastasis Signature
BSA	Bovine Serum Albumin
BTB	Blood-Tumor Barrier
C3aRA	C3a-Receptor Antagonist
CCL	C-C Motif Chemokine Ligand
CDK	Cyclin-Dependent Kinase
CEMIP	Cell Migration Inducing Hyaluronidase 1
CK	Cytokeratin
CNC	Central Nervous System
COX2	Cyclooxygenase-2
CSC	Cancer Stem Cell
CTCs	Circulating Tumor Cells
CXCL	C-X-C Motif Chemokine Ligand
CXCR	C-X-C Motif Chemokine Receptor
DAPI	4′,6-diamidino-2-phenylindole
DFS	Disease-Free Survival
DMEM	Dulbecco’s Minimal Essential Media
EBM-2	Endothelial Basal Medium-2
ECM	Extracellular Matrix
ECs	Endothelial Cells
EGFR	Epidermal Growth Factor Receptor

EMT	Epithelial-to-Mesenchymal Transition
ER	Estrogen Receptor
EVs	Extracellular Vesicles
FABP7	Fatty-Acid-Binding Protein 7
FAK	Focal Adhesion Kinase
FBS	Fetal Bovine Serum
GBM	Glioblastoma
GLUT1	Glucose Transporter 1
GM-CSF	Granulocyte-Macrophage Colony- Stimulating Factor
GSTA5	Glutathione S-Transferase Alpha 5
hCMEC/D3	Human Cerebral Microvascular Endothelial Cell Line
HER2	Human Epidermal Growth Factor Receptor 2
HK2	Hexokinase 2
HMC3	Human Microglial Clone 3
HR	Hormone Receptor
IDC	Invasive Ductal Carcinoma
IFN-g	Interferon gamma
IGFR1	Insulin-Like Growth Factor 1 Receptor
IGFs	Insulin-Like Growth Factors
IL	Interleukin
ILC	Invasive Lobular Carcinoma
IP	Intraperitoneal Injection
IV	Intravenous Injection
JAG	Jagged
KM	Kaplan Meier
L1CAM	L1 Cell Adhesion Molecule
LEF1	Lymphoid Enhancer-Binding Factor-1
lncRNA	Long Noncoding RNA
MFsd2A	Major Facilitator Superfamily Domain 2A
MMP	Matrix Metalloproteinase
NaHCO3	Sodium Bicarbonate
NaOH	Sodium Hydroxide
NCAM	Neuronal Cell Adhesion Molecule
NF-kβ	Nuclear Factor Kappa B
NH4Cl	Ammonium Chloride

NMDAR	N-Methyl-D-Aspartate Receptors
NSCs	Neuronal Stem Cells
NT-3	Neurotrophin-3
OS	Overall Survival
Parental 231	MDA-MB-231
PAs	Plasminogen Activators
PBS	Phosphatase-Buffer Saline
PDGFRβ	Platelet-derived Growth Factor Receptor Beta
PD-L1	Programmed Death-Ligand 1
PDPK1	3-Phosphoinositide-Dependent Protein Kinase-1
PDX	Patient-Derived Xenograft
p-ERK1/2	Phosphrorylated-ERK1/2
PFA	Paraformaldehyde
PI-3K	Phosphoinositide 3-Kinase
PMN	Pre-Metastatic Niche
PR	Progesterone Receptor
PTHRP	Parathyroid Hormone-Related Protein
ROI	Region of Interest
RT	Room Temperature
SDF-1α	Stromal Cell-Derived Factor 1α
SP	Substance P
TDSFs	Tumor-Derived Secreted Factors
TEER	Transendothelial Electrical Resistance
TGFβ	Transforming Growth Factor-Beta
TNBC	Triple-Negative Breast Cancer
TNF-α	Tumor Necrosis Factor Alpha
VEGF	Vascular Endothelial Growth Factor
VEGFR1	Vascular Endothelial Growth Factor Receptor 1
VGF	Nerve Growth Factor Inducible Protein
VLA-4	Very late antigen 4 or Integrin α4β1
XIST	X-Inactive-Specific Transcript

TABLE OF CONTENTS

Table of Contents

AGRADECIMENTOS viii
ABSTRACT xvi
RESUMO xx
TABLE OF CONTENTS xxxii
CHAPTER I. GENERAL INTRODUCTION ..... - 36 -
1. Breast Cancer ..... - 38 -
1.1 Epidemiology and risk factors ..... - 38 -
1.2 Histological & molecular classification ..... - 40 -
2. Metastatic breast cancer ..... - 44 -
2.1 Metastatic organotropism ..... - 46 -
2.2 Molecular subtypes and organotropism ..... - 47 -
3. Breast Cancer Brain Metastasis ..... - 48 -
3.1 Brain specific metastatic regulators and signaling pathways ..... - 50 -
4. Brain Microenvironment ..... - 52 -
4.1 Metastatic niche formation ..... - 52 -
4.2 Resident cells' contribution to the establishment of the brain (pre) metastatic niche - 54 -
4.2.1 Blood-Brain Barrier ..... - 54 -
4.2.2 Neurons ..... - 56 -
4.2.3 Pericytes ..... - 56 -
4.2.4. Microglia ..... - 57 -
4.2.5. Astrocytes ..... - 58 -
5. The secretome as a modulator of the brain pre-metastatic niche ..... - 61 -
CHAPTER II. RATIONAL AND AIMS ..... - 64 -
CHAPTER III. MATERIALS AND METHODS ..... - 70 -
CHAPTER IV. RESULTS ..... - 88 -
I. Secretomes of brain organotropic breast cancer cells affect the blood-brain barrier integrity…… ..... - 90 -
II. Secretomes of brain organotropic breast cancer cells promote microglia activation - 92 -
III. The secretome of brain organotropic breast cancer cells affects the stability of 3D cortical spheroids ..... - 94 -
IV. Extracellular vesicles secreted by brain organotropic breast cancer cells are inefficient to modulate the blood-brain barrier ..... - 95 -
V. Secretome of brain organotropic breast cancer cells promotes brain colonization .. - 97 -

VI. The secretome from brain organotropic breast cancer cells show a brain-specific protein signature ..... - 98 -
VII. VGF promotes BBB disruption and microglia activation ..... - 100 -
VIII. VGF expression is associated with a worse prognosis for breast cancer patients- 105 -
IX.VGF expression is a poor prognostic factor for breast cancer brain metastases ... - 108 -
CHAPTER V. DISCUSSION ..... - 117 -
CHAPTER VI. FUTURE PERSPECTIVES ..... - 127 -
REFERENCES ..... - 131 -
ANNEX - PUBLICATIONS ..... - 147 -

CHAPTER I. GENERAL INTRODUCTION

1. Breast Cancer

1.1 Epidemiology and risk factors

Breast cancer (BC) is a significant global health issue, with a high incidence and mortality among women. The latest Globocan data (in reference to the year 2020) reported nearly 2.3 million new cases and 685,000 deaths from BC worldwide (Figure 1) [1, 2]. Not surprisingly, the incidence of BC has been rising over the years. It is estimated that by 2040, there will be over 3 million new BC cases and 1 million deaths worldwide. This increase is primarily attributed to population growth and aging. [2].

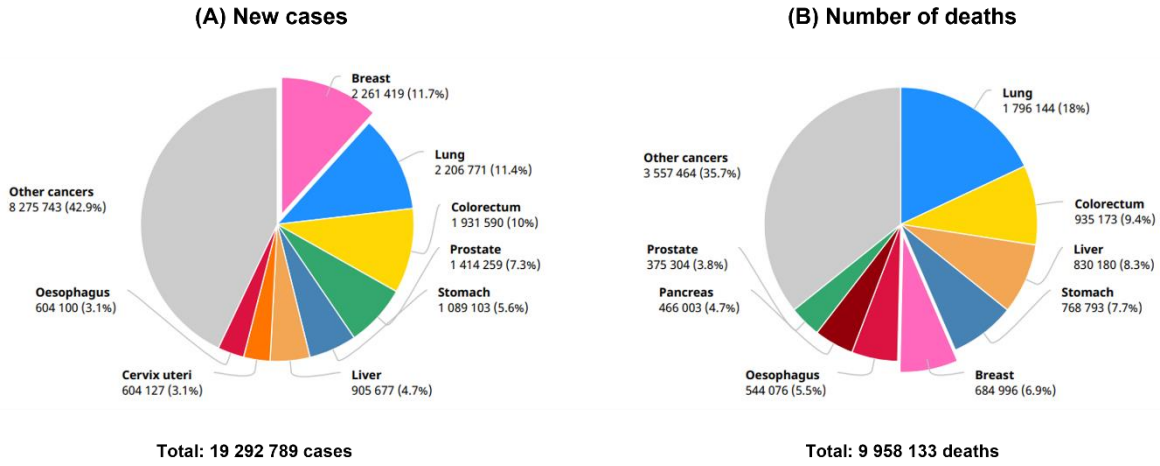


Figure 1. Estimated numbers of new cancer cases **(A)** and deaths **(B)** worldwide for both genders and all ages in 2020 [1].

According to the most recent Globocan projections (for the year 2020), there were 7,041 new cases reported in Portugal annually, with an incidence rate of 70.8 cases per 100,000 people. Moreover, the BC mortality rate in the Portuguese population was 12.7 cases per 100,000 people, resulting in approximately 1,864 deaths each year (Source: Liga Portuguesa contra o Cancro and Globocan 2020). Due to this reality, it is understandable that BC is one of the main research interests among the national cancer research community.

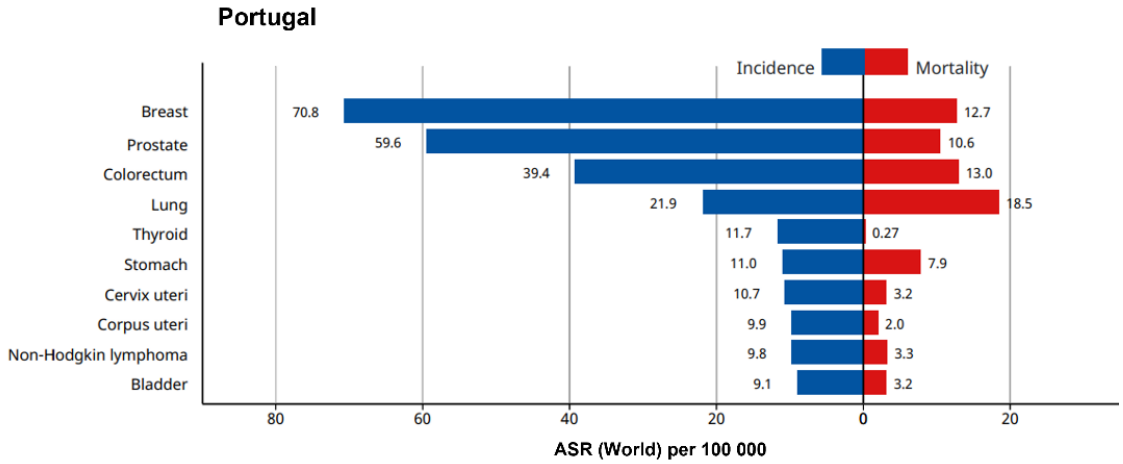


Figure 2. The **GLOBOCAN 2020** data on the annual incidence and mortality rates of the most common types of cancer for both genders in Portugal provide a detailed view of the cancer burden in the country. **Age standardization** is a crucial technique that allows for comparison between populations with different age profiles by adjusting incidence and mortality rates to a common age structure. These data offer valuable insights into the trends of cancer rates in Portugal and enable comparative analysis with other countries, aiding the development of more effective public health policies.**Source: GLOBOCAN 2020**.

The vast majority of BC cases are considered sporadic, and the etiology is not fully understood. However, it is believed that BC results from a complex interaction of genetic, hormonal, and environmental factors. The risk of BC increases with age, with the majority of BC cases occurring in women over 50 years old [3]. This can be attributed to several factors, including prolonged contact with potential carcinogens, cumulative genetic damage, and hormonal changes associated with aging. Additionally, there are other factors that potentially increase the risk of BC, particularly those influencing hormone balance, such as early age at menarche (before 12 years old), late menopause (after the age of 55), postmenopausal weight gain, and long-term use of oral contraceptives (which increase breast exposure to elevated estrogen levels) [4]. Moreover, breast alterations, such as atypical mammary or preneoplastic lesions, frequently detected through biopsy or imaging methods like mammography or magnetic resonance imaging, also indicate an elevated risk of developing BC [5]. Importantly, other significant factors, such as late pregnancy or never having been pregnant, ionizing radiation, a high-saturated fat diet, alcohol consumption, smoking, a sedentary lifestyle, and hormone replacement therapy, also contribute to an increased risk of this type of malignancy [6-9].

Approximately 5% to 10% of BC cases are hereditary, caused by inherited germline mutations in BC susceptibility genes like BRCA1 and BRCA2, significantly increasing the risk of developing BC [10-13].

1.2 Histological & molecular classification

Breast tumors are complex and diverse entities, displaying a wide range of clinical behaviors, morphologies, outcomes, and biological characteristics. Within invasive BC, there are various histological subtypes, including invasive ductal carcinoma (IDC), invasive lobular carcinoma (ILC), ductal/lobular mixed histology, mucinous (colloid), tubular, medullary, papillary carcinomas, among others [14].

Notably, invasive carcinoma is further classified into three grades: grade 1 (well-differentiated), grade 2 (moderately differentiated), and grade 3 (poorly differentiated). This classification is based on factors such as nuclear pleomorphism, glandular/tubule formation, and mitotic index, providing insights into disease progression and treatment responses [15]. Each histological subtype displays distinct microscopic characteristics that unveil significant insights into disease progression and treatment efficacy.

Despite the insights offered by histological classification, it does not fully encompass the molecular complexity of BC, hindering a precise evaluation of the disease's clinical progression and necessitating clear decision-making regarding treatment strategies.

To address this limitation, a new classification system has emerged, aiming to correlate disease molecular characteristics, prognosis, and therapeutic approaches more accurately. Gene expression profile studies, pioneered by Perou and Sorlie et al., improved our understanding of BC, since allowed the stratification of BC patients into distinct molecular subtypes, reflecting the intricate biological diversity of breast tumors. Importantly, these molecular subtypes are associated with variations in prognosis, treatment responsiveness, and potential therapeutic targets. This paradigm shift has revolutionized personalized medicine strategies, enabling the development of tailored treatment plans based on the specific molecular profile of each patient's tumor. These molecular subtypes are defined by variations in the expression of specific genes, namely the estrogen receptor (ER), progesterone receptor (PR), and human epidermal growth factor receptor 2 (HER2) [16-18].

ER and PR are nuclear hormone receptors (HRs) functioning as transcription factors, holding pivotal roles in BC's development and progression. These receptors stand out as two of the most prognostic and predictive markers in BC. Endocrine therapy, also known as hormonal therapy, is an effective treatment option for patients with ER-positive and/or PR-positive breast tumors since it inhibits tumor growth by blocking the actions of these hormones.

HER2 is a membrane tyrosine kinase receptor that regulates cell growth, proliferation, and survival through several signaling pathways, which adds another layer of complexity to BC treatment [19]. The amplification of HER2 serves as a robust prognostic biomarker, strongly

linked to aggressive behavior in BC [20, 21]. Notably, therapeutic strategies targeting HER2, such as humanized monoclonal antibodies (like trastuzumab and pertuzumab), which precisely binds to HER2's extracellular domain, have ushered in a notable improvement in outcomes for patients with HER2-enriched BC [22].

At present, BC clinical classification encompasses four distinctive subtypes: Luminal A, Luminal B, HER2-enriched, and triple-negative BC (TNBC) **(Figure 3)** [23]. These subtypes have distinct gene expression patterns and are associated with different clinical outcomes, as well as to different responses to treatment.

Moreover, ongoing research continues to unveil finer nuances within these BC subtypes. For instance, the emergence of Luminal B as a more aggressive subtype within the Luminal group, highlights the importance of detailed molecular profiling in guiding treatment decisions [24, 25]. Additionally, within TNBC, further subcategorization is being explored based on specific genetic alterations, potentially leading to more tailored therapeutic approaches for this challenging BC subtype [26, 27]. As we delve deeper into the molecular intricacies of BC, the promise of precision medicine approaches becomes increasingly tangible, with the potential to significantly enhance patient outcomes.

Luminal-like tumors are the most common molecular subtypes of BC, accounting for approximately 60-70% of all cases [28]. Within this category, a further division into two distinct subtypes occurs: Luminal A and Luminal B. These subtypes are marked by contrasting gene expression patterns, carrying significant implications for clinical diagnosis and prognosis.

Luminal A tumors are characterized by being HR-positive (ER-positive and PR-positive) and HER2-negative. Clinically, they exhibit attributes of low-grade and slow growth, owing to their minimal proliferative activity. These characteristics contribute to a more favorable prognosis, evidenced by lower relapse rates [29, 30]. Moreover, when compared with other molecular subtypes, Luminal A tumors show a reduced likelihood of lymph node invasion. Treatment strategies for BC patients with the Luminal A molecular subtype typically involve the use of selective ER modulators (SERMs) or ER downregulators (SERDs), such as tamoxifen and fulvestrant, which target the HRs. Additionally, aromatase inhibitors are used to inhibit estrogen production. Furthermore, cyclin-dependent kinase (CDK) 4/6 inhibitors, such as palbociclib, ribociclib, and abemaciclib, may be used in combination with endocrine therapy to enhance treatment efficacy in the Luminal A subtype. These inhibitors block the activity of CDK 4 and 6, thereby suppressing cell cycle progression and inhibiting tumor growth [31, 32].

Luminal B tumors are categorized into two distinct groups based on the expression of the HER2 receptor: Luminal B HER2-negative or positive [31].

- **Luminal B HER2-negative:** is characterized by being ER-positive, PR-low, and HER2-negative. A distinctive feature of Luminal B HER2-negative BC is its higher proliferation rate, as indicated by markers like Ki-67 (higher than 14%). This means that cancer cells divide and multiply more rapidly than in Luminal A tumors, making them more aggressive [33]. In terms of lymph node invasion risk, Luminal B tumors are in the intermediate range among the different subtypes. Due to its more aggressive nature, Luminal B HER2-negative typically has a less favorable prognosis compared to Luminal A breast tumors. Hormonal therapy, such as selective ER modulators (e.g., tamoxifen) or aromatase inhibitors (e.g., letrozole), along with possible chemotherapy, are commonly used for the treatment of Luminal B HER2-negative tumors.

- **Luminal B HER2-positive:** Regardless of progesterone levels and their proliferative capacity, if breast tumors are ER-positive and HER2-positive, they are categorized as Luminal B HER2-positive. For the Luminal B HER2-positive subtype, hormonal therapy targeting the ER is a cornerstone, along with HER2-targeted therapy to address the HER2-positive aspect of the tumor. Monoclonal anti-HER2 antibodies such as trastuzumab (Herceptin) and pertuzumab (Perjeta) are commonly employed in this context. T-DM1 is more commonly used in HER2-positive BC cases that have progressed after prior treatment with trastuzumab and taxane chemotherapy. However, in some cases where Luminal B BC is also HER2-positive and has progressed after initial treatments, T-DM1 may be considered as a therapeutic option. This decision would be based on factors such as the patient's overall health, previous treatments received, tumor characteristics, and response to prior therapies. Additionally, inhibitors targeting receptor tyrosine kinase activity, such as lapatinib and neratinib, have demonstrated efficacy in treating these tumors [34-37].

HER2-enriched breast tumors constitute about 10-15% of all breast tumors and are characterized by a lack or absence of HR expression (ER-negative and PR-negative) and the amplification of HER2. Consequently, these tumors exhibit highly proliferative cells, with 75% displaying a high histological grade, and around 40% presenting mutations in the TP53 gene [38]. Known for their inherently aggressive behavior, HER2-enriched breast tumors are associated with worse prognoses, a heightened risk of lymph node invasion, and

increased metastatic potential. Despite these challenges, advancements in targeted therapies have significantly improved outcomes for patients with HER2-overexpressing BC. The commonly used anti-HER2 treatment is the monoclonal antibody trastuzumab (Herceptin), often administered in combination with chemotherapy. In certain cases, the addition of pertuzumab (Perjeta) to the trastuzumab and chemotherapy regimen may offer additional benefits. As mentioned earlier, in cases where patients with HER2-positive BC have experienced progression following treatment with trastuzumab and taxanes, T-DM1 emerges as another crucial therapeutic option. Moreover, inhibitors targeting the activity of receptor tyrosine kinases have demonstrated efficacy in treating these tumors [22, 37, 39-42].

Triple-negative breast cancer (TNBC) accounts for 15-20% of all breast carcinomas. This molecular subtype is defined by the absence of ER, PR, and HER2 expression. TNBC tends to exhibit heightened aggressiveness compared to other subtypes, often displaying increased lymph node involvement and extensive lymph node metastases. The prognosis for TNBC is notably worse in contrast to other BC subtypes, featuring a heightened recurrence risk. TNBC frequently shows cases with elevated genetic instability, a higher rate of cell proliferation, and a propensity for metastasis to distant organs. Given that TNBC lacks the expression of ER, PR, and HER2, standard hormonal and HER2-targeted therapies prove ineffective. Therefore, its current treatment options rely mostly on anthracycline-based chemotherapy (like doxorubicin or epirubicin) followed by taxane-based chemotherapy (such as paclitaxel or docetaxel) as the standard of care for early-stage TNBC [43]. Given the aggressive nature of TNBC and the limited treatment options available, current research is dedicated to discovering novel targeted therapies and immunotherapies aimed at improving treatment outcomes for TNBC patients. [42, 44-46]. Notably, Keytruda (pembrolizumab) has recently gained approval for the treatment of early-stage triple-negative disease with a high risk of recurrence, along with PD-L1-positive TNBC [45, 47]. This approval represents a significant advancement in the management of TNBC. Due to its heterogeneous nature, TNBC can be classified into different molecular subtypes based on distinct genetic and molecular profiles. Some of the identified subtypes include basal-like, immune-mediated, mesenchymal, luminal androgen receptor (LAR), and others. This molecular heterogeneity can influence the response to treatment and prognosis of patients with TNBC, emphasizing the importance of a personalized and targeted approach to managing this disease [26, 48].

In summary, TNBC and HER2-enriched breast tumors experience early relapses, compared with patients with luminal subtypes (A and B) that present a more favorable prognosis. It's

noteworthy that within the luminal category, Luminal B patients tend to have a worse prognosis than their Luminal A counterparts. Continuing advancements in our understanding of BC subtypes and ongoing research efforts offer hope for refining treatments and improving outcomes for patients across these diverse BC molecular subcategories.

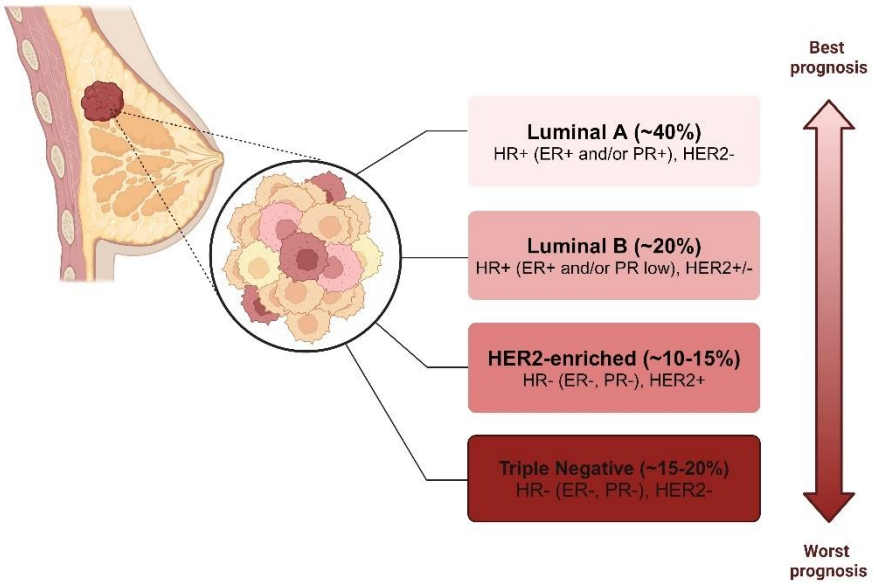


Figure 3. Molecular subtypes of breast cancer. According to the expression of ER, PR, and HER2, breast cancer can be classified into 4 clinically relevant molecular subtypes: Luminal A (ER^+, PR^+, $HER2^-$), Luminal B (ER^+, PR^{low}, $HER2^{-\text{ or }+}$), HER2-overexpressing (ER^-, PR^-, $HER2^+$) and Triple-Negative (ER^-, PR^-, $HER2^-$). (HR – hormone receptor, ER – estrogen receptor, PR – progesterone receptor, HER2 – human epidermal growth factor receptor 2). **Created in Biorender**.

2. Metastatic breast cancer

Despite significant advances in BC treatment and subsequent improvements in survival rates in recent years, there remains a 20-30% chance that women diagnosed with early-stage BC will experience relapse and develop distant metastases [49]. In addition to these patients, approximately 6-10% of BC patients are diagnosed with metastatic disease at the time of initial diagnosis [50, 51]. Diverse prognoses are observed between patients with recurrent distant disease and those with metastatic BC due to variations in tumor biology and treatment responses [52]. Metastasis represents an obstacle to cure BC patients, therefore being the leading cause of compromised quality of life and mortality.

Metastatic BC can potentially occur in several distant organs, such as distal lymph nodes, bones, lungs, liver, and brain [53-56]. This metastatic dissemination presents a multifaceted process involving several sequential steps, each imposing distinct challenges for cancer cells **(Figure 4)** [48-50]:

1. **Tumor evasion -** A pivotal initial step involves cancer cells evading the confines of the primary breast tumor. This escape is facilitated by an intricate interplay of factors, including the tumor microenvironment, epithelial-mesenchymal transition (EMT), and evasion of the immune system.

2. **Migration, invasion, and intravasation -** The invasion of adjacent tissues starts when cancer cells breach the basement membrane, a specialized extracellular matrix (ECM) layer. Subsequently, intravasation occurs, either through lymphatic vessels or blood vessels. This process is regulated by factors within the tumor microenvironment and specific molecular interactions.

3. **Survival in circulation -** The ability of BC cells to survive in the bloodstream potentiates their capacity to establish distant metastases. However, the majority of circulating tumor cells (CTCs) fail to initiate metastatic colonies. Various challenges confront CTCs in the circulation, including immune surveillance, shear forces, and resistance to anoikis, a type of apoptosis induced when cells are in anchorage-independent conditions and lack ECM attachment. For instance, some studies indicate that CTCs engage with platelets and potentially undergo reversible metabolic alterations to enhance resistance against oxidative stress [57, 58].

4. **Extravasation and colonization –** For successful extravasation, CTCs need to overcome the vascular barrier (endothelium) to access the parenchyma of the target organ. Subsequent metastatic colonization requires cancer cells to adapt to the foreign microenvironment of the secondary site. This microenvironment typically differs from that of the primary tumor, encompassing variations in stromal cells, ECM components, and tissue architecture. The interactions between cancer cells and the metastatic microenvironment significantly influence cell survival, growth, and colonization. This dynamic interplay implies mutual influence and constant interaction between cancer cells and the surrounding environment [59]. Cancer cells are capable of adapting to their environment and exploiting its resources to support their growth and survival. On the other hand, cancer cells have the ability to modify and impact the microenvironment, resulting in a feedback loop that promotes metastasis formation. Notably, metastatic colonization is a highly inefficient process that culminates in the death of the majority of cancer cells. Nonetheless, a small fraction (~2%) is able to adapt to the new metastatic niche to form micrometastases [60].

5. **Sustained growth of metastatic cancer cells -** A mere fraction of disseminated cancer cells successfully survive the inhospitable microenvironment of the metastatic niche, proliferating to ultimately give rise to macrometastases - a process that is exceedingly rare (approximately 0.02%) [60, 61].

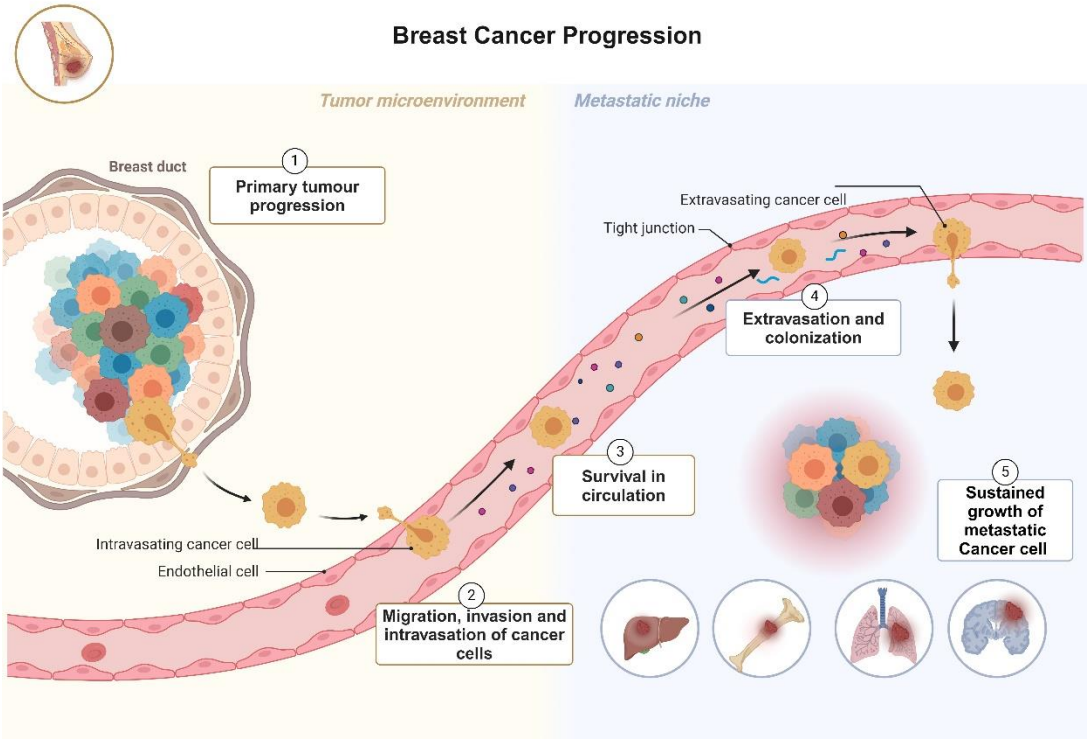


Figure 4. Breast cancer metastasis: schematic representation of the principal events of the metastatic cascade. The metastatic cascade is a complex multistep process. Metastatic breast cancer cells detach from the primary tumour, migrate, invade the surrounding tissue and ultimately enter into circulation, where they have the ability to survive, which is an important hallmark of these cells. Following extravasation, metastatic cancer cells might have the ability to colonize the microenvironment of distant organs and to proliferate, giving rise to metastases. **Created in Biorender**.

2.1 Metastatic organotropism

According to Paget's theory, metastasis is not a random occurrence but is shaped by the interplay between cancer cells (termed “seeds”) and the microenvironment of metastasis (termed “soil”) [53, 62, 63]. This theory underscores that the microenvironment in distant organs will determine the formation of metastases. This concept provides an elegant explanation for organotropism, where specific metastatic niches are favored [54, 64-66]. In the 1930s, James Ewing challenged Paget's view, proposing that cancer cell dissemination is driven by mechanical factors dictated by the vascular system's anatomical structure [67]. This perspective was widely accepted for many years, until Isaiah Fidler's research in the 1970s [68]. Fidler's research demonstrated that the success of the metastatic process is

not solely guided by mechanical flow dynamics. Instead, he showed that distinct tumor types exhibit distinct patterns of metastasis to specific organs, supporting Paget's theory. Since then, research has focused on unraveling molecular and cellular mechanisms governing organ-specific metastasis, emphasizing cancer cell properties and gene-pathway interplay guiding organotropism. For instance, BC cells express specific chemokine receptors, like C-X-C motif receptor (CXCR) 4 and 7, which form partnerships with chemokine ligands found in particular organs, such as lymph nodes (C-X-C motif chemokine (CXCL) 12) and lungs (C-C motif chemokine ligand (CCL) 21). This interaction serves as a navigational system, directing metastatic BC cells to their predetermined destinations [69].

Interestingly enough, it has also been shown by David Lyden and his research team that this organotropism starts already in the early begins of the metastatic cascade by the release of exosomes by cancer cells carrying specific molecules that allow them to selectively home in on target metastatic organs [70-72]. This discovery highlights the potential for intervention in the initial stages of cancer spread by controlling the release or uptake of these organotropic exosomes. Moreover, identifying the unique molecules carried by these exosomes holds promise as biomarkers for predicting organ-specific metastasis, revolutionizing prognostic assessments, and enabling tailored treatment strategies for individual patients.

In addition to molecules present in EVs, soluble factors may also play a crucial role in BC organotropism. For example, BC cells secrete osteoclast-stimulating growth factors, such as parathyroid hormone-related protein (PTHrP) and granulocyte-macrophage colony-stimulating factor (GM-CSF), thereby fostering bone metastasis and contributing to the observed organ-specific metastatic patterns [73].

Furthermore, recent research has highlighted another aspect of this intricate process. A study revealed that BC cells secrete Activin A (ActA), a member of the transforming growth factor-beta (TGF-β) superfamily. This secretion leads to elevated blood levels in tumor-bearing mice and fosters lung metastasis by upregulating profibrotic factors in lung fibroblasts. Consequently, this enhances collagen deposition in the PMN, ultimately contributing to poor patient survival [74].

This complex interplay between cancer cells and the microenvironment of distant organs involves an array of molecular and cellular factors that collectively contribute to the observed organ-specific metastasis. Understanding the underlying mechanisms of metastatic organotropism is imperative for advancing our knowledge of the metastatic process and devising effective strategies for therapeutic intervention.

2.2 Molecular subtypes and organotropism

Predicting the risk of BC metastases is challenging due to its heterogeneity. Traditionally,

clinicians rely on factors such as tumor size, grade, stage, and HR status to assess disease progression and anticipate metastatic patterns. However, emerging research suggests that molecular subtypes play a critical role in shaping the BC metastatic landscape.

Despite variations in molecular subtypes, bone metastasis remains the most prevalent, affecting approximately 70% of patients with metastatic BC [73]. Following bone metastasis, the liver emerges as the second most common site, impacting around 30% of patients [75]. Additionally, the brain represents the third most frequent location of metastasis in BC, affecting between 10% to 30% of patients [76].

Notably, certain molecular characteristics further influence the likelihood of metastasis in BC. For instance, BC with HR expression and simultaneous expression of Ki67 increases the chance of metastasis from 27.8% to 42.9%, and when HER2 is expressed, the chance of metastasis rises to 47.9%. HER2 expression alone leads to a 51.4% chance of metastasis, while the absence of receptor expression results in a 43.1% [77].

A study conducted by Shengrong Sun et al. investigated the relationship between BC subtypes and the sites of distant metastasis [78]. The data suggests that all BC subtypes have a propensity for bone metastases, with a particularly pronounced tendency in the Luminal B HER2-positive subtype. Furthermore, the HER2 overexpression subtype presents a greater likelihood of brain metastasis compared to both the Luminal A and B subtypes. Moreover, the HER2 overexpression subtype exhibits a higher incidence of liver metastases when compared to the other molecular subtypes. TNBC subtype significantly increases the rate of metastasis to the brain, lungs, and distant lymph nodes. In contrast, the basal-like subtype is particularly associated with a lower incidence of liver and bone metastases. Therefore, understanding these variations in metastatic tendencies among BC subtypes is essential for healthcare professionals when devising treatment plans and strategies for monitoring patients.

3. Breast Cancer Brain Metastasis

BC brain metastases incidence has increased in the past few years since the recently used therapies show improved control of the systemic disease but are inefficient in controlling metastatic progression. These develop in approximately 10%–30% of patients with metastatic BC, occurring frequently after metastasis in other systemic organs (such as bone, lung, and liver) and displaying the strongest and worst impact on the survival of BC patients [79, 80]. Several factors contribute to an increased risk of developing brain metastasis, including younger age, advanced tumor stage, presence of lymph node

metastases, multiple metastatic sites (more than 2), larger tumor size, and HR-negative (ER and PR) or HER2-overexpression [81].

Despite recent therapeutic advancements, patients with brain metastases typically experience a mean survival of around 6–16 months after diagnosis. Therefore, understanding (1) how cancer cells specifically reach the brain, (2) whether and how they prepare the brain for their arrival, and (3) which are the critical factors that allow cancer cells to survive in this distant location will be crucial for the development of efficient treatments for brain metastatic and resistant tumors. Interestingly, different BC molecular subtypes not only display different incidences of brain metastases but also different prognostic values. Luminal subtype patients exhibit a lower risk for brain metastasis and tend to have the most favorable brain metastasis-free survival (BMFS). On the other hand, patients with HER2 overexpression and TNBC show a significantly higher risk of developing brain metastases and consequently present poorer BMFS [82-85] **(Figure 5)**.

Still, evidence has emerged demonstrating that, regardless of the BC molecular subtype, brain metastatic cells share certain biological characteristics. For instance, it has been observed that tumors from patients who have metastasized primarily to the brain were negative for HRs, positive for basal markers (such as cytokeratin (CK) 5), and for cancer stem cell (CSC) markers (nestin, CD133, and CD44) [86, 87]. Interestingly, some of these markers have also been found in glioblastomas (GBM), a highly aggressive primary brain tumor [88].

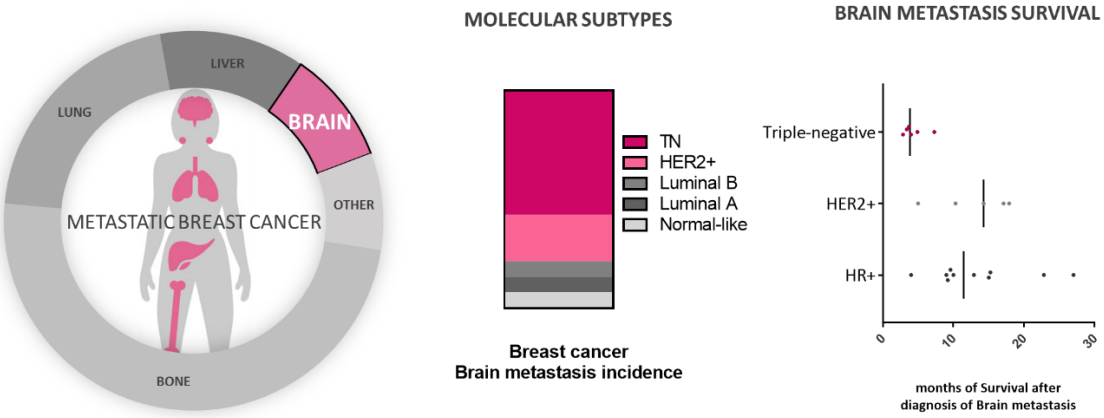


Figure 5. Brain metastases occur in 10%–30% of patients with metastatic breast cancer and are more frequently associated with the HER2-overexpressing and triple-negative breast cancer molecular subtypes. Triple-negative breast cancer shows a significantly increased risk of developing brain metastases, as well as exhibiting the poorest brain metastasis-free survival (BMFS) [89].

3.1 Brain specific metastatic regulators and signaling pathways

Brain metastases represent a significant challenge in cancer management, and understanding the molecular mechanisms underlying their development and progression is crucial for improving patient outcomes. Actually, the spread of cancer cells from primary tumors to the brain involves two critical competences in order to successfully metastasize to the brain. First, cancer cells must acquire the ability to cross the blood-brain barrier (BBB), a specialized and complex barrier structure that separates the blood circulation from the brain. Once cancer cells enter the brain, they face the challenge of adapting to and remodeling the brain microenvironment. Brain metastases are thought to arise mainly due to hematogenous distribution [90]. After travelling from the primary site to the brain, cancer cells often arrest in the dense brain capillary network [91]. Upon the initial arrest, cancer cells may either remain as quiescent cells or actively proliferate to establish a secondary lesion [63, 91]. However, some studies have revealed an intriguing finding that only a very small percentage of cancer cells that stop within the brain's microvasculature develop into metastases, emphasizing the significance of subsequent steps for successful colonization of the brain by metastatic cancer cells [92].

In recent years, several groups have addressed the processes underlying breast-to-brain metastases. The breakthrough in this area began with the establishment of BC cell models with tropism to the brain, generated through successive *in vivo* selection [93]. In a comparative analysis between the gene expression profiles of brain organotropic BC cells and their respective parental cell line, around 250 genes were found to be deregulated. From this list, the authors established a 17-gene list designated as the brain metastasis signature (BrMS).

Importantly, this work, together with more recent data, has uncovered interesting pathways associated with brain metastasis, such as EGFR signaling, cell-matrix interactions, stem cell pathway activation, and glucose metabolic alterations. For example, several EGFR family members and their downstream mediators are widely involved in BC brain metastasis [94-97]. While EGFR seems to be mostly involved in BC cell migration and invasion into the brain [98], HER2 and HER3 overexpression seem to impact the outgrowth of brain metastases [99, 100]. In addition, inhibition of EGFR and cyclooxygenase-2 (COX2) signaling counteracts the transmigration of BC cells through the BBB [101].

Importantly, BC cells can acquire specific molecular characteristics that allow them to interact with and extravasate through the BBB. For example, the membrane glycosyltransferase ST6GALNAC5 has been demonstrated to mediate BC cell adhesion to the brain endothelium, facilitating the passage of cancer cells across the BBB [93]. Additionally, activation of α3β1 integrin has also been proposed to be involved in the

modulation of brain metastases by the interaction between BC cells and brain endothelial cells (ECs) (via αB-crystallin) and by increasing angiogenesis through vascular endothelial growth factor (VEGF) activation [100, 102, 103].

In parallel, stem cell-related pathways have also been reported to play an important role. In fact, Wnt and Notch stem cell markers, and their downstream targets (such as Jagged (JAG) 1, 2, and Interleukin (IL)-1β), are both associated with CSC features and are frequently deregulated in different types of cancers, namely GBM [104] and also in brain metastasis [105-107]. Additionally, the BC stem cell marker CD44, through its interaction with hyaluronic acid, has been shown to facilitate cancer cells passage through the BBB [108, 109].

Following extravasation, cancer cells face various potential outcomes. They may succumb to cell death, influenced by the distinctive conditions of the brain microenvironment [110]. Alternatively, they might enter a dormant state characterized by slow cell-cycle progression [93, 111], or they could survive and generate brain metastasis. Once within the brain, proliferating cancer cells engage in intricate interactions with the brain's microenvironment that promote their outgrowth. For example, molecules associated with metabolism, such as hexokinase 2 (HK2), glucose transporter 1 (GLUT1), fatty acid-binding protein 7 (FABP7), GRP94, and the transcription factor lymphoid enhancer-binding factor-1 (LEF1), have also been described to play a role in the survival of cancer cells in the brain microenvironment [112-117].

Despite this process not yet being fully understood, it is established that the metastatic colonization process is marked by the initiation of neuroinflammatory cascades and the reshaping of the vascular niche. Notably, cancer cells that survive within the brain appear to preferentially position themselves near the perivascular niche [92, 118].

This specific localization of cancer cells offers access to oxygen and nutrients from the blood circulation. It provides a strategic point for attachment within the basal lamina of vessels and enables direct exposure to angiocrine factors released by ECs, fostering tumor growth. Notably, brain metastatic cancer cells have been observed to capitalize on the brain's existing vasculature, foregoing the development of an independent vascular supply system through the angiogenesis process [110]. In the brain microenvironment, cancer cells typically engage with the preexisting vascular network and extend growth along the abluminal side of the vessels, in a phenomenon referred to as vascular co-option [119]. Subsequently, these cells reconfigure the structure of the associated vasculature, integrating it into the evolving metastatic mass. This architectural transformation is a hallmark of brain metastasis and is termed angiocentric growth. A key mechanism underlying this process is intussusceptive angiogenesis, wherein new vessels emerge through the remodeling and bifurcation of preexisting ones [120-122]. Several critical

molecules are involved in vascular co-option namely, CCL2, L1 cell adhesion molecule (L1CAM), and β1 integrin [118, 123, 124].This intricate interplay between metastatic cells and the brain's vasculature underscores the adaptability of these cells and their adeptness at exploiting the brain's unique microenvironment to fuel their growth and progression.

4. Brain Microenvironment

4.1 Metastatic niche formation

The concept of the formation of a metastatic niche is a complex and well-coordinated process that significantly impacts the progression of the disease and the effectiveness of treatments. Even before cancer cells enter the bloodstream, they establish communication with distant organs where metastasis can occur. This communication occurs through the release of tumor-derived molecular components (tumor-derived secreted factors (TDSFs) and/or extracellular vesicles (EVs)). By releasing these factors, cancer cells efficiently mobilize immune cells and activate resident cells. They also play a role in reshaping the ECM, promoting the growth of new blood vessels, and fine-tuning the mechanisms that guide cancer cells to specific organs (organotropism). The combined effect of these interactions is the creation of a pre-metastatic niche (PMN) – a microenvironment that not only provides a welcoming environment but actively supports the survival, growth, and adaptation of cancer cells, even in adverse conditions. [70, 89, 125, 126]. The formation of the PMN relies on three key factors: TDSFs or EVs, bone marrow-derived cells (BMDCs) mobilized by the cancer cells, and the local stromal microenvironment of the host (which includes the components of the future metastatic organ). The PMN plays a significant role in various stages of the metastatic process, contributing in a step-by-step and distinct manner **(Figure 6)** [127]:

1. **Priming -** In the priming phase, primary tumors undergo uncontrolled proliferation, leading to hypoxia and inflammation. Cancer cells release a variety of soluble factors and/or EVs into the bloodstream, mobilizing BMDCs and regulatory/suppressive immune cells to metastatic organs, thereby initiating stromal education and reprogramming. However, at this stage, the PMN is still considered “immature” and not fully prepared for the seeding and colonization of CTCs.

2. **Licensing –** During the licensing phase, continuous recruitment of BMDCs and regulatory/suppressive immune cells to metastatic organs is induced by the soluble factors and EVs released by cancer cells. These factors influence the

microenvironment of the target metastatic site, triggering changes such as inflammation, immune cell recruitment, ECM remodeling, and angiogenesis. These changes prepare a mature PMN for the arrival of CTCs.

3. **Initiation-** As the initiation phase begins, CTCs reach the fully developed PMN. Some of these cells survive or enter a state of dormancy, awaiting the creation of a more favorable environment for them to grow. The well-prepared PMN provides the necessary support for the seeding, colonization, and eventual outgrowth of cancer cells, ultimately leading to the development of micrometastases.

4. **Progression-** During the progression phase, successfully colonized cancer cells continue to proliferate, forming larger metastatic tumors within the secondary organ. As these tumors grow, they can disrupt the organ's normal function and lead to the formation of macrometastases, which have a substantial impact on the patient's health and prognosis.

Understanding the intricate interplay between cancer cells and the evolving microenvironment of the PMN is crucial to decipher the mechanisms underlying metastatic progression. Such insights hold the potential to pave the way for novel therapeutic strategies aimed at disrupting or controlling the metastatic cascade.

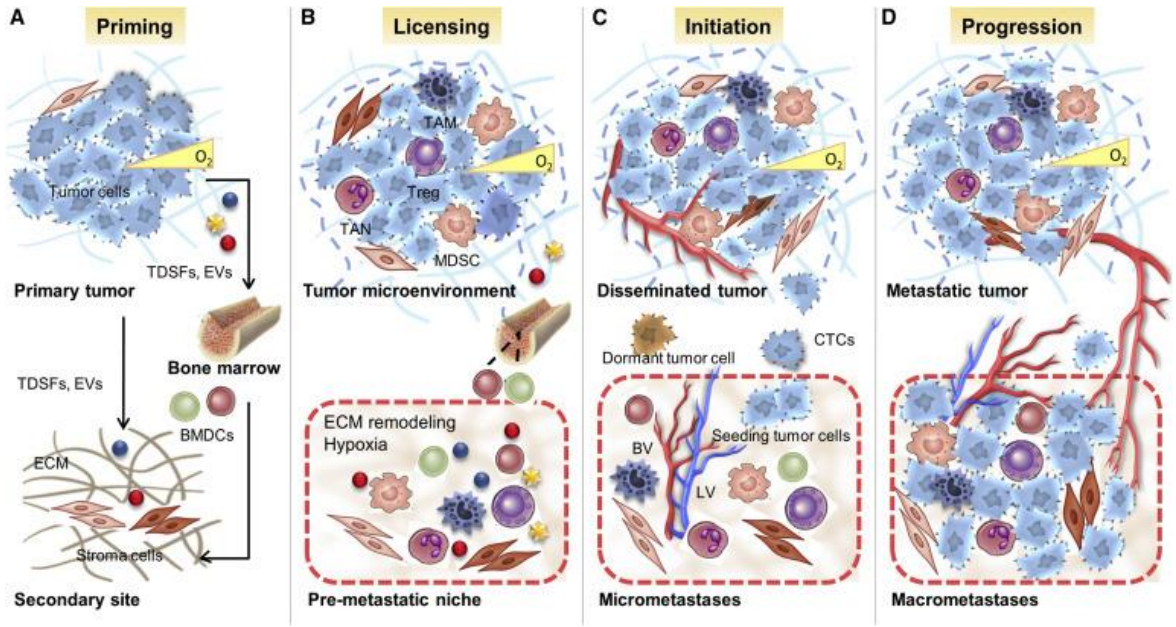


Figure 6. Role of the pre-metastatic niche in the promotion of metastasis (A) In the priming phase, cancer cells secrete soluble factors and/or EVs, to trigger the formation of an immature pre-metastatic niche in the metastatic organ. **(B)** In the licensing phase, bone marrow-derived cells and regulatory/suppressive immune cells are recruited into the metastatic sites in

response to tumor-derived factors. The interactions between factors/recruited cells and host stroma modify the local microenvironment, and finally establish a mature pre-metastatic niche for the seeding and colonization of circulating tumor cells. **(C)** In the initiation phase, circulating tumor cells arrive and colonize at the mature pre-metastatic niche, some of them survive or enter dormancy until the niche environment becomes suitable. The well-prepared pre-metastatic niche can support the seeding, colonization, and outgrowth of cancer cells, resulting in micrometastases. **(D)** In the progression phase, the pre-metastatic niche can host more migrated cancer cells and directly promote metastatic cancer cells to grow, leading to macrometastases. TDSF-tumor derived secreted factors; EVs – extracellular vesicles [127].

4.2 Resident cells' contribution to the establishment of the brain (pre) metastatic niche

The formation of the brain metastatic niche involves the participation of various resident cells within the brain microenvironment. These resident cells play essential roles in creating a favorable environment that supports the growth and survival of metastatic BC cells in the brain. Among these resident cells, ECs, neurons, pericytes, microglia, and astrocytes have been identified as key contributors. Understanding these interactions could lead to the identification of potential therapeutic targets to prevent or disrupt the formation of PMN or metastatic niches. **(Figure 7)**.

4.2.1 Blood-Brain Barrier

The BBB serves as a specialized and distinctive selective barrier within the brain, characterized by its unique vascular structure. Comprising specialized brain capillary ECs, the BBB boasts a tight arrangement facilitated by junctional complexes. Furthermore, the presence of pericytes in contact with the vascular basement membrane, along with astrocytic end feet enveloping the blood vessels, collectively form the neurovascular unit. This intricate arrangement has a critical role in regulating drug delivery while acting as a formidable hindrance to the infiltration of cancer cells into the brain. However, in the context of the brain metastatic process, the integrity of EC junctions within the BBB can be compromised, thus facilitating the extravasation of cancer cells into the brain. This extravasation predominantly occurs through paracellular transmigration, signifying the passage of cancer cells between EC cell junctions [128, 129]. In addition to paracellular migration, breast cancer cells have demonstrated the capability to transmigrate across the BBB while leaving the endothelial cells completely intact. This suggests the involvement of a transcellular route [130]. These distinct mechanisms of migration, both paracellular and transcellular, highlight the adaptability and versatility of cancer cells in navigating the complex barriers posed by the BBB during the metastatic process.

Several genetic determinants play a key role in the extravasation of metastatic BC cells through this highly selective barrier. As already mentioned, the brain metastatic regulators (expressed by cancer cells) HER2, ST6GALNAC5, COX2, EGFR, αB-crystallin, CD44, Syndecan-1, GLUT1, and breast cancer resistance protein (BCRP) are involved in the modulation of BBB permeability [101].

Avraham and colleagues demonstrated that the neuropeptide Substance P (SP), released by BC cells, triggers a process that facilitates the movement of breast cancer cells through the BBB. This process involves activating brain endothelial cells, which then release tumor necrosis factor-alpha (TNF-α) and angiopoietin-2 (Ang-2). This sequence of events leads to BBB impairment and enables the colonization of tumor cells within the brain [131]. In another study, researchers highlighted the connection between the remodeling of tight junctions (specifically ZO-1 and claudin-5) and the Ang-2 protein. This remodeling was found to be partially associated with an increased expression of VEGF in BC cells [132]. This protein, VEGF, is also secreted by BC cells, and its secretion has been demonstrated to promote the disruption of brain ECs [133, 134]. Notably, additional secreted factors have been found to play a role in the development of brain metastases. For instance, stromal cell-derived factor (SDF)-1α has been identified as a factor that induces the activation of phosphoinositide 3-kinase (PI3K), AKT, and focal adhesion kinase (FAK) pathways [135] in BC cells, thereby facilitating their transendothelial migration.

Blocking activated leukocyte cell adhesion molecule (ALCAM) and very late antigen-4 (VLA-4) led to a notable decrease in the number of BC brain metastases. This highlights the vital role that these adhesion molecules play in forming the PMN, which is essential for facilitating the growth of metastatic colonies within the brain microenvironment [136].

Interestingly, it has been demonstrated that EVs are involved in EC-cell adhesion disruption during BC brain metastasis. Specifically, EVs derived from metastatic BC cells have been found to promote the disruption of the vascular endothelial barrier through miR-181c. This miR-181c leads to the reduction of 3-phosphoinositide-dependent protein kinase-1 (PDPK1) and consequently induces the delocalization of actin filaments [137]. Similarly, exosomes containing miR-105, which originate from BC cells, lead to BBB breakdown and brain metastatic progression by decreasing ZO-1 expression within EC tight junctions [138]. Supporting this, both miR-181c and miR-105 were found in the serum of patients at early stages of brain metastatic disease, namely during brain PMN formation [137, 138].

More recently, Lu and colleagues demonstrated that exosomal long noncoding RNA (lncRNA) GS1-600G8.5 secreted by brain organotropic BC cells increased *in vitro* BBB permeability, thus promoting the passage of BC cells across the EC monolayer [139]. Moreover, recent findings revealed that brain organotropic BC cells secrete exosomes containing elevated levels of Cell Migration Inducing Hyaluronidase 1 (CEMIP) that can be

taken up by ECs and microglial cells, inducing vascular remodeling and inflammation in the brain microenvironment [140].

Furthermore, using a model of patient-derived xenograft (PDX) of brain metastasis, it has been demonstrated that the disruption of the BBB is linked to the loss of the major facilitator superfamily domain containing 2A (MFSD2A) in ECs. This loss is due to the absence of astrocytes, which typically release molecules like TGF-β1 and basic fibroblast growth factor (bFGF) to maintain BBB integrity [141]. More recently, Carolin and colleagues demonstrated that serum from BC brain metastasis patients with high levels of cytokines, namely CXCL1 and CXCL13, can impact BBB integrity *in vitro* [142].

4.2.2 Neurons

Neurons play a crucial role in transmitting signals between cells and are among the most vital and abundant components of the brain. Until recently, their influence on the development of brain metastases from BC remained largely unexplored. Neman and colleagues demonstrated that brain metastases show increased upregulation of gamma-aminobutyric acid (GABA) transporters and GABA receptors. This augmentation encourages elevated uptake of the GABA neurotransmitter, leading to enhanced NADPH production and subsequent stimulation of BC cell proliferation [88]. However, recent research by Zeng et al. has brought forth significant insights. They unveiled the interaction between neurons and metastatic BC cells, instigating the activation of glutamine-stimulated N-methyl-D-aspartate receptors (NMDAR), particularly the GluN2B-mediated signaling, within brain-infiltrating BC cells. Their findings underscore the pivotal role of NMDAR activation in successfully establishing metastatic colonies in brain tissue [143].

Furthermore, a recent study unveiled that co-culturing BC cells with neurons results in an increase in the expression of genes linked to classical neurotransmitter receptors and synaptic mediators [144].

4.2.3 Pericytes

Pericytes are perivascular cells located on capillaries between ECs and the brain parenchyma, that mediate several microvascular functions, such as BBB maintenance, blood vessel stabilization, angiogenesis, cerebral blood flow regulation, and the migration of immune cells into the brain [145, 146]. The role of these brain resident cells has largely been deciphered in the context of primary brain tumors, showing that a reduction in pericyte density decreases tumor growth due to increased vessel leakiness and blood supply [147,

148]. However, most recent reports show that loss of pericyte coverage facilitates the brain metastatic process [147].

Xian et al. demonstrated for the first time the role of pericytes as regulators of metastases in neural cell adhesion molecule (NCAM)-deficient mice. This study suggested that NCAM deficiency disturbed pericyte-EC interaction, contributing to metastatic progression [149]. Another study revealed that the contact of metastatic cancer cells with the microvessel wall in a pericyte-like position appears to be a critical step for the extravasation and brain colonization of melanoma and lung cancer cells [150]. Interestingly, two distinct pericyte subpopulations were identified in the blood-tumor barrier (BTB) in BC brain metastasis. The authors showed that CD13+ pericytes were decreased in brain metastases with high permeability, whereas Desmin+ pericytes were increased in brain metastases, with the increase being more pronounced in highly permeable lesions [151]. This study suggested that Desmin+ pericytes could be used as a potential therapeutic target to improve chemotherapeutic efficacy in patients with BC brain metastasis.

A recent study led by Molnár and colleagues has highlighted the crucial role of pericytes in the development of brain metastasis originating from TNBC. Pericytes directly engage with metastatic BC cells by releasing proteins from the ECM, as well as insulin-like growth factors (IGFs) and other molecules that promote attraction, adhesion, and growth. An important molecule, called IGF2, is found in higher levels in pericytes. It interacts with the insulin-like growth factor 1 receptor (IGF1R) on TNBC cells, driving their proliferation. When pericytes increase their production of collagen type IV and fibronectin, TNBC cells respond by increasing activity in certain cell signaling pathways (focal adhesion kinase and Src phosphorylation), leading to the creation of focal adhesions with the newly formed ECM. Additionally, pericytes disturb the adhesion between cancer cells, resulting in migratory and invasive behavior in the metastatic TNBC cells. [152].

4.2.4. Microglia

Microglial cells are the resident immune cells of the central nervous system (CNS), involved in the first line of defense against brain injury and immunological stimuli, while also capable of detecting microenvironmental changes [153-155]. The impact of microglia on brain metastases is less explored, although the role of inflammation and activation of macrophages in cancer progression is widely known.

Similar to what has been observed in both astrocytes and macrophages, microglial cells remain in a resting state until stimulated [156]. After these cells are activated, they can polarize into different states (as observed in tumor-associated macrophages), such as M1 pro-inflammatory and tumor-suppressive, and M2 anti-inflammatory and pro-tumoral

phenotypes. [157]. Although M2 microglial cells are known to be a central component of the immune response to primary brain tumors, their role in the context of brain metastases is less understood [158, 159]. Very few studies report the role of these immune resident cells during the brain metastatic cascade or show the impact of cancer cell secreted factors on microglial activation.

Pukrop et al. reported that activation of M2 microglial cells promoted BC cell invasion and colonization of the brain in a Wnt-dependent manner [160]. In line with the pro-tumoral functions of microglia, loss of long non-coding RNA X-inactive-specific transcript (XIST) by BC cells promoted the secretion of exosomal miR-503, stimulating M2 microglial activation, which in turn proMmoted an increase in programmed death-ligand 1 (PD-L1) expression. This affected the proliferation of T-cells, creating a more amenable microenvironment niche, and favoring the colonization and growth of metastatic cancer cells [161]. In contrast, another study demonstrated that neurotrophin-3 (NT-3) promoted the growth of BC brain metastasis by decreasing microglial cell activation [162].
Finally, metastatic BC cells are found to be surrounded by activated microglial cells, suggesting their important role in initiating the brain metastatic cascade [163-166]. The impact of microglial cells during cancer progression highlights the importance of studying the communication between cancer cells and microglia, particularly during the poorly understood brain PMN remodeling process.

4.2.5. Astrocytes

Astrocytes, the most abundant glial cells found in the brain microenvironment, are crucial for paracrine crosstalk with cancer cells since they are known to secrete different peptides with an impact on brain metastasis progression. Strikingly, a seminal work by Lorger et al. has shown that brain metastatic cancer cells can activate astrocytes even before they extravasate [167]. Their endfeet at the BBB suggests they play a role in this process. This study suggested that astrocytes are activated at early stages of the brain metastatic cascade.
Due to their proximity, astrocytes interact with cancer cells during their entry into the brain. They have been observed to trigger Fas-dependent cell death in both lung and BC cells that have entered the brain [118, 168, 169]. Interestingly, metastatic cells from both breast and lung cancer express elevated levels of serpins, such as Neuroserpin and Serpin B2. These serpins specifically target plasminogen activators (PAs), which neutralize the anti-metastatic impact of astrocytes that rely on plasmin to hinder metastasis. Consequently, this promotes the development of the PMN [118].

Additionally, certain astrocytes expressing STAT3 can be found near metastatic borders in the brain, supporting metastatic growth through suppression of the innate immune system [170].

Astrocytes can also interact with metastatic cells through gap junctions, which could develop between protocadherin 7 on metastatic cells and connexin 43 on astrocytes. This connection triggers the elevation of survival genes, such as STAT1 and the nuclear factor kappa B (NF-κB) signaling pathway, contributing to the promotion of metastasis [171].

Emerging data has been revealing that activated astrocytes, on the other hand, secrete many biological factors, such as proteolytic enzymes, cytokines, chemokines, growth factors, and EVs, that support modifications in the brain tissue during the metastatic process [172-174]. Many of these secreted factors can function as pro-tumoral signals for metastatic BC cells, such as IL-6 and TGF-β [174, 175].

Actually, co-culture experiments have demonstrated that astrocytes produce pro-invasive and pro-migrating factors that affect the tumorigenic capacities of BC cells [176]. Activated astrocytes were shown to increase the levels of phosphorylated-ERK1/2 (p-ERK1/2), leading to an increase in matrix metalloproteinase (MMP)-2 in BC cells. In a later study, Wang et al. identified both MMP-2 and MMP-9 as important mediators for astrocyte-induced tumor cell invasion [177].

Likewise, exosomes secreted by astrocytes may function as mediators of brain metastasis and promote their outgrowth through PTEN knockdown [178]. Interestingly, the authors showed that miR-19a not only targets PTEN but also increases the expression of CCL2, promoting the recruitment of myeloid cells and further associating it with brain metastatic progression.

Gril and team reported that a subpopulation of activated astrocytes expresses phosphorylated platelet-derived growth factor receptor beta (PDGFRβ) [179]. Curiously, in response to soluble factors derived from metastatic BC cells, human astrocytes increased the expression of astrocytic PDGFRβ. Furthermore, inhibition of astrocytic PDGFRβ prevented brain colonization by metastatic BC cells.

Aside from regulating brain metastasis, astrocytes are also associated with brain tumor stem cell properties and with modulating cancer cells' resistance to chemotherapeutic agents, thereby increasing the malignancy in both primary brain tumors and brain metastasis. During the brain metastatic process, CSCs can establish their niche through cooperation with astrocytes. An *in vitro* study demonstrated that bone morphogenetic protein 2 (BMP2) is upregulated in brain metastatic BC cells. Moreover, co-cultures with neural stem cells (NSCs) promoted their differentiation into astrocytes through paracrine communication involving BMP2, a member of the TGF-β signaling pathway [180-182]. This data suggests that breast cancer cells can influence the fate and behavior of nearby neural

stem cells (NSCs), leading to their differentiation into astrocytes. More recently, it was found that increased expression of COX2 and prostaglandins in BC cells with tropism to the brain activated astrocytes, which in turn promoted the secretion of CCL7 responsible for the self-renewal of metastatic breast CSC [183]. In addition, the co-culture of BC cells and astrocytes promotes the upregulation of the glutathione S-transferase alpha 5 (GSTA5), BCL2L1, and TWIST survival genes [168]. Interestingly enough, the upregulation of these genes mediates chemotherapeutic resistance to cisplatin treatment. Finally, exosomal miR-122 released by BC cells modifies glucose metabolism in astrocytes, favoring brain colonization [184].

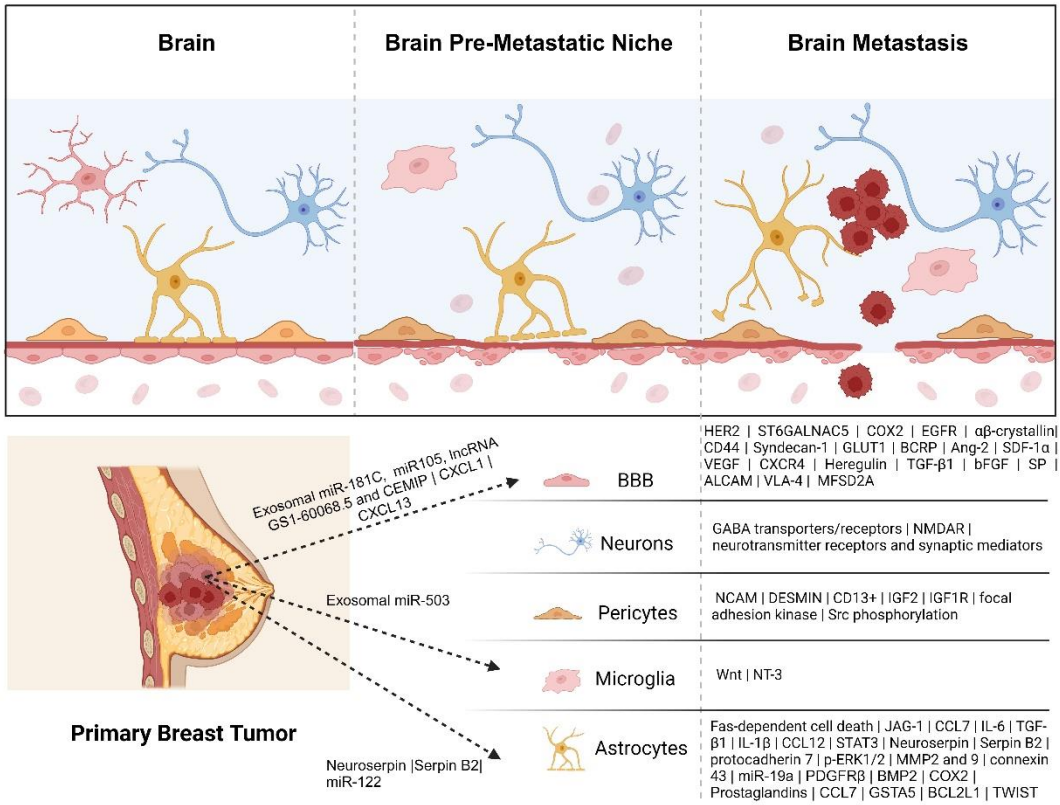


Figure 7. Several changes occur in the brain metastatic niche during breast cancer progression. During the pre-metastatic niche formation, the secretome of cancer cells disturbs the blood-brain barrier and activates brain resident cells. Later, circulating tumor cells reach the BBB, are extravasated into the brain parenchyma, and proliferate in this new microenvironment, generating breast cancer metastasis. The known regulators for each step of the process and each component of the brain metastatic niche are described below. **Adapted from R.Carvalho et al.,2020** [89].

5. The secretome as a modulator of the brain pre-metastatic niche

In recent years, several efforts have been made to uncover and characterize the cancer cell's secretome, aiming to identify biomarkers of metastasis. In fact, there is a plethora of evidence demonstrating that cancer cells prepare the metastatic organ in the early stages of disease progression; long before intravasation, cancer cells communicate with distant metastatic organs, mainly by secreting soluble factors and/or EVs that activate resident cells, immune cells, promote ECM remodeling, and angiogenesis, priming a permissive PMN [185-189].

The factors released by cancer cells collectively compose the "cancer cell secretome," which is regarded as a promising source for the discovery of new molecular targets involved in the crosstalk between the primary tumor and distant metastatic organs. Interestingly, very few data are known regarding the impact of the secretome on the modulation of the brain PMN, despite the growing body of data for other metastatic organs, such as lung, bone, and liver [185, 190].

In recent years, David Lyden and his team have demonstrated that exosomes derived from organotropic BC cells can be endocytosed by resident cells of the respective metastatic organ, in order to prepare the PMN. Surprisingly, the exosomal proteomic analysis demonstrated that distinct integrin profiles correlated with organotropism, although these results were only validated in serum collected from BC patients with liver and lung metastases, but not in those from patients with brain metastasis. Particularly, in the brain, it was recently demonstrated that the CEMIP exosomal protein preconditions the brain microenvironment, enhancing cancer cell outgrowth [140]. Important research efforts have been made to identify players involved in this process, and how cancer cells can directly modulate the brain PMN [191]. Still, it is an unexplored and very challenging area of research.

Innovative high-throughput proteomic technologies have allowed researchers to identify and quantify promising biomarkers in the cancer cell's secretome from body fluids, uncovering new opportunities to develop useful therapies [192-194]. Nevertheless, cancer secretome studies have not always been conclusive due to the complex nature of human samples, encompassing a huge diversity of protein concentrations, thus hampering the detection of molecules with low representation. The majority of secretome studies were performed through *in vitro* cell cultures and subsequently validated in clinical samples using more sensitive techniques, such as ELISA, western blot, and mass spectrometry analysis. [195]. Overall, a large number of secretome studies of cancer cell lines have been published in recent years, including the secretome of BC cells [196].

Bioinformatic analyses using both RNASeq and CYTOF approaches have initiated the examination of the immune microenvironment of BC brain metastasis. However, the majority of these studies have not yet provided information on the early changes in the brain microenvironment during the formation of the pre-metastatic/metastatic niche, but they do provide new insights into the distinct tumor microenvironment surrounding these metastases once they have been established [197-199]. Studying the secretome of cancer cells holds thus a significant potential for understanding these interactions and advancing therapeutic goals. Furthermore, it offers the opportunity to identify biomarkers that indicate the progression of cancer, along with potential targets for disrupting the interactions between the secreted factors and the resident cells within the PMN [200, 201].

CHAPTER II. RATIONALE AND AIMS

Rationale and Aims

Brain metastases are associated with an alarming poor prognosis, with a mean of 6 months survival after diagnosis. This underscores the pressing need for prognostic biomarkers and efficacious therapeutic interventions. To address this critical issue, research has increasingly focused on understanding the complex interplay between BC cells and the brain microenvironment, seeking to uncover the factors responsible for promoting metastatic colonization in the brain. Before intravasation into the bloodstream, BC cells initiate the establishment of the PMN by secreting soluble factors or EVs. This preparatory phase constitutes a pivotal event in the metastatic cascade, presenting promising avenues for therapeutic intervention.

General Aim:

In light of these considerations, the overarching aim of this thesis was to elucidate the soluble factors secreted by brain organotropic breast cancer cells that induce modifications in the brain microenvironment, ultimately impacting their metastatic potential. This research endeavors to unveil the paracrine interactions between breast cancer cells and the brain microenvironment, focusing specifically on identifying key molecular determinants responsible for these interactions. To achieve this overarching goal, four specific objectives were formulated as follows:

Specific aims:

1. To investigate how the secretome of brain organotropic BC cells affects brain PMN formation and colonization.

2. To identify the molecular determinants within the secretome from brain organotropic BC cells that will be responsible for brain PMN modulation.

3. To study the impact of the previously identified markers on the remodeling of the brain PMN and colonization.

4. To clinically validate the relevance of previously identified molecular markers as a predictive factor for BC brain metastasis patients.

.

The findings documented for each of these aims will be discussed further in **Chapter V.**

CHAPTER III. MATERIALS AND METHODS

Materials and Methods

This chapter describes the materials and the methods that were used to generate all the data presented in chapter IV.

Cell Culture. The parental BC cell line MDA-MB-231 (parental 231) was obtained from the American Type Culture Collection (ATCC), Manassas, VA, USA, while its organotropic BC variants lung (231.Lung) [202], bone (231.Bone) [203], brain (231.Brain) [93] and brain with HER2 overexpression (231.Brain.HER2) [100] clones were obtained from J Massagué (MSKCC) and P. Steeg (NCI) **(Figure 8)**. The five cell lines were maintained in Dulbecco's Modified Eagle Medium (DMEM), supplemented with 10% fetal bovine serum (FBS), and 1% antibiotic solution penicillin/streptomycin (all reagents from Invitrogen, Carlsbad, CA, USA).

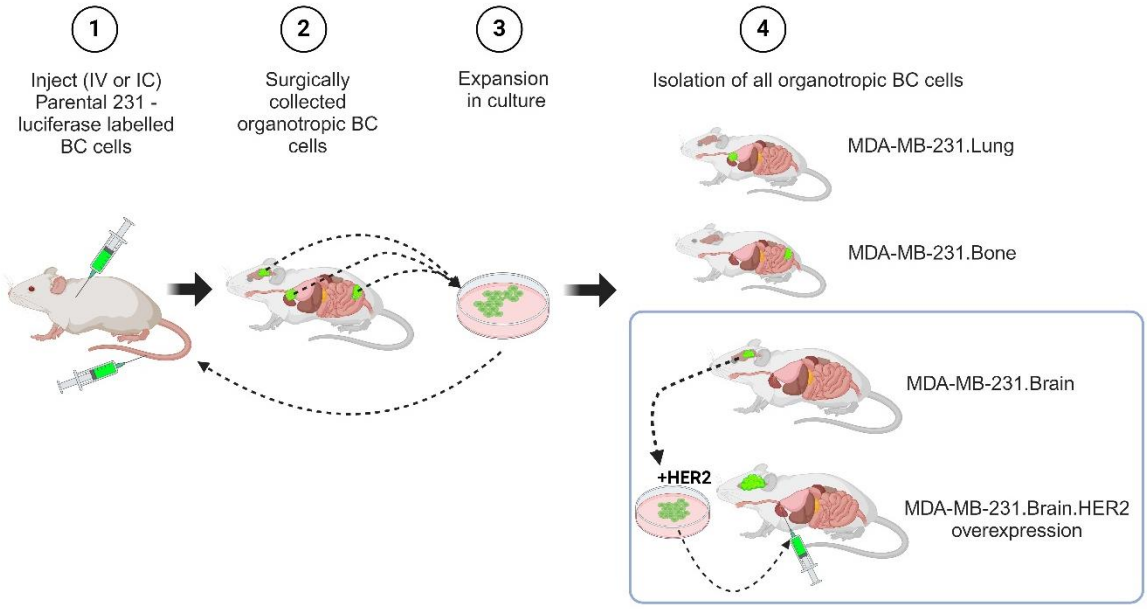


Figure 8. Organotropic MDA-MB-231 breast cancer cell model. This model was developed by the injection of the parental 231 cell line into mice by the intracardiac (IC) route and the brain and bone metastases formed were extracted and expanded in culture. These cells were intracardiac re-injected into mice and the process was repeated at least 6 times, originating 231.Brain and 231.Bone organotropic breast cancer cell lines. The same methodology was applied to generate the 231.Lung organotropic breast cell model; however, intravenous (IV) injection in the tail vein was performed. Additionally, the 231.Brain organotropic BC cells were transfected to overexpress HER2 (231.Brain.HER2). **Created in Biorender.**

The human cerebral microvascular endothelial cell line (hCMEC/D3), used as an *in vitro* model of the BBB [204], was kindly provided by Pierre-Olivier Couraud (Institute Cochin, Université René Descartes, Paris, France). This cell line was cultured in Endothelial Basal Medium-2 (EBM-2; Lonza, Walkersville, MD) supplemented with 1% chemically defined lipid concentrate (Invitrogen, Inchinnan Business Park, UK), 1 ng/ml basic fibroblast growth

factor (bFGF; Sigma-Aldrich), 10 mM 4-(2-hydroxyethyl)-1-piperazineethanesulfonic acid (Lonza), 1.4 µM hydrocortisone (Sigma-Aldrich), 5 µg/ml ascorbic acid (Sigma-Aldrich), 1% penicillin-streptomycin (Gibco), and 5% FBS (Invitrogen) on culture plates coated with collagen Type I (R&D Systems, Inc., Minneapolis, MN). The medium was changed every 2 days until the cells reached confluence. The human microglial clone 3 cell line (HMC3) was purchased from ATCC (ATCC® CRL-3304™) and grown in Eagle's Minimum Essential Medium (EMEM; ATCC, VA, USA), supplemented with 10% FBS and 1% penicillin/streptomycin (all reagents from Invitrogen, Carlsbad, CA, USA). All the cell lines were cultured at 37ºC in a humidified atmosphere with 5% CO2. Cells were used in experiments upon reaching 70–80% confluence.

Secretomes Preparation. Using the parental 231 and their organotropic BC variants for the lung, bone, and brain (without or with HER2 overexpression), we plated ($3x10^5$ cells) in a 6 well-plate, which were subsequently embedded in collagen type I (Merck) to mimic the BC ECM. After 24 hours, we added 1 mL serum-free DMEM to the 3D cultures and left them for 72 hours. The secretomes were recovered, centrifuged (to eliminate cell debris), and used to perform all *in vitro* experiments.

To study the impact of the secretomes *in vivo*, we plated BC cells ($6x10^6$ cells) embedded in collagen type I in a T175 flask. After 24 hours, we added 10 mL serum-free DMEM and left them for 72 hours. The secretomes from the collagen-embedded BC cells were recovered, centrifuged, and concentrated using an Amicon® Ultra-15 3KDa Centrifugal Filter (Millipore) until a final volume of 500µL was reached. To ensure the integrity of the factors present in the secretomes, we aliquoted 30 µL and froze them at -80ºC **(Figure 9)**.

The collagen type I from the rat tail (final concentration of 0.2 mg/mL) was mixed with phosphate-buffered saline (PBS), serum-free DMEM, sodium bicarbonate (NaHCO3), and sodium hydroxide (NaOH), under ice-cold conditions.

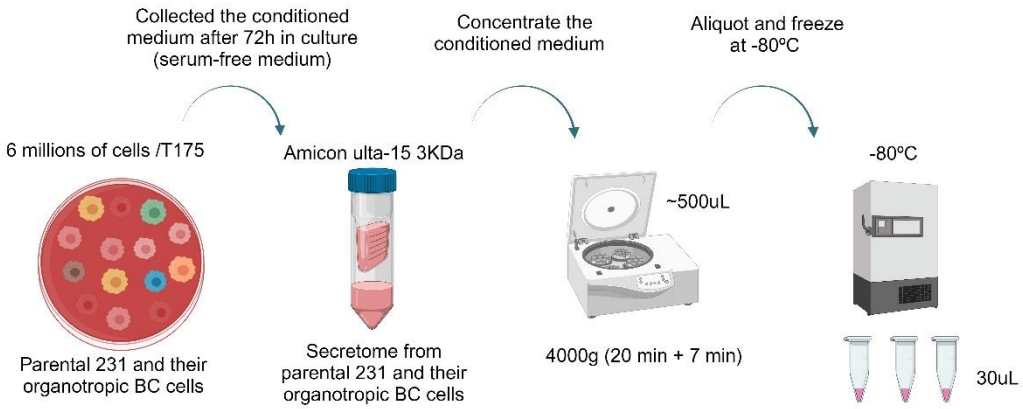


Figure 9. Secretomes Preparation. To understand the impact of the secretomes of parental 231 and their organotropic breast cancer cells *in vivo*, we plated 6x106 cells embedded in collagen type I in a T175 flask. After 24 hours, we added 10 mL of serum-free DMEM for 72 hours. The secretome from the collagen-embedded breast cancer cells was recovered, centrifuged, and concentrated with Amicon® Ultra-15 3KDa Centrifugal Filter (final volume of 500µL). To guarantee the integrity of the factors present in the secretomes, aliquots of 30 µL were prepared and frozen at -80ºC. **Created in Biorender.**

***In vitro* evaluation of brain EC monolayer integrity.** Brain endothelial cell (EC) monolayer integrity was determined by measuring the transendothelial flux of fluorescent 4kDa macromolecules across the hCMEC/D3 cells and by measuring their transendothelial electrical resistance (TEER), as previously described [205]. Briefly, hCMEC/D3 were grown on collagen type I (R&D Systems, Inc., Minneapolis, USA) coated 12 mm Transwell filters (Costar, Corning, NY, USA) at a density of $5.4x10^4$ cell/cm^2, and were maintained for 7 days in a 5% CO_2 incubator at 37°C in regular culture medium for endothelial monolayer formation. On the seventh day, the culture medium from the upper compartment was removed and replaced with secretomes from parental 231 and from their organotropic variants for 24 hours. ECs exposed to fresh serum-free DMEM were used as a control.

In addition, exogenous human purified TLQP-21 peptide at a concentration of 100 nM (Bachem, Bubendorf, Switzerland) was added to the serum-free DMEM. To determine whether TLQP-21 was involved in EC barrier dysfunction, the complement component 3a-receptor antagonist (C3aRA; Sigma-Aldrich; 290157) was added to ECs at a concentration of 10µM during incubation with the secretome of 231.Brain.HER2 overexpression or exogenous TLQP-21, respectively.

To evaluate the permeability of EC monolayer, 1mg/mL fluorescein isothiocyanate (4kDa FITC; Sigma-Aldrich) was added to the apical side of the transwell containing ECs monolayers, diluted in serum-free DMEM or in secretomes of parental 231 and their organotropic BC variants. Samples (50µL) were collected from the basal chamber (and replaced by the corresponding medium) at 20-minute intervals for 180 minutes after

treatments. The fluorescence of samples was measured in a microplate reader (Biotek, Synergy HT, Winooski, VT) and plotted against time. Permeability was determined from linear slope changes after treatments. TEER of ECs monolayers was measured using an STX-2 electrode coupled to an EVOM resistance meter (World Precision Instruments, Hertfordshire, UK). TEER readings of cell-free inserts were subtracted from the values obtained with cells, and results were expressed as a percentage of control. TEER measurements were performed 24 hours after the replacement of the cell culture medium by the above-mentioned secretomes or serum-free DMEM (in the control condition). Only EC monolayers with a TEER above 50 Ωcm^2 were used in subsequent experiments and were obtained by subtracting the TEER of empty inserts, providing the specific TEER of EC monolayers.

***In vitro* microglial phagocytosis assay.** HMC3 cells were seeded ($2.5x10^4$ cells) in a 12-well for 24 hours. Then, we treated the microglial cells with the secretomes from parental 231 and their organotropic BC cells for 8 hours. Microglial cells exposed to serum-free DMEM were used as a control. In addition, we treated microglia cells with 0.2 mg/mL Interferon-γ (IFN-y; Citomed; 285-IF-100) as a positive control.
Exogenous TLQP-21 peptide at a concentration of 100 nM (Bachem, Bubendorf, Switzerland) was added to serum-free DMEM. To determine whether TLQP-21 was involved in microglial phagocytic capacity, the C3aRA was added to microglia cells at a concentration of 10 µM during incubation with exogenous TLQP-21 for 8 hours. To evaluate phagocytic capacity, microglial cells were incubated with 0.0025% (w/w) 1 µm fluorescent latex beads for 75 minutes at 37 °C. At the end of the incubation period, cells were fixed with freshly prepared 4 % (w/v) paraformaldehyde (PFA) in PBS for 10 minutes and then washed with PBS four times to remove unbound beads. Total microglial cells and the number of ingested beads per cell were counted per condition using ImageJ software to determine the percentage of phagocytic cells [206]. We only considered microglial phagocytic capacity when we found more than 5 fluorescent latex beads per cell.

Mouse experiments. In this study, we optimized an *in vivo* secretome-induced model to study the impact of the secretome from parental 231 and of their organotropic BC cells on the remodeling of BBB integrity and microglia modulation. Additionally, we also evaluated the impact of mouse TLQP-21 *in vivo* [207, 208].
In detail, 3 to 4 female N:NIH(S)II-nu/nu mice per condition, with 6–8 weeks of age, were pre-treated via intraperitoneal injection (IP) with 30 µL serum-free DMEM (control condition), 30 µL secretome from 231 parental and their organotropic BC variants, as well as with 30

µL of MCF7 secretome as a negative control (non-metastatic BC cells), for 15 consecutive days.

To understand the impact of TLQP-21 on BBB integrity, animals were pre-treated (4 Female N:NIH(S)II-nu/nu mice per condition, 6–8 weeks of age) with mouse TLQP-21 (4.5 mg/kg; Tocris) for 3 days. Mice follow-up was performed as previously described [209].

Near-infrared fluorescence imaging was performed 30 minutes after intravenous injection (IV) of Cy7.5-dextran 5 kDa (1.5 mg/kg; Nancocs) dye to evaluate BBB permeability **(Figure 10)**.

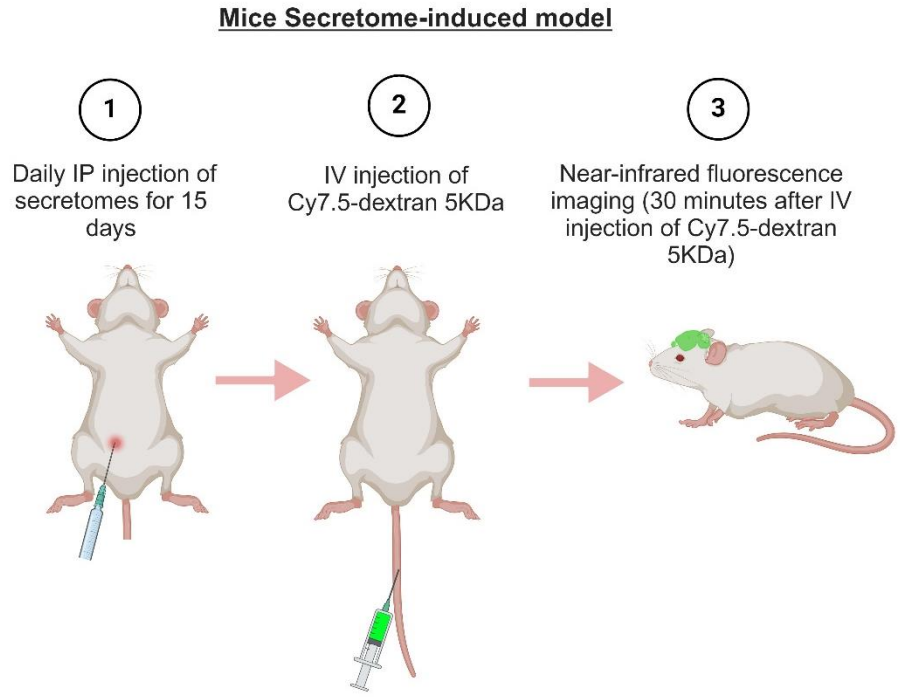


Figure 10. Mice secretome-induced model. The mice with 6–8 weeks of age were pre-treated daily over 15 days with 30 µL of secretome or serum-free DMEM (control condition). At the end of the experiment, near-infrared fluorescence imaging was performed 30 minutes after intravenous injection (IV) of Cy7.5-dextran 5 kDa dye to evaluate blood-brain barrier integrity. **Created in Biorender.**

At the end of the experiment, mice were anesthetized with sodium pentobarbital (80 mg/kg, i.p., Sigma-Aldrich) and transcardially perfused with 10 mL of 0.05 mol/L sodium citrate in 1% PFA (pH 4.2, 37°C), followed by 20 mL of 4% PFA in 0.01 mol/L PBS, pH 7.4. Brains were removed and embedded in paraffin for further immunofluorescence and immunohistochemistry analyses.

To assess brain colonization, nude mice were pre-treated with secretomes (parental 231 and 231.Brain.HER2) or TLQP-21 for 15 and 3 consecutive days, respectively. One day after the final treatment, the mice were intracardially injected with 1×10^5 231.Brain luciferase-expressing cells in PBS. After 3 weeks, the animals were anesthetized and perfused as previously mentioned, and their brains were removed. IVIS Spectrum CT

bioluminescence imaging system (PerkinElmer) was used for brain metastasis imaging **(Figure 11)**.

The analysis of bioluminescent images was conducted using the Living Image software. To quantify the bioluminescent signal, a region of interest (ROI) was delineated around the lesions.

Mice were housed, bred, and maintained at the i3S animal housed in a pathogen-free environment under controlled conditions of light and humidity. All experiments were conducted with the application of the 3Rs (replacement, reduction, and refinement) (JP_2016_02 Project, animal ethics committee, and animal welfare body of i3S) [210].

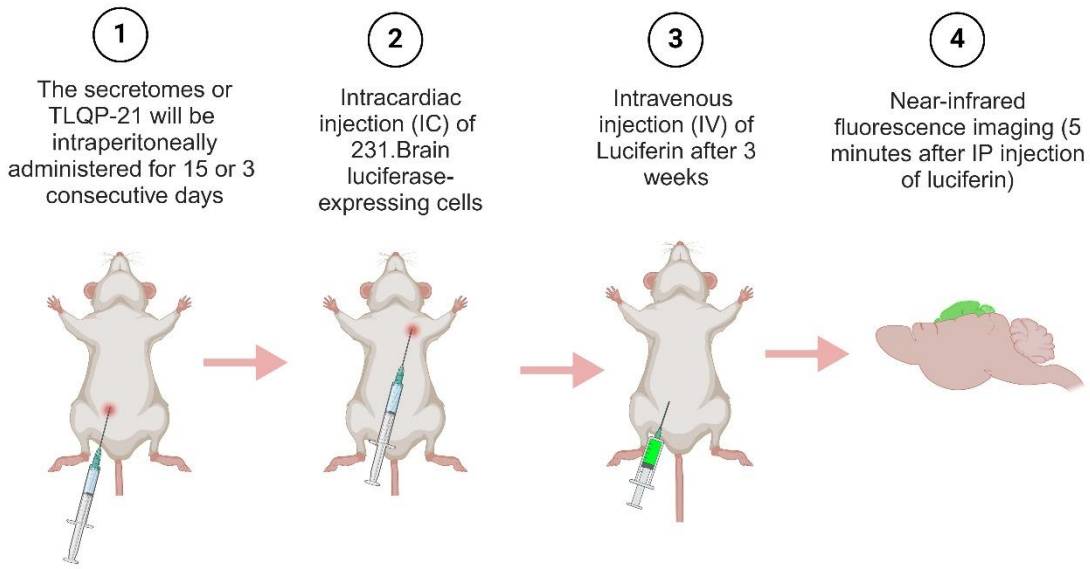


Figure 11. *In vivo* Brain Colonization. Nude mice received pre-treatment with secretomes (from parental 231 and 231.Brain.HER2 cells) or TLQP-21 for 15 and 3 consecutive days, respectively. Following the final treatment, mice were intracardially injected with 1×10^5 231.Brain luciferase-expressing cells in PBS. After 3 weeks, mice were anesthetized, perfused, and their brains were extracted. Brain metastasis imaging was conducted using the IVIS Spectrum CT bioluminescence imaging system. **Created in Biorender.**

3D cortical spheroids production and culture. Primary cortexes were obtained from E16 embryos of Mus musculus pulps (C57BL/6). Trypsin (Gibco, 27250018, 1:250) was dissolved in HBSS (Gibco, 14170-080), to a final concentration of 1.5 mg/mL and filtered with a 0.2 µm sterile syringe filter (VWR, #514-0073) coupled to a 10 mL syringe. After collecting the tissue, a volume of 7 mL of cortexes was incubated with 3 mL of the prepared trypsin solution (final concentration: 0.5 mg/mL), for 8-12 minutes at 37 °C, shaking every 2 minutes. The trypsin solution was carefully removed in a laminar flow hood and the tissue was incubated in a 10% FBS (Gibco, 10270-106) in HBSS and washed with HBSS. The HBSS was removed; the tissue was mechanically dissociated (by pipetting) and filtered

using a 70 µm cell strainer. The total cell number and viability were determined, using a hemocytometer and Trypan Blue (Gibco, 15250-061, 0.4%).
Cortical spheroids were formed using a 96-well U-bottom plate (Thermo Nunclon Sphera, #174925). Neurobasal medium (ThermoFisher, #21103049) was supplemented with B27 (Thermofisher Scientific, #17504044; final concentration 1:50), 200 mM L-glutamine (commercial solution, ThermoFisher Scientific, #25030081), 25 µM L-glutamate (Sigma, #G5889) and 50 µg/mL gentamycin (ThermoFisher Scientific, #15750037; final concentration 50 mg/mL). The cortical cell suspension was diluted in this supplemented medium and placed in the wells, with a concentration of 0.04 $x10^6$ cells/mL (200 µL per well; 8000 cells/spheroid). The plate was centrifuged for 5 minutes, at 200xg, and incubated at 37 °C with a 5% CO_2 atmosphere. After 4 days *in vitro*, half the conditioned medium was replaced with a new supplemented medium (without L-glutamate), every 3 days. The spheroids were fully formed and matured on day 14.
On the 14th day, the cortical spheroids were treated with serum-free DMEM (control condition) and 50µL of the secretome of parental 231 and their organotropic BC cells. The treatments were modified every three days over a span of 14 days.

Analysis of spheroid morphology. Cortical spheroids were imaged using InCell Analyzer 2000 on day 0 before starting treatments and after 14 days of treatments with the secretomes. The acquisition parameters were obtained using the brightfield channel. A focus between 2100 and 2300 was chosen and the plates were scanned with 4x4 binning. The preferred morphological parameters used for the analysis were area and circularity. Morphological parameters were measured from the two-dimensional projection of the three-dimensional spheroids. Using InCell Investigator, stitching and collapsing protocols were employed, generously provided by André Maia, of the i3S Biosciences Screening Platform. Data were then analyzed using a semi-automated quantification method in Fiji/ImageJ, using custom-made macros, generously provided by Mafalda Sousa, of the i3S Scientific Platform of Advanced Light Microscopy.

Extracellular vesicles isolation and treatment. EVs released by parental 231 and their organotropic BC cells were isolated by sequential ultracentrifugation. Briefly, we plated parental 231 and their organotropic BC cells ($2x10^6$cells) embedded in collagen type I in a T75 flask. After 24 hours, we added 8 mL of serum-free medium and left them for 72 hours. The secretomes from the collagen-embedded BC cells were recovered and centrifuged at 300xg for 10 minutes, to remove any cells, and then at 2000xg for 20 minutes, to clear away any cell debris or apoptotic that might be present in cell culture media. EVs were then collected from the later supernatant by an ultracentrifugation step of 100,000xg for 70

minutes. EVs collection was followed by a washing step through resuspension of the pellet in PBS 1x followed by ultracentrifugation at 100,000xg for 70 minutes. All EVs used in biological assays were purified from freshly cultured media, collected and maintained in sterile conditions, and kept on ice at all times when not in use. All centrifugation steps were performed at 4 ºC using the Beckman 70Ti rotor. EVs size distribution and particle number were analyzed using the DS500 nanoparticle characterization system (NanoSight, Malvern Instruments). To quantify the total number of particles secreted per cell, we normalized the overall number of particles/mL by considering the final number of cells and accounting for the applied dilution.

To determine the impact of EVs released by parental 231 and its organotropic BC cells on EC barrier dysfunction, we treated EC monolayers with an equal number of EVs for each condition ($7x10^8$ particles) for 24 hours. Subsequently, we measured permeability and TEER as previously described in this chapter.

Immunofluorescence. Cells were cultured on glass coverslips, fixed with 4% PFA for 20 minutes, treated with ammonium chloride (NH4Cl) (50 mM) for 10 minutes, washed with PBS, and permeabilized with 0.1% Triton X-100 in PBS for 5 minutes, at room temperature (RT). Non-specific binding was blocked by treatment with 5% bovine serum albumin (BSA) in PBS, for 30 minutes at RT. Cells were then stained with Rhodamine Phalloidin (1:200, Life Technologies), for 30 minutes to visualize F-actin, or with anti-β-catenin (1:150), and anti-ZO-1 (1:100) overnight at 4ºC followed by conjugated goat anti-mouse and anti-rabbit secondary IgG (Dako Cytomation, Carpinteria, CA, USA), for 1 hour at RT. After another wash with PBS, each sample was mounted with Vectashield (Vector Laboratories, Inc., Burlingame, CA, USA) containing 4′,6-diamidino-2-phenylindole (DAPI) and visualized with Zeiss LSM 710 confocal microscope (Carl Zeiss AG, Jena, Germany).

Brain tissues were postfixed in 4% PFA for 24 hours at RT and transferred to 30% sucrose in 0.01 mol/L PBS, pH 7.4, for at least 24 hours at 4°C. Next, coronal sections (12 µm) were cut on a cryostat (Leica CM3050S, Nussloch, Germany), and mounted directly onto super-frost microscope slides (Thermo Scientific, Menzel GmbH & Co KG, Braunschweig, Germany) and stored at - 80°C until further use. Then, slices were rinsed in 0.01 mol/L PBS, blocked with 5% BSA in 0.01 mol/L PBS for 1 hour at RT, and incubated overnight at 4°C with rabbit anti-collagen IV (1:200; Abcam) and goat anti-albumin (1:2000; Bethyl Laboratories, Inc, Montgomery, TX, USA) antibodies. Afterward, slices were incubated with Alexa Fluor 488 and Alexa Fluor 594 secondary antibodies (1:200; Invitrogen) for 1 hour at RT, followed by nuclei staining with 5 µg/mL Hoechst 33342 (Sigma-Aldrich) for 5 minutes at RT in the dark. Finally, slices were mounted with Dako fluorescence medium (Dako North

America), and images were recorded using an LSM 710 Meta Confocal microscope (Carl Zeiss).

Western Blot. Cells were lysed with PBS containing 1% Nonidet/P40 (Sigma-Aldrich, Darmstadt, Germany), 1% Triton X100 (Sigma-Aldrich, Darmstadt, Germany), 1:7 Protease Inhibitors Cocktail (Roche Diagnostics GmbH, Mannheim, Germany), and 1:100 Phosphatase inhibitor (Sigma-Aldrich, Darmstadt, Germany).
Protein concentration (cell lysates or secretomes) was determined using the Bio-Rad protein assay (BIO-RAD, Richmond, CA, USA) and samples were loaded into a 10% polyacrylamide gel and transferred onto a nitrocellulose membrane (GE Healthcare Life Sciences, Sheffield, UK) at 100 V for 90 minutes. Membranes were blocked in 0.5% Tween 5% nonfat dry milk for 1 hour, stained with specific primary antibodies overnight at 4º C, and with secondary antibodies for 1 hour at RT. Detection was assessed using the ECL Chemiluminescence detection kit (BIO-RAD, Richmond, CA, USA). Primary antibodies used were anti-VGF (dilution 2 µg/ml, Abcam), anti-phospho-Stat3 (Tyr705) (dilution 1:2000, Cell Signaling), anti-Stat3 (dilution 1:1000, Cell Signaling) and anti-tubulin (dilution 1:1000, Sigma-Aldrich, Darmstadt, Germany). Peroxidase-conjugated secondary antibodies (anti-rabbit and anti-mouse) were purchased from Santa Cruz Biotechnology Inc. (Heidelberg, Germany).
To visualize proteins present in secretomes following protein electrophoresis and transfer, we employed the Revert™ 700 Total Protein Stain method, a well-established protocol designed for protein detection and visualization.
First, the membrane is rinsed with ultrapure water to prepare it for staining. Subsequently, the membrane is treated with the Revert 700 Total Protein Stain, allowing the proteins to be distinctly marked for visualization. Following staining, a thorough rinse with a wash solution is performed to remove any excess stain. A final rinse with ultrapure water ensures a clean background for accurate imaging. To capture images of the membrane, we used an Odyssey® Imaging System with the 700 and 800 nm channels, where the scan intensity or acquisition time were adjusted to prevent saturation.

Proteomic analysis. Proteins were reduced and alkylated with 100 mM Tris pH 8.5, 1% sodium deoxycholate, 10 mM tris (2-carboxyethyl) phosphine (TCEP), and 40 mM chloroacetamide for 10 minutes at 95ºC at 1000 rpm (Thermomixer, Eppendorf). Next, 100 µg of protein were processed for proteomics analysis following the solid-phase-enhanced sample-preparation (SP3) protocol as described by Hughes et al [211]. Enzymatic digestion was performed with Trypsin/LysC (2 µg) overnight at 37ºC at 1000 rpm. The resulting peptides were cleaned-up and desalted with C18 micro columns and further

quantified. Protein identification was performed by nanoLC-MS/MS. This equipment is composed of an Ultimate 3000 liquid chromatography system coupled to a Q-Exactive Hybrid Quadrupole-Orbitrap mass spectrometer (Thermo Scientific, Bremen, Germany). Peptides were loaded onto a trapping cartridge (Acclaim PepMap C18 100Å, 5 mm x 300 µm i.d., 160454, Thermo Scientific) in a mobile phase of 2% ACN, 0.1% FA at 10 µL/min. After 3 minutes loading, the trap column was switched in-line to a 50 cm by 75µm inner diameter EASY-Spray column (ES803, PepMap RSLC, C18, 2 µm, Thermo Scientific, Bremen, Germany) at 300 nL/minute. Separation was generated by mixing A: 0.1% FA, and B: 80% ACN, with the following gradient: 5 minutes (2.5% B to 10% B), 120 minutes (10% B to 30% B), 20 minutes (30% B to 50% B), 5 minutes (50% B to 99% B) and 10 minutes (hold 99% B). Subsequently, the column was equilibrated with 2.5% B for 17 minutes. Data acquisition was controlled by Xcalibur 4.0 and Tune 2.9 software (Thermo Scientific, Bremen, Germany). The mass spectrometer was operated in data-dependent (dd) positive acquisition mode alternating between a full scan (m/z 380-1580) and subsequent HCD MS/MS of the 10 most intense peaks from the full scan (normalized collision energy of 27%). ESI spray voltage was 1.9 kV. Global settings: use lock masses best (m/z445.12003), lock mass injection Full MS, chrom. peak width (FWHM) 15s. Full scan settings: 70k resolution (m/z 200), AGC target 3e6, maximum injection time 120 ms. dd settings: minimum AGC target 8e3, intensity threshold 7.3e4, charge exclusion: unassigned, 1, 8, >8, peptide match preferred, exclude isotopes on, dynamic exclusion 45s. MS2 settings: microscans 1, resolution 35k (m/z 200), AGC target 2e5, maximum injection time 110 ms, isolation window 2.0 m/z, isolation offset 0.0 m/z, spectrum data type profile. The raw data was processed using the Proteome Discoverer software (Thermo Scientific) and searched against the UniProt database for Homo sapiens Proteome. The Sequest HT search engine was used to identify tryptic peptides. The ion mass tolerance was 10 ppm for precursor ions and 0.02 Da for-fragment ions. The maximum allowed for missing cleavage sites was set to 2. Cysteine carbamidomethylation was defined as a constant modification. Methionine oxidation and protein N-terminus acetylation were defined as variable modifications. Peptide confidence was set to high. The processing node Percolator was enabled with the following settings: maximum delta Cn 0.05; decoy database search target FDR 1%, validation based on q-value. Imputation of missing values was performed only when a peptide was detected in at least half (two) of the replicates analyzed. Quantitative proteomic evaluation was performed by pairwise comparisons of all detected peptides and the median ratio was used for protein level comparison. Significance assessment was performed using the background-based ANOVA method implemented in Proteome Discoverer 2.4.1.15 and multiple comparison adjustment of the p values was performed. A minimum of two unique peptides and quantitation in at least half of the samples were required for further evaluation

of each protein. The Venn diagrams were generated with the web tool available at bioinformatics (https://csbg.cnb.csic.es/BioinfoGP/venny.html).

Kaplan Meier plotter survival analysis for VGF mRNA. The Kaplan-Meier (KM) Plotter online survival analysis tool (https://kmplot.com) was used to assess the impact of VGF mRNA levels on overall survival (OS) in BC patients, with the probe set 205586_x_at. The "Auto select best cut-off" option was used, which computes all possible cut-off values and determines the best-performing threshold for the survival analysis. Using these parameters, the analysis was carried out on 1879 patients for OS.

Primary Breast Cancer cohort. A series of 218 primary breast carcinomas diagnosed between 1978–1992, were retrieved from the Pathology Department, Hospital Xeral-Cíes, Vigo, Spain. Patient follow-up information was available for the 218 **(Table 1)**, with a maximum follow-up of 120 months after diagnosis. The tumors were characterized for clinical and pathological features, as previously described [212]. The disease-free survival (DFS) interval was defined as the time from diagnosis to the date of BC-derived relapse (DFS: mean with 95% confidence interval (CI) of 85.5 +/− 2.1 months), whereas overall survival (OS) was considered as the number of months from diagnosis to the disease-related death (OS: mean with 95% CI of 90.0 +/− 2.0 months). BC patients followed the adequate protocols for chemotherapy, radiotherapy, and hormone therapy given at that time. All patients were treated with adjuvant chemotherapy, which consisted of a protocol of six cycles of cyclophosphamide, methotrexate, and fluorouracil. Patients with ER-positive tumors were treated with hormonal therapy, which was carried out exclusively with tamoxifen. Patients with HER2-overexpressing carcinomas were not treated with specific targeted therapy (trastuzumab). No neo-adjuvant treatment was used in the patients included in this series. The present study was conducted under the national regulative law for the usage of biological specimens from tumor banks, where the samples are exclusively available for research purposes in the case of retrospective studies. All analyses were performed according to the reporting recommendations for tumor MARKer prognostic studies (REMARK) recommendations for prognostic and tumor marker studies.

Metastatic Breast Cancer cohort. We used two complementary paired primary and metastatic BC series **(Table 1)**. The first one was retrospectively collected from the archives of the Department of Pathology of the Portuguese Oncology Institute of Porto (IPO Porto) and includes primary breast tumors that metastasized to the lung (n=17), bone (n=56), and brain (n=4). The tumors corresponded to biopsy and/or surgical resections and were formalin-fixed and paraffin-embedded as per routine diagnostics, being evaluated by a

dedicated BC pathologist. All patients were treated by the same multidisciplinary team of professionals in the BC Clinic of IPO Porto. The second one is an exclusive BC brain metastases series with paired primary breast tumors and their corresponding brain metastasis (n=27), which was retrospectively collected from Barretos Cancer Hospital, Brazil. Breast carcinomas were classified considering European Society for Medical Oncology guidelines into luminal A (ER/ PR positive, HER2 negative, and Ki67 low), luminal B (ER/PR positive, HER2 and/or Ki67 high), HER2-overexpressing (ER/PR negative, HER2 positive), and triple-negative (ER/PR/HER2 negative) carcinomas. Metastases present in BC patients were collected after surgical resection or postmortem, preserved and fixed in formalin, embedded in paraffin, and carefully evaluated by neuropathologists. Clinical and pathological features were retrieved for this study from clinical charts. At diagnosis, the majority of patients were stage IV (26.8%, 15/56), followed by stage III (19.6%, 11/56), stage II (26.7%, 15/56), stage I (14.3%, 8/56), and for 7 patients we did not have information about the tumor stage. Information regarding prior metastatic dissemination to the brain was not complete and it was not used in the analysis. Whenever data were available, patients were grouped into intrinsic molecular subtypes: luminal (positive for ER and/or PR, HER2-negative), HER2-positive (HER2-positive/amplified, negative or positive for ER and PgR), and triple-negative (ER-negative and PgR-negative, HER-2-negative). Patient follow-up information was available for those who were diagnosed between 2007–2008 (Barretos Cancer Hospital), with a maximum follow-up of 223 months after diagnosis. These BC patients followed the established protocols of chemotherapy, radiotherapy, and hormone therapy at that time. No neo-adjuvant treatment had been used in the patients included in this series.

The present study was conducted with the approval of the Ethical Commission from both cancer centers, under the national regulative law for the usage of biological specimens from tumor banks, where the samples are exclusively available for research purposes in retrospective studies (Ethical approvals: Portuguese Oncology Institute of Porto (CES. 64/023) and Barretos Cancer Hospital/Fundação Pio XII (2-777-372)).

. **Table 1.** Characterization of the different cohorts

Database	Breast Cancer	Breast Cancer Metastasis	Brain Metastasis
Country	Spain	Portugal	Brazil
Hospital	CHUVI	IPO-P	Barretos
Ethical protocol number/Approval	-	CES.64/023	2.777.372
Type breast tumors	Primary	Primary and matched Metastasis	Primary and mateched Metastasis
Metastasis	No information	Bone, Lung, and Brain	Brain
Number	218	83	27
Type	Retrospective	Retrospective	Retrospective
Date	1978-1992	1996-2016	2012-2018
Age at diagnosis	59,98 ± 12,637 (32-90)	51,07 ± 12,35 (28-76)	49,04 ± 12,73 (27-71)
Follow-up duration	120.0	120.0	120.0
DFS (months)	84,58 ± 44,7 (1-120)	73,18 ± 52,37 (0-120)	28,2 ± 28,23 (0-110)
OS (months)	88,25 ± 341,4 (2-120)	87,34 ± 34,58 (18-120)	53,29 ± 33,98 (6-120)

Immunohistochemistry. Immunohistochemistry for IBA1, pan-Cytokeratin, and VGF was performed on 3 µm sections. Slides were placed in a Clear-Rite bath (Thermo Fisher Scientific, Waltham, MA, USA), rehydrated through a descending series of ethanol washes, and finally placed in distilled water. Epitope exposure was performed for 15 minutes (IBA1 antibody), 1 hour (pan-cytokeratin antibody), and 30 minutes (VGF antibody) at 95 ◦C with citrate buffer (ThermoScientific, Freemont, CA, USA). The following antibodies were used: IBA1 (Thermo Fisher Scientific; GT10312; 1:200), pan-cytokeratin (Sigma; C2562; 1:200), and VGF (Abcam;115609; 5µg/mL). Primary antibodies were detected using the horseradish peroxidase polymer (Cytomation Envision System HRP; DAKO, USA), according to the manufacturer's instructions. Diaminobenzidine was used as the chromogen.

Immunohistochemical evaluation. The expression of VGF was independently evaluated by one pathologist (F.S.) based on grading systems previously established for other markers [213, 214]. Positive staining of VGF was considered when detected in the cytoplasm of cancer cells and at the tumor-adjacent stroma. Cases were classified as negative/low when scored as (0), (1+), (2+), whereas (3+) were determined as high expressing cases. Additionally, VGF expression in the stroma was classified as positive

when present and negative when absent. VGF positivity was considered when high expression of VGF (3+) was found in cancer cells and when VGF was positive in the tumor-adjacent stroma.

Data mining from publicly available datasets. Results were validated using NCBI GEO microarray-based transcriptome datasets GSE2603 and GSE12276, assessed using the Affymetrix U133A and Affymetrix HG-U133 Plus 2.0 chips, respectively. Gene expression was measured at the probe level using the RMA (Robust Multi-array Average) methodology for background subtraction and normalization of probe intensities, employing the oligo package (version 1.64.1) in R (v. 4.3.1). The quality of the data was assessed using principal component analysis. RMA values from VGF were z-scored for each dataset to remove chip-specific effects, and these values were used for survival analysis.
Metastasis-free survival analysis was conducted using the Kaplan-Meier method. Plots were generated in R using the "survival" and "survminer" packages. The best separation cut-off method was utilized to cluster individuals into "high" and "low" gene expression groups. This cut-off refers to the value, within the second quartile, that yields the lowest log-rank P-value in the comparison between the groups.

Statistical analyses. Error bars in graphical data represent the mean ± standard error of the mean (SEM). Reference to the number of independent biological replicates performed for each experiment, as well as the sample size of each experimental group/condition, is provided in the respective figure legend of each experiment. Statistical significance was determined with one-way ANOVA or t-test, in which P values smaller than 0.05 were considered statistically significant. The variance was similar between the groups that were statistically compared. GraphPad Prism version 9.0c software (GraphPad Software, San Diego, CA, USA) was used for statistical analysis and graphical data presentation. ImageJ was used for image processing and analysis. Survival analyses for the primary breast tumor were estimated by the Kaplan–Meier method and compared using the log-rank test. For statistical analysis of the immunohistochemistry results, chi-square tests were carried out using IBM® SPSS® statistics V.26 software package for Windows (SPSS, Inc., Chicago, IL, USA). All statistical tests were two-sided.

CHAPTER IV. RESULTS

I. Secretomes of brain organotropic breast cancer cells affect the blood-brain barrier integrity.

Our goal was to evaluate the impact of the secretomes produced by brain organotropic BC cells on the preparation of the brain PMN, with a particular emphasis on BBB permeability and microglia activation. As models, brain organotropic BC cells (without or with HER2 overexpression), derived from the parental 231, were used **(Figure 8)**. To control for brain metastatic specificity, the results were always compared to data obtained with 231.Lung and 231.Bone organotropic BC cells.

To investigate the impact of the secretome of brain organotropic BC variants on the remodeling of the brain PMN, we started by evaluating BBB integrity. We found that the secretome of both brain organotropic BC variants showed a specific and significant increase in cell permeability **(Figure 12A)** and a decrease in TEER **(Figure 12B)** of hCMEC/D3 monolayers. Interestingly, this significant effect was not seen with the secretome of the parental 231, nor with those from the non-brain organotropic BC variants. By immunofluorescence analysis, we observed a significant decrease in β-catenin expression in hCMEC/D3 cells, in the presence of the secretomes of both brain organotropic BC variants **(Figure 12C-D)**, indicating an *in vitro* disruption of the EC intercellular junctions.

These results were further confirmed by the *in vivo* mice secretome-induced model. After priming mice with secretomes for 15 days, we showed a significant and specific impact of the secretome of both brain organotropic BC variants on BBB permeability. This was evidenced by an increased accumulation of a fluorescent dye in the brain, compared to the secretome of the parental 231, MCF7 (non-metastatic BC cells), and serum-free DMEM (control condition) **(Figure 12E-F)**. Although the secretome from the non-brain organotropic BC variants also showed a small impact on *in vivo* permeability after region of interest (ROI) measurement **(Figure 12F)**, this effect was more pronounced and specific when nude mice were pre-treated with the secretome from both brain organotropic BC cells. Further ex-vivo BBB analysis showed that the brains of these animals tended to have increased fluorescence intensity of collagen IV after treatment with the secretomes from all organotropic BC cells, although not statistically significant **(Figure 12H)**. Nevertheless, the immunofluorescence images revealed evident disorganization and clustering of collagen IV, particularly seen after treatment with secretomes from brain organotropic BC cells **(Figure 12G)**, which could explain the observed increase in BBB permeability *in vivo*. Additionally, we observed a significant and very pronounced accumulation of albumin in the brains of mice treated exclusively with secretomes from brain organotropic BC cells **(Figures 12G and I)**, confirming structural and functional changes in BBB integrity in the prefrontal cortex.

Taken together, these data provide strong evidence that the secretome of brain organotropic BC cells causes BBB disruption, thus promoting the passage of molecular factors through this unique brain barrier.

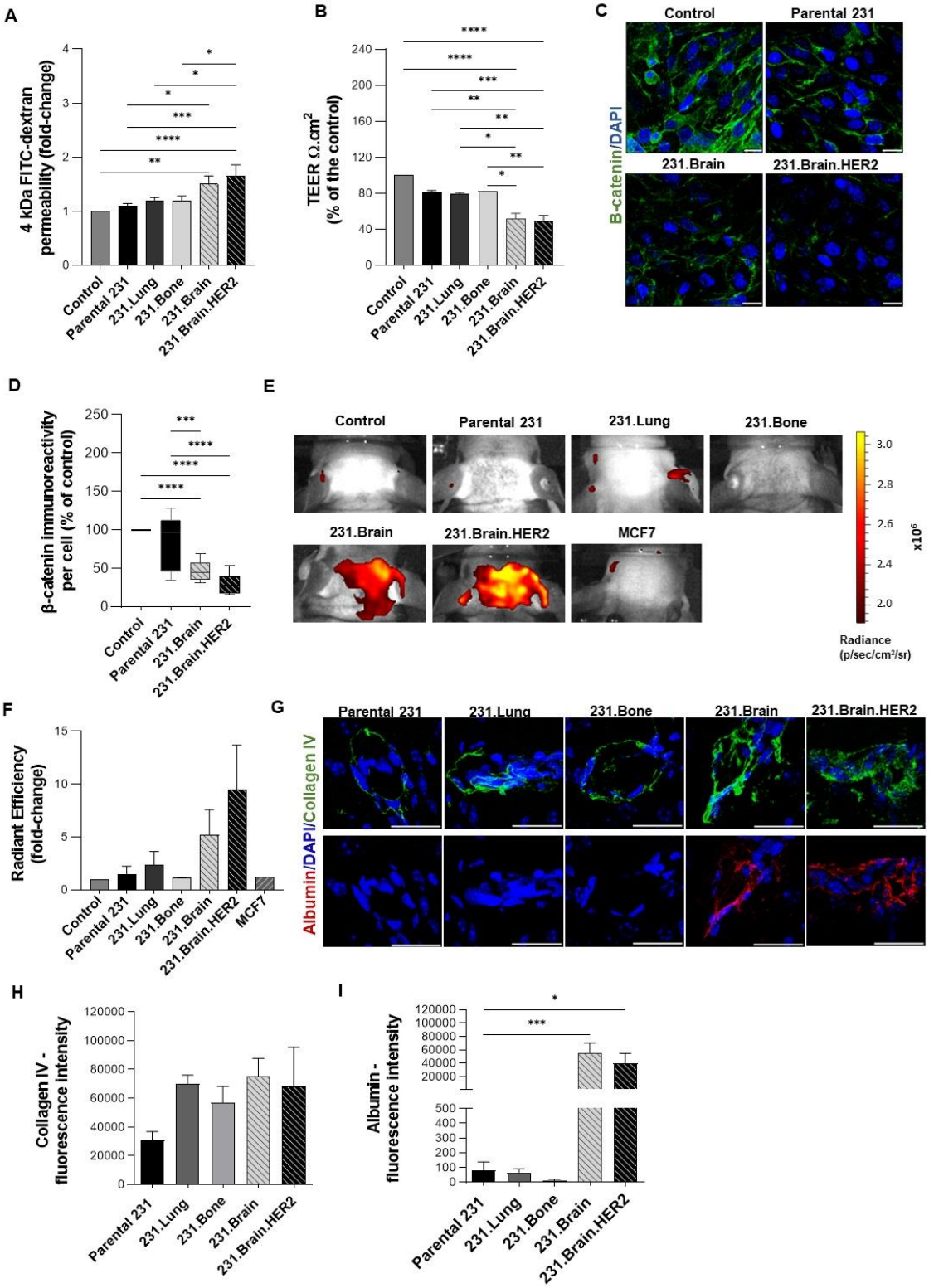


Figure 12. The secretome of brain organotropic breast cancer cells promotes BBB disruption. (A-D) Human cerebral microvascular endothelial cells (ECs) (hCMEC/D3 cells) monolayers were treated with serum-free medium (control condition) and secretomes collected from parental 231 cells and their organotropic breast cancer variants. **(A)** *In vitro* permeability was

assessed using 4kDa FITC-dextran, and **(B)** transendothelial electrical resistance (TEER) assay was performed after 24 hours of treatment (n=4 biological replicates; results presented as mean ± SEM). **(C)** Representative confocal images of β-catenin staining. β-catenin is shown in green and DAPI in blue. (Scale bar corresponds to 20 µm). **(D)** Quantification of β-catenin expression after treatment with the secretome of parental 231 and brain organotropic variants (n=3 biological replicates; results presented as mean ± SEM). **(E)** *In vivo* near-infrared fluorescent brain imaging was conducted after 15 days of treating mice with serum-free medium (control condition), the secretome of parental 231 cells and their organotropic breast cancer cells, and the secretome of MCF7 (a non-metastatic breast cancer cell line, serving as a negative control). Representative images of mice brains acquired at 30 minutes post-injection of Cy7.5-dextran 5 kDa. **(F)** Quantification of radiant efficiency in equal-sized regions of interest (ROI) corresponding to the top of the skull (3/4 animals/group; results presented as mean ± SEM). **(G)** Representative confocal images of collagen IV (a marker of the basal membrane supporting brain vessels) and albumin (a marker of BBB disruption) staining after treatment with parental 231 and their organotropic BC cells. Collagen IV is shown in green, albumin in red and DAPI in blue. (Scale bar corresponds to 20 µm). **(H and I)** Quantification of collagen IV and Albumin mean fluorescence intensity (MFI). (2 mice/per group, 10 independent areas; the results are expressed as mean ± SEM). Statistical significance was assessed using one-way ANOVA. *P < 0.05, **P < 0.01, ***P < 0.001, ****P < 0.0001.

II. Secretomes of brain organotropic breast cancer cells promote microglia activation

Some studies have demonstrated that microglia can be recruited and activated during brain metastatic colonization [162, 167, 215-219]. However, little is known about its role in the remodeling of the brain microenvironment in the early stages of the metastatic cascade, more specifically during the formation of the brain PMN. To understand the impact of the secretomes of brain organotropic BC cells on microglia activation, HMC3 cells were pre-treated with the secretomes collected from the parental 231 and their organotropic BC variants to evaluate their phagocytic capacity, as well as their Stat3 phosphorylation.

Our *in vitro* data demonstrate that the secretome of both brain organotropic BC cells promotes microglia activation, as this treatment significantly increased both phagocytic capacity **(Figure 13A-B)** and Stat3 phosphorylation **(Figure 13C-D)** of microglia cells compared to the control condition. Nevertheless, the secretome of the other non-brain organotropic variants also induced microglia activation, indicating that the previously observed specificity for the BBB is not occurring in this setting.

To validate these findings, we evaluated the role of all secretomes on the microglial cell population in the cerebral cortex of mouse models. Immunohistochemical analysis for IBA1 (a microglia marker) **(Figure 13E)**, was conducted, where microglia cells were counted in the cerebral cortex, and the positive area and staining intensity for each cell were quantified to measure their degree of activation. Interestingly, we demonstrated that the secretome of parental 231 and the secretome of 231.Bone significantly increased the positive area; however, the results were more pronounced with the secretome of both brain organotropic BC cells **(Figure 13F)**. In addition, these secretomes significantly increased the staining intensity per cell **(Figure 13G)**, an effect not observed with the secretome of parental 231

and the other organotropic BC cells. These data suggest that factors present in the secretome of both brain organotropic BC cells trigger a more prominent response on microglia cells during the brain PMN formation.

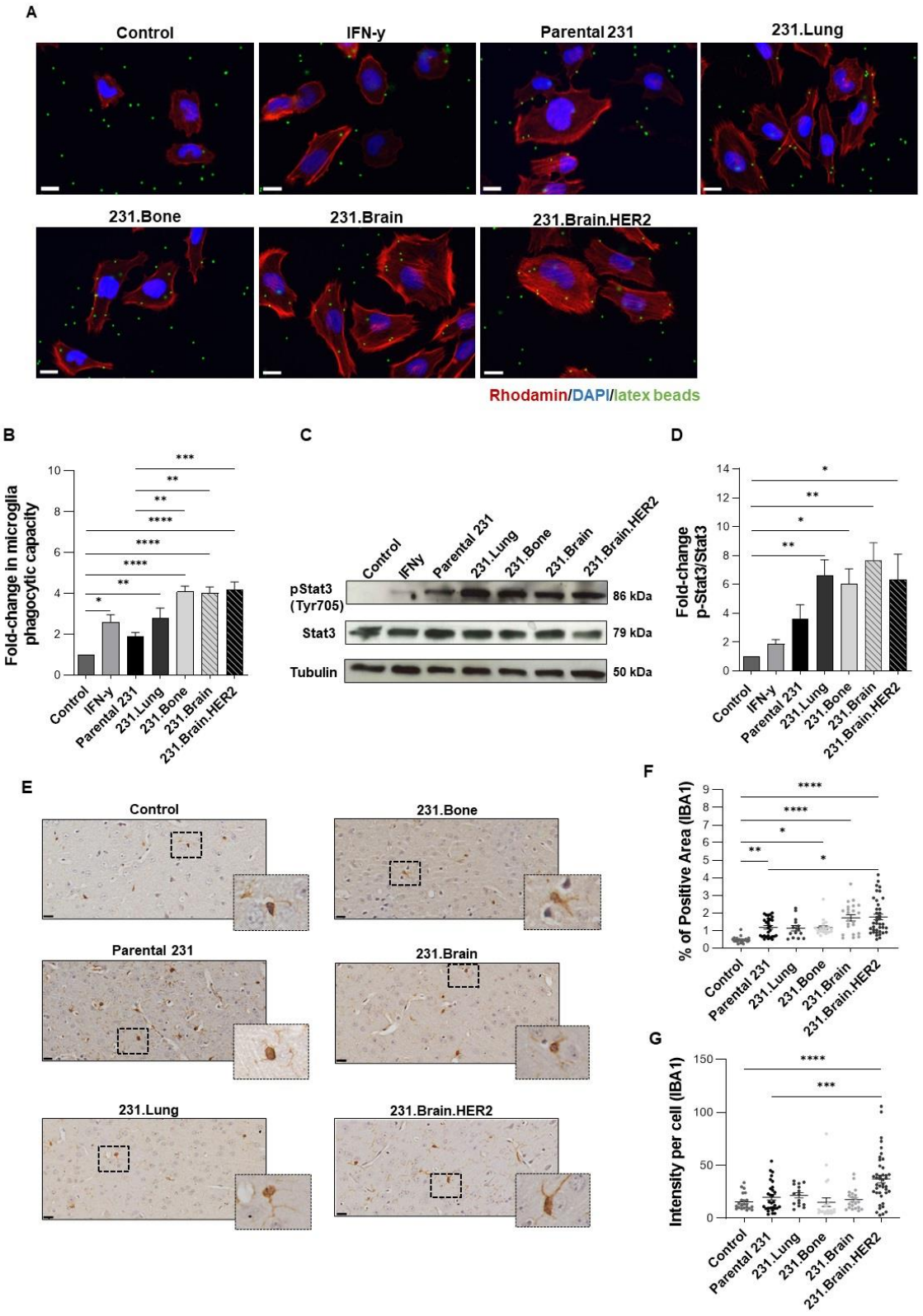


Figure 13. The secretome of brain organotropic breast cancer cells impacts microglia activation. (A) Representative confocal images of microglia phagocytic capacity of 1 µm fluorescent latex beads after treatment with serum-free DMEM

(control condition), IFN-y (positive control), as well as with the secretomes of parental 231 and their organotropic breast cancer variants for 8 hours. (Scale bar corresponds to 20 µm). **(B)** Quantification of microglia phagocytic capacity after treatment with serum-free DMEM (control condition), IFN-y (positive control), as well as with the secretomes of parental 231 and their organotropic breast cancer variants for 8 hours. (n=4 biological replicates; the results are expressed as mean ± SEM). **(C)** Western blot of Stat3 phosphorylation (pStat3 Tyr705) and Stat3 in HMC3 cell lysates after 8 hours of treatment with the serum-free DMEM (control condition), IFN-y (positive control), as well as with the secretomes of parental 231 and their organotropic breast cancer variants. **(D)** Quantification of Stat3 phosphorylation over Stat3 normalized to tubulin. (n=3 biological replicates; the results are expressed as mean ± SEM). **(E)** Representative images of IHC staining for IBA1 (a marker of microglia cells) in the cerebral cortex of mice after 15 days of treatment with serum-free DMEM (control condition), as well as with the secretomes from the parental 231, and their organotropic breast cancer variants. (Scale bar corresponds to 20 µm). **(F)** Quantification of microglia positive area and **(G)** staining intensity per microglia cell in the cerebral cortex of mice after 15 days of treatment with serum-free DMEM (control condition), as well as with the secretomes from the parental 231, and their organotropic breast cancer variants (IBA1- a marker of microglia cells). (3 mice/per group, 6-8 cerebral cortex independent areas; the results are expressed as mean ± SEM). .Statistical significance was assessed using one-way ANOVA .*P < 0.05, **P < 0.01, ****P < 0.0001.

III. The secretome of brain organotropic breast cancer cells affects the stability of 3D cortical spheroids

3D cortical spheroids could be an important tool to study the remodeling of brain resident cells in the early stages of brain metastatic cascade. Derived from the cerebral cortex of mouse embryos, these cortical spheroids encompass four distinct brain resident cell types: microglia, astrocytes, neurons, and oligodendrocytes [220]. They prove to be a highly effective model for accurately recreating the cell complexities found in the *in vivo* cerebral cortex.

We used this model to simulate the brain microenvironment and evaluate the impact of the BC cell's secretome on brain dynamics. After 14 days of treatment, we observed that the secretome of all organotropic BC cells significantly increased the area of the 3D brain spheroids when compared with the serum-free DMEM (control condition) **(Figure 14A-B)**. Interestingly, this effect was not observed after treatment with the secretome of parental 231.

Furthermore, we found that the secretome of both brain organotropic BC cells led to a significant reduction in the circularity of the 3D cortical spheroids. This effect was not seen with the secretome from the parental 231 or the non-brain organotropic BC cells **(Figure 14A and C)**. Although we haven't yet deciphered which population of brain resident cells is affected after treatment, we can conclude that factors present in the secretome of organotropic BC variants, especially with tropism to the brain promote the remodeling of these brain resident cells. This conclusion arises from the observation that, under normal conditions, these cortical spheroids tend to compact over time.

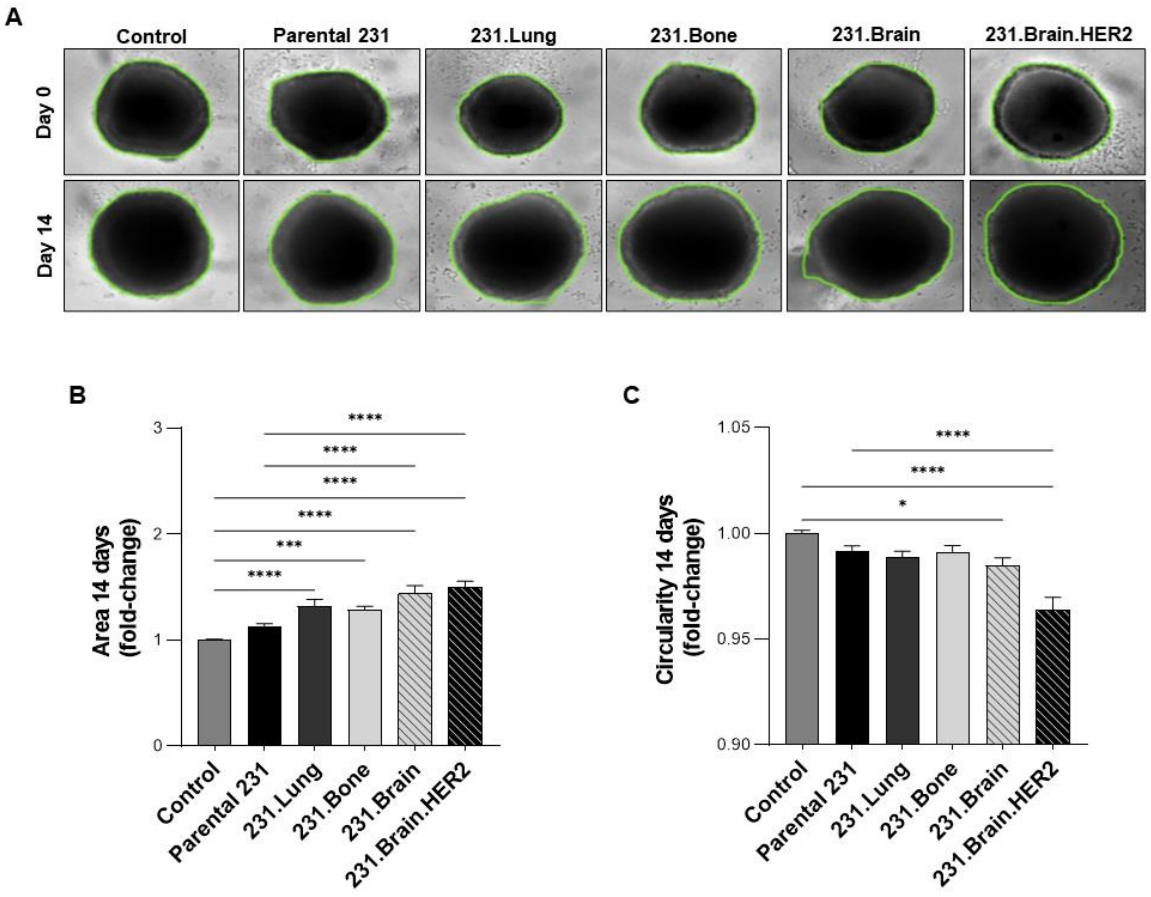


Figure 14. The secretome of brain organotropic breast cancer cells affects the stability of 3D cortical spheroids. (A) Representative images of 3D spheroids on day 0 without treatment and after 14 days of treatment with serum-free medium (control condition), the secretome of parental 231, and their organotropic breast cancer cells. **(B)** Quantification of area (n=4 biological replicates; the results are expressed as mean ± SEM). **(C)** Quantification of circularity (n=4 biological replicates; the results are expressed as mean ± SEM). Statistical significance was assessed using one-way ANOVA .*P < 0.05, ***P < 0.001, ****P < 0.0001.

IV. Extracellular vesicles secreted by brain organotropic breast cancer cells are inefficient to modulate the blood-brain barrier

EVs possess a vital function in facilitating communication between cells by carrying diverse biomolecules like proteins, lipids, and nucleic acids. Originating from the endosomal pathway, EVs are released into various body fluids, including blood, lymphatic fluid, saliva, and urine [202]. Several studies demonstrate that EVs are secreted by cancer cells and contribute to the remodeling of pre-metastatic and metastatic niches [70-72, 140].

To try to decipher which fraction of the secretome of brain organotropic BC cells is responsible for the brain PMN remodelling, we isolated EVs from parental 231 and their organotropic BC variants and evaluated their impact on *in vitro* BBB integrity, since this was

the most specifically affected brain component after treatment with the brain organotropic secretomes.

Using Nanosight, we quantified the size and quantity of EVs secreted by the parental 231 cell line and its organotropic variants. To standardize our findings, we normalized the EVs count to the final cell number, enabling us to determine the number of EVs secreted per cell. Curiously, we found that all organotropic BC cells secrete a higher quantity of small EVs (0-150nm) compared to the parental 231 **(Figure 15A)**. However, this result was only statistically significant in the case of small EVs secreted by 231.Bone and 231.Brain.HER2 BC cells. Interestingly, we also observed that 231.Brain.HER2 secrete a large amount of larger EVs (150-900nm) compared to parental 231 and other organotropic BC cells. Next, we treated hCMEC/D3 monolayers with EVs released by parental 231 cells and their organotropic BC cells (adding an equal number of exosomes for each condition) in order to analyze BBB integrity. We found that EVs released by BC cells did not affect the permeability of EC monolayers **(Figure 15B)**. Regarding TEER, we observed a significant decrease after treatment with EVs released by 231.Bone and 231.Brain.HER2 BC cells **(Figure 15C)**. Based on these results, we could conclude that the effect previously observed, for the specific disruption of the BBB integrity by the secretome of brain organotropic BC cells, is not due to the factors transported by EVs. This suggests that soluble factors are probably responsible for the previously observed impact on BBB integrity.

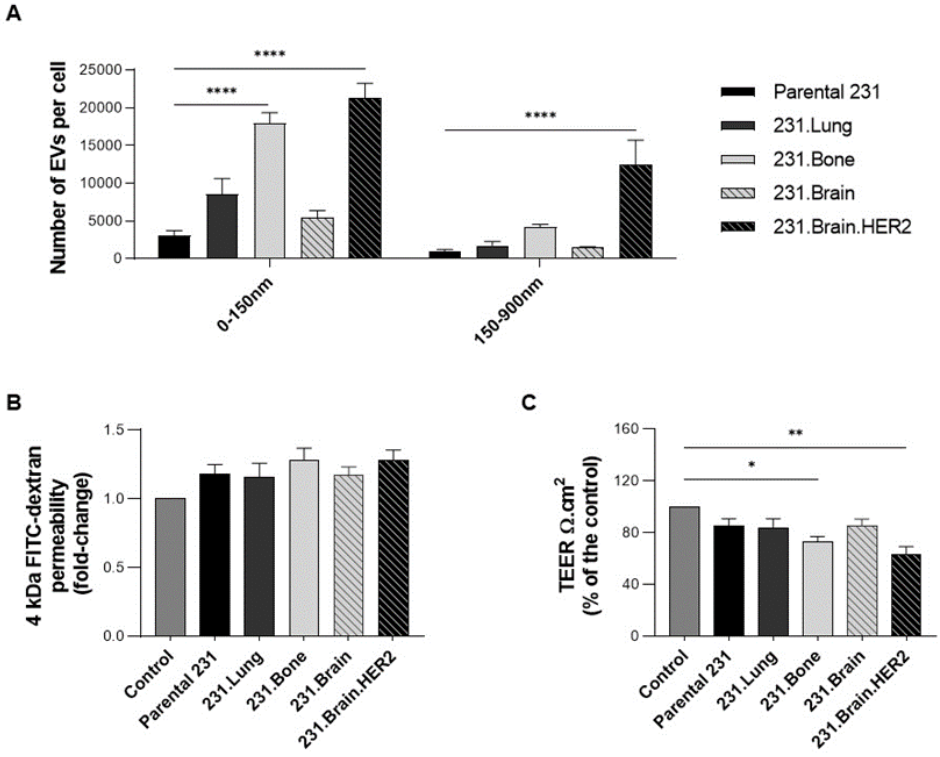


Figure 15. The impact of extracellular vesicles released by brain organotropic breast cancer cells on the blood-brain barrier. **(A)** Quantification of extracellular vesicles secreted by parental 231 and their organotropic breast cancer cells

normalized to the final cell number, enabling us to determine the number of extracellular vesicles secreted per cell. (n=4 biological replicates; the results are expressed as mean ± SEM). **(B)** *In vitro* permeability using a 4kDa FITC-dextran and **(C)** transendothelial electrical resistance (TEER) assay after 24 hours of treatment with extracellular vesicles. (n=4 biological replicates; the results are expressed as mean ± SEM). Statistical significance was assessed using one-way ANOVA.*P < 0.05, **P < 0.01, ****P < 0.0001.

V. Secretome of brain organotropic breast cancer cells promotes brain colonization

To confirm whether these modifications in the brain microenvironment during the early stages of the metastatic cascade promote brain colonization, we still conducted a brain metastasis colonization assay. Interestingly, we observed that mice pre-treated with the secretome of 231.Brain.HER2 cells exhibited an increased luminescence in the brain, when compared with the mice pre-treated with parental 231 secretome, suggesting that BC cells have reached and colonized the brain more efficiently than in the control animals **(Figure 16A-B)**. Immunohistochemical analysis of human Pan-cytokeratin in mouse brain tissue revealed a higher abundance of 231.Brain cells following treatment with the secretome of 231.Brain.HER2 compared to treatment with parental 231 **(Figure 16C)**. This result suggests that the factors in 231.Brain.HER2 secretome plays a key role in creating a favorable environment for brain metastasis.

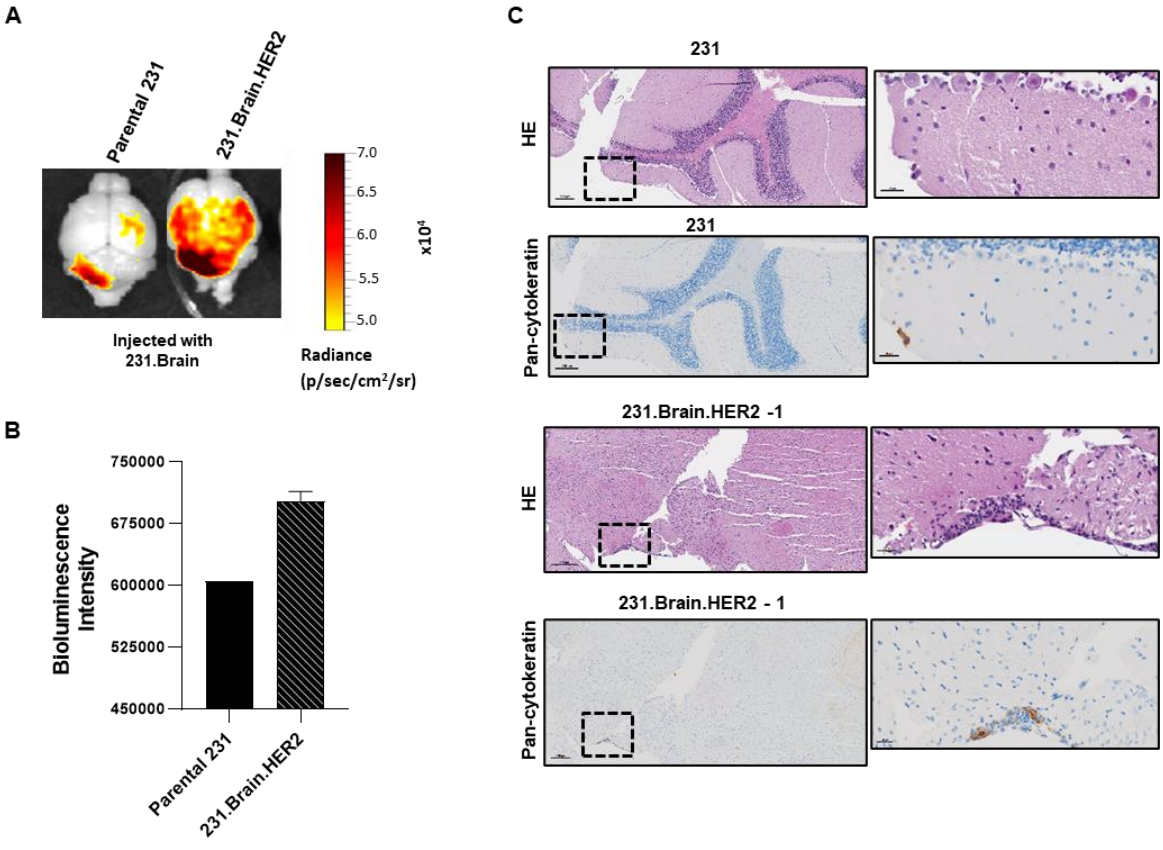


Figure 16. *In vivo* Brain colonization. (A) Animals were pre-treated with the secretome of parental 231 cells (n=2) and 231.Brain.HER2 (n=2) cells for 15 days, followed by intracardial injection of 231.Brain luciferase-expressing cells. Luminescence in the brain was evaluated three weeks post-injection. **(B)** Quantification of bioluminescence in equal-sized regions of interest (ROI). **(C)** Representative hematoxylin and eosin (HE) and immunohistochemistry (IHC) staining for human Pan-cytokeratin in mouse brain tissue, aimed at detecting 231.Brain cell infiltration after treatment with the secretome of parental 231 and 231.Brain.HER2.

VI. The secretome from brain organotropic breast cancer cells show a brain-specific protein signature

To identify a specific brain secretome signature, high-throughput proteomic Label-Free quantitation analysis of the secretome of parental 231 and their organotropic BC variants was performed. We identified a total of 9064 peptides, but only 341 peptides were found to be differentially expressed in the secretome of all organotropic BC cells compared to that of the parental 231. In detail, within these peptides, 120 were differentially expressed in the secretome of 231.Lung, 75 in 231.Bone, 76 in 231.Brain and 70 in 231.Brain.HER2. We observed a specific secretome signature for each metastatic location, as evidenced by unsupervised hierarchical clustering analysis **(Figure 17A)**. Interestingly, by principal component analysis (PCA), we observed the secretome of parental 231 and the secretome of 231.Lung clusters close to each other, whether the secretome of both brain organotropic BC variants are more similar to the secretome of 231.Bone **(Figure 17B)**. To identify the specific deregulated peptides present in the secretome of both brain organotropic BC variants, we intersected the lists of significantly deregulated peptides **(Figure 17C)**.

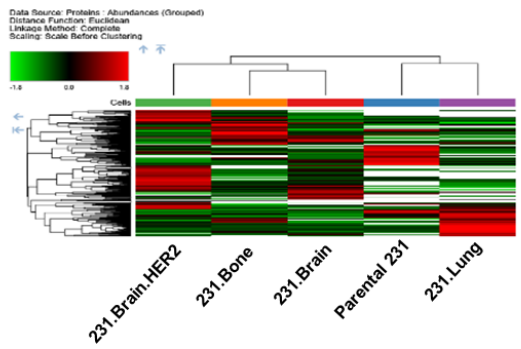
Next, we conducted Gene Ontology enrichment analysis for the peptides specifically deregulated in the secretome of 231.Brain and 231.Brain.HER2 cells. Interestingly, we found that brain organotropic BC cells secrete peptides involved in processes such as inflammatory responses, ECM remodeling, positive regulation of neuronal apoptotic processes, and cell-cell adhesion. These findings suggest that these cells may utilize these processes to enhance their survival and colonization within the brain microenvironment **(Figure 17D)**.

However, we decided to examine the peptides commonly deregulated in both brain-tropic BC cells. From this analysis, we identified six common peptides that were differentially expressed in both brain organotropic BC variants: Ribosomal Protein S15 (SP15), Capping Actin Protein of Muscle Z-Line Subunit Beta (CAPZB), Monoglyceride Lipase (MGLL), Utrophin (UTRN), NOP16 Nucleolar Protein (NOP16) and Nerve Growth Factor Inducible (VGF) **(Figure 17E)**.

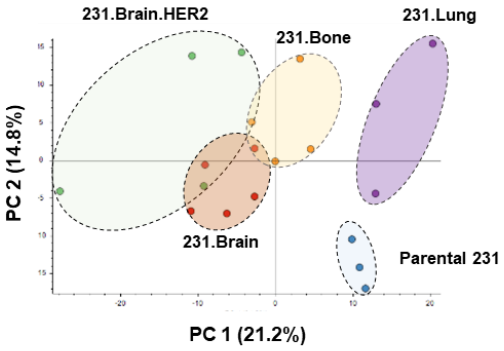
Out of these, we focus on VGF due to its role in brain-related disorders, as well as its increased potential as a putative prognostic factor in BC, as identified by survival analysis

using KM plotter **(Table 2)**. We further validated that VGF was significantly enriched both at the cell level and in the secretome of both brain organotropic BC cells **(Figure 17F-G)**.

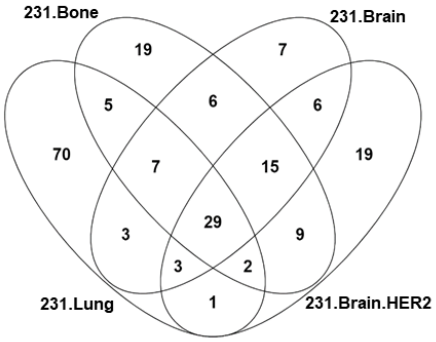
A



B



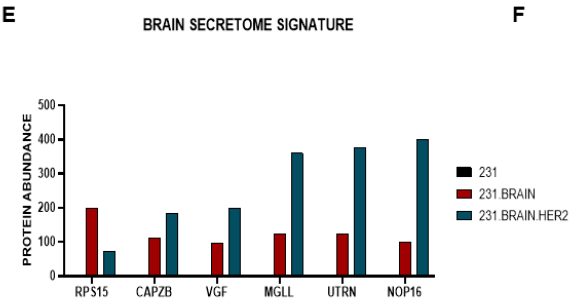
C



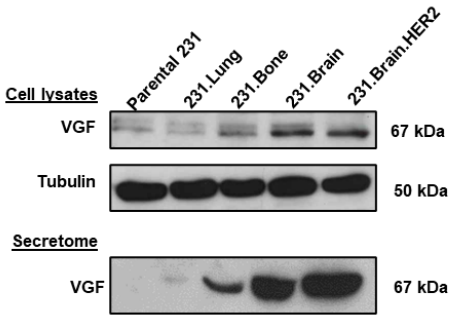
D

	Gene Ontology Term	P-Value
231.Brain	Inflammatory Response	6,10E-03
	Extracellular Matrix Organization	1,00E-02
	Positive Regulation of Neuron Apoptotic Process	1,50E-02
231.Brain.HER2	Cytoskeleton Organization	1.10E-03
	Cell-Cell adhesion	1.00E-02
	Extracellular Matrix Organization	1.50E-02

E



F



G

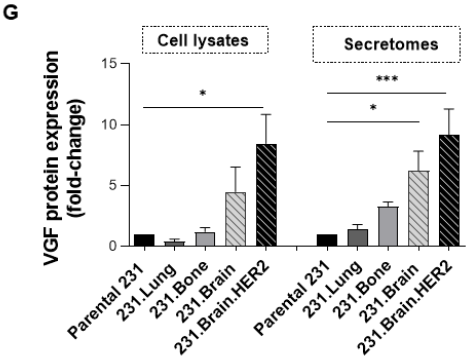


Figure 17. Brain organotropic breast cancer cells exhibit a specific secretome signature. (A) Unsupervised hierarchical clustering analysis of the secretome profiles from parental MDA-MB-231 cells and their brain organotropic breast cancer variants. **(B)** Principal Component Analysis (PCA) illustrating the variance in secretome composition between parental and brain organotropic breast cancer variants. **(C)** Venn diagram identifying the specific deregulated peptides in the secretome of both brain organotropic breast cancer variants. **(D)** Gene Ontology enrichment analysis for the peptides specifically deregulated in the secretome of 231.Brain (7 peptides) and 231.Brain.HER2 cells (19 peptides) **(E)** Protein abundance analysis of differentially expressed proteins in the secretome of brain organotropic breast cancer variants. The bar graph represents the relative levels of Ribosomal Protein S15 (SP15), Capping Actin Protein of Muscle Z-Line Subunit Beta (CAPZB), Monoglyceride Lipase (MGLL), Utrophin (UTRN), NOP16 Nucleolar Protein (NOP16), and Nerve Growth Factor Inducible (VGF). Protein abundance was quantified from secretome analyses, showing significant upregulation in brain metastatic variants compared to the secretome of parental MDA-MB-231 cells. **(F)** Western blot analysis evaluating the expression and presence of VGF in both cell lysates and secretomes. **(G)** Western blot quantification, showing significant differences in VGF expression levels. (n=4–8 biological replicates; data are expressed as mean ± SEM). Statistical significance was assessed using one-way ANOVA (*P < 0.05, ***P < 0.001).

Table 2. Univariate Cox proportional hazard analysis enables the prediction of risk (hazard ratios and corresponding 95% confidence intervals) for overall survival (OS) among breast cancer patients. This analysis utilizes Kaplan-Meier plotter data to assess each of the six common peptides that were differentially expressed in both brain organotropic breast cancer variants across various breast cancer molecular subtypes. A significance level of 5% was considered.

mRNA	Overall Survival (OS)							
	Luminal A		Luminal B		Triple-negative		HER2 Overexpression	
	HR	P-value	HR	P-value	HR	P-value	HR	P-value
VGF (205586_x_at)	0.75 (0.54 - 1.04)	0.079	0.72 (0.47 - 1.08)	0.11	1.84 (1.24 - 2.71)	0.0019	1.93 (1.09 - 3.41)	0.022
RPS15 (200819_s_at)	0.7 (0.5 - 0.98)	0.036	0.64 (0.45 - 0.91)	0.013	1.72 (1.14 - 2.6)	0.0095	1.76 (0.99 - 3.15)	0.051
MGLL (225102_at)	1.99 (1.24 - 3.19)	0.0036	1.74 (0.94 - 3.23)	0.077	1.69 (1.06 - 2.71)	0.026	0.47 (0.23 - 0.93)	0.026
NOP16 (214011_s_at)	1.85 (1.35 - 2.54)	0.00096	0.89 (0.63 - 1.27)	0.53	1.36 (0.87 - 2.12)	0.18	2.34 (1.13 - 4.84)	0.018
UTRN (225093_at)	0.55 (0.33 - 0.9)	0.016	0.56 (0.3 - 1.05)	0.069	1.58 (0.91 - 2.76)	0.1	1.97 (0.76 - 5.11)	0.15
CAPZB (37012_at)	0.74 (0.53 - 1.02)	0.066	1.39 (0.94 - 2.06)	0.097	1.23 (0.81 - 1.85)	0.33	0.61 (0.34 - 1.1)	0.098

VII. VGF promotes BBB disruption and microglia activation

We next investigated the role of VGF in the remodeling of the brain PMN, starting with its impact on BBB structure and function. We pre-treated hCMEC/D3 cell monolayer with TLQP-21, a bioactive C-terminal VGF-derived peptide, for 24 hours. Interestingly, we found similar permeability and TEER values as observed with the secretome of 231.Brain.HER2 when compared with the control condition **(Figure 18A-B)**. Since TLQP-21 binds to the complement component 3a (C3a) receptor-1 (C3aR1), which is expressed in brain ECs [221], we further used a C3aR antagonist in the subsequent experiments. Thus, we co-exposed hCMEC/D3 to the endogenous VGF secreted by 231.Brain.HER2 or exogenous VGF in combination with the selective antagonist for C3aR. Interestingly, we verified that

the increase in endothelial permeability and the decrease in TEER values induced by exogenous and endogenous VGF were significantly prevented, proving that C3aR mediates VGF-induced BBB hyperpermeability. Furthermore, we observed a significant decrease in β-catenin and ZO-1 **(Figure 18C-E)** protein levels in EC monolayers after treatment with the exogenous TLQP-21 peptide, similar to what was observed with the secretome of 231.Brain.HER2. Accordingly, this result was also blocked in the presence of the C3aR antagonist.

The same specific effect was also observed for microglia activation. Pre-treatment with TLQP-21 significantly increased the phagocytic capacity **(Figure 19A and B)** and Stat3 phosphorylation **(Figure 19C-D)** of microglia cells, when compared with the control condition. Interestingly, this effect was abolished when microglia cells were pre-treated with the C3aR antagonist, inhibiting VGF-induced effects **(Figure 19A-D)**.

Importantly, these results were validated *in vivo*. After priming mice with the TLQP-21 for 3 consecutive days, we showed a significant and specific impact on BBB permeability, shown by a significant increase in the accumulation of the fluorescent dye in the brain, compared to the control condition **(Figure 18F and G)**. Immunohistochemical analysis of the mice's brains also revealed that TLQP-21 significantly increased the IBA1-positive area of microglia cells **(Figure 19E-F),** as well as the staining intensity per microglia cell **(Figure 19E-G)**.

Although differences in circularity were not observed, TLQP-21 significantly increased the area of 3D brain spheroids compared to serum-free DMEM (control condition) **(Figure 19H-J).** Similar to the findings with the secretomes of organotropic BC cells, particularly those with tropism to the brain, TLQP-21 also exerts a significant impact on modulating these resident brain cells within the 3D brain spheroids.

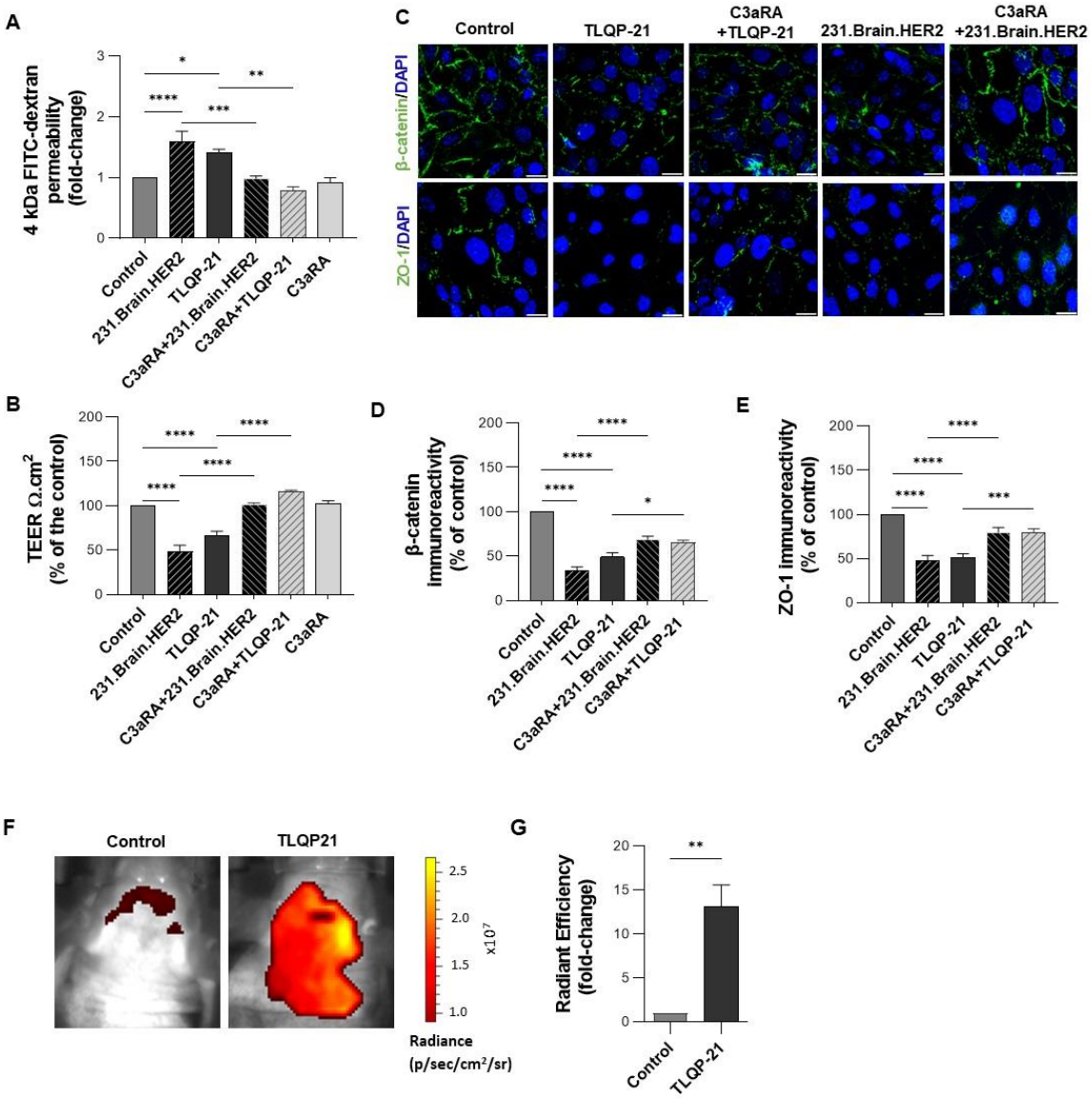


Figure 18. VGF promotes blood-brain barrier disruption. (A-B) Endothelial cells (ECs) monolayers were treated with TLQP-21 (100nM), a VGF derived-peptide, and with a secretome of 231.Brain.HER2 in the absence and presence of the C3a receptor antagonist (10µM) to evaluate **(A)** ECs monolayer permeability using a 4kDa FITC-dextran and **(B)** TEER after 24 hours of exposure. (n=4 biological replicates; the results are expressed as mean ± SEM). **(C)** Representative confocal images of β-catenin and ZO-1 immunoreactivity. β-catenin/ZO-1: green, DAPI: Blue. (Scale bar corresponds to 20 µm). **(D-E)** Quantification of β-catenin and ZO-1 expression. **(F-G)** *In vivo* dynamic near-infrared fluorescent imaging after 3 days of treatment with serum-free DMEM (control condition) and TLQP-21 (4.5 mg/kg). **(F)** Representative images of mice brains acquired at 30 minutes post-injection of Cy7.5-dextran 5 kDa. **(G)** Quantification of radiant efficiency in equal-sized ROI corresponding to the top of the skull. (4 animals/group; the results are expressed as mean ± SEM). Statistical significance was assessed using one-way ANOVA.*P < 0.05, **P < 0.01, ***, P < 0.001, ****P<0,0001.

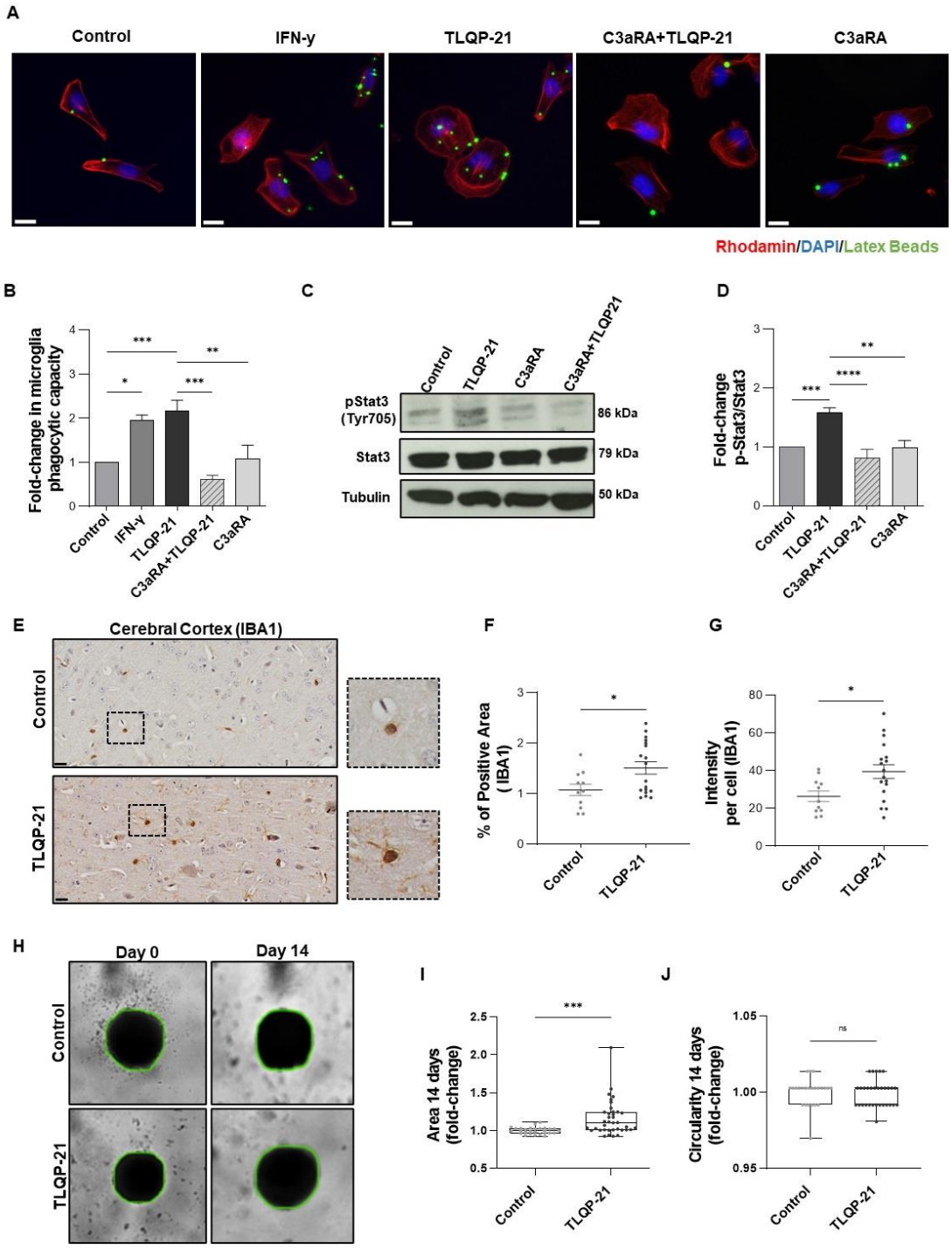


Figure 19. VGF impacts microglia activation. (A) Representative confocal images of microglia phagocytic capacity of 1 µm fluorescent latex beads after treatment with serum-free medium (control condition) and TLQP-21 (100nM) in the absence and presence of the C3a receptor antagonist (10µM) for 8 hours. (Scale bar corresponds to 20 µm). **(B)** Quantification of microglia phagocytic capacity after treatment with serum-free medium (control condition) and TLQP-21 (100nM) in the absence and presence of the C3a receptor antagonist (10µM) for 8 hours. (n=3 biological replicates; the results are expressed as mean ± SEM). **(C)** Western blot of Stat3 phosphorylation (pStat3 Tyr705) and Stat3 in microglia cell lysates (HMC3) after 8 hours of treatment with the serum-free medium (control condition) and TLQP-21 in the presence or absence of C3a receptor antagonist. **(D)** Quantification of Stat3 phosphorylation over Stat3 normalized to tubulin. (n=3 biological replicates; the results are expressed as mean ± SEM). **(E)** Representative IHQ staining for IBA1 in the cerebral cortex of mice after 3 days of treatment

with serum-free medium (control condition) and exogenous mouse TLQP-21 (4.5 mg/kg). (Scale bar corresponds to 20 µm). **(F)** Quantification of IBA1 microglia positive area and **(G)** intensity per microglia cell in the cerebral cortex of mice after 3 days of treatment with serum-free medium (control condition) and TLQP-21 (4.5 mg/kg). (2 mice/per group, 6-8 cerebral cortex independent areas; the results are expressed as mean ± SEM). **(H)** Representative images of 3D spheroids on day 0 without treatment and after 14 days of treatment with serum-free medium (control condition) and TLQP-21 100 µm. **(I)** Quantification of area (n=4 biological replicates; the results are expressed as mean ± SEM). **(J)** Quantification of circularity (n=4 biological replicates; the results are expressed as mean ± SEM). Statistical significance was assessed using one-way ANOVA.*P < 0.05, **P < 0.01, ***, P < 0.001, ****P<0,0001.

Furthermore, we investigated the effect of TLQP-21 on brain metastatic capacity using the same approach as previously described. We observed a trend towards increased metastatic ability in the brain after treatment with TLQP-21 compared to the control condition **(Figure 20A and B).** Immunohistochemical analysis of human Pan-cytokeratin in mouse brain tissue demonstrated an increased number of 231.Brain cells following treatment with TLQP-21 compared to the control condition **(Figure 20C)**. Collectively, these findings support the functional role of VGF in impacting BBB stability and activating microglial cells during the early stages of the brain metastatic cascade. This suggests that VGF plays a crucial role in creating an environment in the brain that promotes the establishment of brain metastasis.

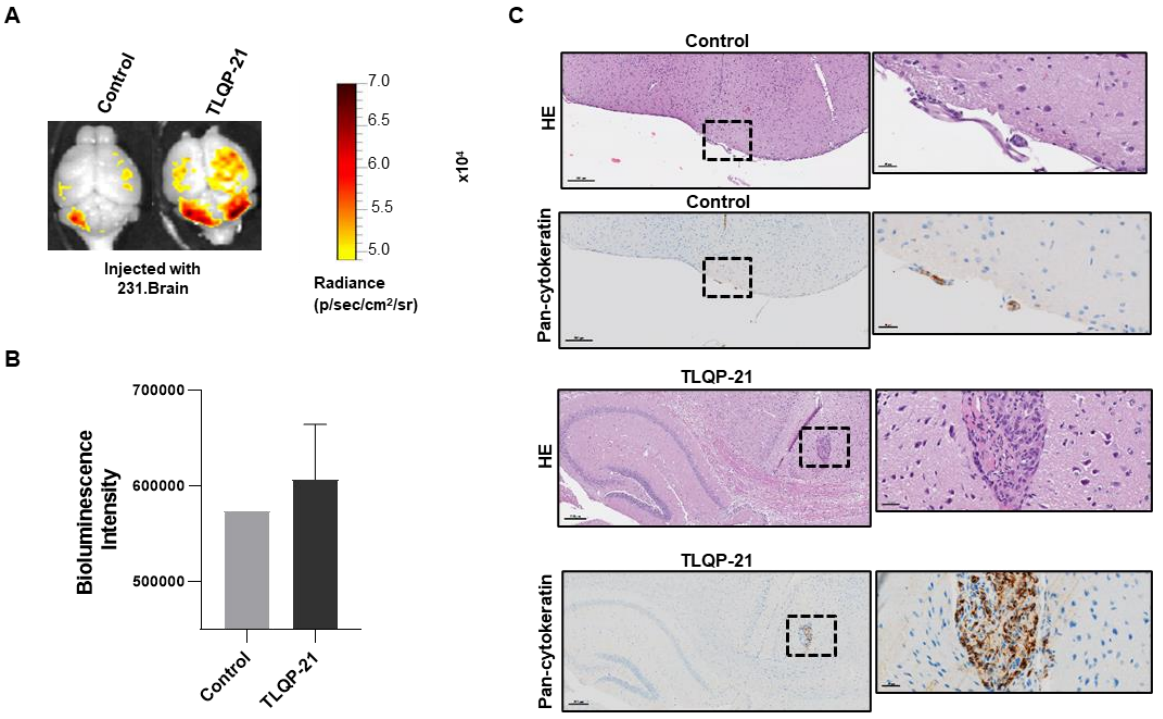


Figure 20. *In vivo* Brain colonization. (A) Animals were pre-treated with TLQP-21(n=2) for 3 days, followed by intracardial injection of 231. Brain luciferase-expressing cells. Luminescence in the brain was evaluated three weeks post-injection. **(B)** Quantification of luminescence. **(C)** Representative hematoxylin and eosin (HE) and immunohistochemistry (IHC) staining for human Pan cytokeratin in mouse brain tissue, aimed at detecting 231.Brain cell infiltration after treatment with control and TLQP-21 (4.5 mg/kg). (Scale bar corresponds to 30 µm and 200 µm).

VIII. VGF expression is associated with a worse prognosis for breast cancer patients

Further, we decided to evaluate the clinical impact of VGF on BC. For that, we started to study VGF mRNA expression using the KM plotter and VGF protein expression using a large series of primary breast carcinomas. KM survival analysis revealed no correlation between VGF mRNA levels and prognosis when considering all molecular subtypes of BC (Overall Survival (OS): hazard ratio (HR) = 1.16; *p=0.12*), as well as Luminal A (OS: HR = 0.75, *p=0.079*) and Luminal B (OS: HR = 0.72, *p=0.11*) subtypes individually. However, VGF mRNA expression was significantly associated with a worse prognosis specifically in triple-negative (10-years OS: HR=1.84, *p=0.0019*) and in HER2 overexpressing (10-years OS: HR=1.93, *p=0.022*) molecular subtypes **(Figure 21A-E)**, which correspond to the molecular subtypes that more frequently metastasize to the brain.

Further, we validate this data in a series of primary breast carcinomas previously characterized by our group [212, 222]. Immunohistochemical staining revealed that VGF was preferentially expressed in the cytoplasm of cancer cells and some cases in the tumor-adjacent stroma, as shown in representative images **(Figure 22A)**. Since we were studying the soluble factors secreted by BC cells that could lead to brain PMN remodeling, we considered VGF positivity when there was concomitant expression in cancer cells as well as in the tumor-adjacent stroma. We found that BC patients with VGF-positive tumors showed significantly lower disease-free survival (DFS) and OS (10-year DFS: *p=0.009*; 10-year OS: *p=0.011*) **(Figure 22B and C)**. In addition, VGF positivity significantly correlated with poor prognostic markers in BC, such as ER negativity (*p=0.010*), and positive expression for EGFR (*p=0.021*), metabolic proteins ((CAIX (*p=0.013*) and GLUT1 (*p=0.004*)). More importantly, VGF-positive tumors were significantly associated with HER2 overexpression and triple-negative (*p=0.029*) molecular subtypes **(Table 3)**, validating the KM survival analysis.

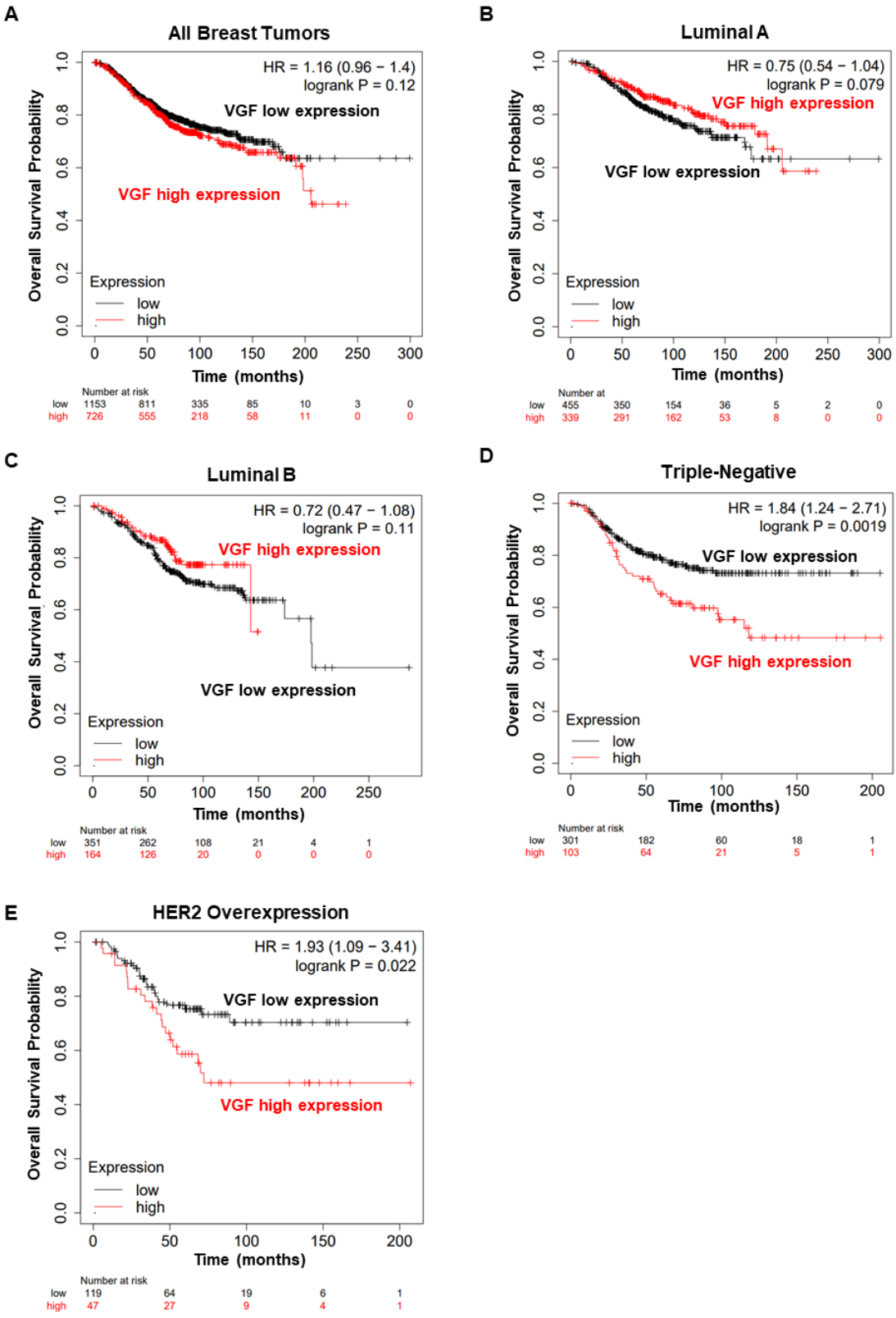


Figure 21. Kaplan-Meier survival curves of breast cancer patients based on VGF mRNA expression. (black lines indicate patients with VGF low expression; red lines indicate patients with VGF high expression). Kaplan-Meier plots comprising **(A)** all breast tumors (Overall-Survival (OS): hazard ratio (HR) =1.16, *p=0.12*)), **(B)** Luminal A (OS: HR=0.75, *p=0.079*), **(C)** Luminal B (OS: HR =0.72, *p=0.11*), **(D)** triple-negative (OS: HR=1.84, *p=0.0019*), and **(E)** HER2 overexpressing breast tumors (OS: HR=1.93, *p=0.022*).

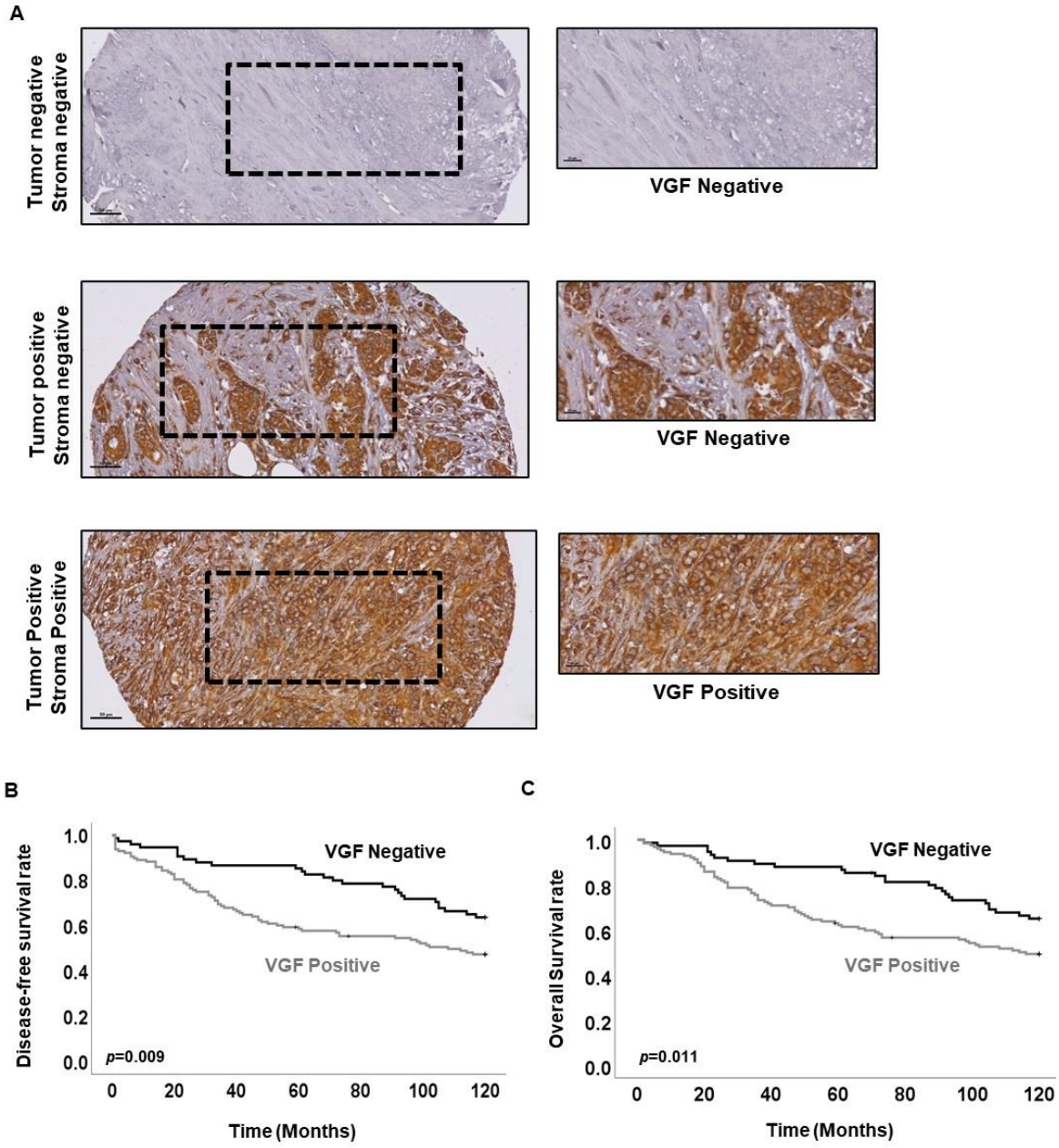


Figure 22. VGF expression is associated with a worse prognosis for breast cancer patients. (A) A breast cancer case was considered VGF positive only when it was found to be concomitantly expressed both in the cancer cells and in the tumor-adjacent stroma. Representative images of VGF-negative cases: Tumor and Stroma negative; Tumor positive/Stroma negative; and VGF-positive cases showing co-expression in tumor and stroma in primary breast tumors. (Scale bar corresponds to 50 and 20 μm). Kaplan Meier plot analysis for **(B)** disease-free survival (DFS) and **(C)** overall survival (OS) based on VGF protein expression using a large series of primary breast carcinomas (DFS:*p=0.009 and* OS:*p=0.011*). (black lines indicate patients with VGF-negative tumors; gray lines indicate patients with VGF-positive tumors). Survival analyses were compared using the log-rank test.

Table 3. Association analysis of VGF expression in primary breast tumors with classical breast cancer poor prognostic factors such as ER (*p=0.010*), EGFR (*p=0.021*), CAIX (*p=0.013*), GLUT1 (p=*0.004*) and breast cancer molecular subtypes (*p*=0.029). The χ^2 test was used to determine associations between groups and the results were considered statistically significant when the p-value was lower than 0.05. ER - Estrogen receptor, PR - Progesterone receptor; EGFR - Epidermal growth factor receptor.

		VGF Negative n= 68		VGF Positive n = 143		p-value
		Frequency	%	Frequency	%	
ER	Negative	15	22,4	54	38,0	0,01
	Positive	52	77,6	88	62,0	
	Missing	2		1		
PR	Negative	36	52,9	88	62,0	n.s
	Positive	32	47,1	54	38,0	
	Missing	0		1		
HER2	Negative	64	94,1	118	84,9	n.s
	Positive	4	5,9	21	15,1	
	Missing	0		4		
EGFR	Negative	67	98,5	128	89,5	0,021
	Positive	1	1,5	15	10,5	
	Missing	0		0		
CAIX	Negative	34	53,1	49	34,8,	0,013
	Positive	30	46,9	92	65,2	
	Missing	4		2		
GLUT1	Negative	60	92,3	105	75,5	0,004
	Positive	5	7,7	34	24,5	
	Missing	3		4		
Molecular subtype	Luminal A-like	27	40,9	44	32,6	0,029
	Luminal B-like	26	39,4	46	34,1	
	HER2 overexpressing	1	1,5	12	8,9	
	Triple-Negative	12	18,2	33	24,4	
	Missing	2		8		

IX. VGF expression is a poor prognostic factor for breast cancer brain metastases

Finally, the impact of VGF expression was evaluated in predicting the metastatic site. For that, we evaluated its expression in a metastatic BC cohort (N=104 patients), which included paired primary and metastatic tumors from BC patients diagnosed with brain metastasis (n=31), lung metastasis (N=17), and bone metastasis (n=56). Brain metastasis series were significantly associated with poor prognostic features, such as high histological grade, age, and molecular subtype (*p<0.0001*) **(Figure 23A-C and Table 4)**. We found that primary

breast tumors that metastasized to the brain were associated with poor prognostic factors, such as ER (*p<0.0001*) and PR (*p=0.002*) negative expression, as well as a higher proliferative index (assessed by Ki67 labeling) (*p=0.005*) when compared with primary breast tumors that metastasized to other locations (lung and bone) **(Figure 24A)**. As expected, primary breast tumors that metastasized to the brain were mainly from the HER2 overexpression and triple-negative molecular subtypes (*p<0.0001*) **(Figure 24B)**. More importantly, we found that primary tumors with VGF-positive expression were significantly associated with an increased propensity to metastasize to the brain (60%), compared with the metastatic propensity to the lung (20%) or bone (25%) (*p=0.003*) **(Figure 25A)**. Our data, from this metastatic cohort, demonstrate that VGF exhibits a sensitivity of 58.1% and a specificity of 71.2% as a predictive biomarker for brain metastasis. Given that HER2 overexpression is linked to an increased risk of developing brain metastasis, we further evaluated the sensitivity and specificity of this marker in our metastatic cohort. Surprisingly, the values were notably lower compared to those obtained for VGF. Specifically, the sensitivity of HER2 as a predictive biomarker for brain metastasis was approximately 25.81%, with a specificity of 50%.

Besides its potential role as a putative predictive biomarker of brain metastasis, a more significant role was observed as a prognostic biomarker. In detail, VGF positivity shows a significantly worse impact on BC patients with metastasis to the brain, with no significant differences observed in the OS of patients with metastasis to the lung or bone (**Figure 25B-D**). This data was further confirmed by an independent TCGA cohort from metastatic BC **(Figure 26A-E)**. In our analysis, we observed that primary tumors expressing VGF maintained this expression in brain metastases. This suggests a consistent pattern of VGF expression retention during the metastatic process specifically in the brain. Conversely, primary tumors from patients with metastases to other organs did not exhibit enrichment in VGF expression in the metastatic tumor (*p=0.001*) **(Figure 25E)**. This disparity in VGF expression dynamics between brain metastases and metastases to other organs underscores the potential significance of VGF as a prognostic biomarker for brain metastasis in BC, opening an interesting avenue for VGF as a potential clinical target in the context of brain metastasis.

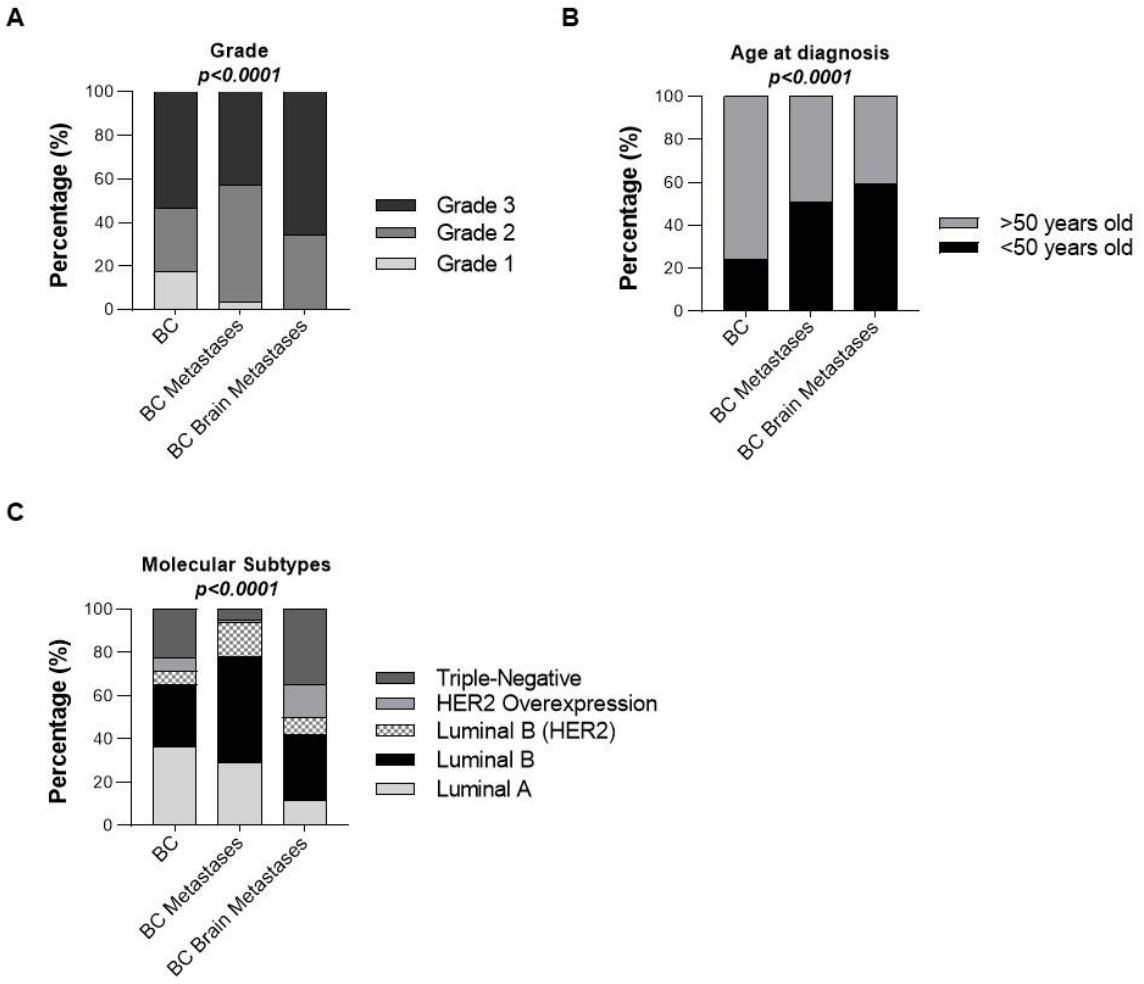


Figure 23. Association of the different breast cancer cohorts with clinicopathological features. Correlation analysis between different breast cancer cohorts with **(A)** histological grade (*p<0.0001*), (B) age (*p<0.001*), and (C) molecular subtypes (*p<0.0001*). The chi-square test was used to determine associations between groups and the results were considered statistically significant when the p-value was lower than 0.05. (BC – primary breast tumors, BC metastases – primary breast tumors with metastases, and BC Brain Metastasis – primary breast tumors with brain metastases only).

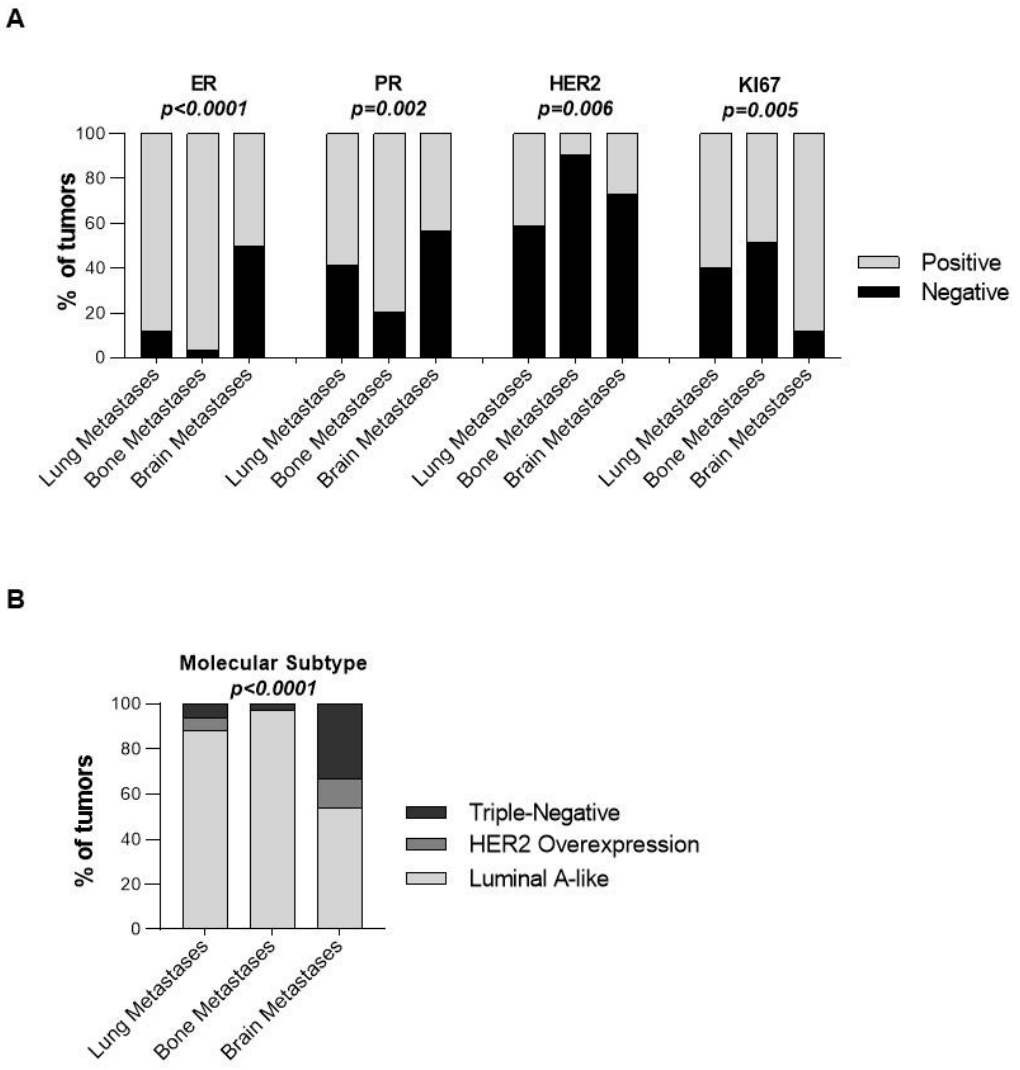


Figure 24. Association between primary breast tumors that metastasize to the lung, bone, and brain with classical poor prognostic factors and molecular subtypes of breast cancer. (A) Correlation analysis of primary breast tumors that metastasize to the lung, bone, and brain with classical breast cancer poor prognostic factors such as ER ($p<0.0001$), PR ($p=0.002$), and Ki67 ($p=0.005$). **(B)** Correlation analysis of primary breast tumors that metastasize to the lung, bone, and brain with breast cancer molecular subtypes ($p<0.0001$). The chi-square test was used to determine associations between groups and the results were considered statistically significant when the p-value was lower than 0.05.

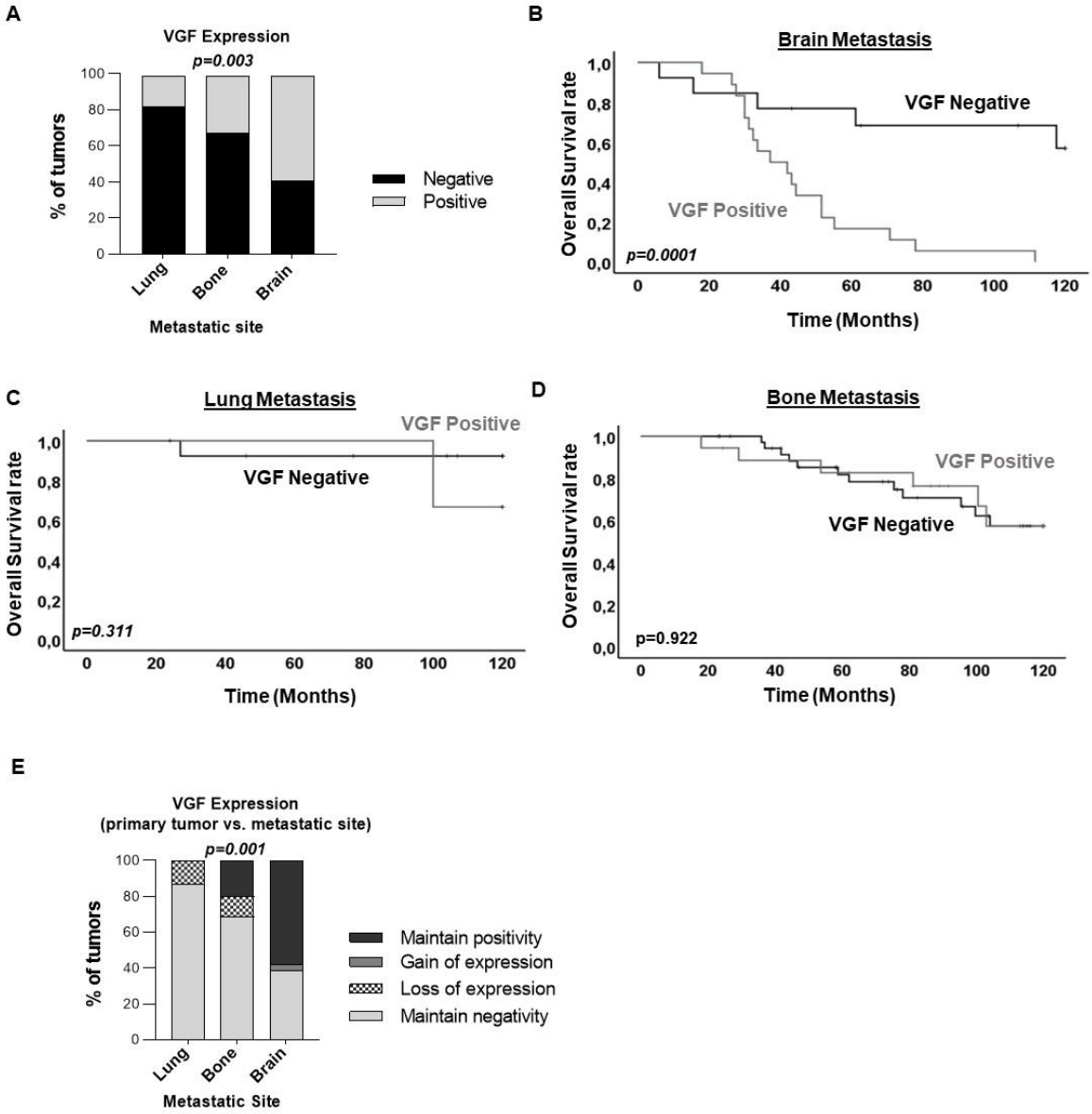


Figure 25. VGF expression is a predictive factor for brain metastases. (A) Correlation analysis of VGF expression in primary breast tumors with their corresponding metastatic location. KM plot analysis for OS based on VGF protein expression in breast cancer metastasis to the **(B)** brain (OS:*p=0.0001*), **(C)** lung (OS:*p=0.311*), and **(D)** bone (OS:*p=0.922*). **(E)** VGF expression in primary breast tumor and its paired metastasis. The chi-square test was used to determine associations between groups and the results were considered statistically significant when the p-value was lower than 0.05.

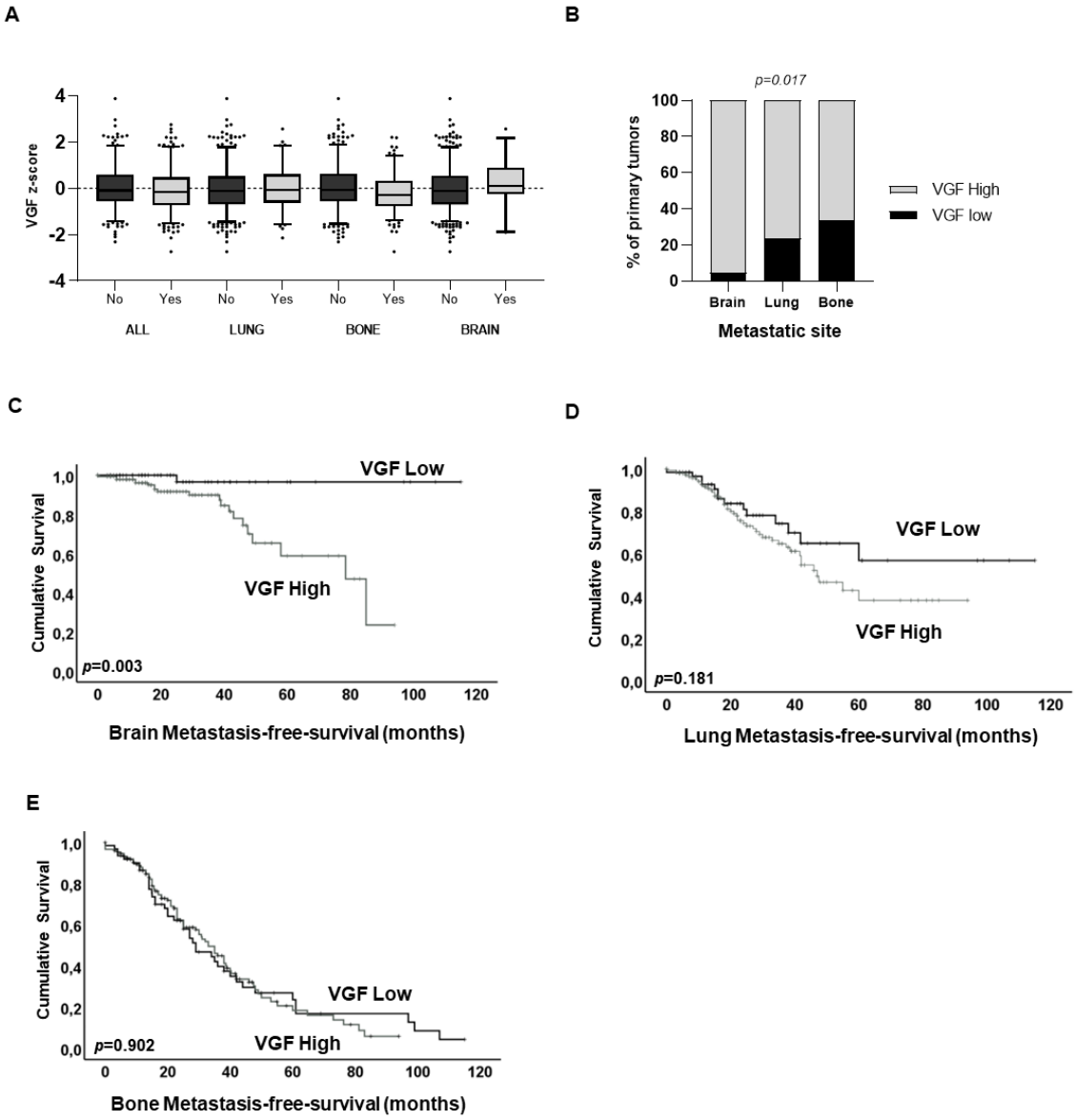


Figure 26. VGF mRNA expression as a predictive factor for breast cancer brain metastases. (A) Z-score analysis of VGF gene expression in primary breast tumors according to their metastatic location. **(B)** Correlation analysis of VGF gene expression in primary breast tumors with their corresponding metastatic location. **(C-E)** Kaplan-Meier plot analysis for overall survival (OS) based on VGF gene expression in breast cancer metastasis to the **(C)** brain (OS:*p=0.003*), **(D)** lung (OS:*p=0.181)*), and **(E)** bone (OS:*p=0.902*). (black lines indicate patients with VGF-negative tumors; gray lines indicate patients with VGF-positive tumors). Survival analyses were compared using the log-rank test.

Table 4. Association of the different breast cohorts with clinicopathological features.*

		Primary Breast Cancer		Breast Cancer Metastasis		Brain Metastasis		p-value
		N = 218		N = 83		N = 27		
		Frequency	%	Frequency	%	Frequency	%	
QT_Neo	No	-	-	74	90,2	16	59.3	-
	Yes	-	-	8	9,8	11	40.7	
	Missing	218		1		0		
Grade	1	37	17,5	3	3,7	0	0	<0,0001
	2	62	29,2	44	53,7	9	34,6	
	3	113	53,3	35	42,7	17	65,4	
	Missing	6		1		1		
Age	< 50 years old	53	24,2	42	50,6	16	59,3	<0,0001
	> 50 years old	165	75,8	41	49,4	11	40,7	
	Missing	0		0		0		
Lymph Node	Negative	63	36,8	19	23,5	8	29.6	n.s
	Positive	108	63,2	62	76,5	18	66.7	
	Missing	47		2		1	3.7	
Metastasis at Diagnosis	Negative	-	-	71	85,5	21	77.8	n.s
	Positive	-	-	12	14,5	6	22.2	
	Undefined	-	-	0		0	0.0	
Molecular subtype	Luminal A-like	76	36,7	24	28,9	3	11,5	<0,0001
	Luminal B-like (HER2 negative)	59	28,5	41	49,4	8	30,8	
	Luminal B-like (HER2 positive)	13	6,3	13	15,7	2	7,7	
	HER 2 overexpressing	13	6,3	1	1,2	4	15,4	
	Triple-Negative	46	22,2	4	4,8	9	34,6	
	Undefined	11		0		1		

*Association of the different breast cancer cohorts (BC, BC metastasis, and Brain metastasis) with QT_Neo, grade, age, lymph node, metastasis at diagnosis, and molecular subtypes. The chi-square test was used to determine associations between groups and the results were considered statistically significant when the p-value was lower than 0.05.

CHAPTER V. DISCUSSION

Discussion

BC is the most common cancer among women worldwide, often metastasizing to various organs, including the brain, which significantly impacts patient survival. The formation of a PMN refers to the process by which cancer cells prepare the tissue for their arrival, allowing them to establish and grow at this new location. Several factors contribute to PMN formation; however, there is limited data regarding brain PMNs, making them the least understood of all potential metastatic sites [89, 223].

In fact, a significant breakthrough in studying the brain metastatic process of BC was the establishment of BC cell models with a specific tropism to the brain, generated through successive *in vivo* selection [93]. Given that brain organotropic BC cells directly interact with the brain microenvironment, they represent a distinctive reservoir of predictive targets for therapeutic intervention aimed at preventing and treating brain metastasis. Through our work with these models, we have been actively involved in defining the impact of bioactive factors released by cancer cells, commonly known as the cancer secretome, in the modulation of the brain's PMN, recognized as crucial players in the initial phases of brain metastasis. The secretome encompasses a broad spectrum of soluble factors, including proteins, growth factors, cytokines, hormones, lipids, and nucleic acids. Additionally, within the realm of secreted molecules, a distinct subset is found enclosed within or associated with the membrane of EVs [224]. These EVs, comprising exosomes, microvesicles, and apoptotic bodies, are small, membrane-bound structures released by both normal and cancer cells, carrying a diverse cargo of bioactive molecules. Thus, exploring the cancer secretome resource holds significant promise in identifying novel molecular targets involved in the communication between the primary tumor and distant metastatic sites.

This concept has been previously explored by other researchers, notably Lyden's team, but with a special focus on EVs rather than other soluble factors. They have demonstrated that exosomes derived from organotropic BC cells have distinct integrin profiles that play a critical role in organotropism by mediating the adhesion and invasion of cancer cells to specific metastatic organs [70]. This particular finding suggests that factors released by cancer cells may be responsible for the formation of niches in several organs, which may control metastatic organotropism.

To explore the mechanisms underlying brain metastasis, we used organotropic MDA-MB-231 cell models for the lung, bone, and brain, which were embedded in collagen type I. We selected this ECM type over other formulations more prevalent in normal breast tissue, containing laminin, collagen IV, or entactin, since collagen type I predominates in the tumor microenvironment and plays a more prominent role in promoting cancer progression [225]. Additionally, another brain organotropic cell line transfected with HER2 (231.Brain.HER2)

was also included, since its overexpression induces extensive brain metastasis occurrence in mice [100].

In our study, we demonstrated that the secretome of brain organotropic BC cells disrupts BBB integrity, suggesting that the secretion of specific factors may play an important role in remodeling the brain microenvironment, creating a more permissive site for cancer cell brain colonization. These findings were contrasted with secretomes from non-brain organotropic cells to ensure brain metastatic specificity. Interestingly, we did not observe a decrease in collagen IV deposition, as commonly observed in BBB disruption situations, but instead a tendency to increase collagen IV expression. Still, a striking and specific pattern of expression was observed in the brains of mice treated with secretomes from brain organotropic cells. Immunofluorescence images revealed disorganization and clustering of collagen IV, which may contribute to increased BBB permeability. This phenomenon has been documented in other pathological conditions, such as epilepsy and stroke, where increased, but delocalized, collagen IV expression is associated with dysfunctional BBB [226, 227]. However, it remains unclear whether this increase in collagen IV expression is directly linked to the formation of new and more leaky blood vessels. Further investigation is warranted to elucidate the underlying mechanisms driving this phenomenon. Nonetheless, the functional impact on BBB integrity was corroborated by the specific accumulation of serum albumin in the brain of mice treated with secretomes from brain organotropic BC cells. This finding highlights the specificity of BBB disruption induced by these secretomes and underscores the potential significance of our observations in understanding the pathophysiology of brain metastasis in BC. Further research in this area may lead to the development of novel therapeutic strategies targeting BBB integrity in metastatic BC.

In fact, our data is in accordance with previous works showing that factors secreted by cancer cells promote BBB dysfunction by altering the expression and localization of key BBB proteins, namely tight junction proteins. This can lead to increased BBB permeability, allowing cancer cells to enter the brain and potentially form metastases [139, 140, 228, 229]. In particular, Lu et al. demonstrated that exosomal lncRNA GS1-600G8.5 secreted by brain organotropic BC cells increases *in vitro* BBB permeability, promoting the passage of BC cells across the EC monolayer [139]. Moreover, it was recently demonstrated that brain organotropic BC cells secrete CEMIP+ exosomes that can be taken up by ECs and microglia, inducing brain vascular remodeling and inflammation [140].

In addition to a restrictive vascular barrier, the brain is composed of unique resident cells, such as microglia, that play an important role in the immune response after injury. Accordingly, considering cancer progression, microglia cells have also been described as being responsible for identifying and attacking cancer cells that have invaded the brain [230,

231]. Nevertheless, some studies suggest that microglia can also promote the growth and spread of metastatic cells in the brain, contrasting with its tumor surveillance function [162, 167, 215-219]. EI Chen et al. demonstrated that NT-3 promotes the growth of metastases by decreasing microglia cell activation [162]. In contrast, another study demonstrated that XIST loss in BC cells increased the release of exosomal microRNA-503, which promotes an *in vitro* anti-inflammatory microglia phenotype [216]. Therefore, using the secretome from brain organotropic BC cells, we looked for microglia modifications and found that, in contrast with the specific impact of brain-derived secretome on BBB integrity, all secretomes from lung, bone, and both brain organotropic cell lines were able to promote microglia activation, as measured by their *in vitro* phagocytic capacity and Stat3 phosphorylation. Considering that *in vitro* microglia cell culture is frequently performed under artificial conditions, which can alter microglia behavior and limit the relevance of experimental findings [232, 233], we also evaluated the impact of the secretomes on microglia using *in vivo* studies. Importantly, we observed that only the secretome of both brain organotropic BC cells could promote modifications in microglia in the cerebral cortex, which is the brain region where metastases most frequently occur [53, 234].

In addition to microglial cells, the brain is comprised of neurons and other glial cells (astrocytes and oligodendrocytes). However, our understanding of how these cells influence the development of brain pre-metastatic or metastatic niches remains limited. For this reason, we aimed to evaluate the impact of secretomes derived from brain organotropic BC cells on different brain resident cell populations using a 3D cortical spheroid model. These spheroids do not require the isolation of progenitor or embryonic cells; they solely rely on mouse postnatal cortex cultures. Within a relatively brief period of two weeks, these spheroids contain neurons, oligodendrocytes, astrocytes, microglia, and a matrix (laminin) synthesized by the cells themselves. They exhibit mechanical properties similar to those of the *in vivo* cortex and display electrical activity. [26, 27]. They provide a more advanced model system for investigating the pathophysiological aspects of the brain, including conditions like stroke [26]. In the field of cancer research, cortical spheroids are used to explore the invasive behavior of GBM cells. Intriguingly, the researchers found that the presence of cortical cells in a matrix-based model enhances GBM invasion, and they also observed neuronal activity [28]. In our study, we exclusively examined the morphological alterations in 3D cortical spheroids following a 14-day treatment with secretomes derived from parental 231 cells and their organotropic BC variants. Interestingly, we observed that the secretomes from all organotropic BC cells had the capacity to increase the surface area of the 3D cortical spheroids. However, it's worth highlighting that only the secretomes derived from brain organotropic BC cells resulted in a noticeable decrease in their circularity. These observations strongly suggest the presence of factors within the

secretome of organotropic BC cells that are responsible for the disturbance of the normal dynamics within the different brain resident cells. However, it is important to note that based solely on this data, we cannot definitively conclude which specific brain resident cells are being modulated. To understand these changes, or to identify the particular brain resident cell populations responsible for these morphological modifications, it would be crucial to individually analyze each of these brain cells through immunofluorescence assays using specific markers designed for each population. Another approach would be to perform sorting of each population and, using specific markers, evaluate parameters such as microglial activation and astrocytic reactivity.

Next, our objective was to identify the fraction of the secretome responsible for the remodeling in the brain microenvironment during the initial stages of the metastatic process, with a specific focus on the BBB, since it was the component of the brain microenvironment where we observed a specific effect from the secretome of brain organotropic models. To accomplish this, we isolated EVs from both parental 231 cells and their organotropic BC variants, subsequently evaluating their impact on *in vitro* BBB integrity. As previously mentioned, earlier studies have indeed demonstrated that factors present in EVs secreted by brain organotropic BC cells can enhance the permeability of EC monolayers [10]. Nevertheless, it's worth noting an alternative mechanism proposed in which EVs secreted by brain organotropic BC cells traverse the BBB through a process of transcytosis and are subsequently taken up by perivascular astrocytes [29, 30]. Interestingly, our experimental results did not reveal a significant increase in permeability following treatment with EVs derived from both parental 231 cells and their organotropic BC variants. Concerning TEER, we observed a significant decrease only when EC monolayers were exposed to EVs secreted by bone and brain organotropic BC cells. Considering that the results obtained from EVs do not correspond with the observations made from the secretome of brain organotropic BC cells, we were inclined to suspect that the factors responsible for the previously observed changes in BBB integrity are likely to be soluble factors.

Based on these results, we sought to determine the soluble factors responsible for these modifications in the brain PMN. Through proteomic analysis, we identified VGF as a significant peptide deregulated in brain organotropic BC secretomes. VGF undergoes proteolytic processing to generate multiple bioactive peptides implicated in various brain biological processes, such as neuronal growth, differentiation, synaptogenesis, and synaptic plasticity [222, 235-239]. While extensively studied in brain disorders, including obesity, diabetes, and neurodegenerative diseases, TLQP-21 emerges as the most prevalent VGF-derived peptide, known for its involvement in these conditions [207, 237, 240-242]. In cancer, VGF impact has been poorly underexplored, although it has been regarded as a marker associated with poorer prognosis in patients with GBM [42], lung

cancer [43], and BC featuring a neuroendocrine component [243]. Significantly, in a recent study, a team of researchers identified an immune-related prognostic signature (IRPS) within BC when compared to normal tissue, with VGF being among the genes included in the signature. Impressively, their findings unveiled a noteworthy correlation between IRPS and various clinicopathological features, establishing it as an independent prognostic factor for BC. These findings provide valuable insights into the potential relevance of VGF in the context of BC, and they may serve as a catalyst for innovative research directions in this field [244]. However, it's worth noting that its role in the context of brain metastasis remains unexplored.

To address this gap, we investigated the impact of TLQP-21 on brain pre-metastatic remodeling. Our study revealed that TLQP-21 influences BBB integrity and modulates microglia activity, both *in vitro* and *in vivo*. However, the effect of TLQP-21 on microglia modulation was less pronounced compared to the secretome of brain organotropic BC cells, indicating the involvement of other factors in microglia activation. Interestingly, prior research in Alzheimer's disease has shown that TLQP-21 affects microglia phagocytic capacity, suggesting its broader role in neuroinflammatory processes. Overall, our findings suggest that VGF, particularly TLQP-21, contributes to brain remodeling, creating a microenvironment conducive to brain metastasis. In fact, the observed increase in brain metastasis-promoting potential further supports this notion, providing a potential mechanism underlying brain metastasis and highlighting the role of VGF signaling in this process.

Finally, we assessed the clinical significance of VGF expression in BC samples. Our findings revealed a significant association between VGF expression, both in the tumor and stroma, and poor prognosis among BC patients. Notably, recent research has linked VGF to resistance against EGFR kinase inhibitors, inducing epithelial-to-mesenchymal transition (EMT) and correlating with adverse outcomes in patients with lung adenocarcinoma [245]. Given the frequent metastasis of both lung and BC to the brain, it is intriguing to note VGF’s dual role in GBM, where it promotes the survival and self-renewal of GBM stem cells while enhancing the proliferation of differentiated GBM cells [246]. Our study revealed a specific association between VGF-positive breast tumors and brain metastasis, distinct from metastases to other organs, like the lung or bone. VGF expression demonstrated a sensitivity of 58.1% and a specificity of 71.2% as a predictive biomarker for brain metastasis, highlighting its potential in this context. Additionally, we assessed the sensitivity and specificity of HER2 overexpression, a known factor in brain metastasis risk, which yielded notably lower values compared to VGF in this specific metastatic cohort. Furthermore, despite exhibiting lower specificity than previously described potential predictive/prognostic biomarkers, like FN14 and GRP94, VGF showed higher sensitivity [247], indicating its

potential as a more sensitive biomarker for identifying BC patients at risk of brain metastasis. Besides its potential impact as a predictive biomarker for brain metastasis, a more important role was shown as a prognostic biomarker. Our data, further confirmed by independent TCGA datasets, have identified VGF as a poor prognostic predictor for BC patients with brain metastasis. Its role as a prognosis biomarker was only significant in the brain metastatic setting, suggesting that VGF would have an important and specific role in the establishment and growth of brain metastasis. In fact, VGF has been described as a crucial secreted factor for the maintenance of GBM stem cells [246], therefore favoring the growth of cancer cells. In accordance, we have also tested the role of VGF in CSC activity, and we have found that TLQP-21 induces the mammosphere forming efficiency of BC cells (data not shown), suggesting that it can have an important role for the maintenance and growth of already established BC brain metastasis. Therefore, further research into the specific mechanisms underlying VGF's involvement in brain metastasis progression are needed.

In conclusion, our research revealed a novel role for VGF in brain remodeling, contributing to BBB disruption and microglia activation, thereby preparing a supportive and receptive PMN for the growth and survival of cancer cells in the brain. Moreover, its specific impact as a poor prognostic predictor for BC patients with brain metastasis, opens new avenues to use VGF as a potential therapeutic target for BC patients at an elevated risk of developing this type of metastasis.

CHAPTER VI. FUTURE PERSPECTIVES

Future perspectives

During this PhD project, we identified VGF as one of the soluble factors secreted by brain organotropic BC cells that promoted BBB disruption and microglial cell activation, both *in vitro* and *in vivo*. Through a pilot assay, we concluded that VGF may also promote brain colonization. Additionally, we found that the expression of VGF is associated with a worse prognosis in BC patients and an increased risk of these patients developing brain metastasis. Therefore, several intriguing questions and challenges remain to be elucidated. Based on our findings, several avenues for future research should be explored:

1. Elucidating the precise mechanisms by which VGF promotes BBB disruption and microglial cell activation, including downstream signaling pathways and interaction partners.

2. Investigating the role of VGF in other aspects of brain metastasis, such as extravasation, survival, and growth of cancer cells in the brain parenchyma.

3. Exploring potential therapeutic strategies targeting VGF or its downstream effectors to prevent or treat brain metastasis in BC patients.

4. Conducting large-scale clinical studies to further validate the prognostic significance of VGF expression in BC patients and its association with brain metastasis development.

5. Assessing the potential of VGF as a biomarker for predicting the risk of brain metastasis in BC patients (in liquid biopsies) and its utility in guiding clinical management decisions.

Overall, continued investigation into the role of VGF in brain metastasis holds promise for advancing our understanding of this complex disease process and identifying novel therapeutic targets for improving patient outcomes.

REFERENCES

References

1. Sung, H., et al., *Global Cancer Statistics 2020: GLOBOCAN Estimates of Incidence and Mortality Worldwide for 36 Cancers in 185 Countries.* CA Cancer J Clin, 2021. **71**(3): p. 209-249.
2. Arnold, M., et al., *Current and future burden of breast cancer: Global statistics for 2020 and 2040.* Breast, 2022. **66**: p. 15-23.
3. Benz, C.C., *Impact of aging on the biology of breast cancer.* Crit Rev Oncol Hematol, 2008. **66**(1): p. 65-74.
4. *Menarche, menopause, and breast cancer risk: individual participant meta-analysis, including 118 964 women with breast cancer from 117 epidemiological studies.* Lancet Oncol, 2012. **13**(11): p. 1141-51.
5. Hartmann, L.C., et al., *Understanding the premalignant potential of atypical hyperplasia through its natural history: a longitudinal cohort study.* Cancer Prev Res (Phila), 2014. **7**(2): p. 211-7.
6. *Type and timing of menopausal hormone therapy and breast cancer risk: individual participant meta-analysis of the worldwide epidemiological evidence.* Lancet, 2019. **394**(10204): p. 1159-1168.
7. Ji, L.W., et al., *Effect of age at first use of oral contraceptives on breast cancer risk: An updated meta-analysis.* Medicine (Baltimore), 2019. **98**(36): p. e15719.
8. Winters, S., et al., *Breast Cancer Epidemiology, Prevention, and Screening.* Prog Mol Biol Transl Sci, 2017. **151**: p. 1-32.
9. Kashyap, D., et al., *Global Increase in Breast Cancer Incidence: Risk Factors and Preventive Measures.* Biomed Res Int, 2022. **2022**: p. 9605439.
10. Mehrgou, A. and M. Akouchekian, *The importance of BRCA1 and BRCA2 genes mutations in breast cancer development.* Med J Islam Repub Iran, 2016. **30**: p. 369.
11. Mahdavi, M., et al., *Hereditary breast cancer; Genetic penetrance and current status with BRCA.* J Cell Physiol, 2019. **234**(5): p. 5741-5750.
12. Fanale, D., et al., *BRCA1/2 variants of unknown significance in hereditary breast and ovarian cancer (HBOC) syndrome: Looking for the hidden meaning.* Crit Rev Oncol Hematol, 2022. **172**: p. 103626.
13. Pujol, P., et al., *Clinical practice guidelines for BRCA1 and BRCA2 genetic testing.* Eur J Cancer, 2021. **146**: p. 30-47.
14. Malhotra, G.K., et al., *Histological, molecular and functional subtypes of breast cancers.* Cancer Biol Ther, 2010. **10**(10): p. 955-60.
15. Rakha, E.A., et al., *Breast cancer prognostic classification in the molecular era: the role of histological grade.* Breast Cancer Res, 2010. **12**(4): p. 207.
16. Perou, C.M., et al., *Molecular portraits of human breast tumours.* Nature, 2000. **406**(6797): p. 747-52.
17. Perou, C.M., et al., *Distinctive gene expression patterns in human mammary epithelial cells and breast cancers.* Proc Natl Acad Sci U S A, 1999. **96**(16): p. 9212-7.
18. Sørlie, T., et al., *Gene expression patterns of breast carcinomas distinguish tumor subclasses with clinical implications.* Proc Natl Acad Sci U S A, 2001. **98**(19): p. 10869-74.
19. Wieduwilt, M.J. and M.M. Moasser, *The epidermal growth factor receptor family: biology driving targeted therapeutics.* Cell Mol Life Sci, 2008. **65**(10): p. 1566-84.
20. Slamon, D.J., et al., *Human breast cancer: correlation of relapse and survival with amplification of the HER-2/neu oncogene.* Science, 1987. **235**(4785): p. 177-82.
21. Seshadri, R., et al., *Clinical significance of HER-2/neu oncogene amplification in primary breast cancer. The South Australian Breast Cancer Study Group.* J Clin Oncol, 1993. **11**(10): p. 1936-42.

22. Mercogliano, M.F., et al., *Emerging Targeted Therapies for HER2-Positive Breast Cancer.* Cancers (Basel), 2023. **15**(7).
23. Goldhirsch, A., et al., *Personalizing the treatment of women with early breast cancer: highlights of the St Gallen International Expert Consensus on the Primary Therapy of Early Breast Cancer 2013.* Ann Oncol, 2013. **24**(9): p. 2206-23.
24. Creighton, C.J., *The molecular profile of luminal B breast cancer.* Biologics, 2012. **6**: p. 289-97.
25. Lopez-Gonzalez, L., et al., *Exploring Biomarkers in Breast Cancer: Hallmarks of Diagnosis, Treatment, and Follow-Up in Clinical Practice.* Medicina, 2024. **60**(1): p. 168.
26. Asleh, K., N. Riaz, and T.O. Nielsen, *Heterogeneity of triple negative breast cancer: Current advances in subtyping and treatment implications.* J Exp Clin Cancer Res, 2022. **41**(1): p. 265.
27. Lehmann, B.D., et al., *Identification of human triple-negative breast cancer subtypes and preclinical models for selection of targeted therapies.* J Clin Invest, 2011. **121**(7): p. 2750-67.
28. Makki, J., *Diversity of Breast Carcinoma: Histological Subtypes and Clinical Relevance.* Clin Med Insights Pathol, 2015. **8**: p. 23-31.
29. Prat, A., et al., *Prognostic significance of progesterone receptor-positive tumor cells within immunohistochemically defined luminal A breast cancer.* J Clin Oncol, 2013. **31**(2): p. 203-9.
30. Gao, J.J. and S.M. Swain, *Luminal A Breast Cancer and Molecular Assays: A Review.* Oncologist, 2018. **23**(5): p. 556-565.
31. Senkus, E., et al., *Primary breast cancer: ESMO Clinical Practice Guidelines for diagnosis, treatment and follow-up.* Ann Oncol, 2015. **26 Suppl 5**: p. v8-30.
32. Mavratzas, A. and F. Marmé, *Treatment of Luminal Metastatic Breast Cancer beyond CDK4/6 Inhibition: Is There a Standard of Care in Clinical Practice?* Breast Care (Basel), 2021. **16**(2): p. 115-128.
33. Inic, Z., et al., *Difference between Luminal A and Luminal B Subtypes According to Ki-67, Tumor Size, and Progesterone Receptor Negativity Providing Prognostic Information.* Clin Med Insights Oncol, 2014. **8**: p. 107-11.
34. da Silva, F.C., et al., *Tailoring Potential Natural Compounds for the Treatment of Luminal Breast Cancer.* Pharmaceuticals, 2023. **16**(10): p. 1466.
35. Schlam, I. and S.M. Swain, *HER2-positive breast cancer and tyrosine kinase inhibitors: the time is now.* npj Breast Cancer, 2021. **7**(1): p. 56.
36. Veeraraghavan, J., et al., *Neratinib plus trastuzumab is superior to pertuzumab plus trastuzumab in HER2-positive breast cancer xenograft models.* npj Breast Cancer, 2021. **7**(1): p. 63.
37. Martínez, M.T., et al., *Treatment of HER2 positive advanced breast cancer with T-DM1: A review of the literature.* Crit Rev Oncol Hematol, 2016. **97**: p. 96-106.
38. Arciero, C.A., et al., *ER(+)/HER2(+) Breast Cancer Has Different Metastatic Patterns and Better Survival Than ER(-)/HER2(+) Breast Cancer.* Clin Breast Cancer, 2019. **19**(4): p. 236-245.
39. Jagosky, M. and A.R. Tan, *Combination of Pertuzumab and Trastuzumab in the Treatment of HER2-Positive Early Breast Cancer: A Review of the Emerging Clinical Data.* Breast Cancer (Dove Med Press), 2021. **13**: p. 393-407.
40. Takada, M. and M. Toi, *Neoadjuvant treatment for HER2-positive breast cancer.* Chinese Clinical Oncology, 2020. **9**(3): p. 32.
41. Vega Cano, K.S., et al., *Systemic Therapy for HER2-Positive Metastatic Breast Cancer: Current and Future Trends.* Cancers (Basel), 2022. **15**(1).
42. Singh, D.D., H.J. Lee, and D.K. Yadav, *Clinical updates on tyrosine kinase inhibitors in HER2-positive breast cancer.* Front Pharmacol, 2022. **13**: p. 1089066.

43. Obidiro, O., G. Battogtokh, and E.O. Akala, *Triple Negative Breast Cancer Treatment Options and Limitations: Future Outlook.* Pharmaceutics, 2023. **15**(7).
44. Emens, L.A., *Immunotherapy in Triple-Negative Breast Cancer.* Cancer J, 2021. **27**(1): p. 59-66.
45. Li, L., et al., *Immunotherapy for Triple-Negative Breast Cancer: Combination Strategies to Improve Outcome.* Cancers (Basel), 2023. **15**(1).
46. Li, Y., et al., *Recent advances in therapeutic strategies for triple-negative breast cancer.* Journal of Hematology & Oncology, 2022. **15**(1): p. 121.
47. Food, U. and D. Administration, *FDA approves pembrolizumab for high-risk early-stage triple-negative breast cancer.* US Food and Drug Administration, 2021.
48. Yin, L., et al., *Triple-negative breast cancer molecular subtyping and treatment progress.* Breast Cancer Res, 2020. **22**(1): p. 61.
49. Riggio, A.I., K.E. Varley, and A.L. Welm, *The lingering mysteries of metastatic recurrence in breast cancer.* Br J Cancer, 2021. **124**(1): p. 13-26.
50. Nordenskjöld, A.E., et al., *Breast cancer survival trends in different stages and age groups - a population-based study 1989-2013.* Acta Oncol, 2019. **58**(1): p. 45-51.
51. Demirors, B., et al., *The Role of Primary Surgery in De Novo Metastatic Breast Carcinoma.* Eur J Breast Health, 2023. **19**(2): p. 110-114.
52. Malmgren, J.A., et al., *Differential presentation and survival of de novo and recurrent metastatic breast cancer over time: 1990-2010.* Breast Cancer Res Treat, 2018. **167**(2): p. 579-590.
53. Chen, W., et al., *Organotropism: new insights into molecular mechanisms of breast cancer metastasis.* NPJ Precis Oncol, 2018. **2**(1): p. 4.
54. Wei, S. and G.P. Siegal, *Surviving at a distant site: The organotropism of metastatic breast cancer.* Semin Diagn Pathol, 2018. **35**(2): p. 108-111.
55. Lu, X. and Y. Kang, *Organotropism of breast cancer metastasis.* J Mammary Gland Biol Neoplasia, 2007. **12**(2-3): p. 153-62.
56. Liang, Y., et al., *Metastatic heterogeneity of breast cancer: Molecular mechanism and potential therapeutic targets.* Semin Cancer Biol, 2020. **60**: p. 14-27.
57. Labelle, M., S. Begum, and R.O. Hynes, *Direct signaling between platelets and cancer cells induces an epithelial-mesenchymal-like transition and promotes metastasis.* Cancer Cell, 2011. **20**(5): p. 576-90.
58. Le Gal, K., et al., *Antioxidants can increase melanoma metastasis in mice.* Sci Transl Med, 2015. **7**(308): p. 308re8.
59. Egeblad, M., E.S. Nakasone, and Z. Werb, *Tumors as organs: complex tissues that interface with the entire organism.* Dev Cell, 2010. **18**(6): p. 884-901.
60. Massagué, J. and A.C. Obenauf, *Metastatic colonization by circulating tumour cells.* Nature, 2016. **529**(7586): p. 298-306.
61. Sousa, B., A.S. Ribeiro, and J. Paredes, *Heterogeneity and Plasticity of Breast Cancer Stem Cells.* Adv Exp Med Biol, 2019. **1139**: p. 83-103.
62. Liu, Q., et al., *Factors involved in cancer metastasis: a better understanding to "seed and soil" hypothesis.* Mol Cancer, 2017. **16**(1): p. 176.
63. Obenauf, A.C. and J. Massagué, *Surviving at a Distance: Organ-Specific Metastasis.* Trends Cancer, 2015. **1**(1): p. 76-91.
64. Paget, S., *The distribution of secondary growths in cancer of the breast. 1889.* Cancer Metastasis Rev, 1989. **8**(2): p. 98-101.
65. Fidler, I.J., *The pathogenesis of cancer metastasis: the 'seed and soil' hypothesis revisited.* Nat Rev Cancer, 2003. **3**(6): p. 453-8.
66. Akhtar, M., et al., *Paget's "Seed and Soil" Theory of Cancer Metastasis: An Idea Whose Time has Come.* Adv Anat Pathol, 2019. **26**(1): p. 69-74.
67. Ewing, J., *THE PROBLEMS OF MELANOMA.* Br Med J, 1930. **2**(3646): p. 852-6.
68. Fidler, I., *L-ASPARAGINASE AND METASTASIS.* The Lancet, 1970. **295**(7650): p. 777-778.

69. Heitz, F., et al., *Cerebral metastases in metastatic breast cancer: disease-specific risk factors and survival.* Ann Oncol, 2011. **22**(7): p. 1571-1581.
70. Hoshino, A., et al., *Tumour exosome integrins determine organotropic metastasis.* Nature, 2015. **527**(7578): p. 329-35.
71. Peinado, H., et al., *Melanoma exosomes educate bone marrow progenitor cells toward a pro-metastatic phenotype through MET.* Nat Med, 2012. **18**(6): p. 883-91.
72. Costa-Silva, B., et al., *Pancreatic cancer exosomes initiate pre-metastatic niche formation in the liver.* Nat Cell Biol, 2015. **17**(6): p. 816-26.
73. Weilbaecher, K.N., T.A. Guise, and L.K. McCauley, *Cancer to bone: a fatal attraction.* Nat Rev Cancer, 2011. **11**(6): p. 411-25.
74. Cohen, N., et al., *Breast Cancer-Secreted Factors Promote Lung Metastasis by Signaling Systemically to Induce a Fibrotic Premetastatic Niche.* Cancer Res, 2023. **83**(20): p. 3354-3367.
75. Hess, K.R., et al., *Metastatic patterns in adenocarcinoma.* Cancer, 2006. **106**(7): p. 1624-33.
76. Bachmann, C., et al., *CNS metastases in breast cancer patients: prognostic implications of tumor subtype.* Med Oncol, 2015. **32**(1): p. 400.
77. Kennecke, H., et al., *Metastatic behavior of breast cancer subtypes.* J Clin Oncol, 2010. **28**(20): p. 3271-7.
78. Wu, Q., et al., *Breast cancer subtypes predict the preferential site of distant metastases: a SEER based study.* Oncotarget, 2017. **8**(17): p. 27990-27996.
79. Weide, R., et al., *Metastatic breast cancer: prolongation of survival in routine care is restricted to hormone-receptor- and Her2-positive tumors.* Springerplus, 2014. **3**: p. 535.
80. Barnholtz-Sloan, J.S., et al., *Incidence proportions of brain metastases in patients diagnosed (1973 to 2001) in the Metropolitan Detroit Cancer Surveillance System.* J Clin Oncol, 2004. **22**(14): p. 2865-72.
81. Koniali, L., et al., *Risk factors for breast cancer brain metastases: a systematic review.* Oncotarget, 2020. **11**(6): p. 650-669.
82. Anders, C.K., et al., *The prognostic contribution of clinical breast cancer subtype, age, and race among patients with breast cancer brain metastases.* Cancer, 2011. **117**(8): p. 1602-11.
83. Niwińska, A., M. Murawska, and K. Pogoda, *Breast cancer subtypes and response to systemic treatment after whole-brain radiotherapy in patients with brain metastases.* Cancer, 2010. **116**(18): p. 4238-47.
84. Oehrlich, N.E., et al., *Clinical outcome of brain metastases differs significantly among breast cancer subtypes.* Oncol Lett, 2017. **14**(1): p. 194-200.
85. Martin, A.M., et al., *Brain Metastases in Newly Diagnosed Breast Cancer: A Population-Based Study.* JAMA Oncol, 2017. **3**(8): p. 1069-1077.
86. Sihto, H., et al., *Breast cancer biological subtypes and protein expression predict for the preferential distant metastasis sites: a nationwide cohort study.* Breast Cancer Res, 2011. **13**(5): p. R87.
87. Guo, L., et al., *Selection of brain metastasis-initiating breast cancer cells determined by growth on hard agar.* Am J Pathol, 2011. **178**(5): p. 2357-66.
88. Jhanwar-Uniyal, M., et al., *Glioblastoma: molecular pathways, stem cells and therapeutic targets.* Cancers (Basel), 2015. **7**(2): p. 538-55.
89. Carvalho, R., J. Paredes, and A.S. Ribeiro, *Impact of breast cancer cells´ secretome on the brain metastatic niche remodeling.* Semin Cancer Biol, 2020. **60**: p. 294-301.
90. Eichler, A.F., et al., *The biology of brain metastases-translation to new therapies.* Nat Rev Clin Oncol, 2011. **8**(6): p. 344-56.
91. Steeg, P.S., K.A. Camphausen, and Q.R. Smith, *Brain metastases as preventive and therapeutic targets.* Nat Rev Cancer, 2011. **11**(5): p. 352-63.
92. Kienast, Y., et al., *Real-time imaging reveals the single steps of brain metastasis formation.* Nat Med, 2010. **16**(1): p. 116-22.

93. Bos, P.D., et al., *Genes that mediate breast cancer metastasis to the brain.* Nature, 2009. **459**(7249): p. 1005-9.
94. Gaedcke, J., et al., *Predominance of the basal type and HER-2/neu type in brain metastasis from breast cancer.* Modern Pathology, 2007. **20**(8): p. 864-870.
95. Adamo, B., et al., *Phosphatidylinositol 3-kinase pathway activation in breast cancer brain metastases.* Breast Cancer Research, 2011. **13**(6): p. R125.
96. Grupka, N.L., et al., *Epidermal growth factor receptor status in breast cancer metastases to the central nervous system. Comparison with HER-2/neu status.* Arch Pathol Lab Med, 2004. **128**(9): p. 974-9.
97. Gumuskaya, B., et al., *EGFR expression and gene copy number in triple-negative breast carcinoma.* Cancer Genet Cytogenet, 2010. **203**(2): p. 222-9.
98. Nie, F., et al., *Involvement of epidermal growth factor receptor overexpression in the promotion of breast cancer brain metastasis.* Cancer, 2012. **118**(21): p. 5198-209.
99. Da Silva, L., et al., *HER3 and downstream pathways are involved in colonization of brain metastases from breast cancer.* Breast Cancer Research, 2010. **12**(4).
100. Palmieri, D., et al., *Her-2 overexpression increases the metastatic outgrowth of breast cancer cells in the brain.* Cancer Res, 2007. **67**(9): p. 4190-8.
101. Bos, P.D., et al., *Genes that mediate breast cancer metastasis to the brain.* Nature, 2009. **459**(7249): p. 1005-U137.
102. Malin, D., et al., *alpha B-Crystallin: ANovel Regulator of Breast Cancer Metastasis to the Brain.* Clinical Cancer Research, 2014. **20**(1).
103. Lorger, M., et al., *Activation of tumor cell integrin alpha(v)beta(3) controls angiogenesis and metastatic growth in the brain.* Proceedings of the National Academy of Sciences of the United States of America, 2009. **106**(26): p. 10666-10671.
104. Espinoza, I., et al., *Notch signaling: targeting cancer stem cells and epithelial-to-mesenchymal transition.* Oncotargets and Therapy, 2013. **6**: p. 1249-1259.
105. Nam, D.H., et al., *Activation of Notch signaling in a xenograft model of brain metastasis.* Clinical Cancer Research, 2008. **14**(13): p. 4059-4066.
106. Xing, F., et al., *Reactive astrocytes promote the metastatic growth of breast cancer stem-like cells by activating Notch signalling in brain.* Embo Molecular Medicine, 2013. **5**(3): p. 384-396.
107. McGowan, P.M., et al., *Notch1 Inhibition Alters the CD44(hi)/CD24(lo) Population and Reduces the Formation of Brain Metastases from Breast Cancer.* Molecular Cancer Research, 2011. **9**(7): p. 834-844.
108. Draffin, J.E., et al., *CD44 potentiates the adherence of metastatic prostate and breast cancer cells to bone marrow endothelial cells.* Cancer Research, 2004. **64**(16): p. 5702-5711.
109. Mine, S., et al., *Hepatocyte growth factor enhances adhesion of breast cancer cells to endothelial cells in vitro through up-regulation of CD44.* Experimental Cell Research, 2003. **288**(1): p. 189-197.
110. Valiente, M., et al., *The Evolving Landscape of Brain Metastasis.* Trends Cancer, 2018. **4**(3): p. 176-196.
111. Malladi, S., et al., *Metastatic Latency and Immune Evasion through Autocrine Inhibition of WNT.* Cell, 2016. **165**(1): p. 45-60.
112. Chen, E.I., et al., *Adaptation of energy metabolism in breast cancer brain metastases.* Cancer Research, 2007. **67**(4): p. 1472-1486.
113. Palmieri, D., et al., *Analyses of Resected Human Brain Metastases of Breast Cancer Reveal the Association between Up-Regulation of Hexokinase 2 and Poor Prognosis.* Molecular Cancer Research, 2009. **7**(9): p. 1438-1445.
114. Yonemori, K., et al., *Disruption of the Blood Brain Barrier by Brain Metastases of Triple-Negative and Basal-Type Breast Cancer But Not HER2/neu-Positive Breast Cancer.* Cancer, 2010. **116**(2): p. 302-308.

115. Cordero, A., et al., *FABP7 is a key metabolic regulator in HER2+ breast cancer brain metastasis.* Oncogene, 2019. **38**(37): p. 6445-6460.
116. Santana-Codina, N., et al., *GRP94 promotes brain metastasis by engaging pro-survival autophagy.* Neuro Oncol, 2020. **22**(5): p. 652-664.
117. Blazquez, R., et al., *LEF1 supports metastatic brain colonization by regulating glutathione metabolism and increasing ROS resistance in breast cancer.* Int J Cancer, 2020. **146**(11): p. 3170-3183.
118. Valiente, M., et al., *Serpins promote cancer cell survival and vascular co-option in brain metastasis.* Cell, 2014. **156**(5): p. 1002-16.
119. Holash, J., et al., *Vessel cooption, regression, and growth in tumors mediated by angiopoietins and VEGF.* Science, 1999. **284**(5422): p. 1994-8.
120. Mentzer, S.J. and M.A. Konerding, *Intussusceptive angiogenesis: expansion and remodeling of microvascular networks.* Angiogenesis, 2014. **17**(3): p. 499-509.
121. Bugyik, E., et al., *Lack of angiogenesis in experimental brain metastases.* J Neuropathol Exp Neurol, 2011. **70**(11): p. 979-91.
122. Paku, S., et al., *A new mechanism for pillar formation during tumor-induced intussusceptive angiogenesis: inverse sprouting.* Am J Pathol, 2011. **179**(3): p. 1573-85.
123. Wang, S., et al., *JAK2-binding long noncoding RNA promotes breast cancer brain metastasis.* J Clin Invest, 2017. **127**(12): p. 4498-4515.
124. Carbonell, W.S., et al., *The vascular basement membrane as "soil" in brain metastasis.* PLoS One, 2009. **4**(6): p. e5857.
125. Xue, H., B. Lu, and M. Lai, *The cancer secretome: a reservoir of biomarkers.* J Transl Med, 2008. **6**: p. 52.
126. Patel, S., et al., *Cancer secretomes and their place in supplementing other hallmarks of cancer.* Adv Exp Med Biol, 2014. **806**: p. 409-42.
127. Liu, Y. and X. Cao, *Characteristics and Significance of the Pre-metastatic Niche.* Cancer Cell, 2016. **30**(5): p. 668-681.
128. Fazakas, C., et al., *Transmigration of Melanoma Cells through the Blood-Brain Barrier: Role of Endothelial Tight Junctions and Melanoma-Released Serine Proteases.* Plos One, 2011. **6**(6).
129. Custódio-Santos, T., M. Videira, and M.A. Brito, *Brain metastasization of breast cancer.* Biochimica et Biophysica Acta (BBA) - Reviews on Cancer, 2017. **1868**(1): p. 132-147.
130. Herman, H., et al., *Paracellular and transcellular migration of metastatic cells through the cerebral endothelium.* J Cell Mol Med, 2019. **23**(4): p. 2619-2631.
131. Rodriguez, P.L., et al., *The proinflammatory peptide substance P promotes blood-brain barrier breaching by breast cancer cells through changes in microvascular endothelial cell tight junctions.* Int J Cancer, 2014. **134**(5): p. 1034-44.
132. Avraham, H.K., et al., *Angiopoietin-2 mediates blood-brain barrier impairment and colonization of triple-negative breast cancer cells in brain.* Journal of Pathology, 2014. **232**(3): p. 369-381.
133. Lee, T.H., et al., *Vascular endothelial growth factor modulates the transendothelial migration of MDA-MB-231 breast cancer cells through regulation of brain microvascular endothelial cell permeability.* Journal of Biological Chemistry, 2003. **278**(7): p. 5277-5284.
134. Fan, J., et al., *Integrin β4 Signaling Promotes Mammary Tumor Cell Adhesion to Brain Microvascular Endothelium by Inducing ErbB2-Mediated Secretion of VEGF.* Annals of Biomedical Engineering, 2011. **39**(8): p. 2223-2241.
135. Lee, B.C., et al., *Involvement of the chemokine receptor CXCR4 and its ligand stromal cell-derived factor 1 alpha in breast cancer cell migration through human brain microvascular endothelial cells.* Molecular Cancer Research, 2004. **2**(6): p. 327-338.
136. Soto, M.S., et al., *Functional role of endothelial adhesion molecules in the early stages of brain metastasis.* Neuro Oncol, 2014. **16**(4): p. 540-51.

137. Tominaga, N., et al., *Brain metastatic cancer cells release microRNA-181c-containing extracellular vesicles capable of destructing blood-brain barrier.* Nature Communications, 2015. **6**.
138. Zhou, W.Y., et al., *Cancer-Secreted miR-105 Destroys Vascular Endothelial Barriers to Promote Metastasis.* Cancer Cell, 2014. **25**(4): p. 501-515.
139. Lu, Y., et al., *Exosomes Derived from Brain Metastatic Breast Cancer Cells Destroy the Blood-Brain Barrier by Carrying lncRNA GS1-600G8.5.* Biomed Res Int, 2020. **2020**: p. 7461727.
140. Rodrigues, G., et al., *Tumour exosomal CEMIP protein promotes cancer cell colonization in brain metastasis.* Nat Cell Biol, 2019. **21**(11): p. 1403-1412.
141. Tiwary, S., et al., *Metastatic Brain Tumors Disrupt the Blood-Brain Barrier and Alter Lipid Metabolism by Inhibiting Expression of the Endothelial Cell Fatty Acid Transporter Mfsd2a.* Scientific Reports, 2018. **8**.
142. Curtaz, C.J., et al., *Serum-derived factors of breast cancer patients with brain metastases alter permeability of a human blood–brain barrier model.* Fluids and Barriers of the CNS, 2020. **17**(1): p. 31.
143. Zeng, Q., et al., *Synaptic proximity enables NMDAR signalling to promote brain metastasis.* Nature, 2019. **573**(7775): p. 526-531.
144. Deshpande, K., et al., *Neuronal exposure induces neurotransmitter signaling and synaptic mediators in tumors early in brain metastasis.* Neuro Oncol, 2022. **24**(6): p. 914-924.
145. Bergers, G. and S. Song, *The role of pericytes in blood-vessel formation and maintenance.* Neuro-Oncology, 2005. **7**(4): p. 452-464.
146. Chen, J.N., et al., *CD146 is essential for PDGFR beta-induced pericyte recruitment.* Protein & Cell, 2018. **9**(8): p. 743-747.
147. Cheng, L., et al., *Glioblastoma Stem Cells Generate Vascular Pericytes to Support Vessel Function and Tumor Growth.* Cell, 2013. **153**(1): p. 139-152.
148. Smyth, L.C.D., et al., *Markers for human brain pericytes and smooth muscle cells.* Journal of Chemical Neuroanatomy, 2018. **92**: p. 48-60.
149. Xian, X., et al., *Pericytes limit tumor cell metastasis.* J Clin Invest, 2006. **116**(3): p. 642-51.
150. Kienast, Y., et al., *Real-time imaging reveals the single steps of brain metastasis formation.* Nature Medicine, 2010. **16**(1): p. 116-U157.
151. Lyle, L.T., et al., *Alterations in Pericyte Subpopulations Are Associated with Elevated Blood-Tumor Barrier Permeability in Experimental Brain Metastasis of Breast Cancer.* Clinical Cancer Research, 2016. **22**(21): p. 5287-5299.
152. Molnár, K., et al., *Pericyte-secreted IGF2 promotes breast cancer brain metastasis formation.* Mol Oncol, 2020. **14**(9): p. 2040-2057.
153. Lenz, K.M. and L.H. Nelson, *Microglia and Beyond: Innate Immune Cells As Regulators of Brain Development and Behavioral Function.* Frontiers in Immunology, 2018. **9**.
154. Menassa, D.A. and D. Gomez-Nicola, *Microglial Dynamics During Human Brain Development.* Frontiers in Immunology, 2018. **9**.
155. Loane, D.J. and A. Kumar, *Microglia in the TBI brain: The good, the bad, and the dysregulated.* Experimental Neurology, 2016. **275**: p. 316-327.
156. Boche, D., V.H. Perry, and J.A.R. Nicoll, *Review: Activation patterns of microglia and their identification in the human brain.* Neuropathology and Applied Neurobiology, 2013. **39**(1): p. 3-18.
157. Sidani, M., et al., *Probing the microenvironment of mammary tumors using multiphoton microscopy.* Journal of Mammary Gland Biology and Neoplasia, 2006. **11**(2): p. 151-163.
158. Wu, K.R., et al., *Roles of the Cyclooxygenase 2 Matrix Metalloproteinase 1 Pathway in Brain Metastasis of Breast Cancer.* Journal of Biological Chemistry, 2015. **290**(15): p. 9842-9854.
159. Matias, D., et al., *Microglia/Astrocytes-Glioblastoma Crosstalk: Crucial Molecular Mechanisms and Microenvironmental Factors.* Frontiers in Cellular Neuroscience, 2018. **12**.
160. Pukrop, T., et al., *Microglia Promote Colonization of Brain Tissue by Breast Cancer Cells in a Wnt-Dependent Way.* Glia, 2010. **58**(12): p. 1477-1489.

161. Xing, F., et al., *Loss of XIST in Breast Cancer Activates MSN-c-Met and Reprograms Microglia via Exosomal miRNA to Promote Brain Metastasis.* Cancer Research, 2018. **78**(15): p. 4316-4330.
162. Louie, E., et al., *Neurotrophin-3 modulates breast cancer cells and the microenvironment to promote the growth of breast cancer brain metastasis.* Oncogene, 2013. **32**(35): p. 4064-77.
163. Lorger, M. and B. Felding-Habermann, *Capturing Changes in the Brain Microenvironment during Initial Steps of Breast Cancer Brain Metastasis.* American Journal of Pathology, 2010. **176**(6): p. 2958-2971.
164. Andreou, K.E., et al., *Anti-inflammatory Microglia/Macrophages As a Potential Therapeutic Target in Brain Metastasis.* Frontiers in Oncology, 2017. **7**.
165. Qiao, S., et al., *Long-term characterization of activated microglia/macrophages facilitating the development of experimental brain metastasis through intravital microscopic imaging.* Journal of Neuroinflammation, 2019. **16**.
166. Simon, A., et al., *Metastatic breast cancer cells induce altered microglial morphology and electrical excitability in vivo.* Journal of Neuroinflammation, 2020. **17**(1): p. 87.
167. Lorger, M. and B. Felding-Habermann, *Capturing changes in the brain microenvironment during initial steps of breast cancer brain metastasis.* Am J Pathol, 2010. **176**(6): p. 2958-71.
168. Kim, S.J., et al., *Astrocytes upregulate survival genes in tumor cells and induce protection from chemotherapy.* Neoplasia, 2011. **13**(3): p. 286-98.
169. Seike, T., et al., *Interaction between lung cancer cells and astrocytes via specific inflammatory cytokines in the microenvironment of brain metastasis.* Clin Exp Metastasis, 2011. **28**(1): p. 13-25.
170. Priego, N., et al., *STAT3 labels a subpopulation of reactive astrocytes required for brain metastasis.* Nat Med, 2018. **24**(7): p. 1024-1035.
171. Hosonaga, M., H. Saya, and Y. Arima, *Molecular and cellular mechanisms underlying brain metastasis of breast cancer.* Cancer Metastasis Rev, 2020. **39**(3): p. 711-720.
172. Hallal, S., et al., *Extracellular Vesicles Released by Glioblastoma Cells Stimulate Normal Astrocytes to Acquire a Tumor-Supportive Phenotype Via p53 and MYC Signaling Pathways.* Molecular Neurobiology, 2019. **56**(6): p. 4566-4581.
173. Hoelzinger, D.B., T. Demuth, and M.E. Berens, *Autocrine factors that sustain glioma invasion and paracrine biology in the brain microenvironment.* Journal of the National Cancer Institute, 2007. **99**(21): p. 1583-1593.
174. Sierra, A., et al., *Astrocyte-derived cytokines contribute to the metastatic brain specificity of breast cancer cells.* Laboratory Investigation, 1997. **77**(4): p. 357-368.
175. Termini, J., J. Neman, and R. Jandial, *Role of the Neural Niche in Brain Metastatic Cancer (vol 74, pg 4011, 2014).* Cancer Research, 2014. **74**(19): p. 5680-5680.
176. Mendes, O., et al., *MMP2 role in breast cancer brain metastasis development and its regulation by TIMP2 and ERK1/2.* Clinical & Experimental Metastasis, 2007. **24**(5): p. 341-351.
177. Wang, T., et al., *Upregulation of Matrix Metalloproteinase-9 in Primary Cultured Rat Astrocytes Induced by 2-Chloroethanol Via MAPK Signal Pathways.* Front Cell Neurosci, 2017. **11**: p. 218.
178. Zhang, L., et al., *Microenvironment-induced PTEN loss by exosomal microRNA primes brain metastasis outgrowth.* Nature, 2015. **527**(7576): p. 100-104.
179. Gril, B., et al., *Pazopanib Inhibits the Activation of PDGFR beta-Expressing Astrocytes in the Brain Metastatic Microenvironment of Breast Cancer Cells.* American Journal of Pathology, 2013. **182**(6): p. 2368-2379.
180. Neman, J., et al., *Co-evolution of breast-to-brain metastasis and neural progenitor cells.* Clinical & Experimental Metastasis, 2013. **30**(6): p. 753-768.

181. Neman, J., et al., *Human breast-to-brain metastases display GABAergic properties in the neural niche.* Cancer Research, 2013. **73**.
182. Neman, J., et al., *Co-evolution of breast-to-brain metastasis and neural progenitor cells.* Clin Exp Metastasis, 2013. **30**(6): p. 753-68.
183. Wu, K., et al., *Roles of the cyclooxygenase 2 matrix metalloproteinase 1 pathway in brain metastasis of breast cancer.* J Biol Chem, 2015. **290**(15): p. 9842-54.
184. Fong, M.Y., et al., *Breast-cancer-secreted miR-122 reprograms glucose metabolism in premetastatic niche to promote metastasis.* Nat Cell Biol, 2015. **17**(2): p. 183-94.
185. Peinado, H., et al., *Pre-metastatic niches: organ-specific homes for metastases.* Nat Rev Cancer, 2017.
186. Liu, Y. and X.T. Cao, *Characteristics and Significance of the Pre-metastatic Niche.* Cancer Cell, 2016. **30**(5): p. 668-681.
187. Aguado, B.A., et al., *Engineering the pre-metastatic niche.* Nature Biomedical Engineering, 2017. **1**(6).
188. Chen, W.J., et al., *Organotropism: new insights into molecular mechanisms of breast cancer metastasis.* Npj Precision Oncology, 2018. **2**.
189. Guo, Y.X., et al., *Effects of exosomes on pre-metastatic niche formation in tumors.* Molecular Cancer, 2019. **18**.
190. Liu, Q., et al., *Factors involved in cancer metastasis: a better understanding to "seed and soil" hypothesis.* Molecular Cancer, 2017. **16**.
191. Geissler, M., et al., *The Brain Pre-Metastatic Niche: Biological and Technical Advancements.* International Journal of Molecular Sciences, 2023. **24**(12): p. 10055.
192. Xue, H., B. Lu, and M. Lai, *The cancer secretome: a reservoir of biomarkers.* Journal of Translational Medicine, 2008. **6**.
193. Patel, S., et al., *Cancer Secretomes and Their Place in Supplementing Other Hallmarks of Cancer.* Advancements of Mass Spectrometry in Biomedical Research, 2014. **806**: p. 409-442.
194. Brandi, J., et al., *Proteomic approaches to decipher cancer cell secretome.* Seminars in Cell & Developmental Biology, 2018. **78**: p. 93-101.
195. Brown, K.J., et al., *Advances in the proteomic investigation of the cell secretome.* Expert Review of Proteomics, 2012. **9**(3): p. 337-345.
196. Ziegler, Y.S., et al., *Integration of Breast Cancer Secretomes with Clinical Data Elucidates Potential Serum Markers for Disease Detection, Diagnosis, and Prognosis.* Plos One, 2016. **11**(6).
197. Klemm, F., et al., *Interrogation of the Microenvironmental Landscape in Brain Tumors Reveals Disease-Specific Alterations of Immune Cells.* Cell, 2020. **181**(7): p. 1643-1660.e17.
198. Friebel, E., et al., *Single-Cell Mapping of Human Brain Cancer Reveals Tumor-Specific Instruction of Tissue-Invading Leukocytes.* Cell, 2020. **181**(7): p. 1626-1642.e20.
199. Kloosterman, D.J. and L. Akkari, *Mapping the Uncharted Territories of Human Brain Malignancies.* Cell, 2020. **181**(7): p. 1454-1457.
200. Brandi, J., et al., *Proteomic approaches to decipher cancer cell secretome.* Semin Cell Dev Biol, 2018. **78**: p. 93-101.
201. Kathryn, M. and E.T. Stella, *Breast-to-brain metastasis: a focus on the pre-metastatic niche.* Breast-to-brain metastasis: a focus on the pre-metastatic niche, 2021. **7**: p. 40.
202. Minn, A.J., et al., *Genes that mediate breast cancer metastasis to lung.* Nature, 2005. **436**(7050): p. 518-24.
203. Yoneda, T., et al., *A bone-seeking clone exhibits different biological properties from the MDA-MB-231 parental human breast cancer cells and a brain-seeking clone in vivo and in vitro.* J Bone Miner Res, 2001. **16**(8): p. 1486-95.
204. Weksler, B.B., et al., *Blood-brain barrier-specific properties of a human adult brain endothelial cell line.* Faseb j, 2005. **19**(13): p. 1872-4.

205. Coelho-Santos, V., et al., *Methylphenidate-triggered ROS generation promotes caveolae-mediated transcytosis via Rac1 signaling and c-Src-dependent caveolin-1 phosphorylation in human brain endothelial cells.* Cell Mol Life Sci, 2016. **73**(24): p. 4701-4716.
206. Silva, S.L., et al., *Features of bilirubin-induced reactive microglia: from phagocytosis to inflammation.* Neurobiol Dis, 2010. **40**(3): p. 663-75.
207. Stephens, S.B., et al., *A VGF-derived peptide attenuates development of type 2 diabetes via enhancement of islet β-cell survival and function.* Cell Metab, 2012. **16**(1): p. 33-43.
208. Kim, J.Y., et al., *SOX9 promotes stress-responsive transcription of VGF nerve growth factor inducible gene in renal tubular epithelial cells.* J Biol Chem, 2020. **295**(48): p. 16328-16341.
209. Ribeiro, A.S., et al., *Extracellular cleavage and shedding of P-cadherin: a mechanism underlying the invasive behaviour of breast cancer cells.* Oncogene, 2010. **29**(3): p. 392-402.
210. Hubrecht, R.C. and E. Carter, *The 3Rs and Humane Experimental Technique: Implementing Change.* Animals (Basel), 2019. **9**(10).
211. Hughes, C.S., et al., *Single-pot, solid-phase-enhanced sample preparation for proteomics experiments.* Nat Protoc, 2019. **14**(1): p. 68-85.
212. Ribeiro, A.S., et al., *P-cadherin functional role is dependent on E-cadherin cellular context: a proof of concept using the breast cancer model.* J Pathol, 2013. **229**(5): p. 705-18.
213. Ricardo, S., et al., *Breast cancer stem cell markers CD44, CD24 and ALDH1: expression distribution within intrinsic molecular subtype.* J Clin Pathol, 2011. **64**(11): p. 937-46.
214. Sousa, B., et al., *The basal epithelial marker P-cadherin associates with breast cancer cell populations harboring a glycolytic and acid-resistant phenotype.* BMC Cancer, 2014. **14**: p. 734.
215. Foo, S.L., et al., *Breast cancer metastasis to brain results in recruitment and activation of microglia through annexin-A1/formyl peptide receptor signaling.* Breast Cancer Res, 2022. **24**(1): p. 25.
216. Xing, F., et al., *Loss of XIST in Breast Cancer Activates MSN-c-Met and Reprograms Microglia via Exosomal miRNA to Promote Brain Metastasis.* Cancer Res, 2018. **78**(15): p. 4316-4330.
217. Andreou, K.E., et al., *Anti-inflammatory Microglia/Macrophages As a Potential Therapeutic Target in Brain Metastasis.* Front Oncol, 2017. **7**: p. 251.
218. Pukrop, T., et al., *Microglia promote colonization of brain tissue by breast cancer cells in a Wnt-dependent way.* Glia, 2010. **58**(12): p. 1477-89.
219. Simon, A., et al., *Metastatic breast cancer cells induce altered microglial morphology and electrical excitability in vivo.* J Neuroinflammation, 2020. **17**(1): p. 87.
220. Ko, E., et al., *Engineering 3D Cortical Spheroids for an In Vitro Ischemic Stroke Model.* ACS Biomater Sci Eng, 2021. **7**(8): p. 3845-3860.
221. Propson, N.E., et al., *Endothelial C3a receptor mediates vascular inflammation and blood-brain barrier permeability during aging.* J Clin Invest, 2021. **131**(1).
222. Quinn, J.P., et al., *VGF as a biomarker and therapeutic target in neurodegenerative and psychiatric diseases.* Brain Commun, 2021. **3**(4): p. fcab261.
223. Geissler, M., et al., *The Brain Pre-Metastatic Niche: Biological and Technical Advancements.* Int J Mol Sci, 2023. **24**(12).
224. Zahari, S., S.E. Syafruddin, and M.A. Mohtar, *Impact of the Cancer Cell Secretome in Driving Breast Cancer Progression.* Cancers (Basel), 2023. **15**(9).
225. Conklin, M.W. and P.J. Keely, *Why the stroma matters in breast cancer: insights into breast cancer patient outcomes through the examination of stromal biomarkers.* Cell Adh Migr, 2012. **6**(3): p. 249-60.
226. Michalski, D., et al., *Increased Immunosignals of Collagen IV and Fibronectin Indicate Ischemic Consequences for the Neurovascular Matrix Adhesion Zone in Various Animal Models and Human Stroke Tissue.* Front Physiol, 2020. **11**: p. 575598.
227. Kyriatzis, G., et al., *In the Rat Hippocampus, Pilocarpine-Induced Status Epilepticus Is Associated with Reactive Glia and Concomitant Increased Expression of CD31, PDGFRβ, and*

Collagen IV in Endothelial Cells and Pericytes of the Blood–Brain Barrier. International Journal of Molecular Sciences, 2024. **25**(3): p. 1693.
228. Arnold, J., et al., *Tubulin Tyrosine Ligase Like 4 (TTLL4) overexpression in breast cancer cells is associated with brain metastasis and alters exosome biogenesis.* J Exp Clin Cancer Res, 2020. **39**(1): p. 205.
229. Feng, S., et al., *Matrix metalloproteinase-2 and -9 secreted by leukemic cells increase the permeability of blood-brain barrier by disrupting tight junction proteins.* PLoS One, 2011. **6**(8): p. e20599.
230. Qiao, S., et al., *Long-term characterization of activated microglia/macrophages facilitating the development of experimental brain metastasis through intravital microscopic imaging.* J Neuroinflammation, 2019. **16**(1): p. 4.
231. Caffarel, M.M. and M.S. Braza, *Microglia and metastases to the central nervous system: victim, ravager, or something else?* J Exp Clin Cancer Res, 2022. **41**(1): p. 327.
232. Cadiz, M.P., et al., *Culture shock: microglial heterogeneity, activation, and disrupted single-cell microglial networks in vitro.* Mol Neurodegener, 2022. **17**(1): p. 26.
233. Warden, A.S., et al., *Tools for studying human microglia: In vitro and in vivo strategies.* Brain Behav Immun, 2023. **107**: p. 369-382.
234. Schroeder, T., et al., *Mapping distribution of brain metastases: does the primary tumor matter?* J Neurooncol, 2020. **147**(1): p. 229-235.
235. Foglesong, G.D., et al., *Role of Hypothalamic VGF in Energy Balance and Metabolic Adaption to Environmental Enrichment in Mice.* Endocrinology, 2016. **157**(3): p. 983-96.
236. Alder, J., et al., *Brain-derived neurotrophic factor-induced gene expression reveals novel actions of VGF in hippocampal synaptic plasticity.* J Neurosci, 2003. **23**(34): p. 10800-8.
237. Koc, G., et al., *Changes in VGF and C3aR1 gene expression in human adipose tissue in obesity.* Mol Biol Rep, 2021. **48**(1): p. 251-257.
238. Benchoula, K., I.S. Parhar, and W.E. Hwa, *The molecular mechanism of vgf in appetite, lipids, and insulin regulation.* Pharmacol Res, 2021. **172**: p. 105855.
239. Lin, W.J., et al., *An increase in VGF expression through a rapid, transcription-independent, autofeedback mechanism improves cognitive function.* Transl Psychiatry, 2021. **11**(1): p. 383.
240. Sahu, B.S., et al., *Peptide/Receptor Co-evolution Explains the Lipolytic Function of the Neuropeptide TLQP-21.* Cell Rep, 2019. **28**(10): p. 2567-2580.e6.
241. Brancia, C., et al., *TLQP Peptides in Amyotrophic Lateral Sclerosis: Possible Blood Biomarkers with a Neuroprotective Role.* Neuroscience, 2018. **380**: p. 152-163.
242. El Gaamouch, F., et al., *VGF-derived peptide TLQP-21 modulates microglial function through C3aR1 signaling pathways and reduces neuropathology in 5xFAD mice.* Mol Neurodegener, 2020. **15**(1): p. 4.
243. Annaratone, L., et al., *Search for neuro-endocrine markers (chromogranin A, synaptophysin and VGF) in breast cancers. An integrated approach using immunohistochemistry and gene expression profiling.* Endocr Pathol, 2014. **25**(3): p. 219-28.
244. Ding, S., et al., *Identification of a novel immune-related prognostic signature associated with tumor microenvironment for breast cancer.* Int Immunopharmacol, 2021. **100**: p. 108122.
245. Hwang, W., et al., *Expression of Neuroendocrine Factor VGF in Lung Cancer Cells Confers Resistance to EGFR Kinase Inhibitors and Triggers Epithelial-to-Mesenchymal Transition.* Cancer Res, 2017. **77**(11): p. 3013-3026.
246. Wang, X., et al., *Reciprocal Signaling between Glioblastoma Stem Cells and Differentiated Tumor Cells Promotes Malignant Progression.* Cell Stem Cell, 2018. **22**(4): p. 514-528.e5.
247. Martínez-Aranda, A., et al., *FN14 and GRP94 expression are prognostic/predictive biomarkers of brain metastasis outcome that open up new therapeutic strategies.* Oncotarget, 2015. **6**(42): p. 44254-73.

ANNEX. PUBLICATIONS

Check for updates

Journal of Pathology
J Pathol October 2024; **264:** 132–147
Published online 29 July 2024 in Wiley Online Library
(wileyonlinelibrary.com) DOI: 10.1002/path.6319

ORIGINAL ARTICLE

Nerve growth factor inducible (VGF) is a secreted mediator for metastatic breast cancer tropism to the brain

Rita Carvalho[1,2,3], Liliana Santos[4,5,6], Inês Conde[1,2,3], Ricardo Leitão[4,5,6], Hugo RS Ferreira[4,5,6], Célia Gomes[4,5,6], Ana Paula Silva[4,5,6], Fernando Schmitt[2,7,8], Carina Carvalho-Maia[9], João Lobo[3,9,10], Carmen Jerónimo[9,10], Joana Paredes[1,2,8] and Ana Sofia Ribeiro[1,2*]

[1] *Cancer Metastasis group, i3S – Institute for Research and Innovation in Health, University of Porto, Porto, Portugal*
[2] *IPATIMUP – Institute of Molecular Pathology and Immunology of the University of Porto, Porto, Portugal*
[3] *Department of Pathology and Molecular Immunology, ICBAS – School of Medicine and Biomedical Sciences, University of Porto, Porto, Portugal*
[4] *Institute of Pharmacology and Experimental Therapeutics, Faculty of Medicine, University of Coimbra, Coimbra, Portugal*
[5] *iCBR – Institute for Clinical and Biomedical Research, Faculty of Medicine, University of Coimbra, Coimbra, Portugal*
[6] *CIBB – Center for Innovation in Biomedicine and Biotechnology, University of Coimbra, Coimbra, Portugal*
[7] *CINTESIS@RISE, Porto, Portugal*
[8] *FMUP – Faculty of Medicine, University of Porto, Porto, Portugal*
[9] *Cancer Biology and Epigenetics Group, IPO Porto Research Center (GEBC CI-IPOP), Portuguese Oncology Institute of Porto (IPO Porto)/Porto Comprehensive Cancer Center Raquel Seruca (P.CCC) & CI-IPOP@RISE (Health Research Network), Porto, Portugal*
[10] *Department of Pathology, Portuguese Oncology Institute of Porto (IPO Porto)/Porto Comprehensive Cancer Center Raquel Seruca (P.CCC), Porto, Portugal*

**Correspondence to: AS Ribeiro, i3S – Instituto de Investigação e Inovação em Saúde da Universidade do Porto, Rua Alfredo Allen 208, 4200-135 Porto, Portugal. E-mail: aribeiro@ipatimup.pt*

Abstract

Brain metastases are one of the most serious clinical problems in breast cancer (BC) progression, associated with lower survival rates and a lack of effective therapies. Thus, to dissect the early stages of the brain metastatic process, we studied the impact of brain organotropic BC cells' secretomes on the establishment of the brain pre-metastatic niche (PMN). We found that BC cells with specific tropism to the brain caused significant blood–brain barrier (BBB) disruption, as well as microglial activation, in both *in vitro* and *in vivo* models. Further, we searched for a brain-organotropic metastatic signature, as a promising source for the discovery of new biomarkers involved in brain metastatic progression. Of relevance, we identified VGF (nerve growth factor inducible) as a key mediator in this process, also impacting the BBB and microglial functions both *in vitro* and *in vivo*. In a series of human breast tumors, VGF was found to be expressed in both cancer cells and the adjacent stroma. Importantly, VGF-positive tumors showed a significantly worse prognosis and were associated with HER2 (human epidermal growth factor receptor 2) overexpression and triple-negative molecular signatures. Further clinical validation in primary tumors from metastatic BC cases showed a significant association between VGF and the brain metastatic location, clearly and significantly impacting on the prognosis of BC patients with brain metastasis. In conclusion, our study reveals a unique secretome signature for BC with a tropism for the brain, highlighting VGF as a crucial mediator in this process. Furthermore, its specific impact as a poor prognostic predictor for BC patients with brain metastasis opens new avenues to target VGF to control the progression of brain metastatic disease.

© 2024 The Pathological Society of Great Britain and Ireland.

Keywords: breast cancer brain metastasis; brain pre-metastatic niche; brain signature; VGF; blood–brain barrier; microglia; prognostic biomarker

Received 26 October 2023; Revised 2 May 2024; Accepted 16 May 2024

No conflicts of interest were declared.

Introduction

Breast cancer (BC) is the most common malignancy and leading cause of cancer death in women due to distant metastases to the bone, lung, liver, and brain [1]. According to Paget's theory, metastases are a non-random process and are instead determined by the interaction between cancer cells (the seeds) and the metastatic microenvironment (the soil) [2–4]. For example, BC expresses chemokine receptors, namely CXCR4 and CCR7, which pair with chemokine ligands expressed in lymph nodes (CXCL12) and lung (CCL21), thus determining the destination of metastases [5]. Several studies have already shown that cancer cells modulate metastatic niches long before they reach the target organ. Several efforts are being made to uncover and characterize the

© 2024 The Pathological Society of Great Britain and Ireland. www.pathsoc.org

molecular factors secreted by cancer cells, aiming to identify metastatic biomarkers. Long before intravasation, cancer cells communicate with distant metastatic organs, mainly by secreting soluble factors and/or extracellular vesicles (EVs), which recruit immune cells and promote resident cells activation, and extracellular matrix (ECM) remodeling, thereby preparing a supportive and receptive pre-metastatic niche (PMN) for the growth and survival of cancer cells [6–9]. These molecular factors released by cancer cells collectively compose the 'cancer cell secretome', which is a promising source of molecular targets involved in the crosstalk between the primary tumor and the future metastatic site [8,10]. Importantly, PMNs may influence the success of metastatic colonization, and understanding their alterations and regulation may help to improve the development of effective therapies.

BC survival rates have improved significantly in recent years, owing to advancements in surveillance and more effective systemic treatments, although 10–30% of patients with metastatic BC will develop brain metastasis during the course of their disease [11–14]. BC brain metastases are a major cause of poor quality of life and the prognosis of patients remains dismal, with survival typically measured in months [15–17]. Current treatments for brain metastases include surgery, stereotactic radiotherapy, whole-brain radiotherapy, and systemic therapy. However, no effective chemotherapeutic options for brain metastasis are available, unlike treatments for lung and bone metastases. It is known that BC patients with HER2 (human epidermal growth factor receptor 2) overexpression and triple-negative molecular subtypes experience metastases more frequently to the brain, suggesting that these cancer cells have specific molecular signatures that afford them an intrinsic advantage to survive in the brain tissue [11,18]. The unique composition of the brain, including the blood–brain barrier (BBB) and specialized resident cells, helps to create a highly protected environment, which is essential for its proper function and long-term health. Thus, the interaction between cancer cells and the brain metastatic niche must present distinct properties compared with other metastatic organs. To prevent and treat brain metastasis, it is critical to identify new molecular drivers responsible for communication between cancer cells and the brain microenvironment.

David Lyden's research has already demonstrated that exosomes secreted by cancer cells contain specific molecules that allow them to home on target metastatic organs, a process known as organotropism [9,19,20]. Particularly, in the brain, it was recently demonstrated that the CEMIP exosomal protein preconditions the brain microenvironment, enhancing cancer cell outgrowth [21]. Significant efforts have been made to identify players involved in this process and to understand how cancer cells directly modulate the brain PMN. However, it remains an unexplored and very challenging area of research.

Therefore, in this work, we aimed to decipher the soluble factors secreted by BC cells responsible for the remodeling of the brain PMN, and how these modifications can impact the brain metastatic capacity of cancer cells. Our data demonstrated that the secretome of brain organotropic BC cells plays an important role in remodeling the brain PMN, namely by affecting BBB integrity and microglial activation. Interestingly, we identified a specific brain secretome signature, with VGF (also known as VGF nerve growth factor inducible) being one of the peptides specifically deregulated in the secretome of brain organotropic BC cells. Notably, we validated its impact on brain PMN remodeling and its potential to be a novel clinical prognostic biomarker for brain metastasis.

Materials and methods

Cell culture

The parental BC cell line MDA-MB-231 (parental 231) was obtained from the American Type Culture Collection (ATCC; Manassas, VA, USA), while its organotropic BC variants lung (231.Lung) [22], bone (231.Bone) [23], brain (231.Brain) [24], and brain with HER2 overexpression (231.Brain.HER2) [25] clones were obtained from J Massagué (Memorial Sloan Kettering Cancer Center, New York, NY, USA) and P Steeg (Center for Cancer Research, National Cancer Institute, Bethesda, MD, USA) (supplementary material, Figure S1). Although the 231.Brain.HER2 organotropic variant does not fully mimic the HER2 molecular subtype, since it was obtained by *ex vivo* transfection of parental 231 with *HER2*, we decided to use it since it shares the same genetic background as the parental cell line (parental 231). Additionally, although both brain organotropic BC cell lines came from different laboratories, they both showed an increased brain metastatic ability.

The human cerebral microvascular endothelial cell line (hCMEC/D3) was kindly provided by Pierre-Olivier Couraud (Institute Cochin, Université René Descartes, Paris, France). The human microglia clone 3 cell line (HMC3) was purchased from ATCC (ATCC® CRL-3304™). Details are provided in Supplementary materials and methods.

Preparation of secretomes

For *in vitro* assays, we plated BC cells (3×10^5 cells in a six-well plate) embedded in collagen type I (Merck, Rahway, NJ, USA) to mimic the BC ECM.

To study the impact of cancer cells' secretomes *in vivo*, we plated BC cells (6×10^6 cells) embedded in collagen type I in a T175 flask (supplementary material, Figure S2). Details are provided in Supplementary materials and methods.

In vitro evaluation of brain endothelial cell monolayer integrity

Brain endothelial cell (EC) monolayer integrity was determined by measuring the transendothelial flux of fluorescent 4 kDa macromolecules across the hCMEC/D3

© 2024 The Pathological Society of Great Britain and Ireland. www.pathsoc.org

10969896, 2024, 2, Downloaded from https://pathsocjournals.onlinelibrary.wiley.com/doi/10.1002/path.6319 by Universidade Do Porto Faculdade de Engenharia, Wiley Online Library on [29/04/2025]. See the Terms and Conditions (https://onlinelibrary.wiley.com/terms-and-conditions) on Wiley Online Library for rules of use; OA articles are governed by the applicable Creative Commons License

cells and by measuring their transendothelial electrical resistance (TEER), as described previously [26]. Details are provided in Supplementary materials and methods.

In vitro microglial phagocytosis assay

To evaluate phagocytic capacity, microglial cells (HMC3) were incubated with 1 µm fluorescent latex beads, 0.0025% (w/w), for 75 min. After incubation, the total number of microglial cells and the number of ingested beads per cell were counted using ImageJ [27]. Details are provided in Supplementary materials and methods.

Mouse experiments

Nude mice were pre-treated via intraperitoneal (i.p.) injection with secretomes (obtained from parental 231 and its organotropic variants) or with TLQP-21 (Bachem, Bubendorf, Switzerland), a VGF-derived peptide that spans residues 556–576 of the precursor sequence, to evaluate their impact on BBB integrity and microglial modulation.

To assess brain colonization, nude mice were pre-treated with secretomes (parental 231 and 231.Brain. HER2) for 15 days or with TLQP-21 for 3 days. One day after the final treatment, mice were injected intracardially with 1×10^5 231.Brain luciferase-expressing cells in phosphate-buffered saline (PBS).

Follow-up of the mice was performed as described previously [28].

All the experiments were conducted with adherence to the 3Rs (replacement, reduction, and refinement) (JP_2016_02 Project, Animal Ethics Committee, and Animal Welfare Body of i3S) [29]. Details are provided in Supplementary materials and methods.

Immunofluorescence

Cells were fixed with 4% paraformaldehyde (PFA) for 20 min. Brain tissues were post-fixed in 4% PFA for 24 h. The protocol and details of antibodies can be found in Supplementary materials and methods.

Western blotting

Western blotting was performed as described previously [30]. The protocol and details of antibodies can be found in Supplementary materials and methods.

Proteomic analysis

Proteins (100 µg) were processed for proteomics analysis following the solid-phase-enhanced sample-preparation (SP3) protocol, as described by Hughes *et al* [31]. The proteomic data have been deposited in the ProteomeXchange Consortium via the PRIDE [32] partner repository with the dataset identifier PXD044100. Additional details are provided in Supplementary materials and methods and raw data are provided in supplementary material, Table S1.

Kaplan–Meier plotter survival analysis for *VGF* mRNA

The Kaplan–Meier (K–M) plotter online survival analysis tool (https://kmplot.com) was used to assess the impact of *VGF* mRNA levels on overall survival (OS) in BC patients. Additional details are provided in Supplementary materials and methods.

Primary breast cancer cohort

A series of 218 primary breast carcinomas diagnosed between 1978 and 1992 were retrieved from the Pathology Department, Hospital Xeral-Cíes, Vigo, Spain. Patient follow-up information was available for all 218 cases (supplementary material, Table S2), with a maximum follow-up of 120 months after diagnosis. The tumors were characterized for clinical and pathological features, as previously described [33]. All analyses were performed according to the REMARK (REporting recommendations for tumor MARKer prognostic studies) recommendations for prognostic and tumor marker studies. Details are provided in Supplementary materials and methods.

Metastasic breast cancer cohort

We used two complementary paired primary and metastatic BC cohorts ($N = 104$) (supplementary material, Table S2). The first cohort was retrospectively collected from the archives of the Department of Pathology of the Portuguese Oncology Institute of Porto (IPO Porto) and includes primary breast tumors that metastasized to the lung ($n = 17$), bone ($n = 56$), and brain ($n = 4$). The second one is an exclusive BC brain metastasis series with paired primary breast tumors and their corresponding brain metastasis ($n = 27$), which was retrospectively collected from Barretos Cancer Hospital, Brazil.

The present study was conducted with the approval of the Ethics Commission from both cancer centers, under the national regulatory law for the usage of biological specimens from tumor banks, where the samples are exclusively available for research purposes in retrospective studies (ethical approvals: Portuguese Oncology Institute of Porto, CES. 64/023; Barretos Cancer Hospital/Fundação Pio XII, 2-777-372). Details are provided in Supplementary materials and methods.

Data mining from publicly available datasets

RNA expression data from a total of 209 primary tumors from BC patients who had relapsed with metastases to the brain ($n = 21$), lung ($n = 59$), and bone ($n = 125$) were downloaded from the Genomic Data Commons on 2 January 2024. The available clinical information was retrieved from Bos *et al* [24]. Details are provided in Supplementary materials and methods.

Immunohistochemistry

Immunohistochemistry for IBA1, pan cytokeratin (C2562; Sigma-Aldrich, Darmstadt, Germany), and

© 2024 The Pathological Society of Great Britain and Ireland. www.pathsoc.org

10969896, 2024, 2, Downloaded from https://pathsocjournals.onlinelibrary.wiley.com/doi/10.1002/path.6319 by Universidade Do Porto Faculdade de Engenharia, Wiley Online Library on [29/04/2025]. See the Terms and Conditions (https://onlinelibrary.wiley.com/terms-and-conditions) on Wiley Online Library for rules of use; OA articles are governed by the applicable Creative Commons License

VGF was performed on 3-µm sections. Further information regarding the protocol and antibodies can be found in Supplementary materials and methods.

Immunohistochemical evaluation

The expression of VGF was independently evaluated by one pathologist (FS) based on grading systems previously established for other markers [34,35]. Details are provided in Supplementary materials and methods.

Statistical analyses

Prism software (GraphPad, v9.0; GraphPad Software Inc., San Diego, CA, USA) and IBM® SPSS® Statistics v.26 (SPSS Inc., Chicago, IL, USA) were used for statistical analysis, as detailed in Supplementary materials and methods.

Results

The secretomes of brain organotropic breast cancer cells affect BBB integrity

Our goal was to evaluate the impact of the secretomes produced by brain organotropic BC cells on the preparation of the brain PMN, with particular emphasis on BBB permeability and microglial activation. As models, brain organotropic BC cells (without or with HER2 overexpression), derived from the parental 231, were used (supplementary material, Figure S1). To control for brain metastatic specificity, the results were always compared with data obtained with 231.Lung and 231. Bone organotropic BC cells.

To investigate the impact of the secretome of brain organotropic BC variants on the remodeling of the brain PMN, we started by evaluating BBB integrity. We found that the secretome of both brain organotropic BC variants showed a specific and significant increase in cell permeability (Figure 1A) and a decrease in TEER (Figure 1B) of hCMEC/D3 monolayers. Interestingly, this significant effect was not seen with the secretome of the parental 231, or with those from the non-brain organotropic BC variants. By immunofluorescence analysis, we observed a significant decrease in β-catenin expression in hCMEC/D3 cells, in the presence of the secretomes of both brain organotropic BC variants (Figure 1C,D), indicating *in vitro* disruption of the EC intercellular junctions.

These results were further confirmed by the *in vivo* mice secretome-induced model (supplementary material, Figure S2). After priming mice with secretomes for 15 days, we showed a significant and specific impact of the secretome of both brain organotropic BC variants on BBB permeability. This was evidenced by an increased accumulation of a fluorescent dye in the brain, compared with the secretome of the parental 231, MCF7 (non-metastatic BC cells), and serum-free culture medium (control condition) (Figure 1E,F). Although the secretome from the non-brain organotropic BC variants also showed a small impact on *in vivo* permeability after region of interest (ROI) measurement (Figure 1F), this effect was more pronounced and specific when nude mice were pre-treated with the secretome from both brain organotropic BC cells. Further *ex vivo* BBB analysis showed that the brains of these animals tended to have increased fluorescence intensity of collagen IV after treatment with the secretomes from all organotropic BC cells, although not statistically significant (Figure 1G,H). Nevertheless, the immunofluorescence images revealed evident disorganization and clustering of collagen IV, particularly seen after treatment with secretomes from brain organotropic BC cells (Figure 1G), which could explain the observed increase in BBB permeability *in vivo*. Additionally, we observed a significant and very pronounced accumulation of albumin in the brains of mice treated exclusively with secretomes from brain organotropic BC cells (Figure 1G,I), confirming structural and functional changes in BBB integrity in the prefrontal cortex.

Taken together, these data provide strong evidence that the secretome of brain organotropic BC cells causes BBB disruption, thus promoting the passage of molecular factors through this unique brain barrier.

The secretomes of brain organotropic breast cancer cells promote microglial activation

Some studies have demonstrated that microglia can be recruited and activated during brain metastatic colonization [36–42]. However, little is known about their role in the remodeling of the brain microenvironment in the early stages of the metastatic cascade, more specifically during the formation of the brain PMN. To understand the impact of the secretomes of brain organotropic BC cells on microglial activation, HMC3 cells were pre-treated with the secretomes collected from the parental 231 and its organotropic BC variants to evaluate their phagocytic capacity, as well as their Stat3 phosphorylation.

Our *in vitro* data demonstrate that the secretome of both brain organotropic BC cell lines promotes microglial activation, as this treatment significantly increased both phagocytic capacity (Figure 2A and supplementary material, Figure S3A) and Stat3 phosphorylation (Figure 2B,C) of microglia cells compared with the control condition. Nevertheless, the secretome of the other non-brain organotropic variants also induced microglial activation, indicating that the previously observed specificity for the BBB does not occur in this setting.

To validate these findings, we evaluated the role of all secretomes on the microglial cell population in the cerebral cortex of mouse models. Immunohistochemical analysis for IBA1 (a marker of microglia) (supplementary material, Figure S3B) was conducted, where microglia cells were counted in the cerebral cortex, and the positive area and staining intensity of each cell were quantified to measure its degree of activation. Interestingly, we demonstrated that the secretome of

© 2024 The Pathological Society of Great Britain and Ireland. www.pathsoc.org

10969896, 2024, 2, Downloaded from https://pathsocjournals.onlinelibrary.wiley.com/doi/10.1002/path.6319 by Universidade Do Porto Faculdade de Engenharia, Wiley Online Library on [29/04/2025]. See the Terms and Conditions (https://onlinelibrary.wiley.com/terms-and-conditions) on Wiley Online Library for rules of use; OA articles are governed by the applicable Creative Commons License

parental 231 and the secretome of 231.Bone significantly increased the positive area; however, the results were more pronounced with the secretome of both brain organotropic BC cell lines (Figure 2D). In addition, these secretomes significantly increased the staining intensity per cell (Figure 2E), an effect not observed

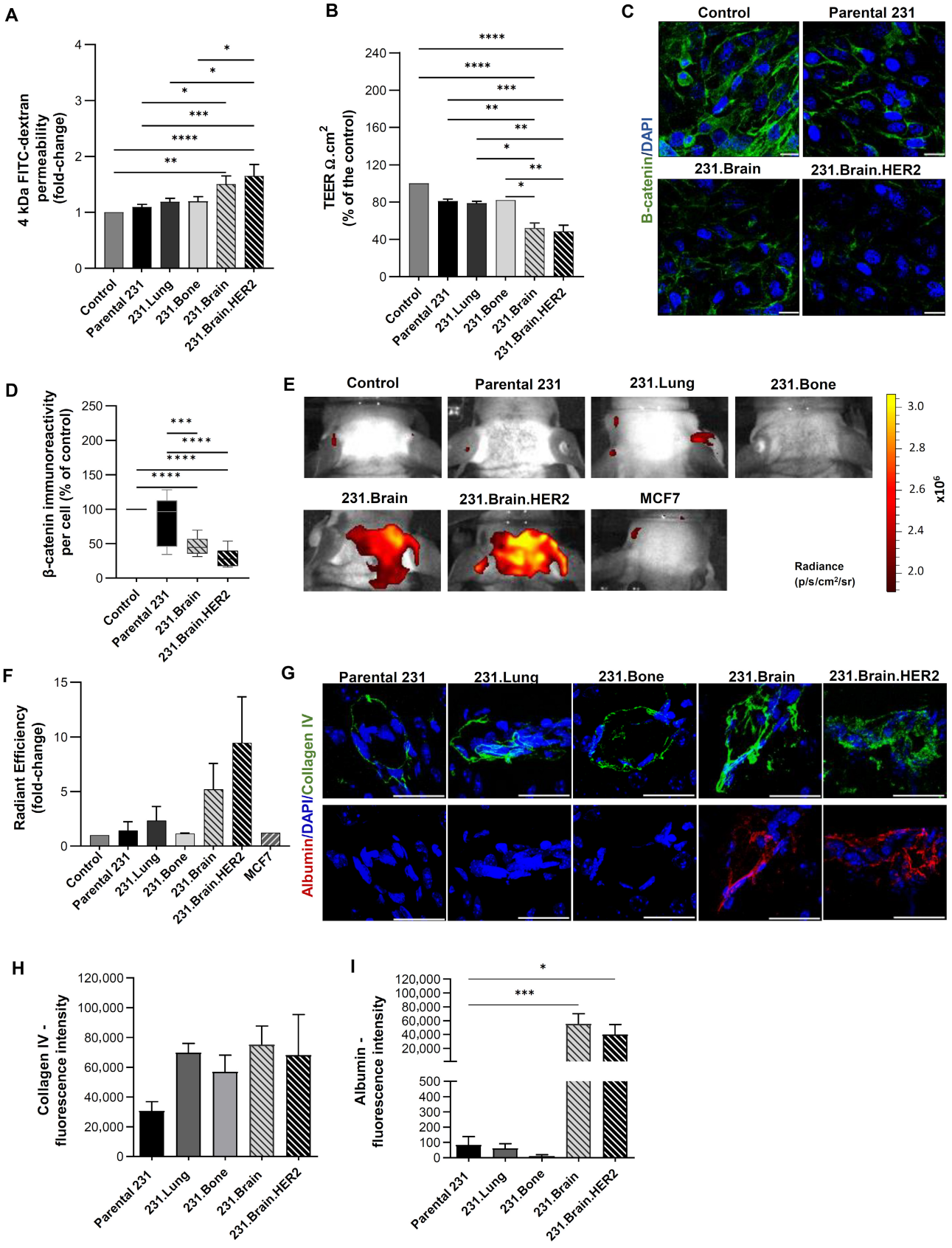


Figure 1 Legend on next page.

© 2024 The Pathological Society of Great Britain and Ireland. www.pathsoc.org

10969896, 2024, 2, Downloaded from https://pathsocjournals.onlinelibrary.wiley.com/doi/10.1002/path.6319 by Universidade Do Porto Faculdade de Engenharia, Wiley Online Library on [29/04/2025]. See the Terms and Conditions (https://onlinelibrary.wiley.com/terms-and-conditions) on Wiley Online Library for rules of use; OA articles are governed by the applicable Creative Commons License

with the secretome of parental 231 and the other organotropic BC cells. These data suggest that factors present in the secretome of both brain organotropic BC cell lines trigger a more prominent response on microglia cells during the brain PMN formation.

To confirm whether these modifications in the brain microenvironment during the early stages of the metastatic cascade promote brain colonization, we conducted a brain metastasis colonization assay. Interestingly, we observed that mice pre-treated with the secretome of 231.Brain.HER2 cells exhibited an increased luminescence in the brain, when compared with the mice pre-treated with 231 secretome, suggesting that BC cells have reached and colonized the brain more efficiently than in the control animals (supplementary material, Figure S6A–C). These results suggest that the secreted factors in the 231.Brain.HER2 secretome play a key role in creating a favorable environment for brain metastasis.

The identification of a brain-specific protein secretome signature

To identify a specific brain secretome signature, high-throughput proteomic label-free quantitation analysis of the secretome of parental 231 and its organotropic BC variants was performed. We identified a total of 9,064 peptides, but only 341 peptides were found to be differentially expressed in the secretome of all organotropic BC cells compared with that of the parental 231. In detail, within these peptides, 120 were differentially expressed in the secretome of 231.Lung, 75 in 231.Bone, 76 in 231.Brain, and 70 in 231.Brain.HER2. We observed a specific secretome signature for each metastatic location, as evidenced by unsupervised hierarchical clustering analysis (supplementary material, Figure S4A). Interestingly, by principal component analysis (PCA), we observed the secretome of parental 231 and the secretome of 231.Lung clusters close to each other, whereby the secretome of both brain organotropic BC variants are more similar to the secretome of 231.Bone (supplementary material, Figure S4B). To identify the specific deregulated peptides present in the secretome of both brain organotropic BC variants, we intersected the lists of significantly deregulated peptides. From this analysis, we identified six common peptides that were differentially expressed in both brain organotropic BC variants: ribosomal protein S15 (SP15), capping actin protein of muscle Z-line subunit beta (CAPZB), monoglyceride lipase (MGLL), utrophin (UTRN), NOP16 nucleolar protein (NOP16), and nerve growth factor inducible (VGF) (Figure 3A). Of these, we focused on VGF due to its role in brain-related disorders, as well as its increased potential as a putative prognostic factor in BC, as identified by survival analysis using the K–M plotter (supplementary material, Table S3). We further validated that VGF was significantly enriched both at the cell level and in the secretome of both brain organotropic BC cell lines (Figure 3B,C and supplementary material, Figure S4C).

VGF promotes BBB disruption and microglial activation

We next investigated the role of VGF in the remodeling of the brain PMN, starting with its impact on BBB structure and function. We pre-treated the hCMEC/D3 cell monolayer with TLQP-21, a bioactive C-terminal VGF-derived peptide, for 24 h. Interestingly, we found similar permeability and TEER values to those observed with the secretome of 231.Brain.HER2, compared with the control condition (Figure 4A,B). Since TLQP-21 binds to the complement component 3a receptor 1 (C3aR1), which is expressed in brain ECs [43], we further used a C3aR antagonist (C3aRA) in the subsequent experiments. Thus, we co-exposed hCMEC/D3 to the endogenous VGF secreted by 231.Brain.HER2 or exogenous VGF in combination with the selective antagonist for C3aR. Interestingly, we verified that the increase in endothelial permeability and the decrease in TEER values induced by exogenous and endogenous VGF were significantly prevented, proving that C3aR mediates VGF-induced BBB hyperpermeability. Furthermore, we observed a significant decrease in β-catenin and ZO-1 (Figure 4C–E) protein levels in EC monolayers after treatment with the exogenous TLQP-21 peptide, similar to what was observed with the secretome of 231.Brain.HER2. Accordingly, this result was also blocked in the presence of the C3aRA.

Figure 1. The secretome of brain organotropic breast cancer cells promotes BBB disruption. (A–D) hCMEC/D3 cell monolayers were treated with serum-free medium (control condition) and secretomes collected from parental 231 cells and their organotropic breast cancer variants. (A) *In vitro* permeability was assessed using 4 kDa FITC-dextran, and (B) transendothelial electrical resistance (TEER) assay was performed after 24 h of treatment ($n = 4$ biological replicates; results presented as mean ± SEM). (C) Representative confocal images of β-catenin staining. β-Catenin is shown in green and DAPI in blue. Scale bar: 20 μm. (D) Quantification of β-catenin expression after treatment with the secretome of parental 231 and brain organotropic variants ($n = 3$ biological replicates; results presented as mean ± SEM). (E) *In vivo* near-infrared fluorescence brain imaging was conducted after 15 days of treating mice with serum-free medium (control condition), the secretome of parental 231 cells and their organotropic breast cancer cells, and the secretome of MCF7 (a non-metastatic breast cancer cell line, serving as a negative control). Representative images of mouse brains acquired at 30 min post-injection of Cy7.5-dextran 5 kDa. (F) Quantification of radiant efficiency in equal-sized regions of interest (ROI) corresponding to the top of the skull (3/4 animals per group; results presented as mean ± SEM). (G) Representative confocal images of collagen IV (a marker of the basal membrane supporting brain vessels) and albumin (a marker of BBB disruption) staining after treatment with parental 231 and their organotropic BC cells. Collagen IV is shown in green, albumin in red, and DAPI in blue. Scale bar: 20 μm. (H, I) Quantification of collagen IV and albumin mean fluorescence intensity (MFI) (two mice per group, ten independent areas; the results are expressed as mean ± SEM). Statistical significance was assessed using one-way ANOVA. $^{*}p < 0.05$, $^{**}p < 0.01$, $^{***}p < 0.001$, $^{****}p < 0.0001$.

© 2024 The Pathological Society of Great Britain and Ireland. www.pathsoc.org

10969896, 2024, 2, Downloaded from https://pathsocjournals.onlinelibrary.wiley.com/doi/10.1002/path.6319 by Universidade Do Porto Faculdade de Engenharia, Wiley Online Library on [29/04/2025]. See the Terms and Conditions (https://onlinelibrary.wiley.com/terms-and-conditions) on Wiley Online Library for rules of use; OA articles are governed by the applicable Creative Commons License

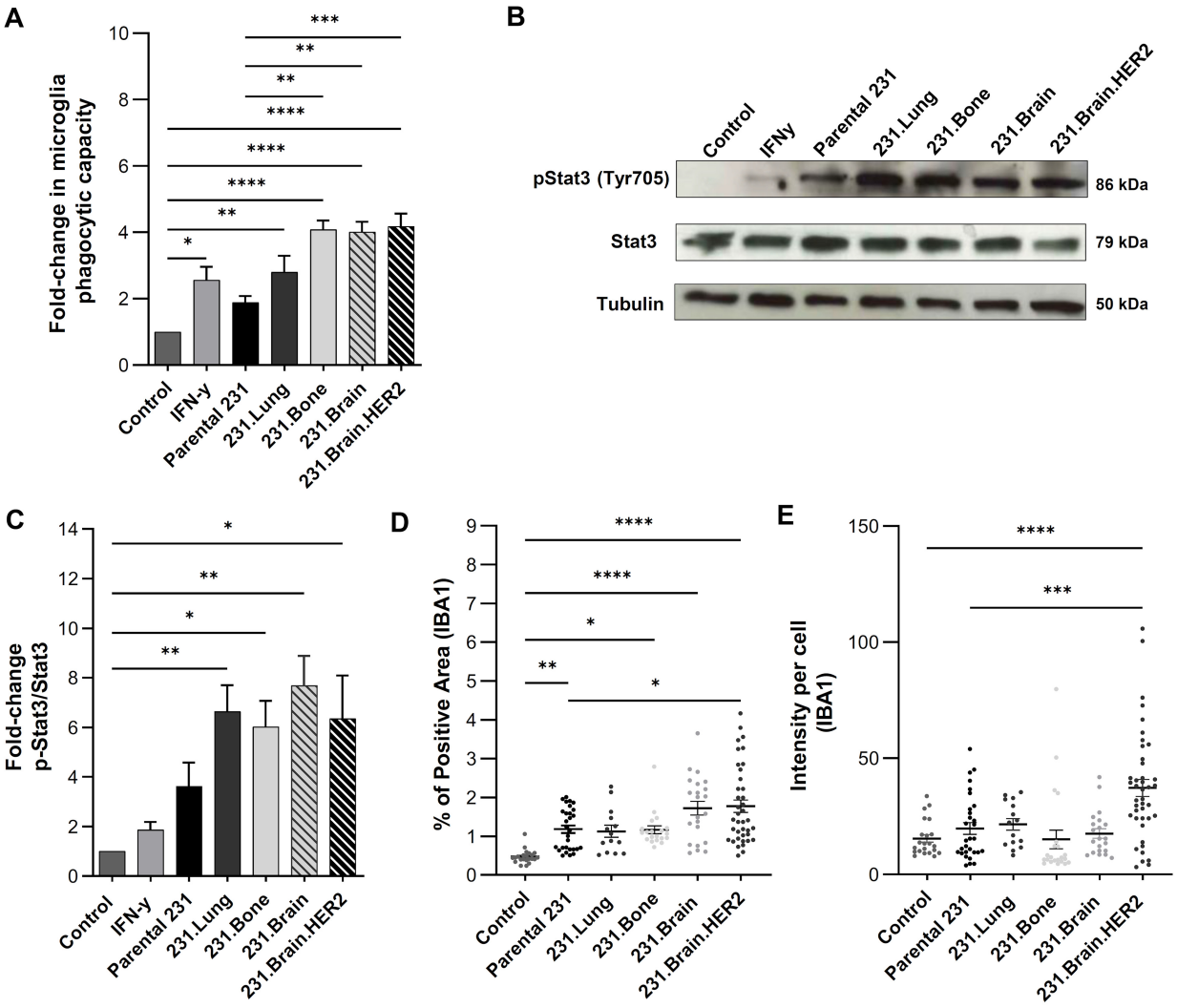


Figure 2. The secretome of brain organotropic breast cancer cells impacts microglia activation. (A) Quantification of microglia phagocytic capacity after treatment with serum-free culture medium (control condition), IFN-γ (positive control), as well as with the secretomes of parental 231 and their organotropic breast cancer variants for 8 h ($n = 4$ biological replicates; the results are expressed as mean ± SEM). (B) Western blot for Stat3 phosphorylation (pStat3 Tyr705) and Stat3 in HMC3 cell lysates after 8 h of treatment with the serum-free culture medium (control condition), IFN-γ (positive control), as well as with the secretomes of parental 231 and its organotropic breast cancer variants. (C) Quantification of Stat3 phosphorylation over Stat3 normalized to tubulin ($n = 3$ biological replicates; the results are expressed as mean ± SEM). (D) Quantification of microglia positive area and (E) staining intensity per microglia cell in the cerebral cortex of mice after 15 days of treatment with serum-free culture medium (control condition), as well as with the secretomes from the parental 231 and its organotropic breast cancer variants (IBA1, a marker of microglia cells) (three mice per group, 6–8 cerebral cortex independent areas; the results are expressed as mean ± SEM). Statistical significance was assessed using one-way ANOVA. *$p < 0.05$, **$p < 0.01$, ***$p < 0.001$, ****$p < 0.0001$.

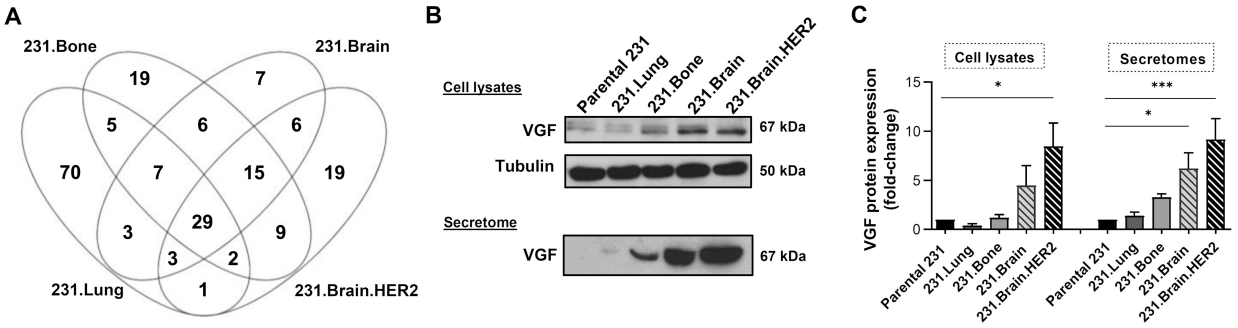


Figure 3. Brain organotropic breast cancer cells show a specific secretome signature. (A) Venn diagram to obtain the specific deregulated peptides in the secretome of both brain organotropic breast cancer variants. (B) Western blot analysis to evaluate the expression and the presence of VGF in cell lysates and the secretomes. (C) Western blot quantification ($n = 4$ and eight biological replicates; the results are expressed as mean ± SEM). Statistical significance was assessed using one-way ANOVA. *$p < 0.05$, ***$p < 0.001$.

© 2024 The Pathological Society of Great Britain and Ireland. www.pathsoc.org

10969896, 2024, 2, Downloaded from https://pathsocjournals.onlinelibrary.wiley.com/doi/10.1002/path.6319 by Universidade Do Porto Faculdade de Engenharia, Wiley Online Library on [29/04/2025]. See the Terms and Conditions (https://onlinelibrary.wiley.com/terms-and-conditions) on Wiley Online Library for rules of use; OA articles are governed by the applicable Creative Commons License

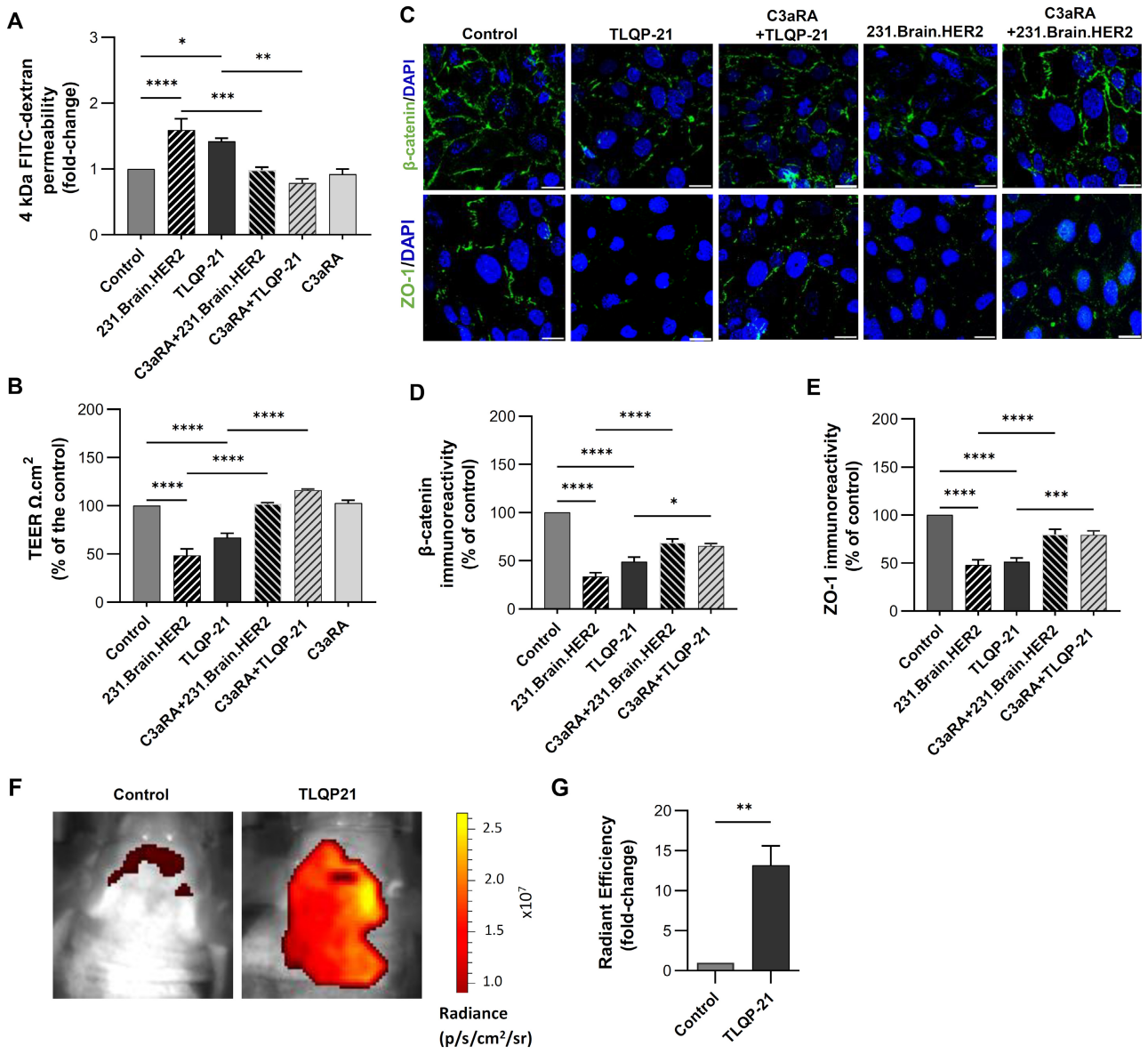


Figure 4. VGF promotes blood–brain barrier disruption. (A, B) Endothelial cell monolayers were treated with TLQP-21 (100 nM), a VGF derived-peptide, and with a secretome of 231.Brain.HER2 in the absence and presence of the C3a receptor antagonist (10 μM) in order to evaluate (A) ECs' monolayer permeability using 4 kDa FITC-dextran and (B) TEER after 24 h of exposure ($n = 4$ biological replicates; the results are expressed as mean ± SEM). (C) Representative confocal images of β-catenin and ZO-1 immunofluorescence. β-Catenin/ZO-1: green; DAPI: blue. Scale bar: 20 μm. (D, E) Quantification of β-catenin and ZO-1 expression. (F, G) *In vivo* dynamic near-infrared fluorescence imaging after 3 days of treatment with serum-free culture medium (control condition) and TLQP-21 (4.5 mg/kg). (F) Representative images of mouse brains acquired at 30 min post-injection of Cy7.5-dextran 5 kDa. (G) Quantification of radiant efficiency in equal-sized ROI corresponding to the top of the skull (four animals per group; results are expressed as mean ± SEM). Statistical significance was assessed using one-way ANOVA. *$p < 0.05$, **$p < 0.01$, ***$p < 0.001$, ****$p < 0.0001$.

The same specific effect was also observed for microglial activation. Pre-treatment with TLQP-21 significantly increased the phagocytic capacity (Figure 5A and supplementary material, Figure S5A) and STAT3 phosphorylation (Figure 5B,C) of microglia cells, compared with the control condition. Interestingly, this effect was abolished when microglia cells were pre-treated with C3aRA, inhibiting VGF-induced effects (Figure 5A–C and supplementary material, Figure S5A).

Importantly, these results were validated *in vivo*. After priming mice with TLQP-21 for three consecutive days, we showed a significant and specific impact on BBB permeability, shown by a significant increase in the accumulation of the fluorescent dye in the brain, compared with the control condition (Figure 4F,G). Immunohistochemical analysis of the mouse brains also revealed that TLQP-21 significantly increased the IBA1-positive area of microglia cells (supplementary material, Figure S5B and Figure 5D), as well as the staining intensity per microglia cell (supplementary material, Figure S5B and Figure 5E).

Furthermore, we investigated the effect of TLQP-21 on brain metastatic capacity using the same approach as previously described. We observed a trend towards increased metastatic ability in the brain after treatment

© 2024 The Pathological Society of Great Britain and Ireland. www.pathsoc.org

10969896, 2024, 2, Downloaded from https://pathsocjournals.onlinelibrary.wiley.com/doi/10.1002/path.6319 by Universidade Do Porto Faculdade de Engenharia, Wiley Online Library on [29/04/2025]. See the Terms and Conditions (https://onlinelibrary.wiley.com/terms-and-conditions) on Wiley Online Library for rules of use; OA articles are governed by the applicable Creative Commons License

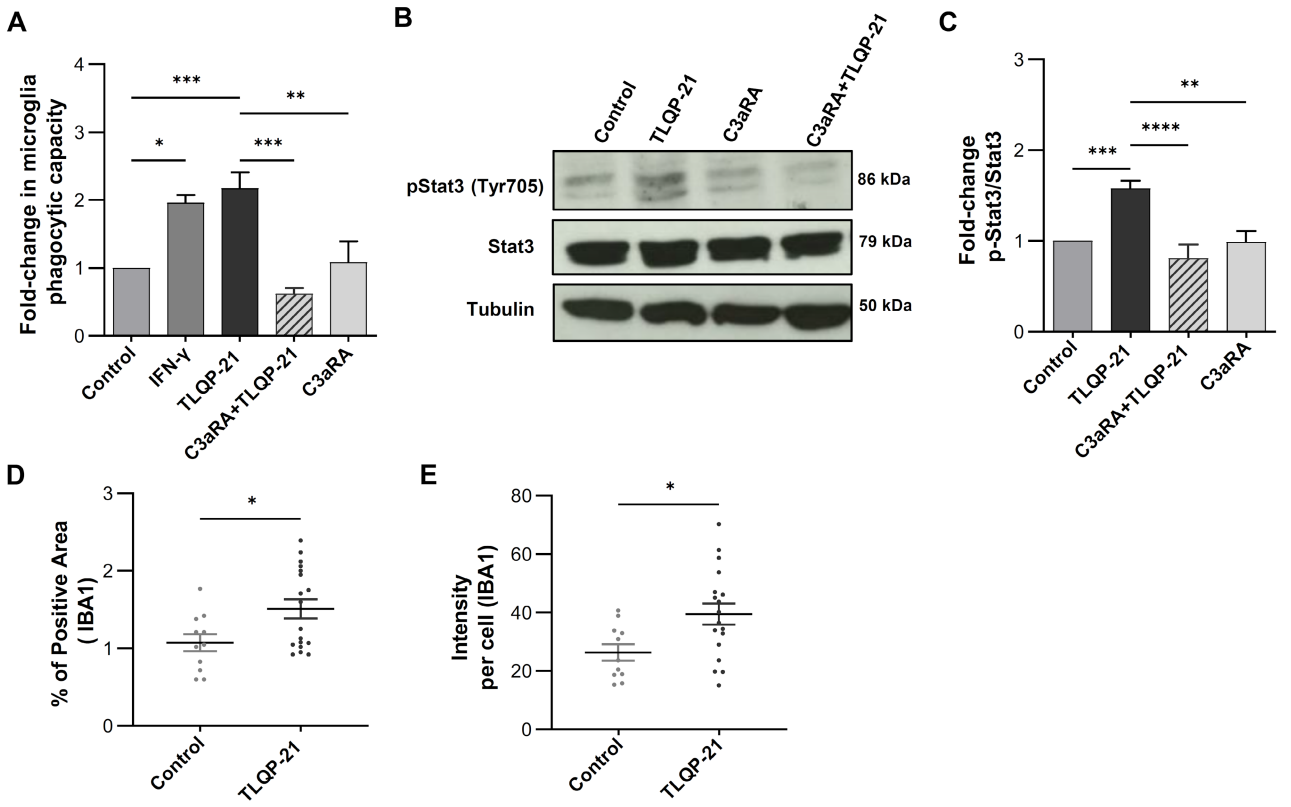


Figure 5. VGF impacts microglia activation. (A) Quantification of microglia phagocytic capacity after treatment with serum-free medium (control condition) and TLQP-21 (100 nM) in the absence or presence of the C3a receptor antagonist (10 μM) for 8 h ($n = 3$ biological replicates; the results are expressed as mean ± SEM). (B) Western blot for Stat3 phosphorylation (pStat3 Tyr705) and Stat3 in microglia cell lysates (HMC3) after 8 h of treatment with serum-free medium (control condition) and TLQP-21 in the presence or absence of the C3a receptor antagonist. (C) Quantification of Stat3 phosphorylation over Stat3 normalized to tubulin ($n = 3$ biological replicates; the results are expressed as mean ± SEM). (D) Quantification of IBA1 microglia positive area and (E) intensity per microglia cell in the cerebral cortex of mice after 3 days of treatment with serum-free medium (control condition) and TLQP-21 (4.5 mg/kg) (two mice per group, 6–8 cerebral cortex independent areas; results are expressed as mean ± SEM). Statistical significance was assessed using one-way ANOVA. *$p < 0.05$, **$p < 0.01$, ***$p < 0.001$, ****$p < 0.0001$.

with TLQP-21 compared with the control condition (supplementary material, Figure S6D–F). Collectively, these findings support the functional role of VGF in impacting BBB stability and activating microglia cells during the early stages of the brain metastatic cascade. This suggests that VGF plays a crucial role in creating an environment in the brain that promotes the establishment of brain metastasis.

VGF expression is associated with a worse prognosis for breast cancer patients

Further, we decided to evaluate the clinical impact of VGF on BC. For that, we started to study *VGF* mRNA expression using the K–M plotter and VGF protein expression in a large series of primary breast carcinomas. K–M survival analysis revealed no correlation between *VGF* mRNA levels and prognosis when considering all molecular subtypes of BC [OS: hazard ratio (HR) = 1.16; $p = 0.12$], as well as luminal A (OS: HR = 0.75, $p = 0.079$) and luminal B (OS: HR = 0.72, $p = 0.11$) subtypes individually. However, *VGF* mRNA expression was significantly associated with a worse prognosis specifically in triple-negative (10-year OS: HR = 1.84, $p = 0.0019$) and in HER2-overexpressing (10-year OS: HR = 1.93, $p = 0.022$) molecular subtypes (supplementary material, Figure S7), which correspond to the molecular subtypes that more frequently metastasize to the brain. Further, we validated these data in a series of primary breast carcinomas previously characterized by our group [33,44]. Immunohistochemical staining revealed that VGF was present in the cytoplasm of cancer cells and in some cases in the adjacent tumor microenvironment, as shown in representative images (supplementary material, Figure S8). Since we were studying the soluble factors secreted by BC cells that could lead to brain PMN remodeling, we considered VGF positivity when there was concomitant expression in cancer cells as well as in the tumor-adjacent stroma. We found that BC patients with VGF-positive tumors showed a significantly lower disease-free survival (DFS) and OS (10-year DFS: $p = 0.009$; 10-year OS: $p = 0.011$) (Figure 6A,B). In addition, VGF positivity significantly correlated with poor BC prognostic markers, such as estrogen receptor (ER) negativity ($p = 0.010$), positive expression for epidermal growth factor receptor (EGFR) ($p = 0.021$), as well as metabolic-associated proteins [CAIX ($p = 0.013$) and GLUT1 ($p = 0.004$)]. More importantly, VGF-positive tumors were significantly associated with HER2 overexpression and triple-negative

© 2024 The Pathological Society of Great Britain and Ireland. www.pathsoc.org

10969896, 2024, 2, Downloaded from https://pathsocjournals.onlinelibrary.wiley.com/doi/10.1002/path.6319 by Universidade Do Porto Faculdade de Engenharia, Wiley Online Library on [29/04/2025]. See the Terms and Conditions (https://onlinelibrary.wiley.com/terms-and-conditions) on Wiley Online Library for rules of use; OA articles are governed by the applicable Creative Commons License

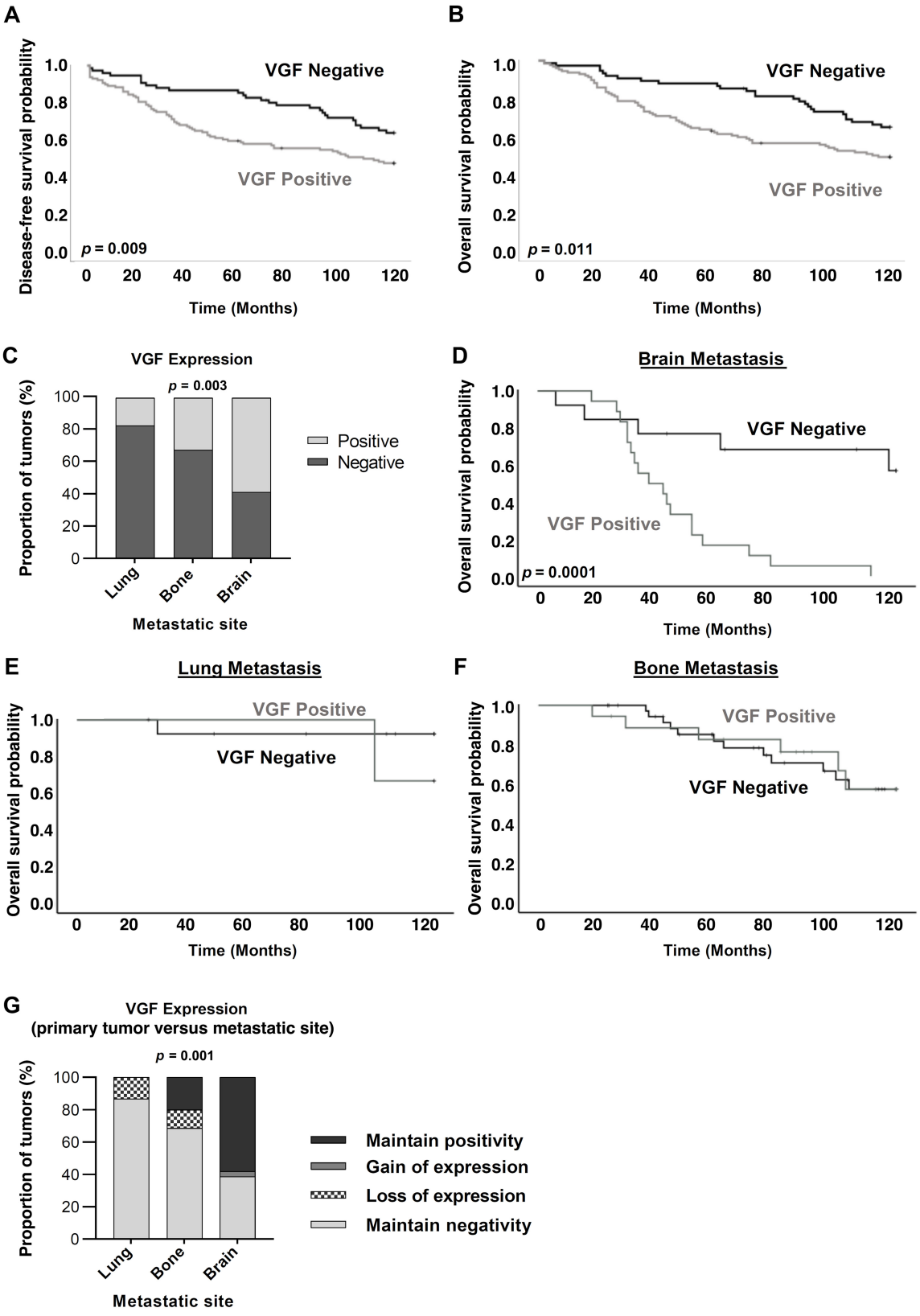


Figure 6. VGF expression is associated with a worse prognosis for breast cancer patients and is a predictive factor for brain metastases. K–M plot analysis for (A) disease-free survival (DFS) and (B) overall survival (OS) based on VGF protein expression using a large series of primary breast carcinomas (DFS: $p = 0.009$ and OS: $p = 0.011$). Black lines indicate patients with VGF-negative tumors; gray lines indicate patients with VGF-positive tumors. Survival analyses were compared using the log-rank test. (C) Correlation analysis of VGF expression in primary breast tumors with their corresponding metastatic location. (D–F) K–M plot analysis for OS based on VGF protein expression in breast cancer metastasis to the brain (OS: $p = 0.0001$) (D), lung (OS: $p = 0.311$) (E), and bone (OS: $p = 0.922$) (F). (G) VGF expression in primary breast tumor and its paired metastasis. The χ^2 test was used to determine associations between groups and the results were considered statistically significant when the p value was less than 0.05.

© 2024 The Pathological Society of Great Britain and Ireland. www.pathsoc.org

10969896, 2024, 2, Downloaded from https://pathsocjournals.onlinelibrary.wiley.com/doi/10.1002/path.6319 by Universidade Do Porto Faculdade de Engenharia, Wiley Online Library on [29/04/2025]. See the Terms and Conditions (https://onlinelibrary.wiley.com/terms-and-conditions) on Wiley Online Library for rules of use; OA articles are governed by the applicable Creative Commons License

($p = 0.029$) molecular subtypes (Table 1), validating the K–M survival analysis.

VGF expression is a poor prognostic factor for breast cancer brain metastases

Finally, the impact of VGF expression was evaluated in predicting the metastatic site. For that, we evaluated its expression in a metastatic BC cohort ($N = 104$ patients), which included paired primary and metastatic tumors from BC patients diagnosed with brain metastasis ($n = 31$), lung metastasis ($n = 17$), and bone metastasis ($n = 56$). The brain metastasis series was significantly associated with poor prognostic features, such as high histological grade, age, and molecular subtype ($p < 0.0001$) (supplementary material, Figure S9A–C and Table S4). We found that primary breast tumors that metastasized to the brain were associated with poor prognostic factors, such as ER ($p < 0.0001$) and progesterone receptor (PR) ($p = 0.002$) negative expression, as well as a higher proliferative index (assessed by Ki-67 labeling) ($p = 0.005$), when compared with primary breast tumors that metastasized to other locations (lung and bone) (supplementary material, Figure S10A). As expected, primary breast tumors that metastasized to the brain were mainly from the HER2 overexpression and triple-negative molecular subtypes ($p < 0.0001$) (supplementary material, Figure S10B). More importantly, we found that primary tumors with VGF-positive expression were significantly associated with an increased propensity to metastasize to the brain (60%), compared with the metastatic propensity to the lung (20%) or bone (25%) ($p = 0.003$) (Figure 6C). Our data from this metastatic cohort demonstrate that VGF exhibits a sensitivity of 58.1% and a specificity of 71.2% as a predictive biomarker for brain metastasis. Given that HER2 overexpression is linked to an increased risk of developing brain metastasis, we further evaluated the sensitivity and specificity of this marker in our metastatic cohort. Surprisingly, the values were notably lower compared with those obtained for VGF. Specifically, the sensitivity of HER2 as a predictive biomarker for brain metastasis was approximately 25.81%, with a specificity of 50%.

Besides its potential role as a putative predictive biomarker of brain metastasis, a more significant role was observed as a prognostic biomarker. In detail, VGF positivity shows a significantly worse impact on BC patients with metastasis to the brain, with no significant differences observed in the OS of patients with metastasis to the lung or bone (Figure 6D–F). These data were further confirmed by an independent TCGA cohort from metastatic BC (supplementary material, Figure S11A–E). In our analysis, we observed that primary tumors expressing VGF maintained this expression in brain metastases. This suggests a consistent pattern of VGF expression retention during the metastatic process specifically in the brain. Conversely, primary tumors from patients with metastases to other organs did not exhibit an enrichment in VGF expression in the metastatic tumor ($p = 0.001$) (Figure 6G). This disparity in VGF expression dynamics between brain metastases and

Table 1. Association analysis of VGF expression in primary breast tumors with classical breast cancer poor prognostic factors such as ER ($p = 0.010$), EGFR ($p = 0.021$), CAIX ($p = 0.013$), GLUT1 ($p = 0.004$), and breast cancer molecular subtypes ($p = 0.029$). The χ^2 test was used to determine associations between groups and the results were considered statistically significant when the p value was less than 0.05.

		VGF-negative		VGF-positive		p value
		$n = 68$		$n = 143$		
		Frequency	%	Frequency	%	
ER	Negative	15	22.4	54	38.0	0.01
	Positive	52	77.6	88	62.0	
	Missing	2		1		
PR	Negative	36	52.9	88	62.0	n.s
	Positive	32	47.1	54	38.0	
	Missing	0		1		
HER2	Negative	64	94.1	118	84.9	n.s
	Positive	4	5.9	21	15.1	
	Missing	0		4		
EGFR	Negative	67	98.5	128	89.5	0.021
	Positive	1	1.5	15	10.5	
	Missing	0		0		
CAIX	Negative	34	53.1	49	34.8.	0.013
	Positive	30	46.9	92	65.2	
	Missing	4		2		
GLUT1	Negative	60	92.3	105	75.5	0.004
	Positive	5	7.7	34	24.5	
	Missing	3		4		
Molecular subtype	Luminal A-like	27	40.9	44	32.6	0.029
	Luminal B-like	26	39.4	46	34.1	
	HER2-overexpressing	1	1.5	12	8.9	
	Triple-negative	12	18.2	33	24.4	
	Missing	2		8		

EGFR, epidermal growth factor receptor; ER, estrogen receptor; PR, progesterone receptor.

© 2024 The Pathological Society of Great Britain and Ireland. www.pathsoc.org

10969896, 2024, 2, Downloaded from https://pathsocjournals.onlinelibrary.wiley.com/doi/10.1002/path.6319 by Universidade Do Porto Faculdade de Engenharia, Wiley Online Library on [29/04/2025]. See the Terms and Conditions (https://onlinelibrary.wiley.com/terms-and-conditions) on Wiley Online Library for rules of use; OA articles are governed by the applicable Creative Commons License

metastases in other organs underscores the potential significance of VGF as a prognostic biomarker for brain metastasis in BC, opening an interesting avenue for VGF as a potential clinical target in the context of brain metastasis.

Discussion

BC is the most common cancer among women worldwide, often metastasizing to various organs, including the brain, which significantly impacts patient survival. To explore the mechanisms underlying brain metastasis, we used organotropic MDA-MB-231 cell models for the lung, bone, and brain, which were embedded in collagen type I. We selected this ECM type over other formulations more prevalent in normal breast tissue, containing laminin, collagen IV, and entactin, since collagen type I predominates in the tumor microenvironment and plays a more prominent role in promoting cancer progression [45]. Additionally, another brain organotropic cell line transfected with HER2 (231.Brain.HER2) was also included since its overexpression induces extensive brain metastasis occurrence in mice [25]. In our study, we demonstrated that the secretome of brain organotropic BC cells disrupts BBB integrity, suggesting that the secretion of specific factors may play an important role in remodeling the brain microenvironment, creating a more permissive site for cancer cell brain colonization. These findings were contrasted with secretomes from non-brain organotropic cells to ensure brain metastatic specificity. Interestingly, we did not observe a decrease in collagen IV deposition, as commonly observed in BBB disruption situations, but instead a tendency to increase collagen IV expression. Still, a striking and specific pattern of expression was observed in the brains of mice treated with secretomes from brain organotropic cells. Our immunofluorescence images revealed disorganization and clustering of collagen IV, which may contribute to increased BBB permeability. This phenomenon has been documented in other pathological conditions, such as epilepsy and stroke, where increased, but delocalized, collagen IV expression is associated with dysfunctional BBB [46,47]. However, it remains unclear whether this increase in collagen IV expression is directly linked to the formation of new and more leaky blood vessels. Further investigation is warranted to elucidate the underlying mechanisms driving this phenomenon. Nonetheless, the functional impact on BBB integrity was corroborated by the specific accumulation of serum albumin in the brains of mice treated with secretomes from brain organotropic BC cells. This finding highlights the specificity of BBB disruption induced by these secretomes and underscores the potential significance of our observations in understanding the pathophysiology of brain metastasis in BC. Further research in this area may lead to the development of novel therapeutic strategies targeting BBB integrity in metastatic BC.

Our data are in accordance with previous studies demonstrating that factors secreted by cancer cells promote BBB dysfunction by altering the expression and localization of key BBB proteins, namely tight junction proteins. This can lead to increased BBB permeability, allowing cancer cells to enter the brain and potentially form metastases [21,48–50]. In particular, Lu *et al* demonstrated that exosomal lncRNA GS1-600G8.5 secreted by brain organotropic BC cells increases *in vitro* BBB permeability, promoting the passage of BC cells across the EC monolayer [49]. Moreover, it was recently demonstrated that brain organotropic BC cells secrete CEMIP^{+} exosomes that can be taken up by ECs and microglia cells, inducing brain vascular remodeling and inflammation [21].

In addition to a restrictive vascular barrier, the brain is composed of unique resident cells, such as microglia, which play an important role in the immune response after injury. Accordingly, considering cancer progression, microglia cells have also been described as being responsible for identifying and attacking cancer cells that have invaded the brain [51,52]. Nevertheless, some studies suggest that microglia can also promote the growth and spread of metastatic cells in the brain, contrasting with its tumor surveillance function [36–42]. Louie *et al* demonstrated that NT-3 promotes the growth of metastases by decreasing microglial cell activation [37]. In contrast, another study demonstrated that XIST loss in BC cells increased the release of exosomal microRNA-503, which promotes an *in vitro* anti-inflammatory microglial phenotype [38]. Therefore, using the secretome from brain organotropic BC cells, we looked for microglial modifications and found that, in contrast with the specific impact of brain-derived secretome on BBB integrity, all secretomes from lung, bone, and both brain organotropic cell lines were able to promote microglial activation, as measured by their *in vitro* phagocytic capacity and Stat3 phosphorylation. Considering that *in vitro* microglial cell culture is frequently performed under artificial conditions, which can alter microglial behavior and limit the relevance of experimental findings [53,54], we also evaluated the impact of the secretomes on microglia using *in vivo* studies. Importantly, we observed that only the secretome of brain organotropic BC cells with HER2 overexpression could promote modifications in microglia in the cerebral cortex, which is the brain region where metastases most frequently occur [3,55].

Based on these results, we sought to determine the soluble factors responsible for these modifications in the brain PMN. Through proteomic analysis, we identified VGF as a significant peptide deregulated in brain organotropic BC secretomes. VGF undergoes proteolytic processing to generate multiple bioactive peptides implicated in various brain biological processes such as neuronal growth, differentiation, synaptogenesis, and synaptic plasticity [44,56–60]. While extensively studied in brain disorders, including obesity, diabetes, and neurodegenerative diseases, TLQP-21 emerges as the most prevalent VGF-derived peptide, known for its involvement in these conditions [58,61–64]. Despite its association with

© 2024 The Pathological Society of Great Britain and Ireland. www.pathsoc.org

10969896, 2024, 2, Downloaded from https://pathsocjournals.onlinelibrary.wiley.com/doi/10.1002/path.6319 by Universidade Do Porto Faculdade de Engenharia, Wiley Online Library on [29/04/2025]. See the Terms and Conditions (https://onlinelibrary.wiley.com/terms-and-conditions) on Wiley Online Library for rules of use; OA articles are governed by the applicable Creative Commons License

poor prognosis in diseases such as glioblastoma [65], lung cancer [66], and BC with neuroendocrine features [67], little is known about VGF's role in brain metastasis. To address this gap, we investigated the impact of TLQP-21 on brain pre-metastatic remodeling. Our study revealed that TLQP-21 influences BBB integrity and modulates microglial activity, both *in vitro* and *in vivo*. However, the effect of TLQP-21 on microglial modulation was less pronounced compared with the secretome of brain organotropic BC cells, indicating the involvement of other factors in microglial activation. Interestingly, prior research into Alzheimer's disease has shown that TLQP-21 affects microglial phagocytic capacity, suggesting its broader role in neuro-inflammatory processes. Overall, our findings suggest that VGF, particularly TLQP-21, contributes to brain remodeling, creating a microenvironment conducive to brain metastasis. The observed increase in brain metastasis-promoting potential further supports this notion. However, it is important to acknowledge that these findings require validation in a larger number of animals to establish their significance definitively. Nevertheless, they provide valuable insights into the potential mechanisms underlying brain metastasis and highlight the role of VGF signaling in this process.

Finally, we assessed the clinical significance of VGF expression in BC samples. Our findings revealed a significant association between VGF expression, both in the tumor and in the stroma, and poor prognosis among BC patients. Notably, recent research has linked VGF to resistance against EGFR kinase inhibitors, inducing epithelial-to-mesenchymal transition (EMT) and correlating with adverse outcomes in patients with lung adenocarcinoma [66]. Given the frequent metastasis of both lung and breast cancer to the brain, it is intriguing to note VGF's dual role in glioblastoma, where it promotes the survival and self-renewal of glioblastoma stem cells while enhancing the proliferation of differentiated glioblastoma cells [65]. Our study revealed a specific association between VGF-positive breast tumors and brain metastasis, distinct from metastases to other organs such as the lung or bone. VGF expression demonstrated a sensitivity of 58.1% and a specificity of 71.2% as a predictive biomarker for brain metastasis, highlighting its potential in this context. Additionally, we assessed the sensitivity and specificity of HER2 overexpression, a known factor in brain metastasis risk, which yielded notably lower values compared with VGF in this specific metastatic cohort. Furthermore, despite exhibiting a lower specificity than previously described potential predictive/prognostic biomarkers such as FN14 and GRP94, VGF showed a higher sensitivity [68], indicating its potential as a more sensitive biomarker for identifying BC patients at risk of brain metastasis. Besides its potential impact as a predictive biomarker for brain metastasis, a more important role was shown as a prognostic biomarker. Our data, further confirmed by independent TCGA datasets, have identified VGF as a poor prognostic predictor for BC patients with brain metastasis. Its role as a prognosis biomarker was only significant in the brain metastatic setting, suggesting that VGF would have an important and specific role in the establishment and growth of brain metastasis. In fact, VGF has been described as a crucial secreted factor for the maintenance of glioblastoma stem cells [65], therefore favoring the growth of cancer cells. In accordance, we also tested the role of VGF in cancer stem cell activity, and we found that TLQP-21 improves the mammosphere-forming efficiency of BC cells (data not shown), suggesting that it can have an important role for the maintenance and growth of already established BC brain metastasis. Therefore, further research into the specific mechanisms underlying VGF's involvement in brain metastasis progression is needed.

In summary, our research revealed a novel role for VGF in brain remodeling, contributing to BBB disruption and microglial activation, thereby preparing a supportive and receptive PMN for the growth and survival of cancer cells in the brain. Moreover, its specific impact as a poor prognostic predictor for BC patients with brain metastasis opens new avenues to use VGF as a potential therapeutic target for BC patients at an elevated risk of developing brain metastasis.

Acknowledgements

MDA-MB-231BC organotropic variants were kindly provided by Joan Massagué's Laboratory (Sloan Kettering Institute, Memorial Sloan Kettering Cancer Center, NY, USA.) The MDA-MB-231.Brain. HER2-overexpressing cells were kindly provided by Patricia S Steeg's Laboratory (Center for Cancer Research, National Cancer Institute, Bethesda, MD, USA). We thank all patients and clinicians for their participation in this study. Dr Cristiano Souza, Márcia Marques, Vinícius Duval da Silva, Alison Barroso, and Daniel Preto compiled patient data from Barretos Cancer Hospital. Jorge Cameselle-Teijeiro compiled patient data from the Pathology Department at Hospital Xeral-Cíes, Vigo, Spain. We acknowledge the i3S Proteomics Scientific Platform. The mass spectrometry technique was performed by Hugo Osório, and the work had the support from the Portuguese Mass Spectrometry Network, integrated into the National Roadmap of Research Infrastructures of Strategic Relevance (ROTEIRO/0028/2013; LISBOA-01-0145-FEDER-022125). We acknowledge the assistance of Nuno Mendes from the HEMS core facility at i3S. The i3S Scientific Platform HEMS is a member of the national infrastructure PPBI – Portuguese Platform of Bioimaging (PPBI-POCI-01-0145-FEDER-022122). We acknowledge the assistance of Bruno Cavadas from the i3S Bioinformatics platform at i3S. This work was funded (in part) by the NORTE 2030 (Programa Operacional Regional do Norte 2021–2027) and co-funded by the European Regional Development Fund under the project 'The Porto Comprehensive Cancer Center Raquel Seruca' with the reference NORTE-

© 2024 The Pathological Society of Great Britain and Ireland. www.pathsoc.org

10969896, 2024, 2, Downloaded from https://pathsocjournals.onlinelibrary.wiley.com/doi/10.1002/path.6319 by Universidade Do Porto Faculdade de Engenharia, Wiley Online Library on [29/04/2025]. See the Terms and Conditions (https://onlinelibrary.wiley.com/terms-and-conditions) on Wiley Online Library for rules of use; OA articles are governed by the applicable Creative Commons License

01-0145-FEDER-072678 – Consórcio P.CCC – Porto. Comprehensive Cancer Center. It was also funded by Fundação para a Ciência e a Tecnologia (FCT) under the project POCI-01-0145-FEDER-030625 and by Hologic Prize 'Saúde da Mulher' 2023. FCT funded the research grants of RC (SFRH/BD/135831/2018) and IC (SFRH/BD/14381/2022).

Author contributions statement

ASR and RC conceived the structure of the work. RC was involved in all experimental work. RC and IC prepared the secretomes. LS and RL performed the brain EC culture experiments and APS and CG performed the respective data analyses. RC, LS, HRSF and ASR performed the *in vivo* experiments. CC-M, JL and CJ compiled patient data from IPOP. FS performed pathology analyses. RC and ASR performed all experimental data analyses. RC and ASR wrote the manuscript. ASR and JP supervised all the work and edited the final version of the manuscript. All authors have read and agreed with the published version of the manuscript.

Data availability statement

The mass spectrometry proteomics data have been deposited in the ProteomeXchange Consortium via the PRIDE partner repository [32] with the dataset identifier PXD044100. All study data are included in the article and/or supplementary material.

References

1. Lin NU, Bellon JR, Winer EP. CNS metastases in breast cancer. *J Clin Oncol* 2004; **22:** 3608–3617.
2. Liu Q, Zhang H, Jiang X, *et al*. Factors involved in cancer metastasis: a better understanding to "seed and soil" hypothesis. *Mol Cancer* 2017; **16:** 176.
3. Chen W, Hoffmann AD, Liu H, *et al*. Organotropism: new insights into molecular mechanisms of breast cancer metastasis. *NPJ Precis Oncol* 2018; **2:** 4.
4. Obenauf AC, Massagué J. Surviving at a distance: organ-specific metastasis. *Trends Cancer* 2015; **1:** 76–91.
5. Müller A, Homey B, Soto H, *et al*. Involvement of chemokine receptors in breast cancer metastasis. *Nature* 2001; **410:** 50–56.
6. Xue H, Lu B, Lai M. The cancer secretome: a reservoir of biomarkers. *J Transl Med* 2008; **6:** 52.
7. Patel S, Ngounou Wetie AG, Darie CC, *et al*. Cancer secretomes and their place in supplementing other hallmarks of cancer. *Adv Exp Med Biol* 2014; **806:** 409–442.
8. Carvalho R, Paredes J, Ribeiro AS. Impact of breast cancer cells' secretome on the brain metastatic niche remodeling. *Semin Cancer Biol* 2020; **60:** 294–301.
9. Hoshino A, Costa-Silva B, Shen TL, *et al*. Tumour exosome integrins determine organotropic metastasis. *Nature* 2015; **527:** 329–335.
10. Zahari S, Syafruddin SE, Mohtar MA. Impact of the cancer cell secretome in driving breast cancer progression. *Cancers (Basel)* 2023; **15:** 2653.
11. Wang Y, Ye F, Liang Y, *et al*. Breast cancer brain metastasis: insight into molecular mechanisms and therapeutic strategies. *Br J Cancer* 2021; **125:** 1056–1067.
12. Nayak L, Lee EQ, Wen PY. Epidemiology of brain metastases. *Curr Oncol Rep* 2012; **14:** 48–54.
13. Nguyen DX, Bos PD, Massagué J. Metastasis: from dissemination to organ-specific colonization. *Nat Rev Cancer* 2009; **9:** 274–284.
14. Franchino F, Rudà R, Soffietti R. Mechanisms and therapy for cancer metastasis to the brain. *Front Oncol* 2018; **8:** 161.
15. Leone JP, Leone BA. Breast cancer brain metastases: the last frontier. *Exp Hematol Oncol* 2015; **4:** 33.
16. Bailleux C, Eberst L, Bachelot T. Treatment strategies for breast cancer brain metastases. *Br J Cancer* 2021; **124:** 142–155.
17. Heitz F, Rochon J, Harter P, *et al*. Cerebral metastases in metastatic breast cancer: disease-specific risk factors and survival. *Ann Oncol* 2011; **22:** 1571–1581.
18. Bryan S, Witzel I, Borgmann K, *et al*. Molecular mechanisms associated with brain metastases in HER2-positive and triple negative breast cancers. *Cancers (Basel)* 2021; **13:** 4137.
19. Peinado H, Alečković M, Lavotshkin S, *et al*. Melanoma exosomes educate bone marrow progenitor cells toward a pro-metastatic phenotype through MET. *Nat Med* 2012; **18:** 883–891.
20. Costa-Silva B, Aiello NM, Ocean AJ, *et al*. Pancreatic cancer exosomes initiate pre-metastatic niche formation in the liver. *Nat Cell Biol* 2015; **17:** 816–826.
21. Rodrigues G, Hoshino A, Kenific CM, *et al*. Tumour exosomal CEMIP protein promotes cancer cell colonization in brain metastasis. *Nat Cell Biol* 2019; **21:** 1403–1412.
22. Minn AJ, Gupta GP, Siegel PM, *et al*. Genes that mediate breast cancer metastasis to lung. *Nature* 2005; **436:** 518–524.
23. Yoneda T, Williams PJ, Hiraga T, *et al*. A bone-seeking clone exhibits different biological properties from the MDA-MB-231 parental human breast cancer cells and a brain-seeking clone *in vivo* and *in vitro*. *J Bone Miner Res* 2001; **16:** 1486–1495.
24. Bos PD, Zhang XH, Nadal C, *et al*. Genes that mediate breast cancer metastasis to the brain. *Nature* 2009; **459:** 1005–1009.
25. Palmieri D, Bronder JL, Herring JM, *et al*. Her-2 overexpression increases the metastatic outgrowth of breast cancer cells in the brain. *Cancer Res* 2007; **67:** 4190–4198.
26. Coelho-Santos V, Socodato R, Portugal C, *et al*. Methylphenidate-triggered ROS generation promotes caveolae-mediated transcytosis via Rac1 signaling and c-Src-dependent caveolin-1 phosphorylation in human brain endothelial cells. *Cell Mol Life Sci* 2016; **73:** 4701–4716.
27. Silva SL, Vaz AR, Barateiro A, *et al*. Features of bilirubin-induced reactive microglia: from phagocytosis to inflammation. *Neurobiol Dis* 2010; **40:** 663–675.
28. Ribeiro AS, Albergaria A, Sousa B, *et al*. Extracellular cleavage and shedding of P-cadherin: a mechanism underlying the invasive behaviour of breast cancer cells. *Oncogene* 2010; **29:** 392–402.
29. Hubrecht RC, Carter E. The 3Rs and humane experimental technique: implementing change. *Animals (Basel)* 2019; **9:** 754.
30. Dionísio MR, Vieira AF, Carvalho R, *et al*. BR-BCSC signature: the cancer stem cell profile enriched in brain metastases that predicts a worse prognosis in lymph node-positive breast cancer. *Cells* 2020; **9:** 2442.
31. Hughes CS, Moggridge S, Müller T, *et al*. Single-pot, solid-phase-enhanced sample preparation for proteomics experiments. *Nat Protoc* 2019; **14:** 68–85.
32. Perez-Riverol Y, Bai J, Bandla C, *et al*. The PRIDE database resources in 2022: a hub for mass spectrometry-based proteomics evidences. *Nucleic Acids Res* 2022; **50:** D543–D552.
33. Ribeiro AS, Sousa B, Carreto L, *et al*. P-cadherin functional role is dependent on E-cadherin cellular context: a proof of concept using the breast cancer model. *J Pathol* 2013; **229:** 705–718.

© 2024 The Pathological Society of Great Britain and Ireland. www.pathsoc.org

10969896, 2024, 2, Downloaded from https://pathsocjournals.onlinelibrary.wiley.com/doi/10.1002/path.6319 by Universidade Do Porto Faculdade de Engenharia, Wiley Online Library on [29/04/2025]. See the Terms and Conditions (https://onlinelibrary.wiley.com/terms-and-conditions) on Wiley Online Library for rules of use; OA articles are governed by the applicable Creative Commons License

34. Ricardo S, Vieira AF, Gerhard R, *et al*. Breast cancer stem cell markers CD44, CD24 and ALDH1: expression distribution within intrinsic molecular subtype. *J Clin Pathol* 2011; **64:** 937–946.
35. Sousa B, Ribeiro AS, Nobre AR, *et al*. The basal epithelial marker P-cadherin associates with breast cancer cell populations harboring a glycolytic and acid-resistant phenotype. *BMC Cancer* 2014; **14:** 734.
36. Foo SL, Sachaphibulkij K, Lee CLY, *et al*. Breast cancer metastasis to brain results in recruitment and activation of microglia through annexin-A1/formyl peptide receptor signaling. *Breast Cancer Res* 2022; **24:** 25.
37. Louie E, Chen XF, Coomes A, *et al*. Neurotrophin-3 modulates breast cancer cells and the microenvironment to promote the growth of breast cancer brain metastasis. *Oncogene* 2013; **32:** 4064–4077.
38. Xing F, Liu Y, Wu SY, *et al*. Loss of XIST in breast cancer activates MSN-c-met and reprograms microglia via exosomal miRNA to promote brain metastasis. *Cancer Res* 2018; **78:** 4316–4330.
39. Lorger M, Felding-Habermann B. Capturing changes in the brain microenvironment during initial steps of breast cancer brain metastasis. *Am J Pathol* 2010; **176:** 2958–2971.
40. Andreou KE, Soto MS, Allen D, *et al*. Anti-inflammatory microglia/macrophages as a potential therapeutic target in brain metastasis. *Front Oncol* 2017; **7:** 251.
41. Pukrop T, Dehghani F, Chuang HN, *et al*. Microglia promote colonization of brain tissue by breast cancer cells in a Wnt-dependent way. *Glia* 2010; **58:** 1477–1489.
42. Simon A, Yang M, Marrison JL, *et al*. Metastatic breast cancer cells induce altered microglial morphology and electrical excitability *in vivo*. *J Neuroinflammation* 2020; **17:** 87.
43. Propson NE, Roy ER, Litvinchuk A, *et al*. Endothelial C3a receptor mediates vascular inflammation and blood–brain barrier permeability during aging. *J Clin Invest* 2021; **131:** e140966.
44. Quinn JP, Kandigian SE, Trombetta BA, *et al*. VGF as a biomarker and therapeutic target in neurodegenerative and psychiatric diseases. *Brain Commun* 2021; **3:** fcab261.
45. Conklin MW, Keely PJ. Why the stroma matters in breast cancer: insights into breast cancer patient outcomes through the examination of stromal biomarkers. *Cell Adh Migr* 2012; **6:** 249–260.
46. Michalski D, Spielvogel E, Puchta J, *et al*. Increased immunosignals of collagen IV and fibronectin indicate ischemic consequences for the neurovascular matrix adhesion zone in various animal models and human stroke tissue. *Front Physiol* 2020; **11:** 575598.
47. Kyriatzis G, Bernard A, Bôle A, *et al*. In the rat hippocampus, pilocarpine-induced status epilepticus is associated with reactive glia and concomitant increased expression of CD31, PDGFRβ, and collagen IV in endothelial cells and pericytes of the blood–brain barrier. *Int J Mol Sci* 2024; **25:** 1693.
48. Arnold J, Schattschneider J, Blechner C, *et al*. Tubulin tyrosine ligase like 4 (TTLL4) overexpression in breast cancer cells is associated with brain metastasis and alters exosome biogenesis. *J Exp Clin Cancer Res* 2020; **39:** 205.
49. Lu Y, Chen L, Li L, *et al*. Exosomes derived from brain metastatic breast cancer cells destroy the blood–brain barrier by carrying lncRNA GS1-600G8.5. *Biomed Res Int* 2020; **2020:** 7461727.
50. Feng S, Cen J, Huang Y, *et al*. Matrix metalloproteinase-2 and -9 secreted by leukemic cells increase the permeability of blood–brain barrier by disrupting tight junction proteins. *PLoS One* 2011; **6:** e20599.
51. Qiao S, Qian Y, Xu G, *et al*. Long-term characterization of activated microglia/macrophages facilitating the development of experimental brain metastasis through intravital microscopic imaging. *J Neuroinflammation* 2019; **16:** 4.
52. Caffarel MM, Braza MS. Microglia and metastases to the central nervous system: victim, ravager, or something else? *J Exp Clin Cancer Res* 2022; **41:** 327.
53. Cadiz MP, Jensen TD, Sens JP, *et al*. Culture shock: microglial heterogeneity, activation, and disrupted single-cell microglial networks *in vitro*. *Mol Neurodegener* 2022; **17:** 26.
54. Warden AS, Han C, Hansen E, *et al*. Tools for studying human microglia: *in vitro* and *in vivo* strategies. *Brain Behav Immun* 2023; **107:** 369–382.
55. Schroeder T, Bittrich P, Kuhne JF, *et al*. Mapping distribution of brain metastases: does the primary tumor matter? *J Neurooncol* 2020; **147:** 229–235.
56. Foglesong GD, Huang W, Liu X, *et al*. Role of hypothalamic VGF in energy balance and metabolic adaption to environmental enrichment in mice. *Endocrinology* 2016; **157:** 983–996.
57. Alder J, Thakker-Varia S, Bangasser DA, *et al*. Brain-derived neurotrophic factor-induced gene expression reveals novel actions of VGF in hippocampal synaptic plasticity. *J Neurosci* 2003; **23:** 10800–10808.
58. Koc G, Soyocak A, Alis H, *et al*. Changes in VGF and C3aR1 gene expression in human adipose tissue in obesity. *Mol Biol Rep* 2021; **48:** 251–257.
59. Benchoula K, Parhar IS, Hwa WE. The molecular mechanism of vgf in appetite, lipids, and insulin regulation. *Pharmacol Res* 2021; **172:** 105855.
60. Lin WJ, Zhao Y, Li Z, *et al*. An increase in VGF expression through a rapid, transcription-independent, autofeedback mechanism improves cognitive function. *Transl Psychiatry* 2021; **11:** 383.
61. Sahu BS, Rodriguez P, Nguyen ME, *et al*. Peptide/receptor co-evolution explains the lipolytic function of the neuropeptide TLQP-21. *Cell Rep* 2019; **28:** 2567–2580.e6.
62. Stephens SB, Schisler JC, Hohmeier HE, *et al*. A VGF-derived peptide attenuates development of type 2 diabetes via enhancement of islet β-cell survival and function. *Cell Metab* 2012; **16:** 33–43.
63. Brancia C, Noli B, Boido M, *et al*. TLQP peptides in amyotrophic lateral sclerosis: possible blood biomarkers with a neuroprotective role. *Neuroscience* 2018; **380:** 152–163.
64. El Gaamouch F, Audrain M, Lin WJ, *et al*. VGF-derived peptide TLQP-21 modulates microglial function through C3aR1 signaling pathways and reduces neuropathology in 5xFAD mice. *Mol Neurodegener.* 2020; **15:** 4.
65. Wang X, Prager BC, Wu Q, *et al*. Reciprocal signaling between glioblastoma stem cells and differentiated tumor cells promotes malignant progression. *Cell Stem Cell* 2018; **22:** 514–528.e5.
66. Hwang W, Chiu YF, Kuo MH, *et al*. Expression of neuroendocrine factor VGF in lung cancer cells confers resistance to EGFR kinase inhibitors and triggers epithelial-to-mesenchymal transition. *Cancer Res* 2017; **77:** 3013–3026.
67. Annaratone L, Medico E, Rangel N, *et al*. Search for neuro-endocrine markers (chromogranin A, synaptophysin and VGF) in breast cancers. An integrated approach using immunohistochemistry and gene expression profiling. *Endocr Pathol* 2014; **25:** 219–228.
68. Martínez-Aranda A, Hernández V, Guney E, *et al*. FN14 and GRP94 expression are prognostic/predictive biomarkers of brain metastasis outcome that open up new therapeutic strategies. *Oncotarget* 2015; **6:** 44254–44273.
69. Weksler BB, *et al*. Blood-brain barrier-specific properties of a human adult brain endothelial cell line. *Faseb j* 2005; **19:** 1872–1874.
70. Kim JY, *et al*. SOX9 promotes stress-responsive transcription of VGF nerve growth factor inducible gene in renal tubular epithelial cells. *J Biol Chem* 2020; **295:** 16328–16341.
71. Ribeiro AS, *et al*. SRC inhibition prevents P-cadherin mediated signaling and function in basal-like breast cancer cells. *Cell Commun Signal* 2018; **16:** 75.

References 69–71 are cited only in the supplementary material.

© 2024 The Pathological Society of Great Britain and Ireland. www.pathsoc.org

10969896, 2024, 2, Downloaded from https://pathsocjournals.onlinelibrary.wiley.com/doi/10.1002/path.6319 by Universidade Do Porto Faculdade de Engenharia, Wiley Online Library on [29/04/2025]. See the Terms and Conditions (https://onlinelibrary.wiley.com/terms-and-conditions) on Wiley Online Library for rules of use; OA articles are governed by the applicable Creative Commons License

SUPPLEMENTARY MATERIAL ONLINE

Supplementary materials and methods

Figure S1. Organotropic MDA-MB-231 breast cancer cell model

Figure S2. Mouse secretome-induced model

Figure S3. The secretome of brain organotropic breast cancer cells impacts microglia activation

Figure S4. Brain organotropic breast cancer cells show a specific secretome signature

Figure S5. VGF impacts microglia activation

Figure S6. Brain metastasis colonization assay

Figure S7. Kaplan–Meier survival curves of breast cancer patients based on *VGF* mRNA expression

Figure S8. VGF expression is associated with a worse prognosis for breast cancer patients

Figure S9. Association of the different breast cancer cohorts with clinicopathological features

Figure S10. Association between primary breast tumors that metastasize to the lung, bone, and brain with classical poor prognostic factors and molecular subtypes of breast cancer

Figure S11. *VGF* mRNA expression as a predictive factor for breast cancer brain metastases

Table S1. Raw data – proteomics

Table S2. Characterization of the different cohorts

Table S3. Univariate Cox proportional hazard analysis enables the prediction of risk (hazard ratios and corresponding 95% confidence intervals) for overall survival (OS) among breast cancer patients

Table S4. Association of the different breast cohorts with clinicopathological features

© 2024 The Pathological Society of Great Britain and Ireland. www.pathsoc.org

10969896, 2024, 2, Downloaded from https://pathsocjournals.onlinelibrary.wiley.com/doi/10.1002/path.6319 by Universidade Do Porto Faculdade de Engenharia, Wiley Online Library on [29/04/2025]. See the Terms and Conditions (https://onlinelibrary.wiley.com/terms-and-conditions) on Wiley Online Library for rules of use; OA articles are governed by the applicable Creative Commons License

Seminars in Cancer Biology 60 (2020) 294–301

Contents lists available at ScienceDirect

Seminars in Cancer Biology

journal homepage: www.elsevier.com/locate/semcancer

Review

Impact of breast cancer cells´ secretome on the brain metastatic niche remodeling

R. Carvalho, J. Paredes, A.S. Ribeiro*

i3S/IPATIMUP, 4200-135, Porto, Portugal

ARTICLE INFO

Keywords:
Secretome
Brain metastasis
Breast cancer
Pre-metastatic niche

ABSTRACT

Brain metastases occur in approximately 10–20% of patients with metastatic breast cancer showing a very poor overall survival. Curiously, different molecular subtypes (that show specific gene expression signatures and differential prognostic significance) are associated with different risks for brain metastases development, suggesting that cancer cells harbor specific molecular programs that award them intrinsic advantages to survive in this specific foreign tissue. Emerging data has been revealing that biophysical and/or mechanical properties of the brain extracellular matrix (ECM), along with those of the brain resident cells, play a crucial role in creating the best conditions for survival, colonization and outgrowth of breast cancer cells in this distinct microenvironment.

Although several reports show that cancer cells modulate metastatic niches way before they reach the target organ, few data exist for the brain metastatic niche. Indeed, little is known concerning how factors secreted by cancer cells activate brain resident cells and/or modify brain ECM biomechanical properties and how these modifications impact cells´ ability to metastasize the brain. The brain is a particular organ, protected by the blood brain barrier (BBB), and containing exclusive functional units and very special cell types. Additionally, it is the organ with the most singular ECM and biomechanical properties. Thus, this cancer cell-brain metastatic niche interaction must present distinct properties. Consequently, the search for putative molecular markers that modulate the brain pre-metastatic niche, thus promoting the successful metastatic homing of cancer cells, is urgently needed.

In this review, we will discuss key aspects regarding breast cancer cells and the brain pre-metastatic niche paracrine communication that is crucial to initiate the metastatic cascade. We will focus on cancer cell`s secretome influence into the brain microenvironment, specifically on its impact on tissue mechanics and on brain resident cells as regulators of the pre-metastatic niche formation, ultimately promoting metastatic colonization.

1. Breast cancer brain metastases

Breast cancer brain metastases incidence has increased in the past few years, since the recently used therapies show an improved control of the systemic disease but are inefficient in controlling metastatic progression. These develop only in 10%–20% of patients with metastatic breast cancer, occurring frequently after metastasis in other systemic organs (such as bone and lung) and displaying the strongest and worse impact on survival of breast cancer patients [1] (Fig. 1). An increased risk to develop brain metastasis is associated with younger patients age, increased tumor stage, presence of lymph node metastases, number of metastatic sites (> 2), large tumor size and hormone receptor–negative, HER2+ and triple-negative tumors [2–7].

Despite recent improvements in breast cancer therapies, patients with brain metastasis show a mean survival of approximately 6–16 months after diagnosis. Therefore, understanding (1) how cancer cells reach specifically the brain, (2) whether and how they prepare the brain for their arrival, and (3) which are the critical factors that allow cancer cell's survival in this distant location will be crucial for the development of efficient treatments for brain metastatic and resistant tumors .

Interestingly, different breast cancer molecular subtypes display not only different brain metastatic incidence, but also different prognostic values (Fig. 1). Breast cancer patients with luminal tumors have a lower risk for brain metastasis and show the most favorable outcome regarding brain metastasis free survival (BMFS). On the other hand, patients bearing HER2 overexpressing and TNBC show a very significant risk to develop metastasis and consequently present a poorest BMFS

* Corresponding author.
E-mail address: aribeiro@ipatimup.pt (A.S. Ribeiro).

https://doi.org/10.1016/j.semcancer.2019.10.011
Received 22 June 2019; Received in revised form 11 October 2019; Accepted 16 October 2019
Available online 09 November 2019
1044-579X/ © 2019 Elsevier Ltd. All rights reserved.

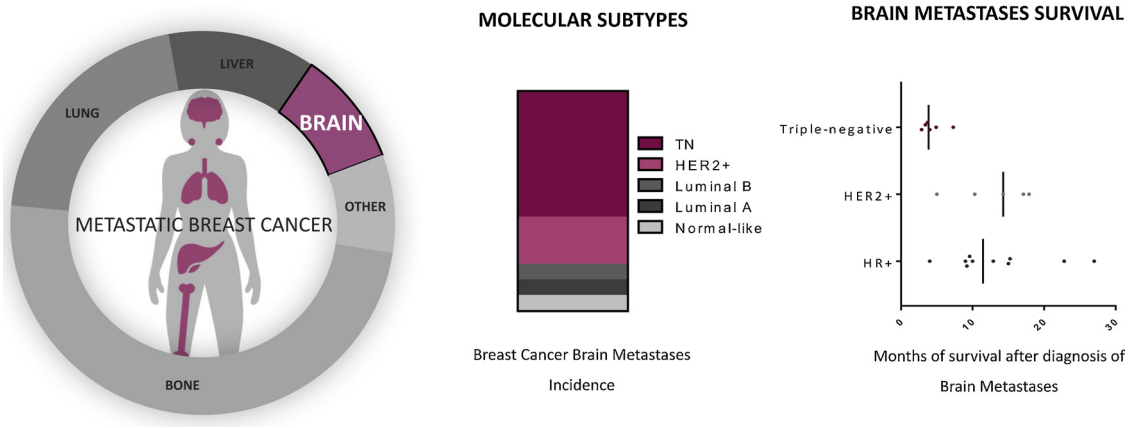


Fig. 1. Brain metastases occur in 10%–20% of patients with metastatic breast cancer and are more frequently associated with the HER2 overexpressing and TNBC molecular subtypes. TNBC show a significant increased risk of developing brain metastasis, as well as exhibit the poorest BMFS (reviewed from [116–118]).

[8–10] (Fig. 1). Still, evidence has emerged demonstrating that, regardless of the breast cancer molecular subtype, brain metastatic cells share certain biological characteristics. For instances, it has been observed that tumors from patients that have metastasized primarily to the brain were negative for hormone receptors, positive for basal markers (such as CK5) and for cancer stem cell (CSC) markers (nestin, CD133 and CD44). Interestingly, some of these markers have also been found in gliobastomas (GBM) .

1.1. Brain specific metastatic regulators and signaling pathways

Brain metastases are thought to arise mainly due to hematogenous distribution [11]. After travelling from the primary site to the brain, cancer cells often arrest in the dense brain capillary network [12]. Upon the initial arrest, cancer cells may either remain as quiescent cells or actively proliferate to establish a secondary lesion [12,13]. Interesting observations reveal that regional distribution of metastatic lesions are associated with the regional blood flow [14], being the majority of the lesions found in cerebral hemispheres and only around 15 % is found within the cerebellum.

In recent years, several groups have addressed the processes underlying breast-to-brain metastases. The breakthrough in this area began with the establishment of breast cancer cell models (CN34 and MDA-231) with tropism to the brain, generated upon successive *in vivo* selection [15,16]. In a gene expression profile comparison between brain tropic breast cancer cells and their respective parental cell line, around 250 genes were found to be deregulated. From this list, the authors established a 17 gene list (designated as brain metastasis signature (BrMS)), found to be significantly associated witnal blood flow [14], being the majority of the lesions found in cerebral hemispheres and only around 15 % is found within the cerebellum.

In recent years, several groups have addressed the processes underlying breast-to-brain metastases. The breakthrough in this area began with the establishment of breast cancer cell models (CN34 and MDA-231) with tropism to the brain, generated upon successive *in vivo* selection [15,16]. In a gene expression profile comparison between brain tropic breast cancer cells and their respective parental cell line, around 250 genes were found to be deregulated. From this list, the authors established a 17 gene list (designated as brain metastasis signature (BrMS)), found to be significantly associated with BMFS in breast cancer patients.

Importantly, this work together with more recent data has uncover interesting pathways associated with brain metastasis, such as EGFR signaling, cell-matrix interactions, stem cell pathways activation and glucose metabolic alterations. For example, several EGFR family members and their downstream mediators are widely involved in breast cancer brain metastases [17–20]. While EGFR seems to be mostly involved in breast cancer cell migration and invasion into the brain [21], HER2 and HER3 overexpression seems to impact on the outgrowth of brain metastases [22,23]. In addition, inhibition of EGFR and COX2 signaling counteracts the transmigration of breast cancer cells through the blood-brain-barrier (BBB) [15]. Considering cell-matrix interactions, two genes have shown to be of interest - ST6GALNAC5 and α3β1 integrin [15,24]. ST6GALNAC5 mediates cancer cell`s adhesion to the brain endothelium [15], facilitating BBB passage of cancer cells. Additionally, activation of α3β1 integrin has also been proposed to be involved in the modulation of brain metastases by the interaction between breast cancer cells and brain endothelial cells (EC) (via αB-crystallin) and by increasing angiogenesis through VEGF activation [23,25,26]. In parallel, stem cell related pathways have also been reported to play an important role. In fact, Wnt and Notch stem cell markers, and their downstream targets (such as JAG1, JAG2 and IL-1β) are both associated with CSC features and are frequently deregulated in different types of cancers, namely GBM [27] and also in brain metastases [28–30]. Additionally, the breast cancer stem cell marker CD44, through its interaction with hyaluronic acid, has been shown to facilitate cancer cells passage through BBB [31,32]. Finally, genes associated with the glucose metabolic pathway, such as HK2 and GLUT1, have also been described to have a role in the survival of cancer cells in the brain microenvironment [33–35].

2. The secretome as a modulator of the brain metastatic niche

In recent years, various efforts have been made to uncover and characterize the cancer cell's secretome, aiming to identify biomarkers of metastization. In fact, there is a plethora of evidence demonstrating that cancer cells prepare the metastatic organ in the early stages of disease progression; long before intravasion, cancer cells communicate with distant tissues or organs, mainly by secreting soluble factors and/or extracellular vesicles (EV) that activate resident cells, immune cells and promote ECM remodeling, priming a permissive pre-metastatic niche [36–40].

These factors released by cancer cells collectively compose the "cancer cell secretome", which is regarded as a promising source for the discovery of new molecular targets involved in the crosstalk between primary tumor and distant metastatic organs. Interestingly, very few data is known regarding the impact of the secretome in the modulation of the brain pre-metastatic niche, despite the growing body of data for other metastatic organs, such as lung, bone and liver [36,41].

Lyden et al. [42] have shown that exosomes derived from organotropic breast cancer cells can be endocytosed by resident cells of the respective metastatic organ, in order to prepare the pre-metastatic niche. Surprisingly, exosomal proteomic analysis demonstrated that distinct integrin profiles correlated with organotropism, although these

results were only validated in serum collected from breast cancer patients with liver and lung metastases, but not in that from patients with brain metastases.

Actually, innovative high-throughput proteomic technologies allowed researchers to identify and quantify promising biomarkers in cancer cell´s secretome from body fluids uncovering new opportunities to develop useful therapies [43–45]. Nevertheless, cancer secretome studies have not always been conclusive due to the complex nature of human samples encompassing a huge diversity of protein concentrations, thus hampering the detection of molecules with low representation. The majority of secretome studies were performed through *in vitro* cell cultures and subsequently validated in clinical samples through the use of more sensitive techniques, such as ELISA, western blot and mass spectrometry analysis [46]. Overall, a large set of secretome studies of cancer cell lines has been published in recent years, including the secretome of breast cancer cells [47].

Importantly, our group has recently established a 3D *in vitro* model mimicking the tumor microenvironment to better determine the breast cancer secretome responsible for the formation of the brain pre-metastatic niche. Our results show that brain organotropic metastatic breast cancer cells secrete higher levels of specific peptides involved in adhesion, migration and matrisome signatures (data not shown), reinforcing the importance of brain tissue remodeling in the early steps of the metastatic cascade. Herein, we provide a review of how secreted factors by cancer cells play a critical role during the development and progression of brain metastases, namely concerning BBB integrity, ECM remodeling, and activation of brain resident cells.

2.1. Blood brain barrier (BBB)

The BBB is a selective barrier with a singular vascular structure composed by brain capillary EC, pericytes in contact with the vascular basement membrane and astrocytic end-feet. It mediates drug delivery, and shows to be an obstacle to the passage of cancer cells into the brain. Still, during brain metastasis, EC junctions can be disturbed, facilitating the extravasion of cancer cells to the brain, preferentially through paracellular transmigration (through EC junctions) [48].

Several genetic determinants have a key role in the infiltration of metastatic cancer cells through this highly selective barrier. As already mentioned, the brain metastatic regulators (expressed by cancer cells) HER2, ST6GALNAC5, COX2, EGFR, αB-crystallin, CD44, Syndecan-1, GLUT1 and BCRP are involved in the modulation of BBB permeability [15]. Also, upregulation of Angiopoietin-2 in brain EC increased BBB permeability by impairing claudin-5 and ZO-1 tight junctions, resulting in metastatic breast cancer cells extravasation and colonization into the brain tissue [49].

However, other interesting secreted factors have also been shown to contribute to brain metastases formation, such as secretion of VEGF that disturbs the endothelial integrity [50], and SDF-1α that promotes PI-3 K, AKT and FAK activation [51] in breast cancer cells, facilitating their transendothelial migration. Interestingly, it has been demonstrated that EVs are involved in the endothelial cell-cell adhesion disruption during breast cancer brain metastases. Indeed, metastatic breast cancer cells-derived EVs promote disruption of the vascular endothelial barrier through miR-181c, decrease 3-phosphoinositide-dependent protein kinase-1 (PDPK1) and consequently induce the delocalization of actin filaments [52]. Likewise, exosomal miR-105 derived from breast cancer cells leads to BBB breakdown and brain metastatic progression by decreasing ZO-1 expression in tight junctions of EC [53]. Supporting this, both miR-181c and miR-105 were found in the serum of patients at early stages of brain metastatic disease, namely during brain pre-metastatic niche formation ((Fig. 2)and(Table 1))[52,53].

More recently, using a model of patient-derived xenograft (PDX) of brain metastases, it has been shown that BBB disruption was associated with loss of major facilitator superfamily domain containing 2A (MFsd2a) in the endothelium, due to the lack of astrocytes that secrete TGFβ1 and bFGF [54].

2.2. Brain extracellular matrix modifications

Much is known about ECM modifications at the primary tumor site; however, cancer cells-mediated ECM remodeling on future metastatic sites has been only recently implicated in the so-called establishment of the pre-metastatic niche. Indeed, a growing amount of evidences suggest that tumors may modify distant sites before their arrival, through paracrine communication with metastatic organ resident cells, that will help priming the pre-metastatic niche [55]. Although the key secreted factors involved in this process are yet to be identified, TNF-α, TGFβ, VEGF-α and MMPs have all been already implicated [56,57].

Most of the information available in this context relies on the study of lung and bone pre-metastatic niche formation, whereas in the brain context, these modifications remain poorly explored. Tumor-secreted Lisil Oxidase(LOX) has a crucial role in bone matrix remodeling [57] whereas in the lung pre-metastatic niche, fibronectin produced by pulmonary fibroblasts promotes the migration and adhesion of VEGFR1 + hematopoietic progenitor cells to the lung niche, which in turn secrete MMP9 [56], further modulating the pre-metastatic niche. In addition, hyaluronic acid (another ECM Component) and its receptor CD44, facilitate signaling through CXCR4/SDF1 axis [58,59], which in turn showed to be crucial for organ-specific metastases of cancer cells to the lung or bone marrow [60].

Finally, MMPs have been also described as crucial players during breast cancer invasion and metastization into the brain, including MMP-1, -2, -3 and -9. Inhibition of these MMPs decreased primary tumor growth and brain metastases formation, reinforcing the role of matrix remodeling for brain metastases [61–63].

These data support the impact of ECM deregulation in the establishment of a pre-metastatic niche. Consequently, the search for putative molecular markers modulating the brain pre-metastatic niche and promoting successful metastatic homing of cancer cells is immediately needed.

2.2.1. ECM biomechanical properties

The ECM biomechanical properties are determined by the composition, concentration and post-translational modifications of the matrix components [57]. The paracrine communication between the tumor and stromal cells promotes pronounced changes in the ECM, facilitating proliferation and invasion within the primary tumor setting [64,65]. The ECM remodeling observed during tumor progression translates into an increase in ECM stiffness, that can be up to 10-fold stiffer when comparing to the normal mammary tissue within breast cancer samples [66]. In general, the stromal and cancer cells start to produce and deposit ECM components, such as collagen type I and fibronectin, that in turn promote increased ECM stiffness [67]. For example, cancer-associated fibroblasts (CAFs) secrete LOX enzymes or modulate Caveolin-1 activity, driving matrix stiffening through collagen crosslinking and facilitating tumor dissemination and metastases [68]. In the opposite direction, conditioned media from cancer cells induced CAF-mediated ECM remodeling, suggesting that cancer cells can activate CAFs via paracrine signals to further induce matrix stiffness [69]. Simultaneously, myofibroblast contraction can induce the release and activation of latent TGF-β from the ECM. This response may generate a positive feedback loop between matrix stiffness and growth factors [70].

In the context of breast cancer, convincing data about the role of biomechanical modulation in tumor progression has been generated [68]. Intriguingly, different breast cancer molecular subtypes metastasize to different organs with very different biomechanical properties. The poor prognostic HER2 and BLBC subtypes are those that metastasize more frequently to the brain and lungs [71,72], which are organs that present low levels of tissue stiffness [66], whereas the luminal subtype metastasizes mostly to the bone [73], which is the organ with the highest stiffness [66]. These data support the Seed and Soil theory,

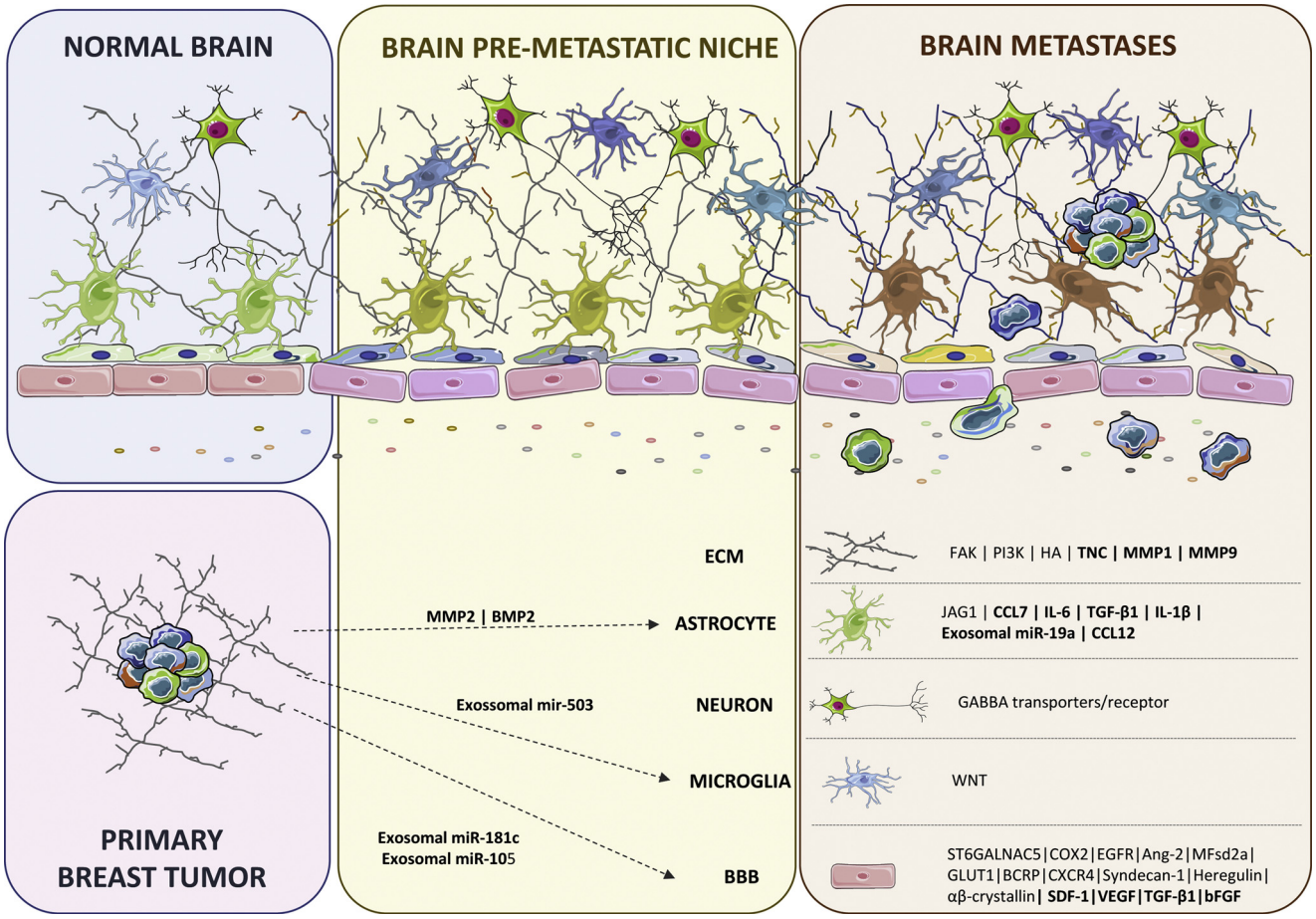


Fig. 2. Several changes occur in the brain metastatic niche during breast cancer progression. During the pre-metastatic niche formation, the secretome of cancer cells disturbs the BBB and activate brain resident cells (as observed by the changes in the color code of the different brain resident cells), that will then modulate the brain ECM. Later, circulating tumor cells reach the BBB, are extravasated into the brain parenchyma and proliferate in this new microenviroment, generating a breast cancer metastasis. The known regulators for each step of the process and for each component of the brain metastatic niche are described below (the secreted factors are listed in bold).

showing that not only cancer cells, but also ECM biophysical and/or mechanical properties, such as stiffness, are crucial for metastases [66,74,75]. In fact, Kostic et al. demonstrated that organotropic breast cancer cells cultured on substrates matching the stiffness of the preferential site of colonization, yielded increased proliferation and migration. This goes in line with previous data showing that breast epithelial cells upregulate proliferation-associated genes, like cyclin D1 and are more proliferative in stiffer matrices [76,77].

Within the most common breast cancer metastatic tissues, brain is the one where the biomechanical crosstalk between cancer cells and ECM is less understood and remains an unexplored area of research. The brain tissue offers a unique, complex and dynamic ECM

Table 1
Summary of secreted proteins involved in the modulation of the brain metastatic niche.

SECRETED FACTORS BY…		EFFECT ON BRAIN…	
		pre-metastatic niche	metastatic microenvironment
CANCER CELLS	**exossomal miR-503**	microglia activation (106)	n.d
	exossomal mir-181c	BBB disruption (52)	n.d
	exossomal mir-105	BBB disruption (53)	n.d
	BMP2	astrocyte activation (116)	n.d.
	MMP2	astrocyte activation (61)	matrix remodelling (113)
	MMP1	n.d.	matrix remodelling (61)
	VEGF	n.d.	Brain endothelial cells (23, 25, 26)
	CCL2	n.d.	Myeloid cells (114)
ASTROCYTES	**MMP9**	n.d.	matrix remodeling (113)
	TGF-β1	n.d	Brain endothelial cells (54)| Breast cancer cells (89, 112)
	bFGF	n.d	Brain endothelial cells (54)
	IL6	n.d.	Breast cancer cells (89, 112)
	exossomal mir-19a	n.d.	Breast cancer cells (114)
	CCL7	n.d.	Breast cancer stem cells (103)
	SDF-1α	n.d.	BBB disruption (51)

microenvironment, providing not only a physical scaffold for cancer cells, but also encompassing important biochemical and biomechanical cues that must be crucial for cancer cells colonization and outgrowth [78]. Most data demonstrating brain tissue remodeling came from studies on brain disorders and on primary brain tumors, showing a significant impact of brain tissue mechanics in regulating GBM aggressive behavior and recurrence [79–82]. For example, gliomas have been shown to progress within a dense ECM, with high HIF1α levels and with an increased stiffness due to tenascin C (TNC)-enriched ECM [83]. In fact, TNC promotes ECM modifications by cross- linking lecticans and hyaluronic acid, forming a complex responsible for increase tumor stiffness relative to the normal soft brain [84,85]. Because increased amounts of hyaluronic acid are produced in primary brain tumors, tissue stiffening is highly increased [85], which in turn influences GBM cancer cell invasion and also the binding of integrins to their ECM substrates [85,86]. In the breast cancer brain metastatic context, Narkhede AA et al. [87] generated hyaluronic acid hydrogels comprising a range of stiffness, recapitulating the brain ECM biomechanical properties. Interestingly, breast cancer cells with tropism to the brain increased their cell adhesion, spreading, proliferation, and migration in increased stiffened hydrogels, a process that was partially mediated through FAK and PI3 K signaling (Fig. 2 and Table 1).

2.3. Brain resident cells

Tumor cells are known to adapt constantly to their environment, either by adjusting their behavior but also by remodeling their surroundings, through activation of resident cells such fibroblasts, immune cells and endothelial cells, which are the main responsible for abnormal ECM production [64,65]. In fact, several reports have shown that cancer cells can modulate the tissue niches before they reach the target organ, by modulating the activity of resident cells. Below, we will describe what is known concerning the impact of cancer cells´ secretome on brain resident cells, and how this modulates the brain metastatic niche (Fig. 2 and Table 1).

2.3.1. Neurons

Neurons, together with glial cells, are the most abundant cells in the brain. Still, their role on brain metastases has not been fully investigated [88,89]. The only data that tackles this issue show that gamma-aminobutyric acid (GABA) transporters and GABA receptor are upregulated in brain metastases, promoting an increase in the uptake of GABBA neurotransmitter, NADPH production, and consequently inducing the proliferation of breast cancer cells [88].

2.3.2. Pericytes

Pericytes are perivascular cells located on capillaries between EC and the brain parenchyma, that mediate several microvascular functions, such as BBB maintenance, blood vessels stabilization, angiogenesis, cerebral blood flow and migration of immune cells into the brain [90,91]. Perivascular cells are characterized by the expression of specific markers, namely platelet-derived growth factor receptor β (PDGFRβ), α-smooth muscle actin (αSMA), desmin, neuro glial antigen-2 (NG2), CD13 and CD146 [92]. The role of these brain resident cells has largely been deciphered in the context of the brain primary tumor, showing that reduction of pericytes density decreases tumor growth, due to increased vessel leakiness and blood supply [93,94]. However, most recent reports show that loss of pericytes coverage facilitates the metastatic process [93].

Xian et al. demonstrated for the first time the role of pericytes as regulators of metastases in neural cell adhesion molecule (NCAM) deficient mice. This study suggested that NCAM deficiency disturbed pericyte-ECs interaction, contributing to metastatic progression {Xian, 2006 #8}.

Finally, only one study revealed that the contact of metastatic cancer cells with microvessel wall in a pericyte like position appears to be a critical step for the extravasation and brain colonization of melanoma and lung cancer cells [95]. More recently, two distinct pericyte subpopulations were identified in the blood-tumor barrier (BTB) in breast cancer brain metastases. The authors showed that CD13 + pericytes were decreased in brain metastases with high permeability, whereas Desmin + pericytes were increased in brain metastases, being more pronounced in highly permeable lesions [96]. This study suggested that Desmin + pericytes could be used as a potential therapeutic target to improve chemotherapeutic efficacy in patients with breast cancer brain metastases. Unfortunately, nothing is known regarding the secretome impact on pericytes function during brain metastatic progression.

2.3.3. Microglia

Microglia cells are the most important immune effector cells in the brain, being involved in the first line of defense against brain injury and immunological stimuli, while also being able to detect microenvironmental changes [97–99]. The microglia impact on brain metastases is less explored, although the role of inflammation and activation of macrophages in cancer progression is widely known. Similarly to what has been observed in both astrocytes and macrophages, microglia cells remain in a resting state until stimulation [100]. After these cells activation, they can polarize into different states (as observed in tumor associated macrophages), such as M1 pro-inflammatory and tumor suppressive, and M2 anti-inflammatory and pro-tumoral phenotypes [101]. The transition from the quiescent to an activated phenotype can occur either by intrinsic (e.g., Runx-1) and extrinsic factors (e.g., CD200 and TREM2). Although M2 microglia cells are known to be a central component of the immune response to primary brain tumors [102,103], very few studies report the role of these immune resident cells during the brain metastatic cascade, or show the impact of cancer cells` secreted factors on microglia activation.

Pukrop et al. reported that activation of M2 microglia cells promoted breast cancer cells invasion and colonization of the brain in a Wnt-dependent manner [104]. In line with pro-tumoral functions of microglia, loss of X-inactive-specific transcript (XIST) by metastatic cancer cells promoted the secretion of exosomal miR-503, stimulating M2 microglia activation that in turn promoted the increase of PD-L1 expression. This affected the proliferation of T-cells, creating a more amenable microenvironment niche, favoring the colonization and growth of metastatic cancer cells [105]. Finally, brain metastatic tumor cells are found to be surrounded by activated microglia cells, suggesting their important role in the beginning of the brain metastatic cascade [106–108].

2.3.4 Astrocytes

Astrocytes, the most abundant glial cells found in the brain microenvironment, are crucial for the paracrine crosstalk with cancer cells, since are known to secrete different peptides with impact on brain metastasis progression. Strikingly, a seminal work by Lorger et al. (2010) has shown that brain metastatic cancer cells are able to activate astrocytes, even before they extravasate [106]. This study suggested that astrocytes are activated at early stages of the brain metastatic cascade, although it remains unclear whether this occurs during the formation of the brain pre-metastatic niche.

Emerging data has been revealing that activated astrocytes, on the other hand, secrete many biological factors, such as proteolytic enzymes, cytokines, chemokines, growth factors and EV that support modifications in the brain tissue during the metastatic process [109–111]. Many of these secreted factors can function as pro-tumoral signals for metastatic cancer cells, such as IL-6 and TGF-β [89,111]. Actually, co-culture experiments have demonstrated that astrocytes produce pro-invasive and pro-migrating factors that affect the tumorigenic capacities of breast cancer cells [61]. Activated astrocytes were shown to increase the levels of phosphorylated-ERK1/2 (p-ERK1/2) leading to an increase of MMP2 in brain metastatic breast cancer cells. In a later study, Wang et al. identified both MMP-2 and MMP-9 as

important mediators for astrocyte-induced tumor cell invasion [112].

Likewise, exosomes secreted by astrocytes may function as mediators of br]. Actually, co-culture experiments have demonstrated that astrocytes produce pro-invasive and pro-migrating factors that affect the tumorigenic capacities of breast cancer cells [61]. Activated astrocytes were shown to increase the levels of phosphorylated-ERK1/2 (p-ERK1/2) leading to an increase of MMP2 in brain metastatic breast cancer cells. In a later study, Wang et al. identified both MMP-2 and MMP-9 as important mediators for astrocyte-induced tumor cell invasion [112].

Likewise, exosomes secreted by astrocytes may function as mediators of brain metastases and promote the outgrowth of breast cancer brain metastases through PTEN knockdown [113]. Interestingly, the authors showed that miR-19a not only targets PTEN, but increases the expression of C-C motif chemokine ligand 2 (CCL2), promoting the recruitment of myeloid cells and further associating with brain metastatic progression.

Gril et al. (2013) reported that a subpopulation of activated astrocytes express phosphorylated PDGFRβ [114]. Curiously, human astrocytes, in response to metastatic breast cancer cells-derived soluble factors, increased the expression of astrocytic PDGFRβ. Furthermore, inhibition of astrocytic PDGFRβ prevented brain colonization by metastatic cancer cells.

Aside from regulating brain metastases, astrocytes are also associated with brain tumor stem cell properties and with modulating cancer cells resistance to chemotherapeutic agents, thereby increasing the malignancy in both primary brain tumors and brain metastases. During the brain metastatic process, CSCs can establish their niche through their cooperation with astrocytes. An *in vitro* study demonstrated that bone morphogenetic protein 2 (BMP2) is upregulated in brain metastatic breast cancer cells. Moreover, co-cultures with neural stem cells (NSCs) promoted their differentiation into astrocytes, through paracrine BMP2 signaling [88,115].

More recently, it was found that increased expression of COX2 and prostaglandins in breast cancer cells, with tropism to the brain, activated astrocytes, that in turn promoted the secretion of chemokine (C-C motif) ligand 7 (CCL7), responsible for the self-renewal of metastatic breast CSCs. In addition, the co-culture of breast cancer cells and astrocytes promotes an upregulation of the glutathione s-transferase alpha 5 (GSTA5), BCL2L1 and TWIST survival genes. Interestingly enough, upregulation of these genes mediates chemotherapeutic resistance to cisplatin treatment.

Together, these findings show that targeting the interactions between metastatic cancer cells and reactive astrocytes may potentially improve both prevention and treatment of brain metastases [102].

3. Conclusions and therapeutic opportunities

It is well established that interactions between cancer cells with resident cells in the tumor microenvironment drive cancer progression towards metastases. Cells are able to survive in new environments by adapting their biological behavior and by remodeling their microenvironment, through activation of resident cells such as stromal cells, EC, immune cells, and fibroblasts [64,65]. In fact, it is know that this paracrine communication can start even before cancer cells reach circulation, preparing a niche favorable to their growth at distant sites (Fig. 2 and Table 1). Consequently, there is the need of searching for putative molecular markers specifically secreted by brain metastatic cancer cells that modulate the brain pre-metastatic niche, thus promoting the successful metastatic homing of cancer cells.

By uncovering clinically relevant predictive biomarkers of brain metastases as well as molecular inhibitors that impair this process, new therapeutic opportunities may arise for patients with metastatic brain tumors or at higher risk to develop brain metastasis. In fact, based combinatorial drug regimens that act synergistically by targeting intrinsic pathways in neoplastic cells alongside extrinsic pro-oncogenic pathways in the tumor microenvironment, must be a priority. As cancer research and clinical oncology progress increasingly towards a new era of integrative cancer therapy, intensive research in deciphering the role of the metastatic microenvironment and of tumor-promoting inflammation will certainly result in innovative therapeutic strategies in the upcoming years.

Declaration of Competing Interest

The authors declare no competing interests.

Acknowledgements and funding

The work is supported by FEDER - Fundo Europeu de Desenvolvimento Regional funds through the COMPETE 2020 - Operacional Programme for Competitiveness and Internationalisation (POCI), Portugal 2020, and by FCT- Fundação para a Ciência e a Tecnologia/ Ministério da Ciência, Tecnologia e Inovação under the projects POCI-01-0145-FEDER-016390, SAICTPAC/0022/2015 and 02/SAICT/2017/030625. RC is funded by FCT (SFRH/BD/135831/2018). JP and ASR are researchers from IPATIMUP/i3S, which is partially supported by FCT in the framework of the project "Institute for Research and Innovation in Health Sciences" (POCI-01-0145-FEDER-007274). We thank to Patricia Carneiro for critical reading of this manuscript.

References

[1] R. Weide, et al., Metastatic breast cancer: prolongation of survival in routine care is restricted to hormone-receptor-and Her2-positive tumors, Springerplus 3 (2014).
[2] F. Heitz, et al., Triple-negative and HER2-overexpressing breast cancers exhibit an elevated risk and an earlier occurrence of cerebral metastases, Eur. J. Cancer 45 (16) (2009) 2792–2798.
[3] F. Heitz, et al., Cerebral metastases in metastatic breast cancer: disease-specific risk factors and survival, Ann. Oncol. 22 (7) (2011) 1571–1581.
[4] K.D. Miller, et al., Occult central nervous system involvement in patients with metastatic breast cancer: prevalence, predictive factors and impact on overall survival, Ann. Oncol. 14 (7) (2003) 1072–1077.
[5] N. Niikura, et al., Treatment outcomes and prognostic factors for patients with brain metastases from breast cancer of each subtype: a multicenter retrospective analysis, Breast Cancer Res. Treat. 147 (1) (2014) 103–112.
[6] B.C. Pestalozzi, et al., Identifying breast cancer patients at risk for Central Nervous System (CNS) metastases in trials of the International Breast Cancer study Group (IBCSG), Ann. Oncol. 17 (6) (2006) 935–944.
[7] R.J. Weil, et al., Breast cancer metastasis to the central nervous system, Am. J. Pathol. 167 (4) (2005) 913–920.
[8] C.K. Anders, et al., The prognostic contribution of clinical breast cancer subtype, age, and race among patients with breast cancer brain metastases, Cancer 117 (8) (2011) 1602–1611.
[9] A. Niwinska, M. Murawska, K. Pogoda, Breast cancer subtypes and response to systemic treatment after whole-brain radiotherapy in patients with brain metastases, Cancer 116 (18) (2010) 4238–4247.
[10] N.E. Oehrlich, et al., Clinical outcome of brain metastases differs significantly among breast cancer subtypes, Oncol. Lett. 14 (1) (2017) 194–200.
[11] A.F. Eichler, et al., The biology of brain metastases-translation to new therapies, Nat. Rev. Clin. Oncol. 8 (6) (2011) 344–356.
[12] P.S. Steeg, K.A. Camphausen, Q.R. Smith, Brain metastases as preventive and therapeutic targets, Nat. Rev. Cancer 11 (5) (2011) 352–363.
[13] A.C. Obenauf, J. Massague, Surviving at a distance: organ-specific metastasis, Trends Cancer 1 (1) (2015) 76–91.
[14] J.Y. Delattre, et al., Distribution of brain metastases, Arch. Neurol. 45 (7) (1988) 741–744.
[15] P.D. Bos, et al., Genes that mediate breast cancer metastasis to the brain, Nature 459 (7249) (2009) 1005–U137.
[16] A.J. Minn, et al., Genes that mediate breast cancer metastasis to lung, Nature 436 (7050) (2005) 518–524.
[17] J. Gaedcke, et al., Predominance of the basal type and HER-2/neu type in brain metastasis from breast cancer, Mod. Pathol. 20 (8) (2007) 864–870.
[18] B. Adamo, et al., Phosphatidylinositol 3-kinase pathway activation in breast cancer brain metastases, Breast Cancer Res. 13 (6) (2011).
[19] N.L. Grupka, et al., Epidermal growth factor receptor status in breast cancer metastases to the central nervous system - comparison with HER-2/neu status, Arch. Pathol. Lab. Med. 128 (9) (2004) 974–979.
[20] B. Gumuskaya, et al., EGFR expression and gene copy number in triple-negative breast carcinoma, Cancer Genet. Cytogenet. 203 (2) (2010) 222–229.
[21] F. Nie, et al., Involvement of epidermal growth factor receptor overexpression in

the promotion of breast cancer brain metastasis, Cancer 118 (21) (2012) 5198–5209.
[22] L. Da Silva, et al., HER3 and downstream pathways are involved in colonization of brain metastases from breast cancer, Breast Cancer Res. 12 (4) (2010).
[23] D. Palmieri, et al., Her-2 overexpression increases the metastatic outgrowth of breast cancer cells in the brain, Cancer Res. 67 (9) (2007) 4190–4198.
[24] T. Okajima, et al., Molecular cloning of brain-specific GD1 alpha synthase (ST6GalNAc V) containing CAG/glutamine repeats, J. Biol. Chem. 274 (43) (1999) 30557–30562.
[25] D. Malin, et al., Alpha B-crystallin: a novel regulator of breast cancer metastasis to the brain, Clin. Cancer Res. 20 (1) (2014).
[26] M. Lorger, et al., Activation of tumor cell integrin alpha(v)beta(3) controls angiogenesis and metastatic growth in the brain, Proc. Natl. Acad. Sci. U. S. A. 106 (26) (2009) 10666–10671.
[27] I. Espinoza, et al., Notch signaling: targeting cancer stem cells and epithelial-to-mesenchymal transition, Onco. Ther. 6 (2013) 1249–1259.
[28] D.H. Nam, et al., Activation of Notch signaling in a xenograft model of brain metastasis, Clin. Cancer Res. 14 (13) (2008) 4059–4066.
[29] F. Xing, et al., Reactive astrocytes promote the metastatic growth of breast cancer stem-like cells by activating Notch signalling in brain, EMBO Mol. Med. 5 (3) (2013) 384–396.
[30] P.M. McGowan, et al., Notch1 inhibition alters the CD44(hi)/CD24(lo) population and reduces the formation of brain metastases from breast cancer, Mol. Cancer Res. 9 (7) (2011) 834–844.
[31] J.E. Draffin, et al., CD44 potentiates the adherence of metastatic prostate and breast cancer cells to bone marrow endothelial cells, Cancer Res. 64 (16) (2004) 5702–5711.
[32] S. Mine, et al., Hepatocyte growth factor enhances adhesion of breast cancer cells to endothelial cells in vitro through up-regulation of CD44, Exp. Cell Res. 288 (1) (2003) 189–197.
[33] E.I. Chen, et al., Adaptation of energy metabolism in breast cancer brain metastases, Cancer Res. 67 (4) (2007) 1472–1486.
[34] D. Palmieri, et al., Analyses of resected human brain metastases of breast cancer reveal the association between up-regulation of hexokinase 2 and poor prognosis, Mol. Cancer Res. 7 (9) (2009) 1438–1445.
[35] K. Yonemori, et al., Disruption of the blood brain barrier by brain metastases of triple-negative and basal-type breast cancer but not HER2/neu-positive breast cancer, Cancer 116 (2) (2010) 302–308.
[36] H. Peinado, et al., Pre-metastatic niches: organ-specific homes for metastases, Nat. Rev. Cancer (2017).
[37] Y. Liu, X.T. Cao, Characteristics and significance of the pre-metastatic niche, Cancer Cell 30 (5) (2016) 668–681.
[38] B.A. Aguado, et al., Engineering the pre-metastatic niche, Nat. Biomed. Eng. 1 (6) (2017).
[39] W.J. Chen, et al., Organotropism: new insights into molecular mechanisms of breast cancer metastasis, Npj Precis. Oncol. 2 (2018).
[40] Y.X. Guo, et al., Effects of exosomes on pre-metastatic niche formation in tumors, Mol. Cancer 18 (2019).
[41] Q. Liu, et al., Factors involved in cancer metastasis: a better understanding to "seed and soil" hypothesis, Mol. Cancer 16 (2017).
[42] A. Hoshino, et al., Tumour exosome integrins determine organotropic metastasis, Nature 527 (7578) (2015) p. 329-+..
[43] H. Xue, B. Lu, M. Lai, The cancer secretome: a reservoir of biomarkers, J. Transl. Med. 6 (2008).
[44] S. Patel, et al., Cancer secretomes and their place in supplementing other hallmarks of cancer, Adv. Mass Spectrom. Biomed. Res. 806 (2014) 409–442.
[45] J. Brandi, et al., Proteomic approaches to decipher cancer cell secretome, Semin. Cell Dev. Biol. 78 (2018) 93–101.
[46] K.J. Brown, et al., Advances in the proteomic investigation of the cell secretome, Expert Rev. Proteomics 9 (3) (2012) 337–345.
[47] Y.S. Ziegler, et al., Integration of breast cancer secretomes with clinical data elucidates potential serum markers for disease detection, diagnosis, and prognosis, PLoS One 11 (6) (2016).
[48] C. Fazakas, et al., Transmigration of melanoma cells through the blood-brain barrier: role of endothelial tight junctions and melanoma-released serine proteases, PLoS One 6 (6) (2011).
[49] H.K. Avraham, et al., Angiopoietin-2 mediates blood-brain barrier impairment and colonization of triple-negative breast cancer cells in brain, J. Pathol. 232 (3) (2014) 369–381.
[50] T.H. Lee, et al., Vascular endothelial growth factor modulates the transendothelial migration of MDA-MB-231 breast cancer cells through regulation of brain microvascular endothelial cell permeability, J. Biol. Chem. 278 (7) (2003) 5277–5284.
[51] B.C. Lee, et al., Involvement of the chemokine receptor CXCR4 and its ligand stromal cell-derived factor 1 alpha in breast cancer cell migration through human brain microvascular endothelial cells, Mol. Cancer Res. 2 (6) (2004) 327–338.
[52] N. Tominaga, et al., Brain metastatic cancer cells release microRNA-181c-containing extracellular vesicles capable of destructing blood-brain barrier, Nat. Commun. 6 (2015).
[53] W.Y. Zhou, et al., Cancer-secreted miR-105 destroys vascular endothelial barriers to promote metastasis, Cancer Cell 25 (4) (2014) 501–515.
[54] S. Tiwary, et al., Metastatic brain tumors disrupt the blood-brain barrier and alter lipid metabolism by inhibiting expression of the endothelial cell fatty acid transporter Mfsd2a, Sci. Rep. 8 (2018).
[55] S.S. McAllister, R.A. Weinberg, Tumor-host interactions: a far-reaching relationship, J. Clin. Oncol. 28 (26) (2010) 4022–4028.
[56] S. Hiratsuka, et al., Tumour-mediated upregulation of chemoattractants and recruitment of myeloid cells predetermines lung metastasis, Nat. Cell Biol. 8 (12) (2006) 1369–U31.
[57] J.T. Erler, V.M. Weaver, Three-dimensional context regulation of metastasis, Clin. Exp. Metastasis 26 (1) (2009) 35–49.
[58] T. Netelenbos, et al., Proteoglycans guide SDF-1-induced migration of hematopoietic progenitor cells, J. Leukoc. Biol. 72 (2) (2002) 353–362.
[59] A. Avigdor, et al., CD44 and hyaluronic acid cooperate with SDF-1 in the trafficking of human CD34(+) stem/progenitor cells to bone marrow, Blood 103 (8) (2004) 2981–2989.
[60] D.H. Jones, et al., Regulation of cancer cell migration and bone metastasis by RANKL, Nature 440 (7084) (2006) 692–696.
[61] O. Mendes, et al., MMP2 role in breast cancer brain metastasis development and its regulation by TIMP2 and ERK1/2, Clin. Exp. Metastasis 24 (5) (2007) 341–351.
[62] O. Mendes, H.T. Kim, G. Stoica, Expression of MMP2, MMP9 and MMP3 in breast cancer brain metastasis in a rat model, Clin. Exp. Metastasis 22 (3) (2005) 237–246.
[63] H. Liu, et al., The role of MMP-1 in breast cancer growth and metastasis to the brain in a xenograft model, BMC Cancer 12 (2012).
[64] N.A. Bhowmick, E.G. Neilson, H.L. Moses, Stromal fibroblasts in cancer initiation and progression, Nature 432 (7015) (2004) 332–337.
[65] A. Orimo, et al., Stromal fibroblasts present in invasive human breast carcinomas promote tumor growth and angiogenesis through elevated SDF-1/CXCL12 secretion, Cell 121 (3) (2005) 335–348.
[66] D.T. Butcher, T. Alliston, V.M. Weaver, A tense situation: forcing tumour progression, Nat. Rev. Cancer 9 (2) (2009) 108–122.
[67] P.P. Provenzano, et al., Collagen density promotes mammary tumor initiation and progression, BMC Med. 6 (2008) 11.
[68] M.W. Pickup, J.K. Mouw, V.M. Weaver, The extracellular matrix modulates the hallmarks of cancer, EMBO Rep. 15 (12) (2014) 1243–1253.
[69] F. Calvo, et al., Mechanotransduction and YAP-dependent matrix remodelling is required for the generation and maintenance of cancer-associated fibroblasts, Nat. Cell Biol. 15 (6) (2013) p. 637-+..
[70] M. Prager-Khoutorsky, et al., Fibroblast polarization is a matrix-rigidity-dependent process controlled by focal adhesion mechanosensing, Nat. Cell Biol. 13 (12) (2011) 1457–U178.
[71] S. Dawood, et al., Incidence of brain metastases as a first site of recurrence among women with triple receptor-negative breast cancer, Cancer 118 (19) (2012) 4652–4659.
[72] F. Heitz, et al., Triple-negative and HER2-overexpressing breast cancers exhibit an elevated risk and an earlier occurrence of cerebral metastases, Eur. J. Cancer 45 (16) (2009) 2792–2798.
[73] C.D. Savci-Heijink, et al., Retrospective analysis of metastatic behaviour of breast cancer subtypes, Breast Cancer Res. Treat. 150 (3) (2015) 547–557.
[74] S. Kumar, V.M. Weaver, Mechanics, malignancy, and metastasis: the force journey of a tumor cell, Cancer Metastasis Rev. 28 (1-2) (2009) 113–127.
[75] M.J. Paszek, et al., Tensional homeostasis and the malignant phenotype, Cancer Cell 8 (3) (2005) 241–254.
[76] M.A. Wozniak, et al., ROCK-generated contractility regulates breast epithelial cell differentiation in response to the physical properties of a three-dimensional collagen matrix, J. Cell Biol. 163 (3) (2003) 583–595.
[77] E.A. Klein, et al., Cell-cycle control by physiological matrix elasticity and in vivo tissue stiffening, Curr. Biol. 19 (18) (2009) 1511–1518.
[78] J.M. Barnes, L. Przybyla, V.M. Weaver, Tissue mechanics regulate brain development, homeostasis and disease, J. Cell. Sci. 130 (1) (2017) 71–82.
[79] J. Reinhard, et al., The extracellular matrix niche microenvironment of neural and cancer stem cells in the brain, Int. J. Biochem. Cell Biol. 81 (Pt A) (2016) 174–183.
[80] K.B. Pointer, et al., Association of collagen architecture with glioblastoma patient survival, J. Neurosurg. (2016) 1–10.
[81] C. Wang, X. Tong, F. Yang, Bioengineered 3D brain tumor model to elucidate the effects of matrix stiffness on glioblastoma cell behavior using PEG-based hydrogels, Mol. Pharm. 11 (7) (2014) 2115–2125.
[82] S.S. Rao, et al., Glioblastoma behaviors in three-dimensional collagen-hyaluronan composite hydrogels, ACS Appl. Mater. Interfaces 5 (19) (2013) 9276–9284.
[83] Y.A. Miroshnikova, et al., Tissue mechanics promote IDH1-dependent HIF1alpha-tenascin C feedback to regulate glioblastoma aggression, Nat. Cell Biol. 18 (12) (2016) 1336–1345.
[84] J.K. Mouw, G. Ou, V.M. Weaver, Extracellular matrix assembly: a multiscale deconstruction, Nat. Rev. Mol. Cell Biol. 15 (12) (2014) 771–785.
[85] Y. Kim, S. Kumar, CD44-based adhesion and mechanotransductive signaling on engineered hyaluronic acid matrices, Biophys. J. 106 (2) (2014) p. 523a-523a.
[86] M.M. Knupfer, et al., CD44 expression and hyaluronic acid binding of malignant glioma cells, Clin. Exp. Metastasis 17 (1) (1999) 71–76.
[87] A.A. Narkhede, et al., The influence of matrix stiffness on the behavior of brain metastatic breast cancer cells in a biomimetic hyaluronic acid hydrogel platform, J. Biomed. Mater. Res. A. 106 (7) (2018) 1832–1841.
[88] J. Neman, et al., Human breast-to-brain metastases display GABAergic properties in the neural niche, Cancer Res. 73 (2013).
[89] J. Termini, J. Neman, R. Jandial, Role of the neural niche in brain metastatic cancer (vol 74, pg 4011, 2014), Cancer Res. 74 (19) (2014) p. 5680-5680.
[90] G. Bergers, S. Song, The role of pericytes in blood-vessel formation and maintenance, NeuroOncology 7 (4) (2005) 452–464.
[91] J.N. Chen, et al., CD146 is essential for PDGFR beta-induced pericyte recruitment, Protein Cell 9 (8) (2018) 743–747.
[92] T. Yamazaki, Y.S. Mukouyama, Tissue specific origin, development, and pathological perspectives of pericytes, Front. Cardiovasc. Med. 5 (2018).

[93] L. Cheng, et al., Glioblastoma stem cells generate vascular pericytes to support vessel function and tumor growth, Cell 153 (1) (2013) 139–152.
[94] L.C.D. Smyth, et al., Markers for human brain pericytes and smooth muscle cells, J. Chem. Neuroanat. 92 (2018) 48–60.
[95] Y. Kienast, et al., Real-time imaging reveals the single steps of brain metastasis formation, Nat. Med. 16 (1) (2010) 116–U157.
[96] L.T. Lyle, et al., Alterations in pericyte subpopulations are associated with elevated blood-tumor barrier permeability in experimental brain metastasis of breast cancer, Clin. Cancer Res. 22 (21) (2016) 5287–5299.
[97] D.J. Loane, A. Kumar, Microglia in the TBI brain: the good, the bad, and the dysregulated, Exp. Neurol. 275 (2016) 316–327.
[98] K.M. Lenz, L.H. Nelson, Microglia and beyond: innate immune cells as regulators of brain development and behavioral function, Front. Immunol. 9 (2018).
[99] D.A. Menassa, D. Gomez-Nicola, Microglial dynamics during human brain development, Front. Immunol. 9 (2018).
[100] D. Boche, V.H. Perry, J.A.R. Nicoll, Review: activation patterns of microglia and their identification in the human brain, Neuropathol. Appl. Neurobiol. 39 (1) (2013) 3–18.
[101] M. Sidani, et al., Probing the microenvironment of mammary tumors using multiphoton microscopy, J. Mammary Gland Biol. Neoplasia 11 (2) (2006) 151–163.
[102] K.R. Wu, et al., Roles of the cyclooxygenase 2 matrix metalloproteinase 1 pathway in brain metastasis of breast cancer, J. Biol. Chem. 290 (15) (2015) 9842–9854.
[103] D. Matias, et al., Microglia/astrocytes-glioblastoma crosstalk: crucial molecular mechanisms and microenvironmental factors, Front. Cell. Neurosci. 12 (2018).
[104] T. Pukrop, et al., Microglia promote colonization of brain tissue by breast cancer cells in a Wnt-dependent way, Glia 58 (12) (2010) 1477–1489.
[105] F. Xing, et al., Loss of XIST in breast cancer activates MSN-c-met and reprograms microglia via exosomal miRNA to promote brain metastasis, Cancer Res. 78 (15) (2018) 4316–4330.
[106] M. Lorger, B. Felding-Habermann, Capturing changes in the brain microenvironment during initial steps of breast cancer brain metastasis, Am. J. Pathol. 176 (6) (2010) 2958–2971.
[107] K.E. Andreou, et al., Anti-inflammatory microglia/macrophages as a potential therapeutic target in brain metastasis, Front. Oncol. 7 (2017).
[108] S. Qiao, et al., Long-term characterization of activated microglia/macrophages facilitating the development of experimental brain metastasis through intravital microscopic imaging, J. Neuroinflammation 16 (2019).
[109] S. Hallal, et al., Extracellular vesicles released by glioblastoma cells stimulate normal astrocytes to acquire a tumor-supportive phenotype via p53 and MYC signaling pathways, Mol. Neurobiol. 56 (6) (2019) 4566–4581.
[110] D.B. Hoelzinger, T. Demuth, M.E. Berens, Autocrine factors that sustain glioma invasion and paracrine biology in the brain microenvironment, J. Natl. Cancer Inst. 99 (21) (2007) 1583–1593.
[111] A. Sierra, et al., Astrocyte-derived cytokines contribute to the metastatic brain specificity of breast cancer cells, Lab. Investig. 77 (4) (1997) 357–368.
[112] T. Wang, et al., Upregulation of matrix Metalloproteinase-9 in primary cultured rat astrocytes induced by 2-chloroethanol via MAPK signal pathways, Front. Cell. Neurosci. 11 (2017) 218.
[113] L. Zhang, et al., Microenvironment-induced PTEN loss by exosomal microRNA primes brain metastasis outgrowth, Nature 527 (7576) (2015) 100–104.
[114] B. Gril, et al., Pazopanib inhibits the activation of PDGFR beta-expressing astrocytes in the brain metastatic microenvironment of breast cancer cells, Am. J. Pathol. 182 (6) (2013) 2368–2379.
[115] J. Neman, et al., Co-evolution of breast-to-brain metastasis and neural progenitor cells, Clin. Exp. Metastasis 30 (6) (2013) 753–768.
[116] M. Smid, et al., Subtypes of breast cancer show preferential site of relapse, Cancer Res. 68 (9) (2008) 3108–3114.
[117] H. Kennecke, et al., Metastatic behavior of breast cancer subtypes, J. Clin. Oncol. 28 (20) (2010) 3271–3277.
[118] S. Wei, G.P. Siegal, Surviving at a distant site: the organotropism of metastatic breast cancer, Semin. Diagn. Pathol. 35 (2) (2018) 108–111.

Molecular Oncology

FEBS PRESS science publishing by scientists

Cadherin-3 is a novel oncogenic biomarker with prognostic value in glioblastoma

Eduarda P. Martins[1,2], Céline S. Gonçalves[1,2], Marta Pojo[1,2], Rita Carvalho[3], Ana S. Ribeiro[3], Vera Miranda-Gonçalves[1,2], Ricardo Taipa[4], Fernando Pardal[5], Afonso A. Pinto[6], Carlos Custódia[7], Cláudia C. Faria[7,8], Fátima Baltazar[1,2], Nuno Sousa[1,2], Joana Paredes[3,9] and Bruno M. Costa[1,2]

1 Life and Health Sciences Research Institute (ICVS), School of Medicine, University of Minho, Braga, Portugal
2 ICVS/3B's - PT Government Associate Laboratory, Braga/Guimarães, Portugal
3 i3S – Instituto de Investigação e Inovação em Saúde, Universidade do Porto, Porto, Portugal
4 Neuropathology Unit, Department of Neurosciences, Centro Hospitalar do Porto, Porto, Portugal
5 Department of Pathology, Hospital de Braga, Portugal
6 Department of Neurosurgery, Hospital de Braga, Portugal
7 Instituto de Medicina Molecular, Faculdade de Medicina, Universidade de Lisboa, Portugal
8 Neurosurgery Department, Hospital de Santa Maria, Centro Hospitalar Lisboa Norte (CHLN), Portugal
9 Faculty of Medicine of the University of Porto, Portugal

Keywords
biomarker; *CDH3*/P-cadherin; glioblastoma; survival; tumor aggressiveness

Corresponding author
B. M. Costa, Life and Health Sciences Research Institute (ICVS), School of Medicine, University of Minho, Campus Gualtar, 4710-057 Braga, Portugal
Fax: +351 253604831
Tel: +351 253604837
E-mail: bfmcosta@med.uminho.pt

(Received 6 April 2020, revised 1 December 2021, accepted 15 December 2021, available online 10 June 2022)

doi:10.1002/1878-0261.13162

Glioblastoma (GBM) is the most common and malignant primary brain tumor in adults. The prognosis of patients is very poor, with a median overall survival of ~ 15 months after diagnosis. Cadherin-3 (also known as P-cadherin), a cell–cell adhesion molecule encoded by the *CDH3* gene, is deregulated in several cancer types, but its relevance in GBM is unknown. In this study, we investigated the functional roles, the associated molecular signatures, and the prognostic value of *CDH3*/P-cadherin in this highly malignant brain tumor. *CDH3*/P-cadherin mRNA and protein levels were evaluated in human glioma samples. Knockdown and overexpression models of P-cadherin in GBM were used to evaluate its functional role *in vitro* and *in vivo*. *CDH3*-associated gene signatures were identified by enrichment analyses and correlations. The impact of *CDH3* in the survival of GBM patients was assessed in independent cohorts using both univariable and multivariable models. We found that P-cadherin protein is expressed in a subset of gliomas, with an increased percentage of positive samples in grade IV tumors. Concordantly, *CDH3* mRNA levels in glioma samples from The Cancer Genome Atlas (TCGA) database are increased in high-grade gliomas. P-cadherin displays oncogenic functions in multiple knockdown and overexpression GBM cell models by affecting cell viability, cell cycle, cell invasion, migration, and neurosphere formation capacity. Genes that were positively correlated with *CDH3* are enriched for oncogenic pathways commonly activated in GBM. *In vivo*, GBM cells expressing high

Abbreviations
CI, confidence interval; CNS, central nervous system; DGAV, Direção Geral de Alimentação e Veterinária; DMEM, Dulbecco's modified Eagle's medium; ES, Enrichment Score; FBS, fetal bovine serum; FDR, false discovery rate; FELASA, Federation of European Laboratory Animal Science Associations; FFPE, formalin-fixed paraffin-embedded; FPKM-UQ, fragments per kilobase of transcript per Million mapped reads upper quartile; GBM, glioblastoma; GO, gene ontology; GSEA, gene set enrichment analysis; H&E, hematoxylin and eosin; HR, hazard ratio; IHC, immunohistochemistry; KEGG, Kyoto encyclopedia of genes and genomes; KPS, Karnofsky Performance Score; NSG, Nod *scid* gamma; NT, nontumor; OS, overall survival; PI, propidium iodide; qRT-PCR, quantitative reverse transcription-polymerase chain reaction; RPMI, Roswell Park Memorial Institute medium; RT, room temperature; TCGA, The Cancer Genome Atlas; WB, western blot; WHO, World Health Organization.

This is an open access article under the terms of the Creative Commons Attribution License, which permits use, distribution and reproduction in any medium, provided the original work is properly cited.

levels of P-cadherin generate larger subcutaneous tumors and cause shorter survival of mice in an orthotopic intracranial model. Concomitantly, high *CDH3* expression is predictive of shorter overall survival of GBM patients in independent cohorts. Together, our results show that *CDH3*/P-cadherin expression is associated with aggressiveness features of GBM and poor patient prognosis, suggesting that it may be a novel therapeutic target for this deadly brain tumor.

1. Introduction

Gliomas represent a major portion of primary central nervous system (CNS) tumors, being glioblastoma (GBM) the most common and malignant form in adults [1]. Patients diagnosed with GBM present a median overall survival (OS) of approximately 15 months under standard-of-care treatment, based on tumor surgical resection and postoperative chemoradiotherapy [2,3]. Despite many advances in our understanding of the cellular and molecular characteristics of GBM, treatments did not significantly improve over the last few decades [4]. More recently, a variety of immunotherapies [5] (e.g., with immune checkpoint inhibitors [6,7]) and oncolytic virus therapies (e.g., with the recombinant oncolytic poliovirus PVSRIPO [8]) have emerged as potentially useful for GBM patients, but their value to improve overall survival is still limited. The identification of new molecular players relevant for GBM aggressiveness may allow a better stratification and understanding of this malignancy, potentially contributing to a better clinical management of patients.

Cadherins are cell–cell adhesion molecules dependent on calcium with a crucial role in tissue morphogenesis and maintenance of structural and functional tissues [9]. P(Placental)-cadherin, encoded by the *CDH3* gene, is a type I classical cadherin, firstly identified in murine placenta [10]. In humans, P-cadherin is also expressed in the placenta, but at lower levels than in mice, and is mainly found in basal layers of epithelial tissues [11–13]. In the last years, similarly to other classical cadherins, the relevance of P-cadherin in various cancers has been highly documented [14,15]. In breast cancer, P-cadherin overexpression is associated with poor clinical outcome and tumor aggressiveness, associating with tumor stem cell properties and invasiveness capacity [16–19]. Paradoxically, in malignant melanoma, P-cadherin induces an anti-invasive behavior by promoting cell–cell adhesion [20,21], highlighting the dual oncogenic or tumor-suppressor roles of P-cadherin according to the tumor type and particular molecular context (reviewed in ref. [15]). Interestingly, the relevance of P-cadherin in malignant gliomas was not previously studied.

In this work, using *in vitro* and *in vivo* models, as well as patient-derived samples, we have established *CDH3*/P-cadherin as a novel oncogenic player in human GBM, deciphering its functional roles, and as a novel prognostic biomarker predictive of shorter survival in GBM patients.

2. Materials and methods

2.1. Cell lines and cell culture

The human GBM cell lines U87MG and U373MG (kindly provided by Dr. Joseph Costello, University of California San Francisco, CA, USA), SNB19 (DSMZ, German Collection of Microorganisms and Cell Cultures, Braunschweig, Germany), U251MG, A172, LN229 (ATCC, American Type Culture Collection, Manassas, VA, USA), and the GBM patient-derived cultures GBML18 (previously established in our group [22]), GBML24, GBML45, and GBML95 were cultured in Dulbecco's modified Eagle's medium (DMEM, Biochrom GmbH, Berlin, Germany), supplemented with 10% fetal bovine serum (FBS, Biochrom GmbH). The GBM patient-derived culture GBML42 (established in our group, as previously described [23]) was maintained in Roswell Park Memorial Institute (RPMI, Biochrom GmbH) 1640 medium, supplemented with 10% FBS. Human embryonic kidney HEK293T cells (kindly provided by Dr. Andreia Neves-Carvalho, ICVS/University of Minho, Portugal) used for lentiviral packaging were cultured in DMEM supplemented with 10% FBS. Complete medium is defined as DMEM or RPMI (according to the cell culture) supplemented with 10% FBS. All cells were maintained in a humidified atmosphere, with 5% (v/v) CO_2 and at 37 °C, unless otherwise stated. GBM cell lines were authenticated by short tandem repeat profiling. All cultures were tested for mycoplasma contamination every month.

2.2. Glioma samples

Glioma tumors were obtained at Hospital de Braga (Braga, Portugal) and Hospital de Santa Maria (Lisbon, Portugal) during craniotomy surgeries for tumor resection or biopsy. Samples from both hospitals were used for mRNA expression levels evaluation. For that, samples were transported in dry ice from the Hospital to the laboratory and stored at −80 °C until further treatment. The samples from Hospital de Braga used for immunohistochemical analyses were formalin-fixed and paraffin-embedded.

2.3. *CDH3* overexpression in GBM cell line

U87MG cells were plated at an initial density of 2×10^5 cells per well (in a 6-well plate). On the next day, cells were transfected with the vector pIRES2-EGFP-CDH3 (U87-CDH3) that contains full-length cDNA encoding *CDH3*, or with the empty vector pIRES2-EGFP (U87-Ctrl) [24] using the lipofectamine 3000 transfection reagent (Invitrogen, Thermo Fisher Scientific, Waltham, MA, USA). Lipofectamine 3000 transfection reagent (4 μL per well) was diluted in Opti-Modified Eagle Reduced Serum Medium (Opti-MEM, Gibco, Thermo Fisher Scientific, Waltham, MA, USA), and the DNA mix was prepared by diluting the transfection vector (1 μg) in Opti-MEM and adding P3000 reagent (2 μL per μg DNA). Afterward, diluted DNA was incubated with the diluted lipofectamine for 15 min at room temperature (RT) and added dropwise to the cells. Cells were incubated with the transfection medium for 48 h. Transfected cells were selected through the incubation with geneticin (G418, 800 $\mu g \cdot mL^{-1}$, Santa Cruz Biotechnology, Dallas, TX, USA) in complete medium.

2.4. *CDH3* silencing in GBM primary cultures by siRNA and shRNA

For the transfection with siRNAs, GBML18 cells were plated at an initial density of 8×10^5 cells per T25 cm^2 culture flask. On the next day, cells were transfected with a small interfering RNA (siRNA) specific for *CDH3* (50 nM; Hs_CDH3_6, Qiagen, Hilden, Germany; GBML18-siCDH3) or the scramble siRNA (Qiagen; GBML18-siCtrl) using lipofectamine 3000 transfection reagent according to manufacturer's recommendations. Briefly, after the incubation of lipofectamine reagent (lipofectamine/siRNA ratio of 1 : 2) with Opti-MEM, siRNA diluted in Opti-MEM was added and incubated for 15 min at RT. This final solution was dropwise added to the cells that were maintained at regular culture conditions. Six hours after transfection, the medium was replaced by fresh complete culture medium and, 48 h after, cells were collected for *CDH3* silencing testing and platted for functional assays.

For lentiviral production, HEK293T cells were seeded at an initial density of 5×10^5 cells per well in 6-well plate and transfected with 1.2 μg of packaging plasmids (TR30022, Origene, Rockville, MD, USA) and 1 μg of *CDH3*-specific shRNA [pGFP-C-shLenti, Origene; GBML18-shCDH3 (construct TL314033C), GBML42-shCDH3-C (construct TL314033C), or GBML42-shCDH3-D (construct TL314033D)] or with a scramble control (TR30021, Origene; GBML18-shCtrl and GBML42-shCtrl) using lipofectamine 3000 (as described in Section *CDH3* overexpression in GBM cell line). The lentiviral supernatant was collected three days after transfection and filtered through a 0.45-μm filter. GBM patient-derived cells (GBML18 and GBML42), previously platted at the density of 5×10^5 in 25 cm^2-flask, were infected with lentivirus in the presence of 8 $\mu g \cdot mL^{-1}$ polybrene (Sigma-Aldrich, St. Louis, MO, USA). Successfully infected cells were selected through incubation with puromycin (0.8 $\mu g \cdot mL^{-1}$ for GBML18 and 1.5 $\mu g \cdot mL^{-1}$ for GBML42; Santa Cruz Biotechnology).

2.5. RNA extraction and cDNA synthesis

RNA of GBM patients' samples from Hospital de Santa Maria was extracted directly from the tumor piece, while samples from Hospital de Braga were previously converted to powder. RNA from tumor samples, primary cultures and cell lines was extracted using the TRIzol reagent (Invitrogen), following manufacturer's recommendations. cDNA was synthesized from 1 μg of RNA using the High-Capacity cDNA Reverse Transcription Kit (Applied Biosystems, Thermo Fisher Scientific, Waltham, MA, USA), following manufacturer's recommendations.

2.6. qRT-PCR—quantitative reverse transcription-polymerase chain reactions

CDH3, *WNT1*, *WNT5A*, and *TBP* (TATA Box Binding Protein—reference gene) expression levels were determined by qRT-PCR using TaqMan Fast Advanced Master Mix (1x; Applied Biosystems, Thermo Fisher Scientific). Specific probes were used for *CDH3* (Hs.PT.58.2656432; 1x; IDT, Integrated DNA Technologies, Leuven, Belgium) and *WNT1*, *WNT5A*, and *TBP* (Hs00180529_m1, Hs00998537_m1, and Hs00427620_m1, respectively; 1x; Life

Technologies, Thermo Fisher Scientific). The reactions were performed in duplicate using the 7500 Fast Real-Time PCR software (Applied Biosystems), for 2 min at 50 °C, 20 s at 95 °C, 3 s at 95 °C and 30 s at 60 °C. The last two steps were repeated for 40 cycles. The expression levels of *FZD4*, *PDGFRB*, *ZEB1*, *NANOG*, *VIM*, and *TBP* were assessed using the PowerUp SYBR Green Master Mix (Applied Biosystems). Reactions were performed for 2 min at 50 °C, 2 min at 95 °C, 15 s at 95 °C and 1 min at the respective annealing temperature, and the last two steps repeated for 40 cycles. Primers' sequences and annealing temperatures are displayed in Table S1. mRNA expression was normalized to *TBP* expression, according to the $2^{-\Delta C_t}$ (Ct: threshold cycle; when presented as relative expression) or $2^{-\Delta\Delta C_t}$ (when presented as fold change) methods [25].

2.7. Viability assays

For trypan blue (Gibco, Thermo Fisher Scientific) exclusion assay, cells were plated at an initial concentration of 6×10^3 (U87MG), 1.5×10^4, or 2×10^4 (GBML18, siRNA or shRNA model, respectively), and 6×10^3 (GBML42) per well, in 6-well plates (each condition in triplicates), and counted 6 days after platting.

For MTS (CellTiter 96® AQueous One Solution Cell Proliferation Assay; Promega, Madison, WI, USA), 4×10^3 GBML18 and 2×10^3 GBML42 cells were platted in 24-well and 12-well plates, respectively, and incubated for 6 days. Cultures were incubated with 10% MTS in complete medium for up to 4 h at 37 °C and 5% (v/v) CO_2. Optical density was measured at 490 nm.

2.8. Neurosphere formation assay

Glioblastoma cells were platted at low density (2×10^3 cells per well for U87MG and 1×10^3 cells for GBML18) in low-attachment 24-well plates (Corning Inc., Corning, NY, USA), in DMEM-F12 (Gibco) supplemented with B27 (1%, Invitrogen), EGF (epidermal growth factor, 20 ng·mL^{-1}, Invitrogen), and bFGF (basic fibroblast growth factor, 20 ng·mL^{-1}, Invitrogen). Fresh medium was added every 2–3 days, and the total number of neurospheres formed was counted at day 10 of incubation for U87MG cells and at day 8 for GBML18.

2.9. 3D spheroid cell invasion

Spheroids were obtained following manufacturer's instructions (GravityTRAP™ ULA Plate, InSphero AG, Schlieren, Switzerland). Briefly, 100 or 200 cells/70 µL (U87 and GBML18, respectively) were added to a 96-well from the GravityTRAP™ ULA Plate and left for 24 h in order to form the cellular spheroid. The medium containing 6–8 spheroids was recovered to a tube. The excess medium was removed, and the spheroids were further embedded in rat tail collagen type I matrix ($NaHCO_3$ 0.25 M; NaOH 1 M, Millipore, Burlington, MA, USA). 3D spheroids embedded in collagen type I were plated in an 8-well coverslip bottom chambers (IBIDI, Planegg, Germany) followed by 1 h of incubation at 37 °C to allow polymerization. After this, complete medium without phenol red was added to the cellular 3D spheroid cultures. The *in vitro* behavior was followed by time-lapse microscopy (Leica microscope—DMI6000B with Adaptative Focus Control, Wetzlar, Germany) during 18 h. Further, the images taken every 20 min were converted into a time-lapse movie, and quantitative analysis of the number of isolated cell invasion and protrusions was performed using Leica LASX Software (Leica, Wetzlar, Germany).

2.10. Wound healing assay

GBML18 and GBML42 cells were platted at high density (6×10^4 cells in each compartment) in 2-well inserts (ibidi GmbH, Gräfelfing, Germany) and incubated overnight to allow cells' adhesion. Inserts were removed on the following day, and migration capacity was registered in photographs taken in an inverted microscope (objective lens magnification 4×; Olympus CKX41 microscope, Olympus, Tokyo, Japan). For each time point, two images/areas were recorded per well. Wound widths (in pixels) were calculated using the BEWOUND software (version 1.7, BESURG, Braga, Portugal), and wound closures were determined in percentages.

2.11. Cell cycle

GBML18 and GBML42 cells were platted in 25-cm^2 flasks at the initial density of 3×10^5 cells and collected 48 and 32 h after platting, respectively. Cells were fixed in 70% (v/v) ethanol, washed twice with PBS 1x, and incubated with propidium iodide (20 µg·mL^{-1}, PI, Invitrogen), RNase (250 µg·mL^{-1}, Invitrogen), and Triton X-100 (0.1%) for 1 h in the dark at 50 °C. Cell acquisition was performed on a BD LSRII flow cytometer (BD Biosciences, Franklin Lakes, NJ, USA) with a 488 nm excitation laser and using the FACS DIVA software (BD Biosciences). At least 30000 gated events were acquired. Data were analyzed using the FLOWJO Software (v10.8.0; Tree Star, Ashland, OR, USA). Doublet cells were removed

plotting FSC-area vs FSC-height and double-checked plotting PI-area vs PI-height. The percentage of cells in each phase was obtained applying the Dean-Jett-Fox algorithm. Experiments were performed in quadruplicates.

2.12. Immunohistochemistry (IHC)

Immunohistochemistry was performed in 3-μm formalin-fixed paraffin-embedded (FFPE) tissue sections as previously described for P-cadherin [26], and for Ki-67, NESTIN, SOX2, BCL2, and Cyclin D1 [27] (details about the antibodies and conditions are presented in Table S2). P-cadherin expression in glioma samples was evaluated and semi-quantified by an experienced neuropathologist (Dr. Ricardo Taipa). The percentage of P-cadherin positive cells was defined as: 0–1% and 1–25%. Expression intensity was defined as: negative, mild, and moderate/intense. Normal human skin and breast tissue were used as positive controls. The percentage of stained areas for Ki-67, NESTIN, SOX2, BCL2, and Cyclin D1 in orthotopic GBM tumors formed upon the injection of U87-Ctrl or U87-CDH3 cells in NSG mice were quantified in at least three animals per group (objective lens magnification 20×: median ~ 137 mm^2; Olympus Upright BX61 microscope) using IMAGEJ software (version 1.52a, Bethesda, MD, USA).

2.13. Western blot (WB)

Western blot was performed in protein lysates as previously described [28]. Briefly, protein lysates were prepared from cultured cells using a lysis buffer [1% (v/v) Triton X-100 and 1% (v/v) NP-40 (Sigma) in deionized water Diagnostics GmbH; 1 : 7 Protease Inhibitors Cocktail (Roche Diagnostics Gmbh, Mannheim, Germany) and 1 : 100 Phosphatase inhibitor (Sigma-Aldrich, Darmstadt, Germany)]. Cells were washed twice in PBS and were allowed to lyse in 500 μL of the lysis buffer for 10 min, at 4 °C. Lysates were then submitted to vortex, centrifuged at high-speed and supernatants were collected. Protein concentration was determined using Bio-Rad protein assay (Bio-Rad, Richmond, CA, USA). Samples were then separated by 10% SDS/PAGE. Proteins were transferred into nitrocellulose membranes (Amersham Hybond ECL, Amersham Biosciences, Buckinghamshire, UK) at 100 V for 90 min. For immunostaining, membranes were blocked with 5% (w/v) non-fat dry milk in PBS containing 0.5% (v/v) Tween-20. Membranes were subsequently incubated with primary antibodies (details in Table S2), followed by six 5-min washes in PBS/Tween-20 and incubation with horseradish peroxidase-conjugated secondary antibodies for 1 h. Membranes were then washed for 30 min in PBS/Tween-20. Proteins were detected using ECL Chemiluminescence detection kit (Amersham Pharmacia Biotech, Piscataway, NJ, USA) as a substrate. Blots were exposed to an autoradiographic film. Each immunoblot was performed at least three times, and the ones selected for figures are representative experiments.

2.14. Mice studies

Mice were kept under standard laboratory conditions with artificial 12 h light/dark cycle (all experiments performed during daylight), controlled ambient temperature (21 ± 1 °C), and a relative humidity of 50–60%, always manipulated in a flow hood chamber, except during intracranial surgeries and ultrasound imaging acquisition. Mice had available *ad libitum* irradiated food and autoclaved water, and were housed in groups of 3–5 per cage to allow social interaction. Cages were also enriched with paper to promote nest building and mice hiding. Sentinel mice health status was used as confirmation of specified pathogen-free according to FELASA (Federation of European Laboratory Animal Science Associations).

In vivo subcutaneous GBM xenograft models

To establish the U87 GBM subcutaneous xenograft model in mice, 1×10^6 U87 cells (U87-Ctrl or U87-CDH3) were injected in both flanks of male immunodeficient SHrN® hairless NOD.SCID mice (NOD.Cg-*Prkdc*^{scid}*Hr*^{hr}/NCrHsd; Harlan Laboratories; 3 per group) aged 6–8 weeks, randomly distributed between the two groups. Tumors were measured with a caliper, and the tumor volume was determined by assessing the two largest sides [Volume (cm^3) = (3.14 × L1 × L1 × L2)/6] (L1 = length; L2 = width). All animals were euthanized when the largest side of the tumor of one animal reached 2 cm. After euthanasia, the tumors were collected and fixed by immersion in formalin and subsequently embedded in paraffin for histological analyses.

The subcutaneous patient-derived xenograft model using GBML18 primary culture (GBML18-shCtrl or GBML18-shCDH3) was established by injecting 1.5×10^6 cells in the flank of 4–5 months old male immunodeficient NOD *scid* gamma (NSG) mice—NOD.Cg-*Prkdc*^{scid}*Il2rg*^{tm1Wjl}/SzJ (Charles River Laboratories, Wilmington, MA, USA; 4 GBML18-shCtrl and 5 GBML18-shCDH3), randomly distributed between the two groups. Tumors were measured by ultrasound, as detailed below (Section In vivo ultrasound imaging).

After euthanasia, the tumors were collected and fixed for histological analyses.

In vivo ultrasound imaging

The Vevo 3100 ultra-high-frequency ultrasound imaging station for small animal (FUJIFILM VisualSonics, Toronto, Canada) was used to assess mice subcutaneous tumor volume at the endpoint. Image acquisitions were performed using the MX550D transducer (40 MHz) and the Mouse (Small) Abdominal settings.

Mice were anesthetized with 3% isoflurane in oxygen, and their flanks were depilated using a depilation cream, and immobilized in the prone position and maintained warm in Vevo's mouse handling table. Mice physiological status (heart and respiratory rates, and body temperature) was closely monitored during the entire acquisition session. Mice were imaged using the motorized 3D mode. Transducer focal length, as well as the acquisition width and depth, was adjusted to the tumor area. The B-mode scanning plane was aligned with the 2D cross section showing the tumor at its largest diameter, and the 3D range adjusted to capture the entire tumor of each mouse (step size was automatically set by the Vevo system). Each 3D acquisition was later analyzed in the VEVOLAB software (version 5.5.0, FUJIFILM VisualSonics), using Vevo's multislice method for tumor volume quantification.

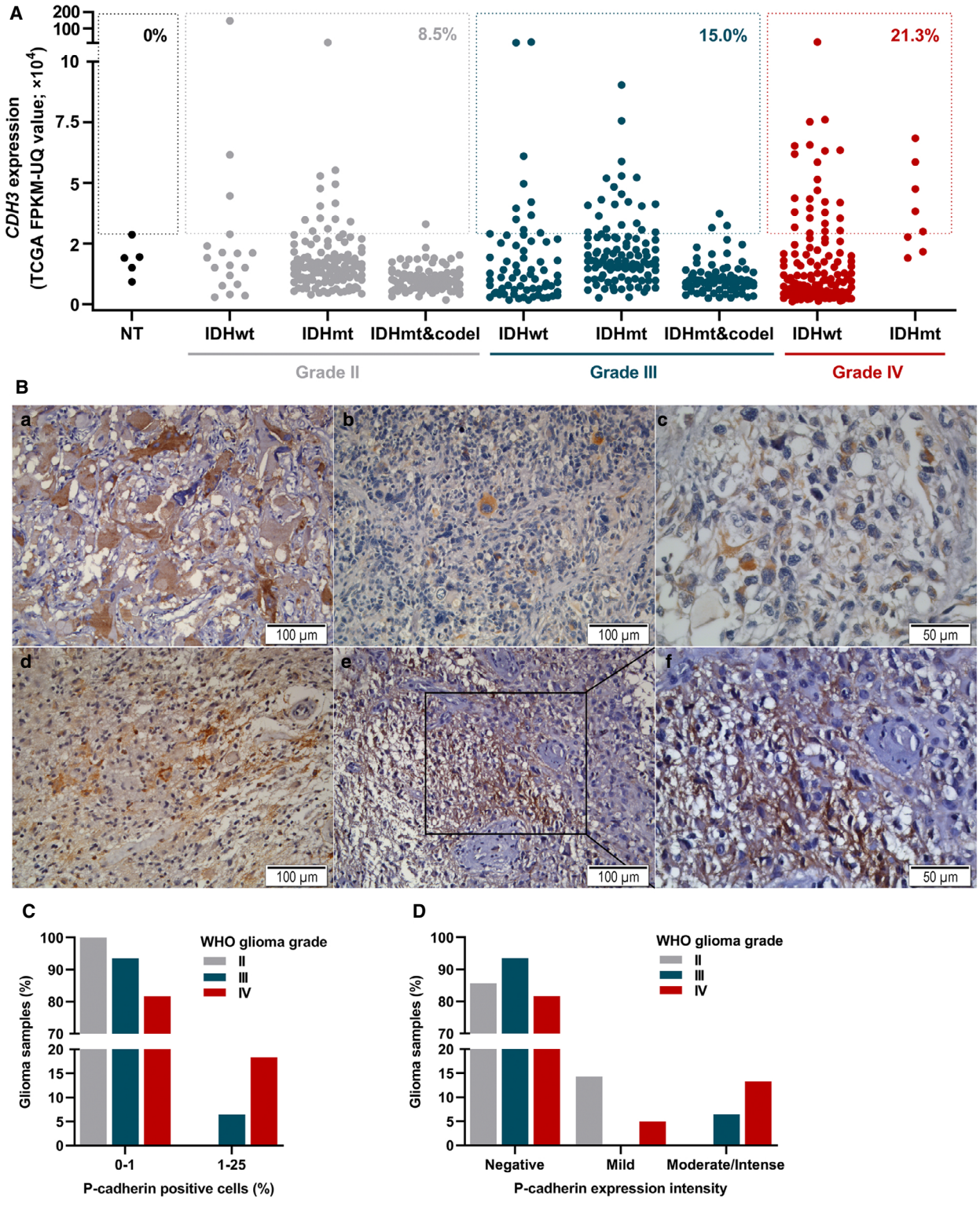
In vivo intracranial orthotopic GBM xenograft model

The intracranial orthotopic model was obtained by injecting U87-Ctrl or U87-CDH3 cells (2×10^5 cells diluted in 5 μL of PBS per animal) stereotactically in the striatum region (+1.8 mm mediolateral, +0.1 mm anteroposterior, −2.5 mm dorsoventral from bregma) of 6- to 10-week-old male immunodeficient NSG mice (Charles River Laboratories). Three independent experiments were performed with a total number of 18 U87-Ctrl and 19 U87-CDH3 animals. Mice were randomly assigned to groups, ensuring no major body weight and age differences between groups. Pre-surgery procedures included anesthesia with ketamine ($75\ mg{\cdot}kg^{-1}$) and medetomidine hydrochloride ($1\ mg{\cdot}kg^{-1}$) intraperitoneally injected, and the analgesic drug butorphanol ($5\ mg{\cdot}kg^{-1}$) that was subcutaneously injected. Cells were injected using a stereotaxic apparatus (digital 3-axis; Stoelting, Wood Dale, IL, USA) and a 10 μL Hamilton syringe (point style 4 beveled and 26 s gauge) at the velocity of $1.7\ \mu L{\cdot}min^{-1}$. Body weight was measured at least every 2 days. The humane endpoint established was 30% weight loss in relation to the maximum weight reached. When the humane endpoint was achieved, the animals were sacrificed by anesthesia overdose. After perfusion using paraformaldehyde 4%, the brain was collected to be latter embedded in paraffin for histological analyses.

2.15. Data mining from publicly available glioma patients' datasets

CDH3 expression data obtained by RNA sequencing (Illumina HiSeq 2000 sequencing system) and expression microarrays (Agilent G4502A 244K), and clinical data were downloaded from The Cancer Genome Atlas (TCGA) database (https://portal.gdc.cancer.gov/) [29]. The IDH mutation and 1p19q codeletion status data were extracted from GlioVis (http://gliovis.bioinfo.cnio.es/) [30]. RNA-Seq expression data contained 5 nontumor unmatched controls, 224 WHO grade II and 240 WHO grade III gliomas, and 141 GBMs. *CDH3* overexpression in glioma samples was considered when higher than the maximum expression of nontumor controls in RNA-Seq data (TCGA FPKM-UQ value > 28 700). Microarray expression data contained 573 GBMs. The median expression value was used whenever more than

Fig. 1. *CDH3*/P-cadherin is overexpressed in a subset of gliomas. (A) *CDH3* mRNA expression in 5 nontumor controls (NT; black dots) and 605 glioma patients from TCGA (RNA-Seq data), comprising 224 grade II (gray dots), 240 grade III (blue dots), and 141 grade IV (red dots). Data are stratified according to IDH mutation and 1p/19q codeletion status, and malignancy grade: 18 IDH-wild-type, 121 IDH-mutant 1p19q non-co-deleted, and 85 IDH-mutant 1p19q co-deleted grade II gliomas; 66 IDH-wild-type, 102 IDH-mutant 1p19q non-co-deleted, and 72 IDH-mutant 1p19q co-deleted grade III gliomas; 133 IDH-wild-type and 8 IDH-mutant grade IV gliomas. The percentage values indicated for each WHO glioma grade correspond to the proportion of patients overexpressing *CDH3* (expression higher than non-tumor controls). (B) Representative IHC images of P-cadherin staining in glioma samples from a cohort of patients from Hospital de Braga ($n = 98$). P-cadherin staining was mostly cytoplasmic in glioma cells (images a and b) and, more rarely, associated with positivity in fibrillary astrocytic networks (images c-f; image f is a magnified region of e). Images a, b, c, e, and f show GBM samples, and image d represents an anaplastic oligodendroglioma. Scale bar = 100 μm, except in image c and f in which scale bar = 50 μm. (C–D) Semiquantitative analysis of P-cadherin IHCs in WHO grades II ($n = 7$), III ($n = 31$), and IV ($n = 60$) gliomas from the Hospital de Braga cohort, showing the percentage of cells expressing P-cadherin (C), and the staining intensity (D). (TCGA: The Cancer Genome Atlas; FPKM-UQ: Fragments Per Kilobase of transcript per Million mapped reads upper quartile; codel, chromosomal 1p/19q codeletion; IDHwt, IDH-wild-type; IDHmt, IDH-mutant; NT, non-tumor; WHO, World Health Organization).



one portion per patient was available. Values were pre-processed and normalized according to 'level 3' specifications of TCGA.

The *CDH3* most positively (Spearman $r > 0.3$) and inversely (Spearman $r < -0.3$) correlated genes (microarray data) were used to test for enriched Reactome

and KEGG pathways and gene ontologies using Enrichr (https://amp.pharm.mssm.edu/Enrichr/) [31,32].

2.16. Gene set enrichment analysis (GSEA)

Gene set enrichment analysis analysis was performed using the GSEA software (www.broad.mit.edu/gsea/) [33] and the microarray expression profile of GBM patients from TCGA (n = 573; Agilent G4502A 244K) [29]. A continuous phenotype profile was used; that is, Pearson's correlation was applied to rank the genes according to *CDH3* expression. Otherwise, default options were used. Gene sets from the molecular signature database C6 collection were used. A gene set was considered significantly enriched when presenting a false discovery rate (FDR) lower than 0.30.

2.17. Statistical analysis

To determine statistical differences between groups in the *in vivo* assays, homoscedasticity was tested using the F test, and afterward, two-sided unpaired t-test was applied, except for longitudinal subcutaneous tumor growth, in which a two-way ANOVA followed by Sidak's multiple comparisons test was used. For *in vitro* assays, two-sided paired t-tests were used, except for migration and cell cycle analyses, where a two-way ANOVA followed by Sidak's multiple comparisons test was applied. For the OS studies (*in vivo* mice models and GBM patients), *CDH3* effect was determined using the log-rank (Mantel-Cox) test (in patients from the Portuguese cohort, the top 30% of samples with lowest expression of *CDH3* were defined as *CDH3*-low GBMs). The prognostic value of *CDH3* was also evaluated using a Cox multivariable analysis adjusted for confounding factors. All analyses were performed in GRAPHPAD PRISM (GraphPad software, Inc., San Diego, CA, USA, version 8) and IBM SPSS STATISTICS (Armonk, New York, NY, USA, version 25) software. Meta-analysis and forest plot were performed in the software Comprehensive Meta-Analysis (Biostat, Inc., Englewood, NJ, USA, version 3) using hazard ratios and confidence intervals of multivariable analyses (random effect was determined). Each statistical test used is reported in figure legends. Statistically significant differences were considered when P-values were lower than 0.05.

2.18. Study approval

Collection of human glioma samples at Hospital de Braga and Hospital de Santa Maria was approved by the respective ethical entity (Subcomissão de Ética para as Ciências da Vida e da Saúde—SECVS 150/2014 and Comissão Nacional de Proteção de Dados—CNPD 7435/2011, respectively) with all patients signing informed consent, according to the Declaration of Helsinki. All animal procedures were approved by the national ethical committee DGAV (Direção Geral de Alimentação e Veterinária, reference no. 017761) and were in accordance with European Union Directive 2010/63/EU.

3. Results

3.1. *CDH3*/P-cadherin is overexpressed in a subset of gliomas

To study the expression pattern of *CDH3* in gliomas, we firstly analyzed its expression levels in patient samples (WHO grades II to IV) deposited in TCGA database with available RNA-seq data (Fig. 1A). In this analysis, we took into consideration the stratification of patients as per their IDH mutation and 1p/19q codeletion status, according to the 2016 WHO classification of CNS tumors [34]. A wide spectrum of expression of *CDH3* was observed in each glioma subgroup, reflecting the remarkable inter-individual heterogeneity typical of glioma. Interestingly, particular cases of high expression of *CDH3* were found in each glioma subtype, both in IDH-wild-type (22.2%, 16.7%, and 18.8% of IDH-wild-type grade II, III, and IV gliomas, respectively) and IDH-mutant cases (11.6%, 21.6%, and 62.5% of gliomas IDH-mutant grade II, III, and IV, respectively). In contrast, IDH-mutant and 1p/19q co-deleted gliomas, classically classified as oligodendroglioma, presented consistently low levels of *CDH3* expression, with only 1.2% and 4.2% of grade II and III cases overexpressing *CDH3*. Focusing on each WHO malignancy grade, independently of IDH mutation and 1p/19q codeletion status, the frequency of *CDH3* overexpression increased with higher tumor grades (8.5% in grade II, 15.0% in grade III, and 21.3% in grade IV gliomas).

We next evaluated P-cadherin protein expression by IHC in our cohort of glioma samples from which FFPE-tissues were available (Hospital de Braga; n = 98), including WHO grades II, III and IV gliomas. The major clinicopathological features, including histological subtype and WHO grade (of which GBM constitutes the majority of cases), age and gender distribution, IDH mutation status, treatment exposure and institution are presented in Table 1. We detected P-cadherin positive samples in all malignancy grades of gliomas (Fig. 1B–D), with a higher frequency within grade IV (GBM) tumors (of note, only 1 out of 7 tested grade II gliomas presented detectable levels of

Table 1. Clinical information of patients included in the Portuguese dataset.

Number of patients[a]	115
Diagnosis, *n* (%)	
Diffuse astrocytoma	3 (2.6%)
Anaplastic astrocytoma	3 (2.6%)
Oligodendroglioma	2 (1.7%)
Anaplastic oligodendroglioma	20 (17.4%)
Oligoastrocytoma	1 (0.9%)
Anaplastic oligoastrocytoma	1 (0.9%)
Glioblastoma	85 (73.9%)
WHO Grade, *n* (%)	
II	6 (5.2%)
III	24 (20.9%)
IV	85 (73.9%)
Lesion, *n* (%)	
Primary	108 (93.9%)
Recurrence	7 (6.1%)
Age, mean (range)	59.5 (20–81)
Gender, *n* (%)	
Male	78 (67.8%)
Female	37 (32.2%)
IDH1/*IDH2* mutation status[b], *n* (%)	
wt	42 (36.5%)
mt	15 (13.0%)
Not specified	58 (50.4%)
MGMT promoter methylation[c], *n* (%)	
Methylated	11 (9.3%)
Unmethylated	14 (11.9%)
Not specified	93 (78.8%)
Treatment, *n* (%)	
Chemotherapy	2 (1.7%)
Radiotherapy	16 (13.9%)
Chemoradiotherapy	83 (72.2%)
Not treated	8 (7.0%)
Not specified	6 (5.2%)
Institution, *n* (%)	
Hospital de Braga	72 (62.6%)
Hospital de Santa Maria	43 (37.4%)

[a]Patients from Hospital de Braga and Hospital de Santa Maria with P-cadherin protein expression evaluated by IHC ($n = 71$) and *CDH3* mRNA expression evaluated by qRT-PCR ($n = 66$).
[b]Determined by restriction fragment length polymorphism (RFLP) or IHC confirmed by Sanger sequencing in dubious cases.
[c]Determined by pyrosequencing technology [80].

P-cadherin expression, but only at mild levels and in less than 1% of the cells; Fig. 1C,D). Semiquantitative analyses demonstrated that an increased percentage of P-cadherin positive cells and higher staining intensity is found in grade IV gliomas (Fig. 1C,D). Representative P-cadherin IHC images of each WHO glioma grade are shown in Fig. S1.

Globally, the increased percentage of *CDH3*/P-cadherin overexpressing samples in grade IV gliomas suggests this molecule may be relevant for tumor aggressiveness.

3.2. P-cadherin is associated with GBM *in vitro* aggressiveness in an overexpression model

Considering the heterogeneity observed in patients, we firstly studied the expression of *CDH3* in a total of 12 GBM *in vitro* cell models, including six GBM cell lines and six patient-derived cultures (Fig. S2). We identified GBM cells with high (SNB19, GBML18, GBML24, and GBML45), intermediate (A172, GBML26, GBML42, and GBML95), and low/undetectable *CDH3* expression (U87MG, U373MG, U251MG, and LN229), nicely recapitulating the heterogeneity observed in patients.

To pinpoint the impact of P-cadherin in GBM, we firstly performed *in vitro* functional assays using an overexpression approach, in which *CDH3*/P-cadherin was overexpressed in U87 cells (a commercially available GBM cell line with very low or undetectable levels of *CDH3*/P-cadherin by qRT-PCR and western blot). Success of transfection and overexpression was confirmed at the mRNA level by qRT-PCR (Fig. 2A) and at the protein level by western blot (Fig. 2B). P-cadherin expression was associated with increased GBM cell viability, as assessed by trypan blue exclusion assay (Fig. 2C). Considering that GBMs are known for their remarkable invasiveness capacity [35], and since P-cadherin has been shown to impact cell invasion in different tumors (e.g., melanoma [20,21] and breast cancer [18]), we also evaluated how P-cadherin affects this cancer hallmark feature by three-dimensional invasion assays (Fig. 2D). P-cadherin was associated with increased cell invasion capacity in GBM cells, as measured by isolated cell invasion events (Fig. 2E) and the total number of protrusions (Fig. 2F). P-cadherin-overexpressing GBM cells also formed more neurospheres than control cells (Fig. 2G, H). Together, these results suggest that P-cadherin regulates several critical hallmarks of cancer in GBM *in vitro*, acting mostly in an oncogenic manner.

3.3. P-cadherin promotes tumor growth *in vivo* and associates with shorter survival in GBM xenograft mouse models

A subcutaneous GBM xenograft model was established in immunodeficient hairless NOD.SCID mice injected with U87 cells previously manipulated for *CDH3* expression. Tumors derived from U87-CDH3 cells presented a significantly higher growth rate than U87-control tumors (Fig. 2I), resulting in tumors with higher volumes (Fig. 2J) and weights (Fig. 2K) at the humane endpoint of the experiment. Tumor histology (Fig. 2L) and long-term P-cadherin protein expression (Fig. 2M) was confirmed.

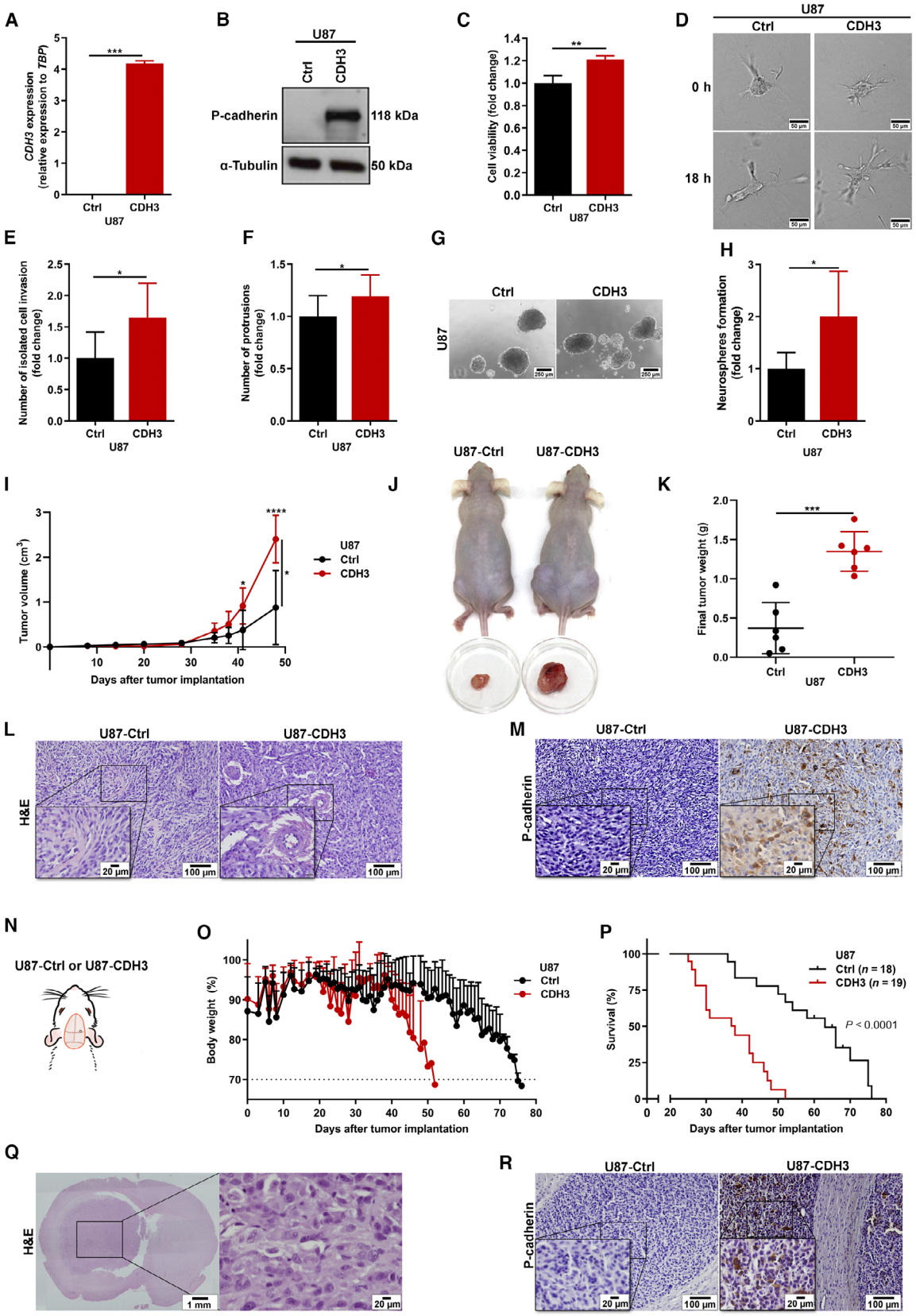
To better mimic the complex GBM microenvironment, we also established an intracranial orthotopic model in immunodeficient NSG mice injecting CDH3-low and CDH3-high U87 GBM cells (Fig. 2N). Mice body weight was registered throughout the experiment, showing that mice injected with U87-CDH3 cells displayed significant weight loss earlier and more drastically than animals injected with U87-Ctrl cells (Fig. 2O). More importantly, mice with tumors overexpressing P-cadherin exhibited significantly shorter survival than mice injected with control GBM cells ($P < 0.0001$; Fig. 2P), suggesting P-cadherin may be prognostically valuable in GBM. Tumor formation was confirmed through hematoxylin and eosin (H&E) staining of the brains (Fig. 2Q), and P-cadherin long-term *in vivo* expression was confirmed in mice tumors by IHC, being exclusively detected in U87-CDH3 tumors (Fig. 2R). Additionally, we evaluated the expression of some cancer-related proteins in *ex vivo* tumors from both groups, including proliferation (Ki-67 and Cyclin D1), anti-apoptotic (BCL2), and stemness (NESTIN and SOX2) markers, collected at distinct time points according to animal survival times (Fig. S3A,B). Interestingly, despite the prominent effect in the survival of mice, there were no significant differences regarding the levels of expression of these proteins between both groups of tumors at the humane endpoint. Of note, intracranial tumors revealed to be highly heterogeneous both histologically and molecularly, with various levels of positive staining for each marker, regardless of P-cadherin status (Fig. S3B).

3.4. *CDH3* knockdown impairs distinct cancer hallmarks in GBM cells

In addition to the overexpression approach, the impact of P-cadherin in GBM cells was also assessed using gene silencing approaches. Firstly, *CDH3* was silenced by siRNA in GBML18 cells (a GBM patient-derived culture with high levels of P-cadherin expression). Efficacy of transient transfections was determined at the RNA (Fig. 3A) and protein (Fig. 3B) levels. Fitting well with the findings in the overexpression model using U87MG cells, the silencing of P-cadherin in GBML18 patient-derived cultured with siRNA resulted in decreased cell viability (Fig. 3C), decreased invasion (Fig. 3D–F), and decreased capacity to form neurospheres (Fig. 3G,H).

Considering the observed effects of transient silencing of P-cadherin with siRNA *in vitro*, we next established a stable knockdown model using a shRNA targeting *CDH3*. After confirming the long-term knockdown of *CDH3*/P-cadherin (Fig. S4A,B), this shRNA-based GBML18 model was validated *in vitro* for key cancer hallmarks, globally recapitulating the association of P-cadherin silencing with compromised GBM cell viability (Fig. S4C,D) and migration capacity (Fig. S4E,F). Furthermore, we confirmed the functional effects of shRNA-mediated *CDH3* silencing in an additional GBM patient-derived culture (GBML42). The stable silencing of *CDH3* was confirmed (Fig. S5A), and *CDH3* functional effects were consistently validated, endorsing its association with

Fig. 2. P-cadherin displays oncogenic functions by regulating key hallmarks of malignancy in GBM *in vitro* and *in vivo*. (A–B) Successful *CDH3* overexpression in the GBM cell line U87MG, as assessed at the mRNA levels by qRT-PCR ($n = 3$) (A) and at protein levels by western blot ($n = 3$, representative experiment is displayed) (B). (C) Effect of P-cadherin in cell viability assessed by trypan blue in U87 cells ($n = 4$). (D–F) Three-dimensional invasion assays of P-cadherin-high and P-cadherin-low GBM cells ($n = 5$; representative images are shown for both conditions (D); scale bar = 50 μm). Quantification of isolated cell invasion (E) and protrusions (F) in GBM cells with high and low P-cadherin expression. (G–H) Influence of P-cadherin in the stemness capacity of GBM cells as assessed by the neurosphere formation assay ($n = 5$; representative images of all conditions are shown (G); scale bar = 250 μm). (H) Quantification of the number of neurospheres formed in GBM cells with high and low levels of P-cadherin. (I) Effect of P-cadherin on tumor growth kinetics of *in vivo* subcutaneous GBM models (bilateral injections per mice, $n = 3$ hairless NOD.SCID mice per group). (J) *In vivo* and *ex vivo* pictures at the experimental endpoint (day = 49) of U87 subcutaneous tumors with high or low P-cadherin expression levels (bilateral injections per mice, $n = 3$ per group). (K) Final tumor weight of subcutaneous tumors formed from U87-Ctrl and U87-CDH3 cells (bilateral injections per mice, $n = 3$ per group). (L) H&E staining of subcutaneous tumors (representative images are displayed; scale bars = 100 μm and 20 μm, as indicated). (M) P-cadherin protein expression in the subcutaneous U87-Ctrl and U87-CDH3 tumors (representative images are displayed; scale bars = 100 μm and 20 μm, as indicated). (N) Intracranial surgery scheme for orthotopic models ($n = 18$ for U87-Ctrl, and $n = 19$ U87-CDH3). (O) Total body weight variation after intracranial injections of *CDH3*-manipulated U87 cells in NSG mice ($n = 18$ for U87-Ctrl, and $n = 19$ for U87-CDH3). (P) Overall survival of mice intracranially implanted with *CDH3*-overexpressing or control-U87 GBM cells ($n = 18$ for U87-Ctrl, and $n = 19$ for U87-CDH3). (Q) H&E staining of brain sections to confirm tumor formation (representative images are displayed; scale bars = 1 mm and 20 μm, as indicated). (R) Long-term P-cadherin expression in GBM tumors formed from U87-Ctrl and U87-CDH3 cells' mice orthotopic injection (representative images are displayed; scale bars = 100 and 20 μm, as indicated). [H&E: hematoxylin and eosin staining; panels A, C, E, F,H two-sided paired *t*-test, data is presented as mean ± SEM; panel K: two-sided unpaired *t*-test, data are presented as mean ± SD; panel I: two-way ANOVA followed by post-hoc Sidak's test, data are presented as mean ± SD; panel O: data are presented as mean ± SD; panel P: log-rank test; $*P < 0.05$; $**P < 0.01$; $***P < 0.001$; $****P < 0.0001$].


A
CDH3 expression (relative expression to TBP)
***
Ctrl
CDH3
U87
B
U87
Ctrl
CDH3
P-cadherin
118 kDa
α-Tubulin
50 kDa
C
Cell viability (fold change)
**
Ctrl
CDH3
U87
D
U87
Ctrl
CDH3
0 h
18 h
50 µm
E
Number of isolated cell invasion (fold change)
*
Ctrl
CDH3
U87
F
Number of protrusions (fold change)
*
Ctrl
CDH3
U87
G
Ctrl
CDH3
U87
250 µm
H
Neurospheres formation (fold change)
*
Ctrl
CDH3
U87
I
Tumor volume (cm³)
****
*
*
U87
Ctrl
CDH3
Days after tumor implantation
J
U87-Ctrl
U87-CDH3
K
Final tumor weight (g)
***
Ctrl
CDH3
U87
L
U87-Ctrl
U87-CDH3
H&E
20 µm
100 µm
M
U87-Ctrl
U87-CDH3
P-cadherin
20 µm
100 µm
N
U87-Ctrl or U87-CDH3
O
Body weight (%)
U87
Ctrl
CDH3
Days after tumor implantation
P
Survival (%)
U87
Ctrl (n = 18)
CDH3 (n = 19)
P < 0.0001
Days after tumor implantation
Q
H&E
1 mm
20 µm
R
U87-Ctrl
U87-CDH3
P-cadherin
20 µm
100 µm

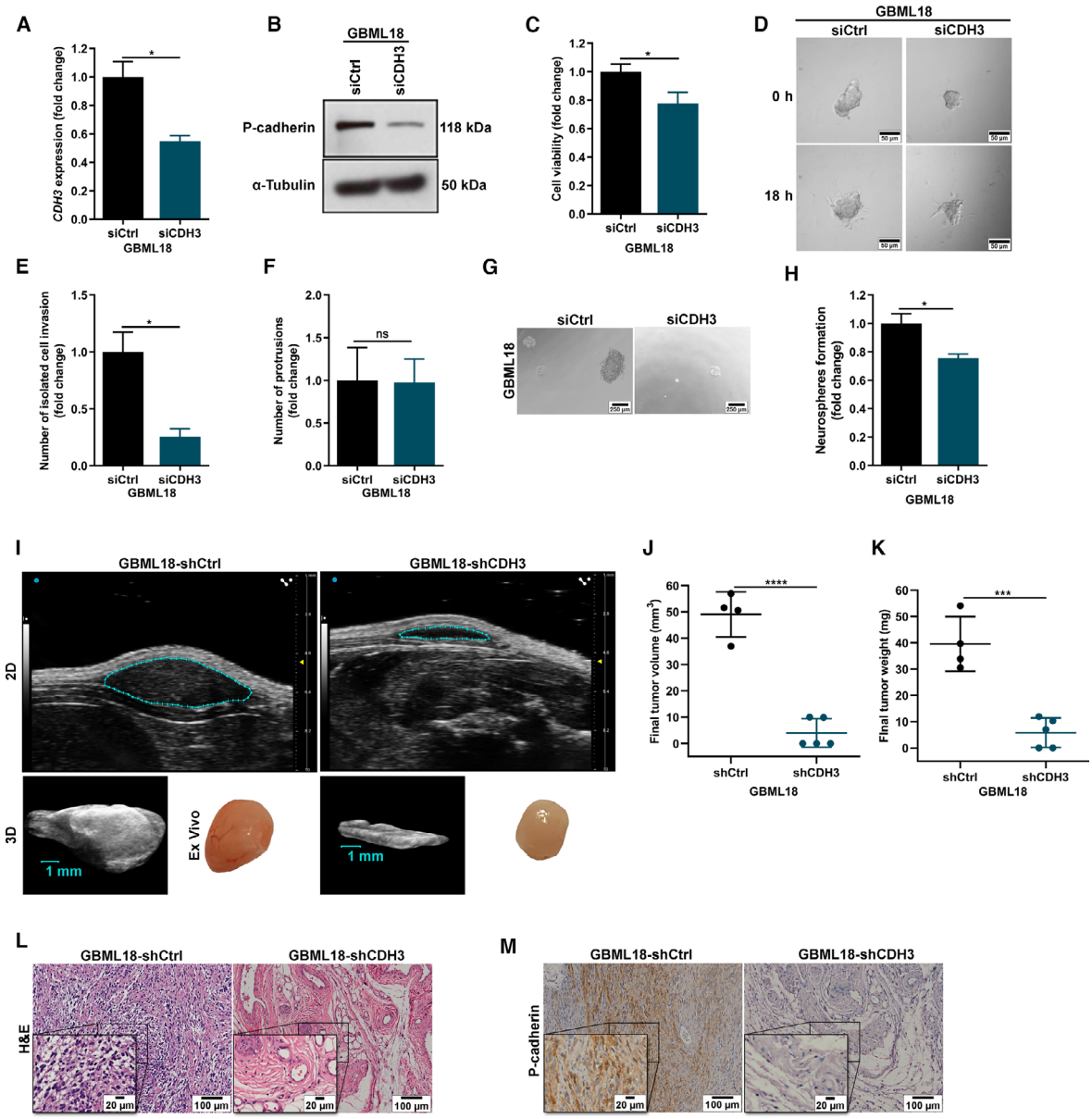


Fig. 3. P-cadherin knockdown impairs distinct cancer hallmarks in GBM cells and diminishes tumor growth *in vivo*. (A–B) Success of transient transfections with siRNA in GBM patient-derived culture GBML18 assessed by RNA ($n = 4$) (A) and protein levels ($n = 3$, representative experiment is displayed) (B). (C) Functional effect of P-cadherin in cell viability (trypan blue exclusion assay, $n = 5$). (D–F) Three-dimensional invasion assay of GBML18-siCtrl and GBML18-siCDH3 [$n = 3$; representative images are shown for each experimental condition (D); scale bar = 50 µm]. Isolated cell invasion (E) and protrusions were quantified (F). (G–H) Neurospheres formation capacity ($n = 5$; representative images in (G); scale bar = 250 µm; and quantification of the number of neurospheres formed in each condition (H). (I) Representative ultrasound images obtained at the endpoint of the experiment for subcutaneous tumors formed from the injection of GBML18 cells stably silencing *CDH3* (GBML18-shCtrl vs GBML18-shCDH3) in NSG mice ($n = 4$ and 5, respectively), at the largest two-dimensional cross-sectional plan and after three-dimensional reconstruction (scale bar = 1 mm). Respective *ex vivo* tumors are shown. (J) Final tumor volume determined by ultrasound after three-dimensional reconstruction and measurements ($n = 4$ for GBML18-shCtrl and $n = 5$ for GBML18-shCDH3). (K) Final tumor weight of the P-cadherin-high and P-cadherin-low subcutaneous tumors determined at the endpoint ($n = 4$ for GBML18-shCtrl and $n = 5$ for GBML18-shCDH3). (L) Histology of the tumors formed assessed by H&E (representative images are displayed; scale bars = 100 µm and 20 µm, as indicated). (M) IHC showing P-cadherin expression in GBML18-shCtrl tumors and silencing in GBML18-shCDH3 group (representative images are displayed; scale bars = 100 µm and 20 µm, as indicated). [H&E: hematoxylin and eosin staining; panels A, C, E, F, H: two-sided paired *t*-test, data are presented as mean ± SEM; panels J, K: two-sided unpaired *t*-test, data are presented as mean ± SD; ns: nonsignificant; $*P < 0.05$; $***P < 0.001$; $****P < 0.0001$].

increased cell viability (Fig. S5B,C), and migration (Fig. S5D,E).

3.5. The stable silencing of *CDH3* disrupts GBM tumor growth *in vivo*

To understand the effects of *CDH3* stable silencing *in vivo*, we then established subcutaneous xenograft tumors by injecting GBML18 cells (GBML18-shCtrl or GBML18-shCDH3) in the flank of NSG mice. Concordantly to the results obtained with the overexpression model (Fig. 2), mice bearing *CDH3*-low cells formed much smaller tumors than the ones injected with *CDH3*-high cells, as observed by ultrasound imaging, both at two-dimensional analyses and after three-dimensional tumor reconstructions (Fig. 3I). The collected tumors were consistently smaller in GBML18-shCDH3 group comparing to GBML18-shCtrl animals, as proven by the reduced final tumor volume (Fig. 3J), and final tumor weight (Fig. 3K). Tumor histology (Fig. 3L) and P-cadherin long-term silencing (Fig. 3M) were confirmed by H&E staining and IHC, respectively.

3.6. *CDH3* influences cell cycle progression in GBM cells

Considering the consistent data in distinct models associating P-cadherin with cell viability and GBM tumor growth *in vivo*, the influence of P-cadherin silencing on cell cycle was also evaluated in our two GBM primary cultures with stable *CDH3* knockdown (Fig. S6). Curiously, the silencing of *CDH3* significantly impacted cell cycle in the two primary cultures, despite cell-specific differences. Specifically, the silencing of *CDH3* in GBML18 cells (Fig. S6A) led to a diminished G0/G1 phase and G2/M enrichment (a hallmark of cells undergoing mitotic cell death and with decreased mitosis/proliferation [36,37]), while in GBML42 (Fig. S6B), *CDH3* knockdown led to an increment of S phase associated with decreased G2/M phase, suggesting an arrest in the DNA replication phase [38].

3.7. *CDH3*-associated gene signatures are enriched for common GBM-related pathways

To gain insights into putative cellular and molecular mechanisms responsible for the oncogenic effects of P-cadherin observed *in vitro* and *in vivo*, we performed GSEA in the large cohort of GBM patients from TCGA ($n = 573$). Using *CDH3* expression as continuous label, we found that *CDH3*-positively correlated genes were enriched for signatures of genes upregulated upon the activation of the WNT-β-catenin signaling, RTK/PI3K/mTOR signaling axis (through *ERBB2*, *VEGF* and *mTOR*), and upon inactivation of the tumor-suppressor genes *PTEN* and *RB*; in addition, *CDH3*-positively correlated genes were enriched for signatures of genes downregulated upon HOXA9 silencing (Fig. 4A).

To validate our *in vitro* results suggesting that P-cadherin influences cell viability, cell cycle, invasion, and stemness capacity, we investigated the expression levels of specific genes belonging to three Gene Ontology (GO) gene sets related to those cancer hallmarks. Interestingly, in GBM patients, *CDH3* was co-expressed with several genes related to cell cycle, cell motility, and stem cells proliferation (heatmaps representing *CDH3*'s top 5 most co-expressed genes belonging to each gene set, Fig. 4B; and representative individual examples of correlation graphs, Fig. 4C). To further complement these data, we searched for gene ontologies and pathways associated with the *CDH3* most positively and negatively correlated genes (Fig. 4D and Fig. S7). In line with our previous data, we observed that *CDH3*-positively correlated genes are enriched for Reactome classes such as cell–cell junction organization, and activation of matrix metalloproteinases (Fig. 4D), as well as with other cancer-related pathways revealed by KEGG analyses, such as cGMP-PKG and Wnt signaling pathways (Fig. S7A). Finally, the expression of particular key players involved in the signaling pathways and/or biological processes identified in the transcriptomic data from this large dataset of GBM patients was also tested in our genetically manipulated GBM patient-derived cultures (Fig. S7E). Despite the differences observed between the two knockdown models, suggesting that some of these expression patterns might be cell-dependent, the overall association between *CDH3* and markers of these pathways was validated (e.g., *CDH3* silencing led to a decreased expression of WNT/β-catenin genes, such as *WNT1* and *WNT5A*), establishing good parallels between our *in vitro* data and that from patients.

Globally, these genome-wide analyses suggest that *CDH3*/P-cadherin might be associated with pro-tumor gene expression signatures that are known to be critical in GBM signaling.

3.8. *CDH3* is predictive of shorter survival in primary GBM patients

Taking into consideration our data implicating P-cadherin with GBM aggressiveness *in vitro*, and to be associated with poor prognosis (shorter OS) in a GBM xenograft model, we questioned if this association was

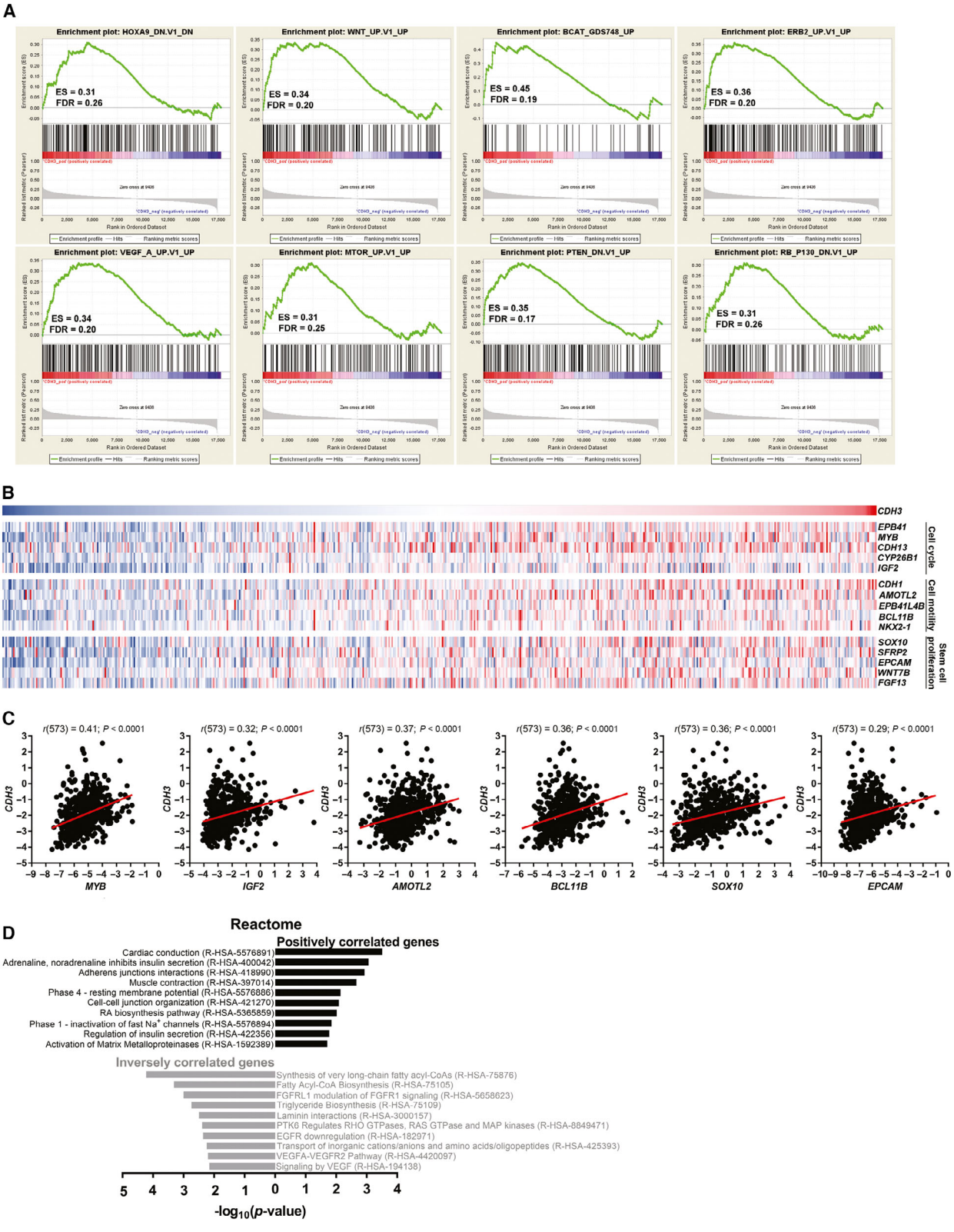

A
Enrichment plot: HOXA9_DN.V1_DN
ES = 0.31
FDR = 0.26
Enrichment plot: WNT_UP.V1_UP
ES = 0.34
FDR = 0.20
Enrichment plot: BCAT_GDS748_UP
ES = 0.45
FDR = 0.19
Enrichment plot: ERB2_UP.V1_UP
ES = 0.36
FDR = 0.20
Enrichment plot: VEGF_A_UP.V1_UP
ES = 0.34
FDR = 0.20
Enrichment plot: MTOR_UP.V1_UP
ES = 0.31
FDR = 0.25
Enrichment plot: PTEN_DN.V1_DN
ES = 0.35
FDR = 0.17
Enrichment plot: RB_P130_DN.V1_UP
ES = 0.31
FDR = 0.26
Rank in Ordered Dataset
Enrichment profile
Hits
Ranking metric scores
B
CDH3
EPB41
MYB
CDH13
CYP26B1
IGF2
CDH1
AMOTL2
EPB41L4B
BCL11B
NKX2-1
SOX10
SFRP2
EPCAM
WNT7B
FGF13
Cell cycle
Cell motility
Stem cell proliferation
C
r(573) = 0.41; P < 0.0001
r(573) = 0.32; P < 0.0001
r(573) = 0.37; P < 0.0001
r(573) = 0.36; P < 0.0001
r(573) = 0.36; P < 0.0001
r(573) = 0.29; P < 0.0001
CDH3
MYB
IGF2
AMOTL2
BCL11B
SOX10
EPCAM
D
Reactome
Positively correlated genes
Cardiac conduction (R-HSA-5576891)
Adrenaline, noradrenaline inhibits insulin secretion (R-HSA-400042)
Adherens junctions interactions (R-HSA-418990)
Muscle contraction (R-HSA-397014)
Phase 4 - resting membrane potential (R-HSA-5576886)
Cell-cell junction organization (R-HSA-421270)
RA biosynthesis pathway (R-HSA-5365859)
Phase 1 - inactivation of fast Na+ channels (R-HSA-5576894)
Regulation of insulin secretion (R-HSA-422356)
Activation of Matrix Metalloproteinases (R-HSA-1592389)
Inversely correlated genes
Synthesis of very long-chain fatty acyl-CoAs (R-HSA-75876)
Fatty Acyl-CoA Biosynthesis (R-HSA-75105)
FGFRL1 modulation of FGFR1 signaling (R-HSA-5658623)
Triglyceride Biosynthesis (R-HSA-75109)
Laminin interactions (R-HSA-3000157)
PTK6 Regulates RHO GTPases, RAS GTPase and MAP kinases (R-HSA-8849471)
EGFR downregulation (R-HSA-182971)
Transport of inorganic cations/anions and amino acids/oligopeptides (R-HSA-425393)
VEGFA-VEGFR2 Pathway (R-HSA-4420097)
Signaling by VEGF (R-HSA-194138)
-log10(p-value)

Fig. 4. *CDH3*-positively correlated genes in GBM patients are enriched for genes involved in common cancer-related pathways. (A) GSEA analyses demonstrating that *CDH3*-positively correlated genes are enriched for genes downregulated upon the knockdown of *HOXA9*, and for genes upregulated upon the activation of the WNT-β-catenin signaling and RTK/PI3K/mTOR signaling axis, or the silencing of *PTEN* and *RB*. (B) Heatmaps of expression levels of *CDH3* and the 5 most positively correlated genes of three distinct GO gene sets (cell cycle—GO:0007049; cell motility—GO:0048870; stem cell proliferation—GO:0072089) in 573 GBM TCGA patients. Darkest blue represents the lowest expression values and darkest red represents the higher expression values of each row. (C) Correlations plots between *CDH3* expression and *MYB*, *IGF2*, *AMOTL2*, *BCL11B*, *SOX10*, and *EPCAM* in TCGA GBM patients (Spearman's correlations *r* and *P* values are shown). (D) Reactome pathways among the most positively (Spearman $r > 0.3$) and inversely (Spearman $r < -0.3$) *CDH3*-correlated genes in 573 GBM patients from TCGA (DN, downregulated; ES, enrichment score; FDR, false discovery rate; GO, gene ontology; GSEA, gene set enrichment analyses; TCGA, The Cancer Genome Atlas; UP, upregulated).

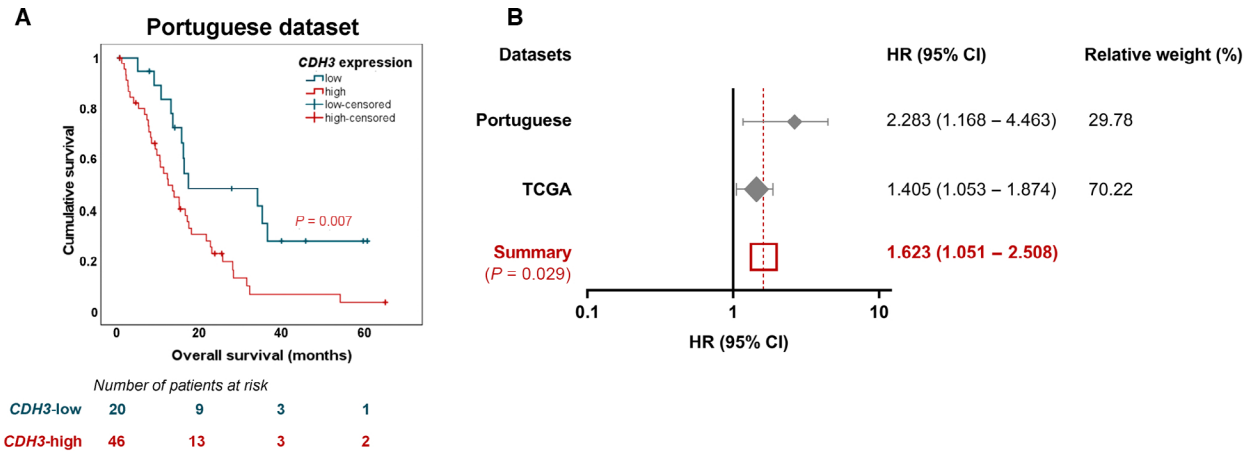


Fig. 5. High *CDH3* expression is associated with shorter overall survival in GBM patients. (A) Kaplan-Meier survival curve of our Portuguese cohort ($n = 66$) regarding low ($n = 20$) and high ($n = 46$) *CDH3* mRNA expression levels in GBM patients, as evaluated by qRT-PCR. The cohort includes 33 IDH wt (50%), and 33 GBM samples with IDH status not specified (50%); 9 *MGMT* promoter methylated (13.6%), 9 *MGMT* promoter unmethylated (13.6%), and 48 GBM samples not evaluated for *MGMT* promoter methylation (72.7%). (B) Meta-analysis of the association of *CDH3* and overall survival in GBM patients from the Portuguese and TCGA datasets. The analysis was performed with the hazard rations obtained with Cox multivariable analyses. Each diamond represents one dataset and its size correlates to the relative weight of the dataset in the analysis. The extending lines indicate the 95% confidence intervals. The red square represents the overall effect (TCGA, The Cancer Genome Atlas; HR, hazard ratio; CI, confidence interval; log-rank test was applied in panel A).

also present in human patients. Interestingly, P-cadherin was already described to associate with poor patient prognosis in other types of cancer [19,39,40]. To test our hypothesis, we evaluated *CDH3* mRNA expression levels by qRT-PCR in primary GBM samples collected at Hospital de Braga and Hospital de Santa Maria ($n = 66$; clinical information in Table 1). The median OS of primary GBM patients in our cohort was 13.7 months, very similar to that described more recently in the literature [3]. We found that GBM patients with high *CDH3* expression present significantly shorter OS than those with low expression levels (Fig. 5A; $P = 0.007$). Importantly, considering the putative effects of age and gender in a multivariable survival analysis, *CDH3* maintained its independent prognostic value (Table 2; $P = 0.016$). This association of *CDH3* with poor prognosis was further validated in the large TCGA dataset using a multivariable Cox model (Table 3; $P = 0.021$), adjusted for the potential confounding effects of *IDH1* mutation status, age at diagnosis, Karnofsky performance status (KPS), gender, treatment with chemo- or radiotherapy, and additional treatments. Importantly,

Table 2. Cox multivariable survival analysis in GBM patients from Portuguese dataset (qRT-PCR data; $n = 66$). Bold-faced values indicate significant *P*-values (CI, Confidence Interval; HR, Hazard Ratio).

	P-value	HR	95% CI
CDH3 expression[a,b]	**0.016**	2.283	1.168–4.463
Age at diagnosis	**0.047**	1.035	1.001–1.070
Gender[a,c]	0.167	0.619	0.314–1.222

[a] *CDH3* expression and gender were used as categorical variables.
[b] *CDH3*-low ($n = 20$) vs. *CDH3*-high expression ($n = 46$).
[c] Male ($n = 49$) vs. Female ($n = 17$).

Table 3. Cox multivariable survival analysis in GBM patients from TCGA (microarray data; $n = 275$). Bold-faced values indicate significant *P*-values (CI, confidence interval; HR, hazard ratio).

	P-value	HR	95% CI
CDH3 expression[a,b]	**0.021**	1.405	1.053–1.874
IDH1 mutation status[a,c]	**0.031**	0.518	0.285–0.941
Age at diagnosis	**0.001**	1.021	1.009–1.034
KPS[a,d]			
0–50	**0.001**	–	–
60–70	**0.004**	0.339	0.162–0.711
80–100	**< 0.001**	0.250	0.122–0.512
Gender[a,e]	0.141	0.793	0.583–1.080
Chemo- or radiotherapy[a,f]	**< 0.001**	0.211	0.122–0.367
Additional chemo- or radiotherapy[a,g]	0.072	0.762	0.566–1.024

[a] *CDH3* expression, *IDH1* mutation status, KPS, gender, chemo- or radiotherapy, and additional chemo- or radiotherapy were used as categorical variables.
[b] *CDH3*-low ($n = 129$) vs. *CDH3*-high expression ($n = 146$), defined based on the median value of expression.
[c] *IDH1*-wild-type ($n = 252$) vs. *IDH1*-mutant ($n = 23$).
[d] KPS 0–50 ($n = 13$); 60–70 ($n = 63$); 80–100 ($n = 199$).
[e] Male ($n = 172$) vs. Female ($n = 103$).
[f] No treatment ($n = 18$) vs. Treatment ($n = 257$).
[g] No additional treatment ($n = 152$) vs. Additional treatment ($n = 123$).

to integrate data from the independent cohorts, a meta-analysis was performed, validating that *CDH3* is significantly associated with shorter OS (Fig. 5B, HR = 1.623, $P = 0.029$). Globally, our data indicate that *CDH3* associates with shorter OS of GBM patients, suggesting its potential as a novel biomarker predictive of poor prognosis in these patients.

4. Discussion

Distinct cadherins are known to play a role in gliomas [41–46]. However, the impact of P-cadherin, which has been implicated in several types of cancer [20,47–51], was still unknown in glioma. While cadherin-6 [52], cadherin-11 [52], T-cadherin [53], R-cadherin [52], and N-cadherin [54] are widely expressed in the brain of distinct species, P-cadherin has been considered largely undetected in various brain regions in mice and humans [10,13,55,56]. Thus, the aberrant expression observed in some gliomas, particularly grade IV gliomas (Fig. 1) may have functional consequences impacting glioma pathophysiology. Other studies reported that P-cadherin is associated with high histological grades in invasive ductal breast carcinoma [51], lung invasive adenocarcinoma [39], and in colorectal tumors [48]. Concordantly with the idea that P-cadherin associates with more aggressive cancers, our study established P-cadherin as a novel oncogenic player in GBM, affecting cell viability, cell cycle, cell invasion, migration, and neurosphere formation (Figs 2 and 3; Figs S4–S6). These data are concordant with the described effect of P-cadherin in breast cancer, in which it is associated with increased invasiveness and stemness capacity [16,17,51]. Contrarily, P-cadherin associates with decreased cell invasion in melanoma [20]. Considering the relevant impact of P-cadherin in stemness in other types of cancer, future studies to specifically address how P-cadherin influences self-renewal capacity of glioma stem cells are warranted. Despite the *in vitro* results and the prominent effect in shortening mice OS (Fig. 2), we did not find significant differences between control- and P-cadherin-overexpressing U87 orthotopic tumors regarding the expression of proteins commonly altered in GBM, including stemness markers (Fig. S3). This result may be partly explained by the fact that all tumors (formed from U87-Ctrl and U87-CDH3 cells) were analyzed at different time points based on the OS of each animal, a stage at which they have reached similar levels of aggressiveness. Future studies should focus on studying the effect of P-cadherin in GBM in mice survival using long-term knockdown approaches.

Cadherins are not considered to have only structural functions. Indeed, different intracellular mediators were reported to interact with P-cadherin (reviewed in [15]). Consistent with this idea, we found that some of the P-cadherin oncogenic effects observed in GBM may result from alterations in critical intracellular signaling pathways. Interestingly, our GSEA analyses in GBM patients (Fig. 4) demonstrated associations between *CDH3*-correlated genes and β-catenin-dependent WNT pathway, described to be associated with GBM aggressiveness [57]. This putative link between P-cadherin and β-catenin was also previously reported in mammary basal epithelial cells [58], and in colon cancer cells, where the inhibition of P-cadherin leads to the downregulation of β-catenin [59]. Furthermore, WNT genes, such as *WNT5A* [60] and *WNT6* [27], were also already described to impact GBM aggressiveness, some of which presented differential expression due to *CDH3* status in our GBM models (Fig. S7E). Interestingly, the associations observed between *CDH3*-correlated genes, *VEGF*, *ERBB2*, and *mTOR* suggest its involvement in oncogenic pathways, such as the RTK/PI3K/mTOR signaling axis [61]. Moreover, the oncogenic value of *CDH3* is reinforced by the upregulation of *CDH3*-positively correlated genes upon knockdown of *RB* and *PTEN* tumor-suppressor genes, and by the association with *HOXA9*, a transcription factor with critical oncogenic functions in GBM [22,62,63]. Data from clinical specimens also

suggested that *CDH3* correlates with genes involved in key biological processes, such as *MYB*, described to be activated in some GBM cell lines [64], and dependent on PI3K [65], further validating our GSEA data. *IGF2*-high expressing GBMs are frequently associated with poor survival [66], and IGF2 can interact with IGF-1R, activating it and leading to a proliferative phenotype through AKT [67]. Interestingly, P-cadherin on its own is described to activate invasion and metastasis capacities in ovarian cancer by interacting with IGF-1R [68]. In addition to these specific genes, we identified a strong positive correlation between *CDH3* and genes involved in cell migration (*AMOTL2* [69] and *BCL11B* [70]] and stemness capacity [*SOX10* [71] and *EPCAM* [72]) in GBM patients, further supporting our *in vitro* data. While these findings result from association and correlation analyses from patient samples, and thus do not establish direct causative relationships, they may shed light into the gene signatures and signaling pathways by which P-cadherin mediates its oncogenic functions in glioma, which could be further explored in future studies.

Despite the advances that resulted in the identification of clinically relevant molecules in GBM, the heterogeneity of these tumors still requires the discovery of novel players to improve the accuracy of diagnosis and prognosis [73]. The prognostic value of *CDH3*, predictive of shorter OS in independent cohorts of GBM patients (Fig. 5 and Tables 2 and 3), is concordant with the results obtained *in vivo*, and fits well with previous reports in breast cancer [19,40] and lung cancer [39]. The prognostic value of other classical cadherins, such as E- and N-cadherin, has been explored in gliomas, but somewhat contradicting findings have been reported, with some authors, suggesting that these cadherins are not suitable as prognostic molecules [74], while others report low levels of *CDH2* (coding N-cadherin protein) as being predictive of longer survival and better response to temozolomide [45], the most used chemotherapeutic agent in the treatment of GBM.

Our findings implicating P-cadherin as a tumor promoting molecule, and the prognostic value of *CDH3* independent of other known prognostic indicators, suggest this cell–cell adhesion molecule may be an attractive new therapeutic target for P-cadherin-positive tumors. Thus, in future, it will be critical to test the therapeutic value of specific inhibitors of P-cadherin in GBM, some of which have been already developed [75–79] and completed phase 1 clinical trials [e.g., an immunoconjugate PCA062 (NCT02375958) and an anti-P-cadherin/anti-CD3-bispecific molecule PF-06671008 (NCT02659631)] in solid tumors, including triple-negative breast cancer, head and neck cancer, and esophageal cancer.

5. Conclusions

In conclusion, our work establishes, for the first time, *CDH3*/P-cadherin as a novel oncogenic molecule in GBM. We demonstrated that this cell adhesion molecule is overexpressed in a subset of high-grade gliomas, and affects GBM aggressiveness *in vitro*. *In vivo*, P-cadherin associates with increased tumor growth and shorter survival. In the clinical setting, *CDH3* correlates with cancer-related signatures and associates with poor prognosis of GBM patients.

Acknowledgements

The authors want to acknowledge to the families and patients who contributed to this study. Financial support was provided by projects (PTDC/CCI-BIO/4180/2020 and PTDC/SAU-GMG/113795/2009 to BMC; SAICTPAC/0022/2015 and 02/SAICT/2017/030625 to JP), and individual funding from the FCT—Foundation for Science and Technology (CEECIND/00072/2018 and IF/00601/2012 to BMC; PD/BDE/143154/2019, co-funded by MCTES, FSE, and UE, to EPM; SFRH/BD/92786/2013 to CSG; SFRH/BD/81042/2011 to MP; SFRH/BD/135831/2018 to RC; and SFRH/BD/51997/2012 to VMG); by Fundação Calouste Gulbenkian (BMC); by ICVS Scientific Microscopy Platform, member of the national infrastructure PPBI - Portuguese Platform of Bioimaging (PPBI-POCI-01-0145-FEDER-022122); by National funds, through the Foundation for Science and Technology (FCT) - project UIDB/50026/2020 and UIDP/50026/2020 and by the projects NORTE-01-0145-FEDER-000013, NORTE-01-0145-FEDER-000039 and NORTE-01-0145-FEDER-000055, supported by Norte Portugal Regional Operational Programme (NORTE 2020), under the Portugal 2020 Partnership Agreement, through the European Regional Development Fund (ERDF).

Conflict of interest

The authors declare no conflict of interest.

Author contributions

EPM, CSG, MP, RC, ASR, and VMG conducted experiments. EPM, CSG, MP, RC, ASR, RT, FB, NS, JP, and BMC analyzed data. FP, AAP, CC, and CCF provided patient samples. EPM and BMC wrote the manuscript. All authors reviewed and approved the manuscript.

Peer Review

The peer review history for this article is available at https://publons.com/publon/10.1002/1878-0261.13162.

Data accessibility

TCGA data used are publicly available (https://doi.org/10.1038/nature07385).

References

1 Ostrom QT, Patil N, Cioffi G, Waite K, Kruchko C, Barnholtz-sloan JS. CBTRUS statistical report: primary brain and other central nervous system tumors diagnosed in the United States in 2013–2017. *Neuro Oncol*. 2020;**22**:iv1–96.

2 Stupp R, Mason WP, van den Bent MJ, Weller M, Fisher B, Taphoorn MJB, et al. Radiotherapy plus concomitant and adjuvant temozolomide for glioblastoma. *N Engl J Med*. 2005;**352**:987–96.

3 Stupp R, Hegi ME, Mason WP, van den Bent MJ, Taphoorn MJ, Janzer RC, et al. Effects of radiotherapy with concomitant and adjuvant temozolomide versus radiotherapy alone on survival in glioblastoma in a randomised phase III study: 5-year analysis of the EORTC-NCIC trial. *Lancet Oncol*. 2009;**10**:459–66.

4 Stoyanov GS, Dzhenkov D, Ghenev P, Iliev B, Enchev Y, Tonchev AB. Cell biology of glioblastoma multiforme: from basic science to diagnosis and treatment. *Med Oncol*. 2018;**35**:27.

5 Lim M, Xia Y, Bettegowda C, Weller M. Current state of immunotherapy for glioblastoma. *Nat Rev Clin Oncol*. 2018;**15**:422–42.

6 Cloughesy TF, Mochizuki AY, Orpilla JR, Hugo W, Lee AH, Davidson TB, et al. Neoadjuvant anti-PD-1 immunotherapy promotes a survival benefit with intratumoral and systemic immune responses in recurrent glioblastoma. *Nat Med*. 2019;**25**:477–86.

7 Reardon DA, Brandes AA, Omuro A, Mulholland P, Lim M, Wick A, et al. Effect of nivolumab vs bevacizumab in patients with recurrent glioblastoma: the CheckMate 143 phase 3 randomized clinical trial. *JAMA Oncol*. 2020;**6**:1003–10.

8 Desjardins A, Gromeier M, Herndon JE II, Beaubier N, Bolognesi DP, Friedman AH, et al. Recurrent glioblastoma treated with recombinant poliovirus. *N Engl J Med*. 2018;**379**:150–61.

9 Halbleib JM, Nelson WJ. Cadherins in development: cell adhesion, sorting, and tissue morphogenesis. *Genes Dev*. 2006;**20**:3199–214.

10 Nose A, Takeichi M. A novel cadherin cell adhesion molecule: its expression patterns associated with implantation and organogenesis of mouse embryos. *J Cell Biol*. 1986;**103**:2649–58.

11 Shimoyama Y, Hirohashi S, Hirano S, Noguchi M, Shimosato Y, Takeichi M, et al. Cadherin cell-adhesion molecules in human epithelial tissues and carcinomas. *Cancer Res*. 1989;**49**:2128–33.

12 Shimoyama Y, Yoshida T, Terada M, Shimosato Y, Abe O, Hirohashi S. Molecular cloning of a human Ca2+-dependent cell-cell adhesion molecule homologous to mouse placental cadherin: its low expression in human placental tissues. *J Cell Biol*. 1989;**109**:1787–94.

13 Imai K, Hirata S, Irie A, Senju S, Ikuta Y, Yokomine K, et al. Identification of a novel tumor-associated antigen, cadherin 3/P-cadherin, as a possible target for immunotherapy of pancreatic, gastric, and colorectal cancers. *Cancer Ther Preclin*. 2008;**14**:6487–95.

14 Berx G, van Roy F. Involvement of members of the cadherin superfamily in cancer. *Cold Spring Harb Perspect Biol*. 2009;**1**:a003129.

15 Vieira AF, Paredes J. P-cadherin and the journey to cancer metastasis. *Mol Cancer*. 2015;**14**:178.

16 Vieira AF, Ricardo S, Ablett MP, Dionísio MR, Mendes N, Albergaria A, et al. P-cadherin is coexpressed with CD44 and CD49f and mediates stem cell properties in basal-like breast cancer. *Stem Cells*. 2012;**30**:854–64.

17 Vieira AF, Ribeiro AS, Dionísio MR, Sousa B, Nobre AR, Albergaria A, et al. P-cadherin signals through the laminin receptor α6β4 integrin to induce stem cell and invasive properties in basal-like breast cancer cells. *Oncotarget*. 2014;**5**:679–92.

18 Ribeiro AS, Paredes J. P-cadherin linking breast cancer stem cells and invasion: a promising marker to identify an "intermediate/metastable" EMT state. *Front Oncol*. 2014;**4**:371.

19 Paredes J, Albergaria A, Oliveira JT, Jeronimo C, Milanezi F, Schmitt FC. P-cadherin overexpression is an indicator of clinical outcome in invasive breast carcinomas and is associated with CDH3 promoter hypomethylation. *Clin Cancer Res*. 2005;**11**:5869–77.

20 Van Marck V, Stove C, Van Den Bossche K, Stove V, Paredes J, Vander Haeghen Y, et al. P-cadherin promotes cell-cell adhesion and counteracts invasion in human melanoma. *Cancer Res*. 2005;**65**:8774–83.

21 Jacobs K, Feys L, Vanhoecke B, Van Marck V, Bracke M. P-cadherin expression reduces melanoma growth, invasion, and responsiveness to growth factors in nude mice. *Eur J Cancer Prev*. 2011;**20**:207–16.

22 Pojo M, Gonçalves CS, Xavier-Magalhães A, Oliveira AI, Gonçalves T, Correia S, et al. A transcriptomic signature mediated by HOXA9 promotes human glioblastoma initiation, aggressiveness and resistance to temozolomide. *Oncotarget*. 2015;**6**:7657–74.

23 Azari H, Millette S, Ansari S, Rahman M, Deleyrolle LP, Reynolds BA. Isolation and expansion of human

glioblastoma multiforme tumor cells using the neurosphere assay. *J Vis Exp*. 2011;**56**:e3633.
24 Paredes J, Stove C, Stove V, Milanezi F, Van Marck V, Derycke L, et al. P-cadherin is up-regulated by the antiestrogen ICI 182, 780 and promotes invasion of human breast cancer cells. *Cancer Res*. 2004;**64**:8309–17.
25 Livak KJ, Schmittgen TD. Analysis of relative gene expression data using real-time quantitative PCR and the 2(-Delta Delta C(T)) method. *Methods*. 2001;**25**:402–8.
26 Sousa B, Paredes J, Milanezi F, Lopes N, Martins D, Dufloth R, et al. P-cadherin, Vimentin and CK14 for identification of basal-like phenotype in breast carcinomas: an immunohistochemical study. *Histol Histopathol*. 2010;**25**:963–74.
27 Gonçalves CS, Vieira de Castro J, Pojo M, Martins EP, Queirós S, Chautard E, et al. WNT6 is a novel oncogenic prognostic biomarker in human glioblastoma. *Theranostics*. 2018;**8**:4805–23.
28 Ribeiro AS, Nobre AR, Mendes N, Almeida J, Vieira AF, Sousa B, et al. SRC inhibition prevents P-cadherin mediated signaling and function in basal-like breast cancer cells. *Cell Commun Signal*. 2018;**16**:75.
29 The Cancer Genome Atlas Research Network. Comprehensive genomic characterization defines human glioblastoma genes and core pathways. *Nature*. 2008;**455**:1061–8.
30 Bowman RL, Wang Q, Carro A, Verhaak RGW, Squatrito M. GlioVis data portal for visualization and analysis of brain tumor expression datasets. *Neuro Oncol*. 2017;**19**:139–41.
31 Chen EY, Tan CM, Kou Y, Duan Q, Wang Z, Meirelles GV, et al. Enrich:interactive and collaborative HTML5 gene list enrichment analysis tool. *BMC Bioinformatics*. 2013;**14**:128.
32 Kuleshov MV, Jones MR, Rouillard AD, Fernandez NF, Duan Q, Wang Z, et al. Enrichr: a comprehensive gene set enrichment analysis web server 2016 update. *Nucleic Acids Res*. 2016;**44**:W90–7.
33 Subramanian A, Tamayo P, Mootha VK, Mukherjee S, Ebert BL, Gillette MA, et al. Gene set enrichment analysis: a knowledge-based approach for interpreting genome-wide expression profiles. *Proc Natl Acad Sci USA*. 2005;**102**:15545–50.
34 Louis DN, Perry A, Reifenberger G, von Deimling A, Figarella-Branger D, Cavenee WK, et al. The 2016 World Health Organization classification of tumors of the central nervous system: a summary. *Acta Neuropathol*. 2016;**131**:803–20.
35 de Gooijer MC, Navarro MG, Bernards R, Wurdinger T, van Tellingen O. An experimenter's guide to glioblastoma invasion pathways. *Trends Mol Med*. 2018;**24**:763–80.
36 Hirose Y, Berger MS, Pieper RO. p53 effects both the duration of G2/M arrest and the fate of temozolomide-treated human glioblastoma cells. *Cancer Res*. 2001;**61**:1957–63.
37 Deeraksa A, Pan J, Sha Y, Liu XD, Eissa NT, Lin SH, et al. Plk1 is upregulated in androgen-insensitive prostate cancer cells and its inhibition leads to necroptosis. *Oncogene*. 2013;**32**:2973–83.
38 Kastan MB, Bartek J. Cell-cycle checkpoints and cancer. *Nature*. 2004;**432**:316–23.
39 Imai S, Kobayashi M, Takasaki C, Ishibashi H, Okubo K. High expression of P-cadherin is significantly associated with poor prognosis in patients with non-small-cell lung cancer. *Lung Cancer*. 2018;**118**:13–9.
40 Vieira AF, Dionísio MR, Gomes M, Cameselle-Teijeiro JF, Lacerda M, Amendoeira I, et al. P-cadherin: a useful biomarker for axillary-based breast cancer decisions in the clinical practice. *Mod Pathol*. 2017;**30**:698–709.
41 Barami K, Lewis-Tuffin L, Anastasiadis PZ. The role of cadherins and catenins in gliomagenesis. *Neurosurg Focus*. 2006;**21**:E13.
42 Appolloni I, Barilari M, Caviglia S, Gambini E, Reisoli E, Malatesta P. A cadherin switch underlies malignancy in high-grade gliomas. *Oncogene*. 2015;**34**:1991–2002.
43 Asano K, Duntsch CD, Zhou Q, Weimar JD, Bordelon D, Robertson JH, et al. Correlation of N-cadherin expression in high grade gliomas with tissue invasion. *J Neurooncol*. 2004;**70**:3–15.
44 Bai Y-H, Zhan Y-B, Yu B, Wang W-W, Wang L, Zhou J-Q, et al. A novel tumor-suppressor, CDH18, inhibits glioma cell invasiveness via UQCRC2 and correlates with the prognosis of glioma patients. *Cell Physiol Biochem*. 2018;**48**:1755–70.
45 Chen Q, Cai J, Jiang C. CDH2 expression is of prognostic significance in glioma and predicts the efficacy of temozolomide therapy in patients with glioblastoma. *Oncol Lett*. 2018;**15**:7415–22.
46 Darweesh MF, Abdel-salam LO, Negm MS. N-cadherin expression in glioblastoma and its correlation with the histopathological findings. *Acad J Cancer Res*. 2016;**9**:7–12.
47 Jarrard DF, Paul R, van Bokhoven A, Nguyen SH, Bova GS, Wheelock MJ, et al. P-cadherin is a basal cell-specific epithelial marker that is not expressed in prostate cancer. *Clin Cancer Res*. 1997;**3**:2121–8.
48 Kumara HMCS, Bellini GA, Caballero OL, Herath SAC, Su T, Ahmed A, et al. P-cadherin (CDH3) is overexpressed in colorectal tumors and has potential as a serum marker for colorectal cancer monitoring. *Oncoscience*. 2017;**4**:139–47.
49 Usui A, Ko SY, Barengo N, Naora H. P-cadherin promotes ovarian cancer dissemination through tumor cell aggregation and tumor-peritoneum interactions. *Mol Cancer Res*. 2014;**12**:504–13.
50 Mandeville JA, Neto BS, Vanni AJ, Smith GL, Rieger-Christ KM, Zeheb R, et al. P-cadherin as a

prognostic indicator and a modulator of migratory behaviour in bladder carcinoma cells. *BJU Int*. 2008;**102**:1707–14.
51 Paredes J, Milanezi F, Viegas L, Amendoeira I, Schmitt F. P-cadherin expression is associated with high-grade ductal carcinoma in situ of the breast. *Virchows Arch*. 2002;**440**:16–21.
52 Redies C. Cadherins in the central nervous system. *Prog Neurogibol*. 2000;**61**:611–48.
53 Ranscht B, Dours-Zimmermann MT. T-cadherin, a novel cadherin cell adhesion molecule in the nervous system lacks the conserved cytoplasmic region. *Neuron*. 1991;**7**:391–402.
54 Hatta K, Takeichi M. Expression of N-cadherin adhesion molecules associated with early morphogenetic events in chick development. *Nature*. 1986;**320**:447–9.
55 Redies C, Müller HAJ. Similarities in structure and expression between mouse P-cadherin, chicken B-cadherin and frog XB/U-cadherin. *Cell Commun Adhes*. 1994;**2**:511–20.
56 Kaji C, Tomooka M, Kato Y, Kojima H, Sawa Y. The expression of podoplanin and classic cadherins in the mouse brain. *J Anat*. 2012;**220**:435–46.
57 Liu X, Wang L, Zhao S, Ji X, Luo Y, Ling F. β-Catenin overexpression in malignant glioma and its role in proliferation and apoptosis in glioblastoma cells. *Med Oncol*. 2011;**28**:608–14.
58 Faraldo MM, Teulière J, Deugnier MA, Birchmeier W, Huelsken J, Thiery JP, et al. β-Catenin regulates P-cadherin expression in mammary basal epithelial cells. *FEBS Lett*. 2007;**581**:831–6.
59 Sun L, Hu H, Peng L, Zhou Z, Zhao X, Pan J, et al. P-cadherin promotes liver metastasis and is associated with poor prognosis in colon cancer. *Am J Pathol*. 2011;**179**:380–90.
60 Hu B, Wang Q, Wang YA, Hua S, Sauvé CEG, Ong D, et al. Epigenetic activation of WNT5A drives glioblastoma stem cell differentiation and invasive growth. *Cell*. 2016;**167**:1281–95.e18.
61 Aldape K, Zadeh G, Mansouri S, Reifenberger G, von Deimling A. Glioblastoma: pathology, molecular mechanisms and markers. *Acta Neuropathol*. 2015;**129**:829–48.
62 Costa BM, Smith JS, Chen Y, Chen J, Phillips HS, Aldape KD, et al. Reversing HOXA9 oncogene activation by PI3K inhibition: epigenetic mechanism and prognostic significance in human glioblastoma. *Cancer Res*. 2010;**70**:453–62.
63 Gonçalves CS, Xavier-Magalhães A, Martins EP, Pinto AA, Pires MM, Pinheiro C, et al. A novel molecular link between HOXA9 and WNT6 in glioblastoma identifies a subgroup of patients with particular poor prognosis. *Mol Oncol*. 2020;**14**:1224–41.
64 Welter C, Henn W, Theisinger B, Fischer H, Zang KD, Blin N. The cellular myb oncogene is amplified, rearranged and activated in human glioblastoma cell lines. *Cancer Lett*. 1990;**52**:57–62.
65 Corradini F, Cesi V, Bartella V, Pani E, Bussolari R, Candini O, et al. Enhanced proliferative potential of hematopoietic cells expressing degradation-resistant c-Myb mutants. *J Biol Chem*. 2005;**280**:30254–62.
66 Soroceanu L, Kharbanda S, Chen R, Soriano RH, Aldape K, Misra A, et al. Identification of IGF2 signaling through phosphoinositide-3-kinase regulatory subunit 3 as a growth-promoting axis in glioblastoma. *Proc Natl Acad Sci USA*. 2007;**104**:3466–71.
67 Oliva CR, Halloran B, Hjelmeland AB, Vazquez A, Bailey SM, Sarkaria JN, et al. IGFBP6 controls the expansion of chemoresistant glioblastoma through paracrine IGF2/IGF-1R signaling. *Cell Commun Signal*. 2018;**16**:61.
68 Cheung LWT, Mak ASC, Cheung ANY, Ngan HYS, Leung PCK, Wong AST. P-cadherin cooperates with insulin-like growth factor-1 receptor to promote metastatic signaling of gonadotropin-releasing hormone in ovarian cancer via p120 catenin. *Oncogene*. 2011;**30**:2964–74.
69 Mojallal M, Zheng Y, Hultin S, Audebert S, van Harn T, Johnsson P, et al. AmotL2 disrupts apical-basal cell polarity and promotes tumour invasion. *Nat Commun*. 2014;**5**:4557.
70 Zhao C, Li X, Han B, You Z, Qu L, Liu C, et al. Gga-MIR-219b targeting BCL11B suppresses proliferation, migration and invasion of Marek's disease tumor cell MSB1. *Sci Rep*. 2017;**7**:4247.
71 Dravis C, Spike BT, Harrell JC, Johns C, Trejo CL, Southard-Smith EM, et al. Sox10 regulates stem/progenitor and mesenchymal cell states in mammary epithelial cells. *Cell Rep*. 2015;**12**:2035–48.
72 González B, Denzel S, Mack B, Conrad M, Gires O. EpCAM is involved in maintenance of the murine embryonic stem cell phenotype. *Stem Cells*. 2009;**27**:1782–91.
73 Reifenberger G, Wirsching H-G, Knobbe-Thomsen CB, Weller M. Advances in the molecular genetics of gliomas — implications for classification and therapy. *Nat Rev Clin Oncol*. 2016;**14**:434–52.
74 Noh M-G, Oh S-J, Ahn E-J, Kim Y-J, Jung T-Y, Jung S, et al. Prognostic significance of E-cadherin and N-cadherin expression in gliomas. *BMC Cancer*. 2017;**17**:583.
75 Fisher TS, Hooper AT, Lucas J, Clark TH, Rohner AK, Peano B, et al. A CD3-bispecific molecule targeting P-cadherin demonstrates T cell-mediated regression of established solid tumors in mice. *Cancer Immunol Immunother*. 2018;**67**:247–59.
76 Root AR, Cao W, Li B, LaPan P, Meade C, Sanford J, et al. Development of PF-06671008, a highly potent anti-P-cadherin/anti-CD3 bispecific DART molecule with extended half-life for the treatment of cancer. *Antibodies*. 2016;**5**:6.

77 Park J, Park E, Han SW, Im SA, Kim TY, Kim WH, et al. Down-regulation of P-cadherin with PF-03732010 inhibits cell migration and tumor growth in gastric cancer. *Invest New Drugs*. 2012;**30**:1404–12.
78 Zhang CC, Yan Z, Zhang Q, Kuszpit K, Zasadny K, Qiu M, et al. PF-03732010: a fully human monoclonal antibody against P-cadherin with antitumor and antimetastatic activity. *Clin Cancer Res*. 2010;**16**:5177–88.
79 Kudo S, Caaveiro JMM, Nagatoishi S, Miyafusa T, Matsuura T, Sudou Y, et al. Disruption of cell adhesion by an antibody targeting the cell-adhesive intermediate (X-dimer) of human P-cadherin. *Sci Rep*. 2017;**7**:39518.
80 Fogli A, Chautard E, Vaurs-Barrière C, Pereira B, Müller-Barthélémy M, Court F, et al. The tumoral A genotype of the MGMT rs34180180 single-nucleotide polymorphism in aggressive gliomas is associated with shorter patients' survival. *Carcinogenesis*. 2015;**37**:169–76.

Supporting information

Additional supporting information may be found online in the Supporting Information section at the end of the article.

Fig. S1. P-cadherin expression in glioma samples.
Fig. S2. Characterization of *CDH3* expression in 12 GBM cell models.
Fig. S3. P-cadherin does not influence the expression of proliferation, anti-apoptotic, and stemness markers in mice intracranial tumors.
Fig. S4. Stable P-cadherin knockdown is associated with decreased aggressiveness features of GBML18 cells *in vitro*.
Fig. S5. Silencing of *CDH3* with distinct shRNA clones affects cancer hallmarks in GBML42, a GBM patient-derived culture.
Fig. S6. *CDH3* influences the cell cycle of GBM cells.
Fig. S7. Molecular signatures associated with *CDH3*-positively and *CDH3*-inversely correlated genes in GBM patients from TCGA, and validation in GBM primary cultures.
Table S1. Sequence of primers used for qRT-PCR studies.
Table S2. Information of antibodies used for western blot and immunohistochemistry.

International Journal of
Molecular Sciences

MDPI

Article

The Chick Chorioallantoic Membrane Model: A New In Vivo Tool to Evaluate Breast Cancer Stem Cell Activity

Marta Teixeira Pinto [1,2,†], Ana Sofia Ribeiro [1,2,†], Inês Conde [1,2], Rita Carvalho [1,2] and Joana Paredes [1,2,3,*]

[1] i3S—Institute of Investigation and Innovation in Health, 4200-135 Porto, Portugal; mtpinto@i3s.up.pt (M.T.P.); aribeiro@ipatimup.pt (A.S.R.); iconde@ipatimup.pt (I.C.); rcarvalho@ipatimup.pt (R.C.)
[2] Ipatimup, Institute of Molecular Pathology and Immunology, University of Porto, 4200-135 Porto, Portugal
[3] Faculty of Medicine, University of Porto, 4200-319 Porto, Portugal
* Correspondence: jparedes@ipatimup.pt; Tel.: +351-225-570-700
† These authors contributed equally to this work.

Abstract: The high plasticity of cancer stem-like cells (CSCs) allows them to differentiate and proliferate, specifically when xenotransplanted subcutaneously into immunocompromised mice. CSCs are highly tumorigenic, even when inoculated in small numbers. Thus, in vivo limiting dilution assays (LDA) in mice are the current gold standard method to evaluate CSC enrichment and activity. The chick embryo chorioallantoic membrane (CAM) is a low cost, naturally immune-incompetent and reproducible model widely used to evaluate the spontaneous growth of human tumor cells. Here, we established a CAM-LDA assay able to rapidly reproduce tumor specificities—in particular, the ability of the small population of CSCs to form tumors. We used a panel of organotropic metastatic breast cancer cells, which show an enrichment in a stem cell gene signature, enhanced $CD44^{+}/CD24^{-/low}$ cell surface expression and increased mammosphere-forming efficiency (MFE). The size of CAM-xenografted tumors correlate with the number of inoculated cancer cells, following mice xenograft growth pattern. CAM and mice tumors are histologically comparable, displaying both breast CSC markers CD44 and CD49f. Therefore, we propose a new tool for studying CSC prevalence and function—the chick CAM-LDA—a model with easy handling, accessibility, rapid growth and the absence of ethical and regulatory constraints.

Keywords: cancer stem cells; chicken chorioallantoic membrane; in vivo model; limiting dilution assay

check for updates

Citation: Pinto, M.T.; Ribeiro, A.S.; Conde, I.; Carvalho, R.; Paredes, J. The Chick Chorioallantoic Membrane Model: A New In Vivo Tool to Evaluate Breast Cancer Stem Cell Activity. *Int. J. Mol. Sci.* **2021**, *22*, 334. https://doi.org/10.3390/ijms22010334

Received: 23 November 2020
Accepted: 25 December 2020
Published: 30 December 2020

Publisher's Note: MDPI stays neutral with regard to jurisdictional claims in published maps and institutional affiliations.

Copyright: © 2020 by the authors. Licensee MDPI, Basel, Switzerland. This article is an open access article distributed under the terms and conditions of the Creative Commons Attribution (CC BY) license (https://creativecommons.org/licenses/by/4.0/).

1. Introduction

Cancer stem-like cells (CSCs), also designated as tumor-initiating cells (TICs), were shown to be critical in inducing tumor heterogeneity, but also in inducing cancer development, progression and metastasis due to their capacity to be chemoresistant, invasive and dormant [1,2]. These cells possess the ability to self-renew, harboring high levels of plasticity and being able to differentiate in different phenotypic populations, especially when engrafted in in vivo models, such as immunocompromised mice. It has been also shown that CSC populations are also enriched in human metastatic lesions [3,4], as well as in metastatic cancer cell lines [5–7], being responsible for therapy resistance.

CSCs have been described as representing a small population of the tumor tissue and expressing specific cell surface markers. In breast cancer, it was shown that cancer cells expressing $CD44^{+}/CD24^{-/low}$ are particularly efficient in forming new tumors, showing the capacity to self-renew and to be therapy-resistant [8]. However, in the last years, several other surface proteins have been indicated as putative biomarkers for breast CSCs, such as CD49f [9] and EpCAM [10], which are usually used in combination to characterize mammary stem cell subpopulations [11]. Breast cancer cells with high ALDH1 activity also demonstrate stem cell properties, namely by contributing to metastases and chemotherapy resistance [12,13], as well as the ones co-expressing P-cadherin, CD44 and CD49f, especially in basal-like breast cancer [14,15]. Therefore, these markers are widely used to

perform the in vitro characterization of breast CSCs [1,15–17], which can be combined with their mammosphere-forming efficiency. Actually, the ability of cells to form multicellular spheroids is the classic in vitro assay to evaluate stem cell properties, which takes advantage of the fact that only cells with stem-like properties are able to survive and proliferate in the absence of attachment to an exogenous substratum [18]. As such, "mammospheres" are highly enriched in mammary stem cells or breast CSCs. Moreover, single cells isolated from mammospheres can generate multilineage colonies when cultured in the presence of serum on a collagen substratum that promotes their differentiation. Mammosphere-derived cells are also capable of generating clonally complex functional structures in reconstituted 3D culture systems, such as Matrigel [1,16–18].

Importantly, one of the most significant drivers of the malignant phenotype is the tumor microenvironment. The components of the extracellular matrix (ECM) and other microenvironment constituents (cellular elements and soluble factors) can also modulate cancer stemness. Importantly, it affects the oxygen concentration, pH and nutrient availability, which will, in turn, modulate the CSC activity and functions (such as self-renewal and chemoresistance) [19], as well as influence the breast cancer stemness and tumor aggressiveness [1]. In order to provide the microenvironmental cues, it is therefore critical to evaluate CSCs in an in vivo context. To assess the tumorigenic capacity, breast cancer cells are traditionally xenotransplanted into the subcutaneous region under the mammary fat pad of female immunocompromised mice in varying cell dilutions [6,15,20–22]. Although these encompass ethical and financial limitations, the limiting dilution assays in mice are the "gold standard" method to evaluate CSC tumorigenicity.

In contrast, the chick embryo chorioallantoic membrane (CAM) is a low cost, reproducible and reliable model used to investigate several functional features of tumor biology, such as the ability of cells to be tumorigenic, to invade and to metastasize into the embryo [23,24]. The CAM is a highly vascularized extraembryonic membrane, thus providing rich nutrient conditions for the spontaneous growth of human tumor cells. Actually, this model has been used for many years to support the growth of numerous types of tumors, including breast cancer [17,25–29]. Additionally, supporting tumor growth, the CAM has a deficient immunological and inflammatory response in earlier stages of the chick development [27,30]. Moreover, it has also been used as a platform to analyze the values of anticancer drugs [29,31] and radiation therapy [30].

Taking into account the several described advantages of the CAM model, our major goal was to develop a new limiting dilution assay in vivo model able to rapidly reproduce tumor specificities—in particular, the ability of the small population of CSCs to form tumors in an immuno-incompetent host. Thus, in this manuscript, we describe, for the first time, the use of a limiting dilution assay to evaluate cancer cells' stemness in the chick CAM, in comparison with the in vivo gold standard mice model, using a panel of organotropic MDA-MB-231 metastatic breast cancer cells. We demonstrated that the size of the tumors formed in the CAM correlates with the number of inoculated cells, following the same cell growth pattern as in mice. Furthermore, the CAM and mice tumors were histologically comparable and displayed a similar pattern of breast CSC markers. These results allowed us to propose that the chick CAM model can be a new tool to evaluate breast CSC properties in vivo.

2. Results

2.1. Organotropic Breast Cancer Cells Show Increased In Vitro CSC Properties

Human metastatic lesions have been described as being enriched in cancer cells with stem cell properties. Therefore, we used the highly metastatic human breast cancer cell line MDA-MB-231 and its organotropic variants (lung, bone and brain) [32–34]. As a first approach to validate their stem cell properties, we performed an in-silico analysis to evaluate the prevalence of a stem cell signature in each of the breast cancer cell lines. We crossed the list of genes previously described as significantly deregulated in each one of the organotropic-derived breast cancer cell lines when compared with the parental 231

breast cancer cell line [32–34] (resumed in Supplementary Table S1), in order to obtain both the specific, and the shared, list of deregulated genes. From this analysis, 80.8% (194 out of 240) of the genes were specifically deregulated in brain metastatic breast cancer cells, compared with 70.5% (60 out of 85) and 62.1% (59 out of 95) specifically deregulated genes for bone and lung metastatic cells, respectively (Figure 1a).

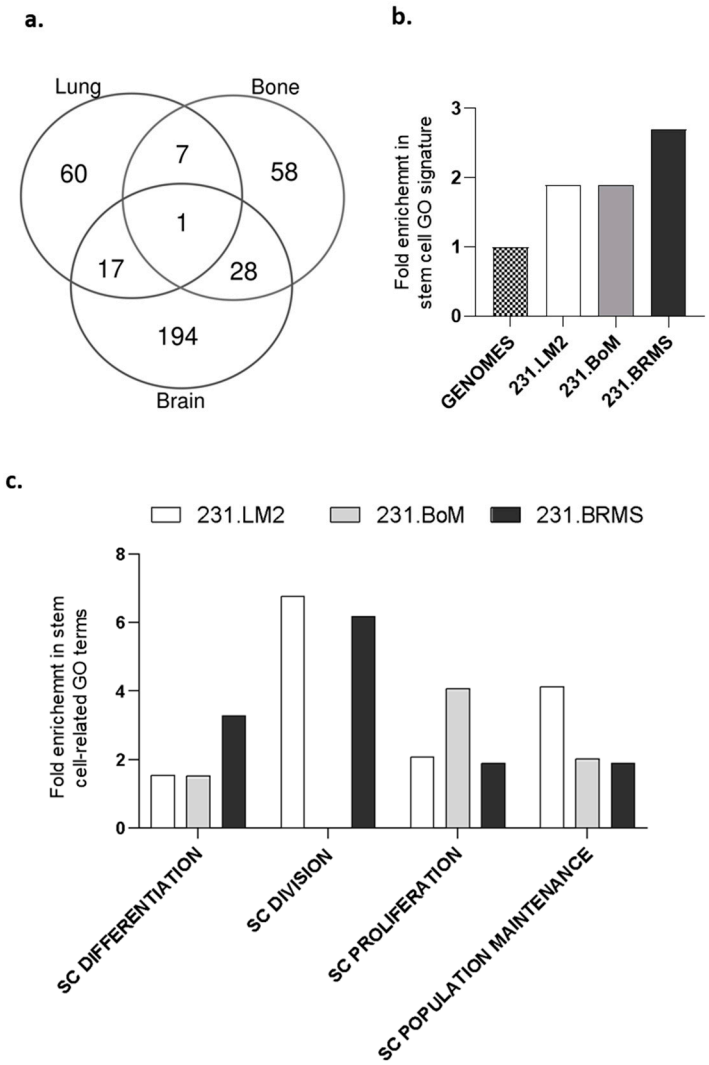


Figure 1. Organotropic breast cancer cell lines show an enriched stem cell-like signature. Enrichment analysis for stem cell gene ontology terms using the significantly deregulated gene (DEG) list between each organotropic breast cancer cell line and the parental MDA-MB-231 cell line. (**a**) Venn diagram showing the common and specific DEGs between the different organotropic variants. (**b**) Overall enrichment in stem cells gene ontology (GO) signature and (**c**) in stem cell-related GO terms after an analysis of the specific DEGs annotated with a stem cell function. SC: stem cell.

Further, we determined the stem cell enrichment for each organotropic breast cancer cell line using the specifically deregulated gene lists by analyzing the stem cell gene ontology (GO) terms retrieved from http://amigo.geneontology.org/amigo/search/bioentity?q=stem. As expected, our results showed that all organotropic breast cancer cells were enriched in genes associated with stem cell functions (Figure 1b)—particularly, the 231.BRMS cell line. Concerning the different stem cell GO terms—SC population maintenance, SC proliferation, SC division and SC differentiation—major differences were observed within the different organotropic breast cancer cells (Figure 1c). 231.LM2 is particularly enriched

in SC division and population maintenance, 231.BoM is mainly enriched in SC proliferation and 231.BRMS is enriched in SC division and differentiation (Figure 1c).

Finally, to validate in vitro the enriched cancer stem cell (CSC) phenotype in the different organotropic metastatic breast cancer cell lines, we performed the in vitro gold-standard methods for CSC identification: characterization in terms of breast CSC markers and the mammospheres-forming assay, which measures the ability of cells to be anoikis-resistant and to grow in anchorage-independent conditions, as well as their capacity to self-renew and differentiate. In particular, the $CD44^{+}CD24^{-}$ phenotype was measured by flow cytometry. Although all the cell lines were constituted by a large subpopulation of $CD44^{+}/CD24^{-/low}$ cells, it was still possible to observe a very significant enrichment in the $CD44^{+}/CD24^{-/low}$ subpopulation in the organotropic variants when compared with the parental cell line (with 80.1% in 231, 99% in 231.LM2, 97.2% in 231.BoM and 96.3% in 231.BRMS) (Figure 2a,b). The enriched stem-like phenotype in the organotropic breast cancer cell lines was further confirmed by the observed increased mammosphere-forming efficiency (MFE, although this effect was only significant in the 231.BoM and 231.BRMS cells when compared with the 231 parental cell line) (Figure 2c,d). Of notice is that these changes were not due to differences in the proliferative capacity of the cells (Figure 2e).

2.2. Establishing a Limiting Dilution Assay for CSC Identification Using the In Vivo Chicken Egg CAM Model

Our main aim was to test the ability of organotropic breast metastatic cells to grow in the non-mammalian chick embryo chorioallantoic membrane (CAM). For that, we adapted the concept of the in vivo limiting dilution assay, which is normally used to determine the cancer-initiating cell frequency of an established suspension cell line. For a proper comparison, we used both CAM and immunocompromised mice xenograft models. Breast cancer cell lines were inoculated at different concentrations in the CAM and in mice, according to the experimental design depicted in Figure 3.

Although all cell lines were able to form tumors in the CAM, a different phenotype was observed between the parental 231 and the organotropic variants. The parental cell line (231) typically formed disaggregated and diffuse tumors, whereas the organotropic variants formed significantly bigger and cohesive tumors (Figure 4a). Further, as described in the previous section, we performed a limiting dilution assay (LDA), in both the CAM and mice, to evaluate the stem cell frequency of the organotropic breast cancer cells. We evaluated the tumor size (Figure 4b,c) and the frequency of tumor formation (Tables 1 and 2). For the CAM-LDA, 18 embryos were inoculated with 1-M cells, 9–11 embryos with 100 K, 10 to 11 with 10-K cells and 8–10 embryos with 1-K cells. All organotropic cells showed significantly bigger tumors when inoculated at 1-M and 100-K cells in the CAM (Figure 4b) in compassion to the parental cell lines. Both the in vitro and in vivo CAM results were consistent with each other. The next step was to validate them using a limiting dilution assay in the in vivo mice model, since this is the gold standard method in the CSC field to prove the stem-like ability of cancer cells. For mice LDA, two–four mice were used per condition (dilution/cell line), and, after three weeks, organotropic cells also showed significantly bigger tumors then the parental cell line 231 when inoculated at 1-M (231.LM2 and 231BRMS) and 100-K (all three cell lines). As in the CAM, no differences were detected when 10-K cells were inoculated; to reduce the number of used animals, the 1-K dilution was not tested in mice (Figure 4c). Though the tumor size differences were not maintained at the lower cell inoculations (10-K and 1-K cells), it was still possible to observed an increase in the frequency of tumor formation (Table 1) that reflected a significant increase in the stem cell frequency of all organotropic breast cancer cells, as calculated by Extreme Limiting Dilution Analysis (ELDA) software [35]. Interestingly, and in accordance with the mammosphere-forming assay, this effect showed to be more pronounced in 231.BoM and 231.BRMS. The number of tumor-initiating cells was higher in 231.BoM and 231.BRMS, as already shown in the previously described CAM-LDA assay. Although with less significance, the same analysis performed for mice LDA showed the same pattern for stem cell frequency (Table 2). In summary, the in vivo chick CAM model recapitulates the in vitro

CSC properties of breast cancer cells, producing tumors with sizes and stem cell frequencies comparable with the ones found with mice LDA assay.

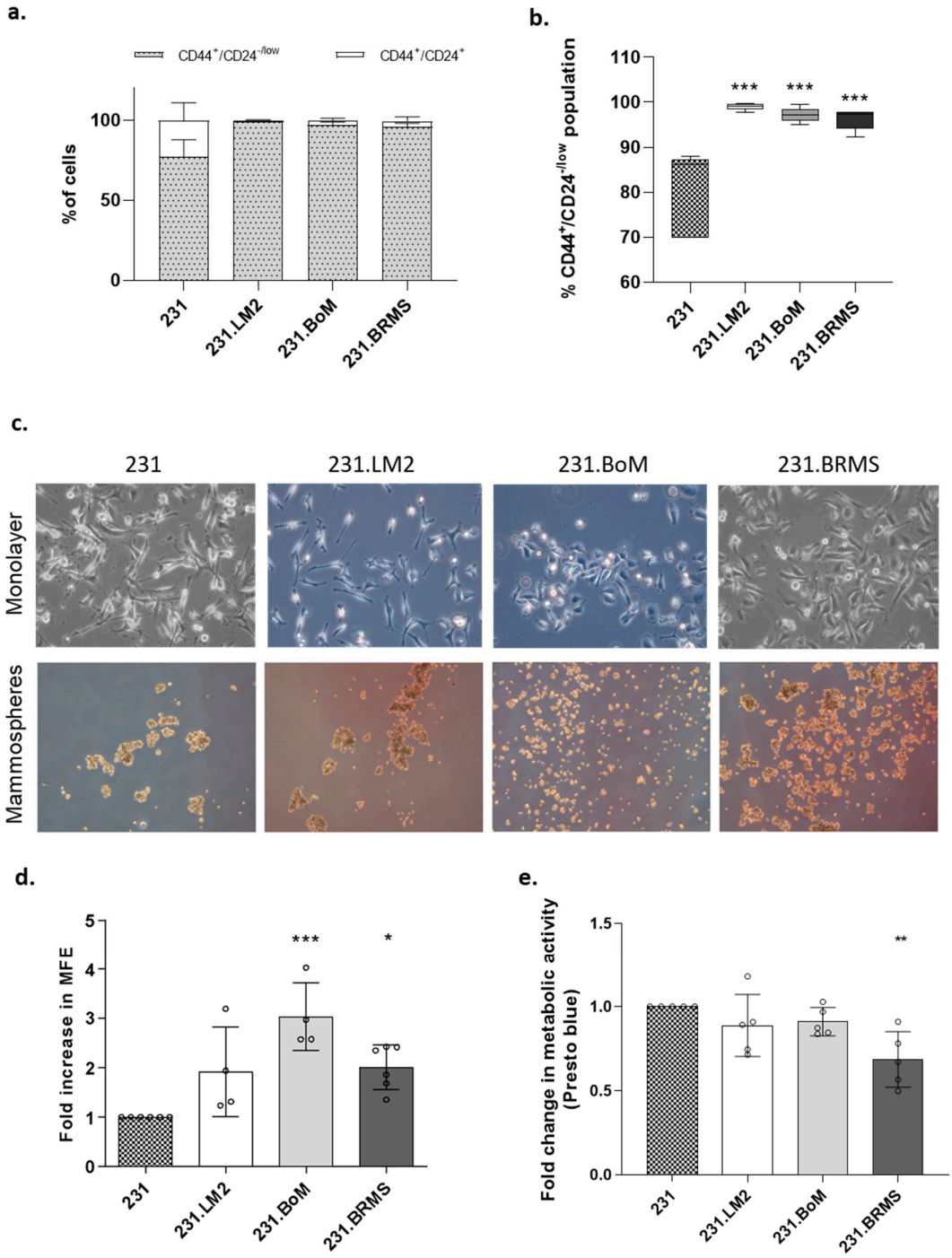


Figure 2. Organotropic breast cancer cells show increased in vitro cancer stem cell (CSC) properties. (**a**) Characterization of the cancer cell populations for CD44 and CD24 CSC markers by flow cytometry analysis in 231 breast cancer cells and its organotropic variants. (**b**) Percentage of the CSC population $CD44^{+}/CD24^{-/low}$ in 231 breast cancer cells and its organotropic variants. (**c**) Representative picture of monolayer (2D) and mammospheres (20× magnification). (**d**) Mammosphere-forming efficiency (MFE) in organotropic breast cancer cells (minimum of 4 biological replicates) compared with parental cells. (**e**) Fold change in cell viability and metabolic activity measured by the Presto blue assay. Five biological replicates; *—$p < 0.05$, **—$p < 0.01$ and ***—$p < 0.001$.

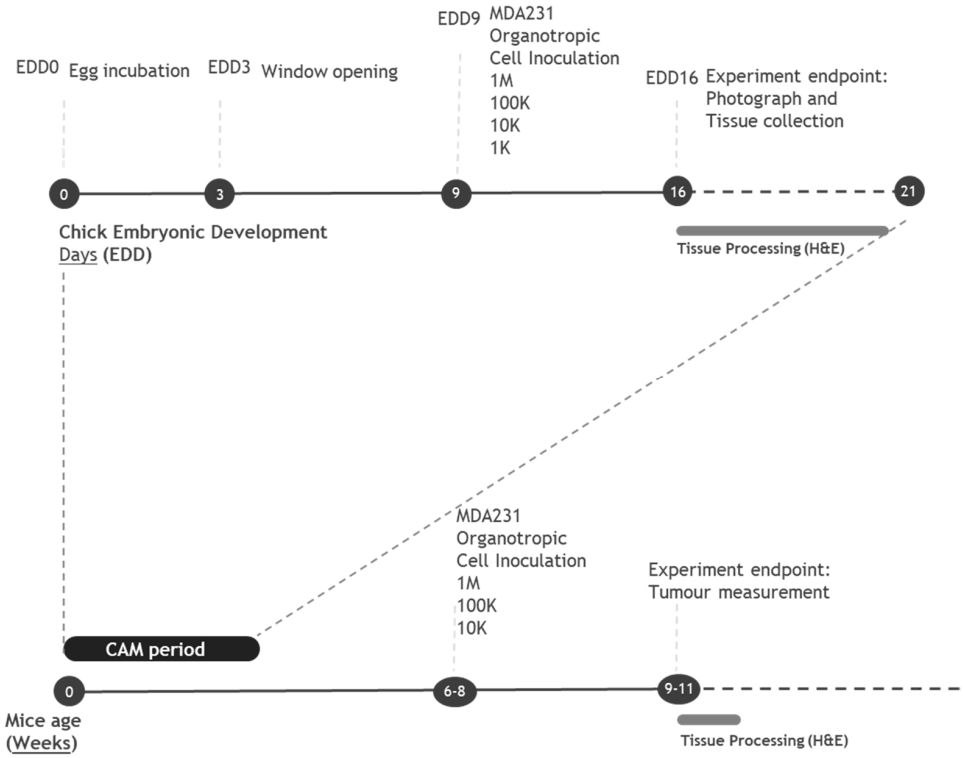


Figure 3. In vivo limiting dilution assay (LDA) workflow: a timeline of the chorioallantoic membrane (CAM) and mice experiments. Fertilized eggs are incubated for 3 days; at which time, a window in the shell is opened. At embryonic development day 9 (EDD9), breast cancer cells are inoculated on top of the CAM. At EDD16, eggs are sacrificed, and the tumor growth is examined. Mice with 6–8 weeks of age are subcutaneously injected with breast cancer cells. Tumor growth is monitored for 3 weeks. At weeks 9–11, mice are sacrificed and tumors are further examined.

Table 1. Stem cell frequency in chorioallantoic membrane (CAM) tumors. Limiting dilution data as the percentage of tumor-forming eggs. The frequency of cancer stem cells (CSCs) was estimated using the Extreme Limiting Dilution Analysis (ELDA) calculating website. Confidence choice entered was 0.95, and *p*-values reflect differences in CSC frequencies between the metastatic cell lines (231.LM2, 231.BoM and 231.BRMS) and the parental cell line (231). N per group varied between 8–18 eggs for a total of 191 eggs inoculated.

Cell Model	Cell Number				Stem Cell Frequency (ELDA)	*p*-Value (Vs 231)
	1 M	100 K	10 K	1 K		
231	18/18 (100%)	5/9 (55.6%)	2/10 (20%)	3/8 (37.5%)	1/68,769	-
231.LM2	18/18 (100%)	10/11 (90.9%)	6/10 (60%)	4/10 (40%)	1/17,209	0.00163
231.BoM	18/18 (100%)	11/11 (100%)	7/11 (63.6%)	3/9 (33.3%)	1/7490	<0.0001
231.BRMS	18/18 (100%)	10/10 (100%)	4/10 (40%)	3/10 (30%)	1/12,215	0.00067

Table 2. Stem cell frequency in mice tumors. Limiting dilution data as the percentage of tumor-forming mice. The frequency of CSC was estimated using the ELDA calculating website. Confidence choice entered was 0.95, and *p*-values reflect differences in CSC frequencies between each of the organotropic cell lines (231.LM2, 231.BoM and 231.BRMS) and the parental cell line (231). N per group varied between 2–4 mice per group for a total of 39 subcutaneously injected mice.

Cell Model	Cell Number			Stem Cell Frequency (ELDA)	*p*-Value (Vs 231)
	1 M	100 K	10 K		
231	2/2 (100%)	2/4 (50%)	0/3 (0%)	1/15,7144	-
231.LM2	3/3 (100%)	4/4 (100%)	0/3 (0%)	1/37,558	ns
231.BoM	3/3 (100%)	4/4 (100%)	2/3 (66%)	1/9099	0.0041
231.BRMS	3/3 (100%)	4/4 (100%)	2/3 (66%)	1/9099	0.0041

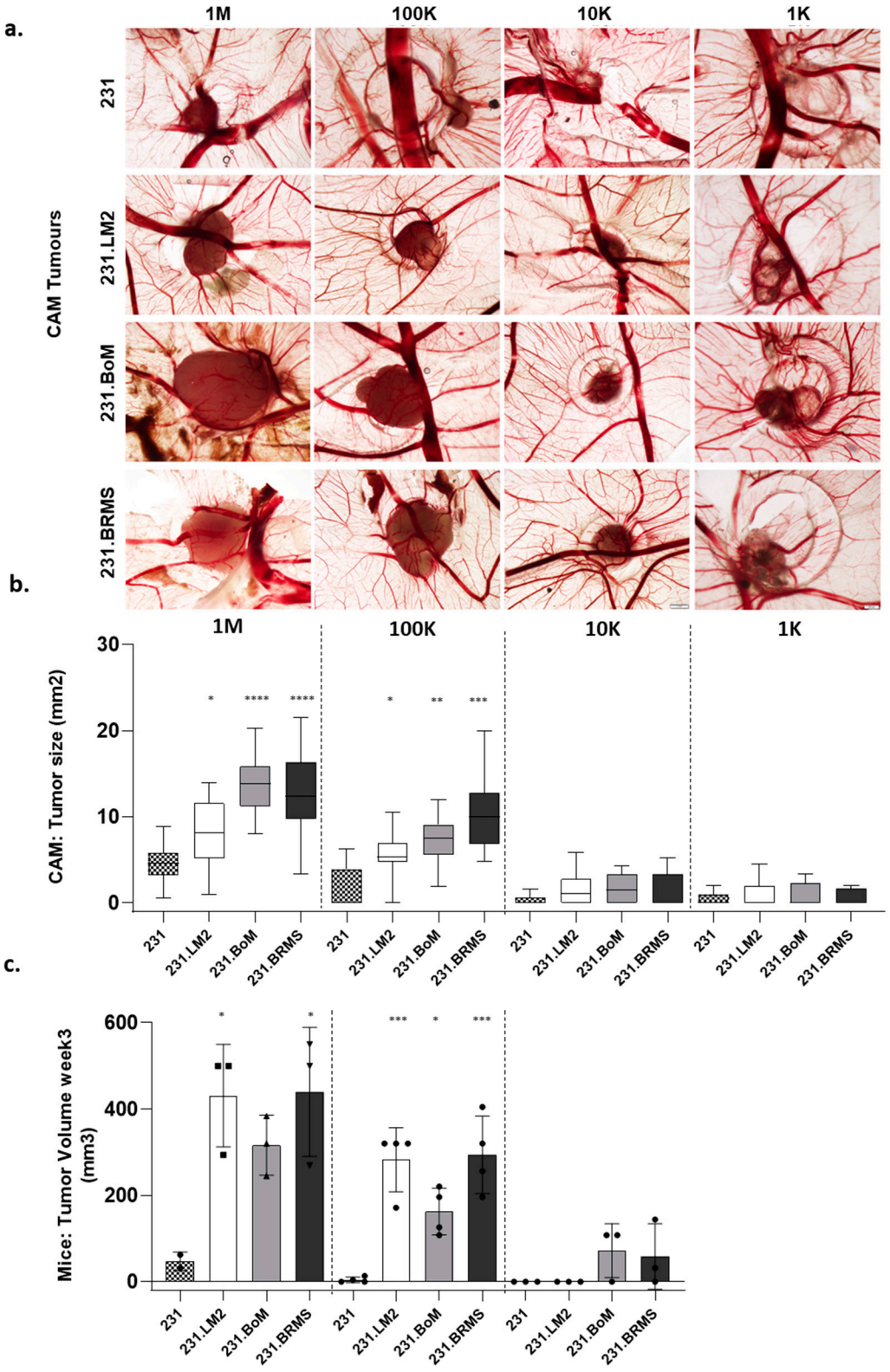


Figure 4. Organotropic breast cancer cells display an increased tumorigenic ability in the choriallantoic membrane of the chick embryo (CAM). (**a**) Representative pictures of CAM xenografted tumors (4 cell lines × 4 cell dilutions); scale bar = 500 µm. (**b**) Tumor size evaluation in the LDA performed in the CAM by inoculations of 1-M, 100-K, 10-K and 1-K cells per egg. (**c**) Tumor size evaluation in a LDA performed in immunodeficient mice by subcutaneous injection of 1-M, 100-K and 10-K cells number per animal. *—$p < 0.05$, **—$p < 0.01$, ***—$p < 0.001$ and ****—$p < 0.0001$).

2.3. Validation of Breast CSC Markers in CAM and Mice Xenografted Tumors

In addition to the previously described macro analysis, the tumors derived from 1-M cells were recovered in both in vivo models and processed for histological analysis. Immunohistochemistry labeling was performed for the CD44 and CD49f breast CSC markers (Figure 5).

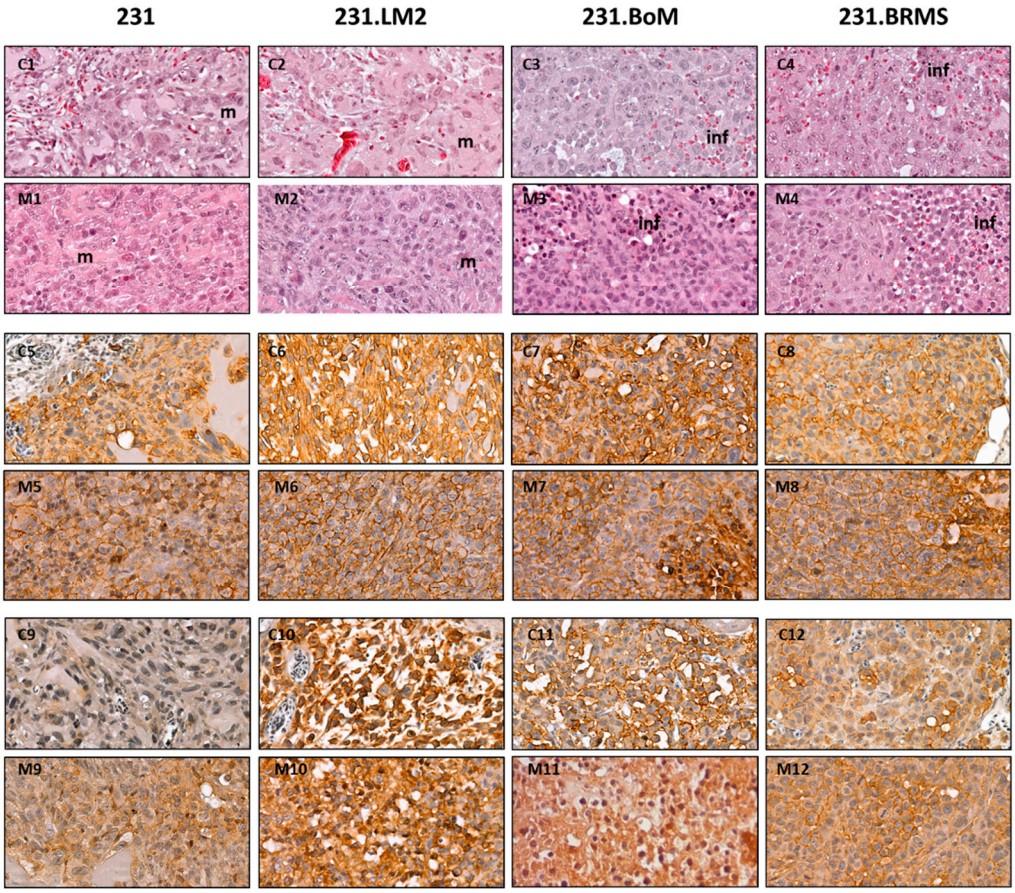


Figure 5. CAM and mice xenografts display similar citocellular organization and stem marker patterns. Each column regards a cell line (231, 231.LM2, 231.BoM and 231.BRMS). (**C1**–**C4**) Hematoxylin–eosin staining in the CAM xenografted tumors (63× magnification); m—Matrigel and inf—infiltrate. (**M1**–**M4**) Hematoxylin–eosin staining in the mice xenografted tumors (63× magnification). (**C5**–**C8**) CD44 labeling in CAM tumors (63 magnification). (**M5**–**M8**) CD44 labeling in mice tumors (63× magnification). (**C9**–**C12**) CD49f labeling in CAM tumors (63× magnification). (**M9**–**M12**) CD49f labeling in mice tumors (63× magnification).

In the CAM, tumors derived from all cell lines were able to invade the CAM and to be vascularized (see Supplementary Figure S1 at 10× magnification). Cellular morphology in the CAM (Figure 5C1–C4) and mice (Figure 5M1–M4) tumors could be compared. The tumors derived from the parental cell line (231) present a clear Matrigel component (m in Figure 5C1,M1), in contrast with the organotropic cell lines, which show a more compact and homogeneous aspect without the detectable presence of Matrigel (Figure 5C2–C4,M2–M4). In agreement with the in vitro results, organotropic breast cancer cell lines show intense and strong staining for both CD44 (Figure 5C6–C8 in comparison to C5 and Figure 5M6–M8 in comparison to M5) and CD49f (Figure 5C10–C12 in comparison to C9 and Figure 5M10–M12 in comparison to M9).

3. Discussion

Tumor progression is a complex multistep process and cancer cells have to display great plasticity in order to survive to the metastatic stepwise cascade [36]. In fact, primary tumors are known to be biologically heterogeneous and composed of different subpopulations of cancer cells with distinct properties, allowing them to adapt to the different processes of the tumor progression cascade. Contributing to this process, the presence of a small subpopulation of cancer cells within the tumor bulk with stem-like properties was demonstrated—cancer stem cells (CSCs) [37]. CSCs are crucial for disease progression, given their self-renewal, plasticity and differentiation capabilities. They are able to induce tumorigenesis, forming or repopulating heterogeneous cancer cell populations [3,14,15,38]. Besides their highly tumorigenic potential, CSCs are resistant to most treatments currently available, and this drug-resistance can promote metastasis and tumor relapses. Therefore, CSC research is an urgent topic in oncology and new and faster tools to evaluate the stem profiles of tumor cells are crucial.

Currently, a combination of in vitro and in vivo assays are used as standard methods to evaluate the self-renewal and differentiation potential of CSCs. Specifically, in breast cancer, an enrichment in CSCs can be identified in vitro by the $CD44^{+}/CD24^{-/low}$ profile and by the formation of mammospheres [18] and by in vivo limiting dilution assays in mice models. Although these mice xenograft models are considered the "gold standard" method to evaluate stemness in vivo, they are invariably associated with high production costs and strict ethical considerations.

Here, we aimed to validate a new in vivo LDA based on the chick embryo chorioallantoic membrane (CAM) as an alternative research tool to be used in the CSC research field. In particular, we demonstrated the ability of the small population of CSCs to form tumors in the CAM, an immuno-incompetent host. In contrast to the mice model, the CAM model has low costs and little regulatory issues; it is also a reproducible and reliable tool to study several aspects of tumor biology, since it has been widely used to study tumor growth and behavior, therapy delivery and efficiency, angiogenesis and metastasis [3,17,23–28].

To establish the new LDA in the chick CAM, a panel of organotropic breast cancer cells was used as cell models. In order to determine if the CAM model would respond to the constraints faced in the in vivo model, we started by characterizing the CSC phenotype of breast cancer cells, previously established by Massagué [32–34], that show tropism to different organs (lung, bone and brain). All organotropic breast cancer cells were shown to be enriched in genes associated with stem cell features. In addition, all of them showed increased in vitro CSC activity when compared with the parental cell line, measured either by the $CD44^{+}/CD24^{-/low}$ profile and by the increased mammosphere-forming efficiency. This effect was more prominent with the bone (231.BoM) and brain (231.BRMS) organotropic breast cancer cells.

Following the in vitro characterization for stem cell features, in vivo LDA was performed in the CAM and in mice. Note that the chick embryo is naturally immune-incompetent, thus allowing the grafting of human tumor cells. Our results in the CAM showed that all cell lines were able to form tumors in seven days, but the organotropic variants formed significantly larger and more compact tumors than those from the parental cell line. In agreement with the previously established stem cell profile, 231.BoM and 231.BRMS formed more prominent tumors. Using mice LDA, tumor formation took three weeks, and the organotropic cell lines were also clearly more tumorigenic; however, for the 1-M cells, differences could only be detected for the 231.LM2 and 231. BRMS cell lines. By using the CAM model, it was possible to achieve 9–18 samples per condition (in contrast with 2–4 in the mice model), thus rendering the statistical analysis more robust in the CAM than in mice LDA. This is clear by the significance levels obtained (that were higher in the CAM-LDA than in mice LDA) but, also, by the consistency obtained between dilutions. Note that 100-K derived tumors were smaller than the 1-M cell derived tumors but followed the same growth pattern between the cell lines.

Besides the tumor size, the stem cell frequency of the organotropic breast cancer cells was determined based on the frequency of tumor formation for each dilution in CAM and mice assays [35]. Consistently with in vitro characterization, all organotropic breast cell lines presented significantly higher stem cell frequency in comparison with the parental cell line when these were inoculated in the CAM. However, for mice LDA, significance was only achieved for 231.BoM and 231.BRMS. Still, the magnitude of the values obtained in the CAM were comparable to the ones found in mice LDA. This analysis demonstrates the importance of a robust set of samples, not always possible to achieve in mice assays. In summary, the in vivo chick CAM model recapitulates the in vitro CSC properties of breast cancer cells, producing tumors with sizes and stem cell frequencies comparable with the ones obtained with the in vivo mice LDA assay.

Finally, xenografted CAM and mice tumors were further analyzed in terms of cell morphology (Hematoxylin–eosin (H&E) staining) and expression of breast CSC markers CD44 and CD49f. As in mice, the morphology of CAM xenografted tumors resembles cancer patient tumors by containing extracellular matrix, stromal cells and extensive vasculature. The tumors formed by the parental cell line, both in CAM and in mice, presented a clear distinct morphology from the ones formed by organotropic cells, demonstrating a more Matrigel-enriched component, where organotropic cell lines formed more compact tumors. Indeed, the presence of a microenvironment is the major advantage of in vivo models, such as the CAM and mice, that contrasts with cancer cell-derived models such as tumor organoids. The expression analysis of the breast CSC markers CD44 and CD49f by immunohistochemistry (IHC) confirmed the in vivo recapitulation of the stem cell features. CAM tumors present stronger staining in organotropic cell lines in comparison with the parental 231. Thus, the CAM system provides the formation of breast cancer-derived tumors that reproduce more faster and accurately the characteristics of CSC-enriched cell models used in this study when compared with mice model.

In a generic way, the in vivo CAM model shows several advantages compared to mice model, namely, easy handling, low cost, accessibility and rapid growth, reproducibility, reliability (reflected in a higher statistical power) and the absence of ethical and regulatory constraints. In particular, for the study of CSCs, we propose the LDA in the chick CAM model as an alternative, appealing and novel research tool to study CSC activity. Although our results are focused on breast cancer, we envisage that the CAM-LDA can be applied to other cancer cell models. However, this should be further validated, where different CSC markers should be selected according to the chosen cancer cell type. This system can still be further explored to test the efficacy of potential anti-CSC drugs with the potential to be used in a personalized medicine context.

4. Materials and Methods

4.1. Cell Culture

The breast cancer cell line MDA-MB-231 (231) was obtained from ATCC (American Type Culture Collection, Manassas, VA, USA), while its organotropic variants lung-metastatic (MDA-MB-231.LM2) [34], bone-metastatic (MDA-MB-231.BoM) [33] and brain-metastatic [MDA-MB-231.BRMS [32]) clones were obtained from J Massagué, the MSK Cancer Center, New York City, NY, USA. The four cell lines were maintained in Dulbecco's minimal essential media (DMEM), supplemented with 10% fetal bovine serum (FBS), I and with 1% antibiotic solution—penicillin/streptomycin (all reagents from Invitrogen, Carlsbad, CA, USA). All the cell lines were cultured at 37 °C in a humidified atmosphere with 5% CO_2 and used in experiments upon reaching 70–80% confluence.

4.2. In Silico Bioinformatics Analysis

To perform the in-silico analysis, the previously described gene expression profiles for significant deregulated genes (DEGs) in brain, bone and lung metastatic breast cancer cells were used [33–35]. After, these gene lists were crossed in order to obtain specific or shared DEGs for each metastatic breast cancer cell line. From this analysis, 80.8% (194 out of 240)

of the genes were specifically deregulated in brain metastatic breast cancer cells (BCC), compared with 70.5% (60 out of 85) and 62.1% (59 out of 95) specifically deregulated genes for bone and lung metastatic BCC, respectively. Gene ontology (GO) terms were retrieved from http://amigo.geneontology.org/amigo/search/bioentity?q=stem.

4.3. Cell Surface Marker Analysis by Flow Cytometry

The expression of CD44 and CD24 on the cell surface of breast cancer cells was determined by flow cytometry analysis. Flow cytometry analysis for these markers was performed as previously described [3].

4.4. Presto Blue Assay

Presto blue assay was performed as previously described [3]. A minimum of 3 independent biological experiments were performed.

4.5. Mammosphere Assay

Mammosphere-forming assay was performed as previously described [3]. A minimum of 5 independent biological experiments were performed.

4.6. Limiting Dilution Assay in the In Vivo CAM Model

The chicken embryo CAM model was used to evaluate the tumorigenic response. Fertilized chick (*Gallus gallus*) eggs were obtained from commercial sources and incubated horizontally at 37 °C in a humidified atmosphere and referred to the embryonic development day (EDD). According to the European Directive 2010/63/EU, ethical approval is not required for experiments using embryonic chickens. Correspondingly, the Portuguese law on animal welfare does not restrict the use of chicken eggs for experimental purposes.

In detail, on EDD3, a square window was opened in the shell after the removal of 1.5–2 mL of albumen to allow detachment of the developing CAM. The window was sealed with a transparent adhesive tape and the eggs returned to the incubator. On EDD9, different numbers of MDA-MB-231 cells and their organotropic variants (resuspended in 5 uL of Matrigel and 5 uL of serum-free medium) were engrafted on top of the growing CAMs. Cells (1×10^6 (1-M), 1×10^5 (100-K), 1×10^4 (10-K) and 1×10^3 (1-K)) were inoculated, per embryo, into a 5-mm silicone ring under sterile conditions. The eggs were resealed and returned to the incubator for an additional 7 days, until EDD16. At this time point, the ring was removed; the CAM was excised from the embryos and photographed ex ovo under a stereoscope at 20× magnification (Olympus, Tokyo, Japan, SZX16 coupled with a DP71 camera). The area of CAM tumors was determined using the Olympus cell Sens Standard 1.14 program. Excised CAMs were fixed in 10% neutral-buffered formalin, paraffin-embedded for slide sections and stained with hematoxylin–eosin for histological examination or processed for immunohistochemistry.

4.7. Limiting Dilution Assay in the In Vivo Mice Model

For the Limiting dilution assay, a subcutaneous injection of the different cancer cells (231, 231.LM2, 231.BoM and 231.BRMS) in the flanks of female N:NIH(S)II-nu/nu mice, 6–8 weeks of age, was performed, using a 25-G needle. In detail, 3 to 4 mice per group and per condition were injected with consecutive cell dilutions ranging from 1×10^6–1×10^4 cells resuspended in Matrigel (1:1). Mice follow-up and tumor volumes were followed, as previously described [3], for a total of 3 weeks. At the end of the experiment, tumors were surgically removed, fixed in 10% buffered formalin, embedded in paraffin, sectioned and stained with hematoxylin and eosin.

The mice were housed, bred and maintained at the i3S Animal House in a pathogen-free environment under controlled conditions of light and humidity. All the experiments were conducted with the application of the 3Rs (replacement, reduction and refinement) (JP_2016_02 Project, animal ethics committee and animal welfare body of i3S).

4.8. Extreme Limiting Dilution Analysis (ELDA)

ELDA software was used to assess the number of self-renewing cells contained within each breast cancer cell line in both the in vivo CAM and mice models. ELDA has the capacity to calculate frequencies for stem cell subpopulations that produce 0% or 100% tumor engraftment, and, therefore, it is preferred for calculating tumor initiation from limited cell numbers. The ELDA software application analyses provided 95% confidence intervals and *t*-test statistical values that distinguished between the numbers of tumor initiating cells from the distinct conditions tested—http://bioinf.wehi.edu.au/software/elda/ [35].

4.9. Immunohistochemistry

Immunohistochemistry for CD44 and CD49f was performed in 3-µm sections of both excised CAM tumors and in mice xenografted tumor sections, as previously described [3].

4.10. Statistical Analysis

GraphPad version 5.0c software (GraphPad Software, San Diego, CA, USA) was used to construct the graphs and to perform the statistical analysis. An ANOVA test was used to calculate the significance of the mammosphere-forming efficiency (followed by Tukey's test) and tumor growth in the CAM and mice assays (followed by Dunnett's test). Flow cytometry experiments were carried out three times, with data pooled from all 3 experiments. Values of $p < 0.05$ were considered to be statistically significant.

Supplementary Materials: The following are available online at https://www.mdpi.com/1422-0067/22/1/334/s1: Figure S1: CAM and mice xenograft images at lower magnification. Table S1: Significantly deregulated genes for each organotropic-derived breast cancer cell line.

Author Contributions: M.T.P., A.S.R. and J.P. conceived the structure of the work. R.C. and I.C. performed the MFE assay and the FACS experiments. A.S.R. and I.C. performed the cell culture experiments. M.T.P. and A.S.R. performed and analyzed the in vivo CAM assay. A.S.R. and R.C. performed the in vivo mice assays. A.S.R. and M.T.P. wrote the manuscript. J.P. supervised the work and edited the final manuscript. All authors have read and agreed to the published version of the manuscript.

Funding: This work was funded by FEDER—Fundo Europeu de Desenvolvimento Regional—funds through the COMPETE 2020—Operacional Programme for Competitiveness and Internationalisation (POCI), Portugal 2020, and by FCT—Fundação para a Ciência e a Tecnologia/Ministério da Ciência, Tecnologia e Ensino Superior under the projects Pest-C/SAU/LA0003/2013, NORTE-01-0145-FEDER-000029, SAICTPAC/0022/2015 and FCT/02/SAICT/2017/030625. FCT funded the research grant of RC (SFRH/BD/135831/2018). IPATIMUP integrated the i3S Research Unit, which was partially supported by FCT in the framework of the project "Institute for Research and Innovation in Health Sciences" (POCI-01-0145-FEDER-007274).

Institutional Review Board Statement: The study was conducted according to the guidelines of the Declaration of Helsinki and approved by the Institutional Review Board (or Ethics Committee) of animal ethics committee and animal welfare body of i3S (JP_2016_02 Project).

Informed Consent Statement: Not applicable.

Data Availability Statement: Not applicable.

Acknowledgments: MDA-MB-231 organotropic cells were provided by the Joan Massagué Laboratory (Memorial Sloan Kettering Cancer Center, New York, NY, USA).

Conflicts of Interest: The authors declare no conflict of interest.

Abbreviations

231	parental MDA-MB-231 breast cancer cells
231.BRMS	brain-metastatic MDA-MB-231
231.LM2	lung-metastatic MDA-MB-231
231.BoM	bone-metastatic MDA-MB-231
APC	allophycocyanin
BCC	breast cancer cell
CAM	chorioallantoic membrane
CSCs	cancer stem-like cells
DEGs	deregulated genes
EDD	embryonic development day
ECM	extracellular matrix
ELDA	extreme limiting dilution assay
FBS	fetal bovine serum
GO	gene ontology
H&E	hematoxilin–eosin
HRP	horseradish peroxidase
IHC	immunohistochemistry
LDA	limiting dilution assay
MFE	mammosphere-forming efficiency
TICs	tumor-initiating cells

References

1. De Angelis, M.L.; Francescangeli, F.; Zeuner, A. Breast Cancer Stem Cells as Drivers of Tumor Chemoresistance, Dormancy and Relapse: New Challenges and Therapeutic Opportunities. *Cancers* **2019**, *11*, 1569. [CrossRef] [PubMed]
2. Smalley, M.; Piggott, L.; Clarkson, R. Breast cancer stem cells: Obstacles to therapy. *Cancer Lett.* **2013**, *338*, 57–62. [CrossRef] [PubMed]
3. Dionisio, M.R.; Vieira, A.F.; Carvalho, R.; Conde, I.; Oliveira, M.; Gomes, M.; Pinto, M.T.; Pereira, P.; Pimentel, J.; Souza, C.; et al. BR-BCSC Signature: The Cancer Stem Cell Profile Enriched in Brain Metastases that Predicts a Worse Prognosis in Lymph Node-Positive Breast Cancer. *Cells* **2020**, *9*, 2442. [CrossRef] [PubMed]
4. Eyre, R.; Alferez, D.G.; Spence, K.; Kamal, M.; Shaw, F.L.; Simoes, B.M.; Santiago-Gomez, A.; Sarmiento-Castro, A.; Bramley, M.; Absar, M.; et al. Patient-derived Mammosphere and Xenograft Tumour Initiation Correlates with Progression to Metastasis. *J. Mammary Gland Biol. Neoplasia* **2016**, *21*, 99–109. [CrossRef]
5. Charafe-Jauffret, E.; Ginestier, C.; Iovino, F.; Wicinski, J.; Cervera, N.; Finetti, P.; Hur, M.H.; Diebel, M.E.; Monville, F.; Dutcher, J.; et al. Breast cancer cell lines contain functional cancer stem cells with metastatic capacity and a distinct molecular signature. *Cancer Res.* **2009**, *69*, 1302–1313. [CrossRef]
6. Liu, H.; Patel, M.R.; Prescher, J.A.; Patsialou, A.; Qian, D.; Lin, J.; Wen, S.; Chang, Y.F.; Bachmann, M.H.; Shimono, Y.; et al. Cancer stem cells from human breast tumors are involved in spontaneous metastases in orthotopic mouse models. *Proc. Natl. Acad. Sci. USA* **2010**, *107*, 18115–18120. [CrossRef]
7. Ren, D.; Zhu, X.P.; Kong, R.; Zhao, Z.; Sheng, J.T.; Wang, J.; Xu, X.Y.; Liu, J.Y.; Cui, K.M.; Zhang, X.H.F.; et al. Targeting Brain-Adaptive Cancer Stem Cells Prohibits Brain Metastatic Colonization of Triple-Negative Breast Cancer. *Cancer Res.* **2018**, *78*, 2052–2064. [CrossRef]
8. Al-Hajj, M.; Wicha, M.S.; Benito-Hernandez, A.; Morrison, S.J.; Clarke, M.F. Prospective identification of tumorigenic breast cancer cells. *Proc. Natl. Acad. Sci. USA* **2003**, *100*, 3983–3988. [CrossRef]
9. Mercurio, A.M.; Bachelder, R.E.; Chung, J.; O'Connor, K.L.; Rabinovitz, I.; Shaw, L.M.; Tani, T. Integrin laminin receptors and breast carcinoma progression. *J. Mammary Gland Biol. Neoplasia* **2001**, *6*, 299–309. [CrossRef]
10. Krebsbach, P.H.; Villa-Diaz, L.G. The Role of Integrin alpha6 (CD49f) in Stem Cells: More than a Conserved Biomarker. *Stem Cells Dev.* **2017**, *26*, 1090–1099. [CrossRef]
11. Eirew, P.; Stingl, J.; Raouf, A.; Turashvili, G.; Aparicio, S.; Emerman, J.T.; Eaves, C.J. A method for quantifying normal human mammary epithelial stem cells with in vivo regenerative ability. *Nat. Med.* **2008**, *14*, 1384–1389. [CrossRef] [PubMed]
12. Croker, A.K.; Rodriguez-Torres, M.; Xia, Y.; Pardhan, S.; Leong, H.S.; Lewis, J.D.; Allan, A.L. Differential Functional Roles of ALDH1A1 and ALDH1A3 in Mediating Metastatic Behavior and Therapy Resistance of Human Breast Cancer Cells. *Int. J. Mol. Sci.* **2017**, *18*, 2039. [CrossRef] [PubMed]
13. Ginestier, C.; Hur, M.H.; Charafe-Jauffret, E.; Monville, F.; Dutcher, J.; Brown, M.; Jacquemier, J.; Viens, P.; Kleer, C.G.; Liu, S.; et al. ALDH1 is a marker of normal and malignant human mammary stem cells and a predictor of poor clinical outcome. *Cell Stem Cell* **2007**, *1*, 555–567. [CrossRef] [PubMed]
14. Vieira, A.F.; Ribeiro, A.S.; Dionisio, M.R.; Sousa, B.; Nobre, A.R.; Albergaria, A.; Santiago-Gomez, A.; Mendes, N.; Gerhard, R.; Schmitt, F.; et al. P-cadherin signals through the laminin receptor alpha6beta4 integrin to induce stem cell and invasive properties in basal-like breast cancer cells. *Oncotarget* **2014**, *5*, 679–692. [CrossRef]

15. Vieira, A.F.; Ricardo, S.; Ablett, M.P.; Dionisio, M.R.; Mendes, N.; Albergaria, A.; Farnie, G.; Gerhard, R.; Cameselle-Teijeiro, J.F.; Seruca, R.; et al. P-Cadherin is Co-Expressed with Cd44 and Cd49f and Mediates Stem Cell Properties in Basal-Like Breast Cancer. *Stem Cells* **2012**, *30*, 854–864. [CrossRef]
16. Schmitt, F.; Ricardo, S.; Vieira, A.F.; Dionisio, M.R.; Paredes, J. Cancer stem cell markers in breast neoplasias: Their relevance and distribution in distinct molecular subtypes. *Virchows Arch.* **2012**, *460*, 545–553. [CrossRef]
17. Yousefnia, S.; Ghaedi, K.; Seyed Forootan, F.; Nasr Esfahani, M.H. Characterization of the stemness potency of mammospheres isolated from the breast cancer cell lines. *Tumor Biol.* **2019**, *41*, 1010428319869101. [CrossRef]
18. Dontu, G.; Al-Hajj, M.; Abdallah, W.M.; Clarke, M.F.; Wicha, M.S. Stem cells in normal breast development and breast cancer. *Cell Prolif.* **2003**, *36* (Suppl. S1), 59–72. [CrossRef]
19. Prager, B.C.; Xie, Q.; Bao, S.; Rich, J.N. Cancer Stem Cells: The Architects of the Tumor Ecosystem. *Cell Stem Cell* **2019**, *24*, 41–53. [CrossRef]
20. Sun, H.; Jia, J.; Wang, X.; Ma, B.; Di, L.; Song, G.; Ren, J. CD44+/CD24− breast cancer cells isolated from MCF-7 cultures exhibit enhanced angiogenic properties. *Clin. Transl. Oncol.* **2013**, *15*, 46–54. [CrossRef]
21. Yang, J.; Zhang, X.; Chen, Z.; Shen, Y.; Wang, F.; Wang, Y.; Liu, Y.; Liu, P.; Yang, J. Angiomotin-p130 inhibits beta-catenin stability by competing with Axin for binding to tankyrase in breast cancer. *Cell Death Dis.* **2019**, *10*, 179. [CrossRef] [PubMed]
22. Zhang, M.; Behbod, F.; Atkinson, R.L.; Landis, M.D.; Kittrell, F.; Edwards, D.; Medina, D.; Tsimelzon, A.; Hilsenbeck, S.; Green, J.E.; et al. Identification of tumor-initiating cells in a p53-null mouse model of breast cancer. *Cancer Res.* **2008**, *68*, 4674–4682. [CrossRef] [PubMed]
23. Palmer, T.D.; Lewis, J.; Zijlstra, A. Quantitative analysis of cancer metastasis using an avian embryo model. *JoVE* **2011**, e2815. [CrossRef] [PubMed]
24. Zhao, S.G.; Shilkrut, M.; Speers, C.; Liu, M.; Wilder-Romans, K.; Lawrence, T.S.; Pierce, L.J.; Feng, F.Y. Development and validation of a novel platform-independent metastasis signature in human breast cancer. *PLoS ONE* **2015**, *10*, e0126631. [CrossRef]
25. Chen, M.J.; Chiou, P.P.; Lin, P.; Lin, C.M.; Siri, S.; Peck, K.; Chen, T.T. Suppression of growth and cancer-induced angiogenesis of aggressive human breast cancer cells (MDA-MB-231) on the chorioallantoic membrane of developing chicken embryos by E-peptide of pro-IGF-I. *J. Cell Biochem.* **2007**, *101*, 1316–1327. [CrossRef]
26. Estrada, M.F.; Rebelo, S.P.; Davies, E.J.; Pinto, M.T.; Pereira, H.; Santo, V.E.; Smalley, M.J.; Barry, S.T.; Gualda, E.J.; Alves, P.M.; et al. Modelling the tumour microenvironment in long-term microencapsulated 3D co-cultures recapitulates phenotypic features of disease progression. *Biomaterials* **2016**, *78*, 50–61. [CrossRef]
27. Nowak-Sliwinska, P.; Segura, T.; Iruela-Arispe, M.L. The chicken chorioallantoic membrane model in biology, medicine and bioengineering. *Angiogenesis* **2014**, *17*, 779–804. [CrossRef]
28. Prazeres, H.; Torres, J.; Rodrigues, F.; Pinto, M.; Pastoriza, M.C.; Gomes, D.; Cameselle-Teijeiro, J.; Vidal, A.; Martins, T.C.; Sobrinho-Simoes, M.; et al. Chromosomal, epigenetic and microRNA-mediated inactivation of LRP1B, a modulator of the extracellular environment of thyroid cancer cells. *Oncogene* **2011**, *30*, 1302–1317. [CrossRef]
29. Vu, B.T.; Shahin, S.A.; Croissant, J.; Fatieiev, Y.; Matsumoto, K.; Le-Hoang Doan, T.; Yik, T.; Simargi, S.; Conteras, A.; Ratliff, L.; et al. Chick chorioallantoic membrane assay as an in vivo model to study the effect of nanoparticle-based anticancer drugs in ovarian cancer. *Sci. Rep.* **2018**, *8*, 8524. [CrossRef]
30. Dunker, N.; Jendrossek, V. Implementation of the Chick Chorioallantoic Membrane (CAM) Model in Radiation Biology and Experimental Radiation Oncology Research. *Cancers* **2019**, *11*, 1499. [CrossRef]
31. Swadi, R.; Mather, G.; Pizer, B.L.; Losty, P.D.; See, V.; Moss, D. Optimising the chick chorioallantoic membrane xenograft model of neuroblastoma for drug delivery. *BMC Cancer* **2018**, *18*, 28. [CrossRef]
32. Bos, P.D.; Zhang, X.H.; Nadal, C.; Shu, W.; Gomis, R.R.; Nguyen, D.X.; Minn, A.J.; van de Vijver, M.J.; Gerald, W.L.; Foekens, J.A.; et al. Genes that mediate breast cancer metastasis to the brain. *Nature* **2009**, *459*, 1005–1009. [CrossRef]
33. Gupta, G.P.; Minn, A.J.; Kang, Y.; Siegel, P.M.; Serganova, I.; Cordon-Cardo, C.; Olshen, A.B.; Gerald, W.L.; Massague, J. Identifying site-specific metastasis genes and functions. *Cold Spring Harb. Symp. Quant. Biol.* **2005**, *70*, 149–158. [CrossRef] [PubMed]
34. Minn, A.J.; Gupta, G.P.; Siegel, P.M.; Bos, P.D.; Shu, W.; Giri, D.D.; Viale, A.; Olshen, A.B.; Gerald, W.L.; Massague, J. Genes that mediate breast cancer metastasis to lung. *Nature* **2005**, *436*, 518–524. [CrossRef] [PubMed]
35. Hu, Y.; Smyth, G.K. ELDA: Extreme limiting dilution analysis for comparing depleted and enriched populations in stem cell and other assays. *J. Immunol. Methods* **2009**, *347*, 70–78. [CrossRef] [PubMed]
36. Chaffer, C.L.; Weinberg, R.A. A perspective on cancer cell metastasis. *Science* **2011**, *331*, 1559–1564. [CrossRef] [PubMed]
37. Shiozawa, Y.; Nie, B.; Pienta, K.J.; Morgan, T.M.; Taichman, R.S. Cancer stem cells and their role in metastasis. *Pharmacol. Ther.* **2013**, *138*, 285–293. [CrossRef] [PubMed]
38. Sousa, B.; Ribeiro, A.S.; Paredes, J. Heterogeneity and Plasticity of Breast Cancer Stem Cells. *Adv. Exp. Med. Biol.* **2019**, *1139*, 83–103. [CrossRef]

cells

MDPI

Article

BR-BCSC Signature: The Cancer Stem Cell Profile Enriched in Brain Metastases that Predicts a Worse Prognosis in Lymph Node-Positive Breast Cancer

Maria Rita Dionísio [1,2,3], André F. Vieira [1,2], Rita Carvalho [1,2], Inês Conde [1,2], Mónica Oliveira [1,2], Madalena Gomes [1,2], Marta T. Pinto [1,2,4], Pedro Pereira [3], José Pimentel [3], Cristiano Souza [5], Márcia M. C. Marques [6,7], Vinícius Duval da Silva [8], Alison Barroso [5], Daniel Preto [5], Jorge F. Cameselle-Teijeiro [9], Fernando Schmitt [1,2,10], Ana Sofia Ribeiro [1,2] and Joana Paredes [1,2,10,*]

1 Epithelial Interactions in Cancer (EPIC) group, i3S, Institute of Investigation and Innovation in Health, University of Porto, 4200-135 Porto, Portugal; medicismilenium@gmail.com (M.R.D.); avieira@ipatimup.pt (A.F.V.); rcarvalho@ipatimup.pt (R.C.); iconde@ipatimup.pt (I.C.); mcc4oliveira@gmail.com (M.O.); madalenassgomes@gmail.com (M.G.); mtpinto@i3s.up.pt (M.T.P.); fschmitt@ipatimup.pt (F.S.); aribeiro@ipatimup.pt (A.S.R.)
2 IPATIMUP- Institute of Pathology and Immunology, University of Porto, 4200-135 Porto, Portugal
3 Centro Hospitalar de Lisboa Norte, 1649-035 Lisboa, Portugal; pedrojfp@gmail.com (P.P.); josepimentel@medicina.ulisboa.pt (J.P.)
4 In vivo CAM assays, i3S - Institute of Investigation and Innovation in Health, University of Porto, 4200-135 Porto, Portugal
5 Department of Breast and Gynecologic Oncology, Barretos Cancer Hospital, Barretos-SP 14784-400, Brazil; crispadua10@gmail.com (C.S.); alison00wagner@gmail.com (A.B.); ddpreto@gmail.com (D.P.)
6 Molecular Oncology Research Center, Barretos Cancer Hospital, Barretos-SP 14784-400, Brazil; mmcmsilveira@gmail.com
7 Barretos School of Health Sciences - FACISB, Barretos-SP 14784-400, Brazil
8 Department of Pathology, Barretos Cancer Hospital, Barretos-SP 14784-400, Brazil; vinids@gmail.com
9 Department of Pathology, Complejo Hospitalario Universitário de Vigo (CHUVI) 36204 Vigo, Spain; videoprimaria@mundo-r.com
10 Department of Pathology, Faculty of Medicine of Porto University (FMUP), 4200-135 Porto, Portugal
* Correspondence: jparedes@ipatimup.pt; Tel.: +35-12-2557-0700

Received: 18 September 2020; Accepted: 4 November 2020; Published: 9 November 2020



Abstract: Brain metastases remain an unmet clinical need in breast oncology, being frequently found in HER2-overexpressing and triple-negative carcinomas. These tumors were reported to be highly cancer stem-like cell-enriched, suggesting that brain metastases probably arise by the seeding of cancer cells with stem features. Accordingly, we found that brain-tropic breast cancer cells show increased stem cell activity and tumorigenic capacity in the chick embryo choriallantoic membrane when compared to the parental cell line. These observations were supported by a significant increase in their stem cell frequency and by the enrichment for the breast cancer stem cell (BCSC) phenotype $CD44^{+}CD24^{-/low}$. Based on this data, the expression of BCSC markers (CD44, CD49f, P-cadherin, EpCAM, and ALDH1) was determined and found to be significantly enriched in breast cancer brain metastases when compared to primary tumors. Therefore, a brain (BR)-BCSC signature was defined (3–5 BCSC markers), which showed to be associated with decreased brain metastases-free and overall survival. Interestingly, this signature significantly predicted a worse prognosis in lymph node-positive patients, acting as an independent prognostic factor. Thus, an enrichment of a BCSC signature was found in brain metastases, which can be used as a new prognostic factor in clinically challenging breast cancer patients.

Keywords: breast cancer; cancer stem cells; stem cell biology; prognostic factors

1. Introduction

Breast cancer is the second leading cause of brain metastases after lung cancer [1]. Of patients with metastatic breast cancer, 15–30% will develop brain metastases during the course of the disease [2]. Specifically, human epidermal growth factor receptor 2 (HER2)-overexpressing and triple-negative breast cancer (TNBC) patients are at higher risk of developing brain metastases [1,3–5].

Metastatic breast cancer dissemination to the central nervous system (CNS) is accompanied by neurological impairments affecting both cognitive and sensory functions, as well as an extremely poor prognosis [6]. Strategies to treat brain metastases are still very limited. Postoperative or preoperative radiation is usually delivered in conjunction with surgical resection to boost local control [7–9]. Further, therapies based in trastuzumab-containing regimens, bevacizumab, or small molecules inhibitors may be contemplated, as they significantly extend overall patient survival (OS) [9]. Conventional chemotherapy has shown limited activity in CNS, the culprit of which has been thought to be the blood–brain barrier along with the molecular structure of the agents [1].

Thus, to improve the management of breast cancer patients and to design prevention strategies for brain metastases, it would be highly relevant to dissect the nature of breast cancer tumor cells that are able to outgrow in the brain. Some years ago, a subpopulation of cancer cells expressing the $CD44^{high}CD24^{-/low}$ cell surface phenotype was identified in primary breast carcinomas as being highly tumorigenic and enriched for stem cell features, namely by their capacity to self-renew and to be therapy resistant [10]. Indeed, a high CD44/CD24 ratio in breast cancer has been shown as an important breast cancer prognosis predictor [11] and also to be enriched in circulating tumor cells [12,13] and in distant metastases, such as in liver [11], bone [14], and lung [15]. Interestingly, further evidence indicated that breast cancer stem cells (BCSC) are probably able to promote the metastatic cascade also to the brain [16]. McGowan and colleagues reported that Notch1 is important for the maintenance of the $CD44^{high}/CD24^{low}$ phenotype in brain-seeking cells [17], whereas Smid and colleagues showed that the expression profile of brain metastases, irrespective of the primary breast cancer subtype, displayed an upregulation of the WNT stem-like signaling pathway [18]. In addition, Sihito and colleagues demonstrated that hormone receptor-negative breast cancer patients, mainly relapsing primarily to the brain, displayed higher expression of nestin and CD133 (prominin-1) in metastases, both of which are regarded as cancer stem cell (CSC) markers of glioblastoma [19]. More recently, Sirkisoon et al. also demonstrated that TGLI1 mediates breast cancer metastasis to the brain by promoting metastasis-initiating CSCs and activating astrocytes in the brain microenvironment [20].

Aside from CD44 and CD24, other biomarkers are also considered to be able to identify and isolate BCSCs, namely, CD49f and EpCAM, which are usually used in combination to characterize cell subpopulations of the breast tissue hierarchy [21–23]. In particular, CD49f, also known as α6-integrin, is a BCSC marker with significant tumor-promoting signaling [24–26] that has been correlated with reduced breast cancer survival [27]. EpCAM is found in breast cancer circulating tumor cells [28] and it has been associated with cancer cell proliferation, survival, migration, invasion [29,30], and enhanced bone metastases' formation [31]. Additionally, the aldehyde dehydrogenase (ALDH) superfamily of enzymes, which is involved in detoxification and/or bioactivation of various intracellular aldehydes, has been identified in both normal and malignant mammary stem cells [32]. Indeed, breast cancer cells expressing high ALDH activity contribute to metastases and chemotherapy resistance [33], and ALDH positivity in breast cancer patients has been associated with early relapse, liver metastases [11], and poor prognosis [32]. Importantly, we have also described P-cadherin as a CSC marker in basal-like breast cancer [34], being closely associated with the phenotype that identifies the luminal progenitor cell of the mammary gland [34,35]. This biomarker is an indicator of poor clinical outcome in primary breast carcinomas and lymph node metastases [36], being a putative valuable marker for axillary-based breast

cancer decisions in the clinical practice [37]. Due to its strong association with invasion [38] and stem cell properties [24,34], we postulate that P-cadherin may also play a role in metastases' colonization or growth [39].

In this work, our aim was to evaluate the stem cell profile and activity of breast cancer cells that colonize the brain, by the use of a brain-tropic breast cancer cell culture system as well as a series of human brain metastases from breast cancer patients. The main goal was to provide evidence that brain metastases are actually enriched in stem cell features. Interestingly, our data revealed a novel signature profile of five distinct BCSC markers enriched in brain metastases—the BR-BCSC signature, which is able to significantly predict poor prognosis of high-risk breast cancer patients and opens the possibility of identifying tumors with potential to metastasize to the brain.

2. Materials and Methods

2.1. Cell Culture

The breast cancer cell line MDA-MB-231 (231) was obtained from ATCC (American Type Culture Collection, Manassas, VA, USA). The human brain-tropic cell line MDA-MB-231.BR (231.Br) and MDA-MB-231.BR.HER2 overexpressing cells (231.Br.HER2) were generated as previously described [40] and were obtained from Patricia Steeg's laboratory—NIH (National Institute of Health, Bethesda, MD, USA). The three cell lines were maintained in Dulbecco's minimal essential media (DMEM, Invitrogen, Carlsbad, CA, USA) supplemented with 10% fetal bovine serum (FBS, Invitrogen) and with 1% antibiotic solution—penicillin streptomycin (Invitrogen). All cell lines were routinely cultured at 37 °C in a humidified atmosphere with 5% CO2. Cells were used in experiments upon reaching 70–80% confluence.

2.2. Cell Surface Marker Analysis by Flow Cytometry

To determine the expression of CD44, CD24, and CD49f on the cell surface of 231, 231.Br, and 231.Br.HER2 cells, we performed flow cytometry analysis. Cells were washed twice with phosphatase buffered saline (PBS) solution and then harvested with versene/0.48 mM EDTA (Invitrogen). Detached cells were washed with PBS supplemented with 0.5% FBS (stain buffer), centrifuged at 1200 rpm for 5 min, and resuspended in stain buffer. A single-cell suspension was incubated with APC-conjugated anti-CD44 (1:20) and PE-conjugated anti-CD24 (1:10), or with PerCP-Cy7-conjugated anti-CD49f (1:20). All antibodies were purchased from BD Biosciences (Temse, Belgium). Primary antibodies or the respective isotype controls (BD Biosciences) were incubated at 4 °C in the dark for 20 min. A cell viability marker was included (1:100 dilution, violet fluorescent reactive dye, Invitrogen) to discriminate dead cells. Cells were analyzed using a BD FACS Canto-II flow cytometer (BD Biosciences, Temse, Belgium).

2.3. Immunoblotting

Cells were lysed with PBS containing 1% Nonidet/P40 (Sigma-Aldrich, Darmstad, Germany), 1% Triton X100 (Sigma-Aldrich, Darmstad, Germany), 1:7 Protease Inhibitors Cocktail (Roche Diagnostics Gmbh, Mannheim, Germany), and 1:100 Phosphatase inhibitor (Sigma-Aldrich, Darmstad, Germany). Protein concentration was determined using the Bio-Rad protein assay (BioIRad, Richmond, CA, USA) and samples were loaded into a 10% polyacrylamide gel and transferred onto a nitrocellulose membrane (GE Healthcare Life Sciences, Sheffield, UK) at 100 V for 90 min. Membranes were blocked in 0.5% Tween 20.5% nonfat dry milk for 1 h and stained with specific primary antibodies overnight at 4 °C and with secondary antibodies for 45 min at room temperature. Detection was assessed using the ECL Chemiluminescence detection kit (Amersham Pharmacia Biotech, Piscataway, NJ, USA). Primary antibodies were anti-CD49f (dilution 1:1000, Sigma-Aldrich), anti-E-cadherin (dilution 1:1000, Cell signaling), anti-N-cadherin (dilution 1:1000, BD Transduction), anti-vimentin, anti-a-tubulin (dilution 1:1000, Sigma-Aldrich, Darmstad, Germany), and anti-GAPDH (Santa Cruz Biotechnology Inc, Heidelberg, Germany), the last of which was used as a loading control. Peroxidase-conjugated

secondary antibodies (anti-rabbit and anti-mouse) were purchased from Santa Cruz Biotechnology Inc. (Heidelberg, Germany).

2.4. Presto Blue Assay

The 1×10^4 cells were seeded in 96-well plates and incubated at 37 °C, 5% CO_2 for 24 h. Cell viability was assessed using Presto Blue reagent: cells were washed with PBS and incubated during 30–45 min with Presto Blue solution (1:10 prepared with Presto Blue, Thermo Fisher, Whatham, MA, USA, and DMEM medium). After the incubation time, fluorescence was measured in Synergy Mx, Biotek Instruments Inc (Winooski, VT, USA) (emission: 560 nm; excitation: 590 nm).

2.5. Zymography Assay

The conditioned medium collected from several cell cultures, which were grown in 6-well plates coated with collagen type I, was analyzed for proteinases' activity using gelatin and β-casein zymography. Gelatin gels were loaded with 12 μg of protein per sample and β-casein gels with 50 μg of protein per sample. Samples were mixed with sample buffer (0.03% bromophenol blue, 0.25 M Tris-HCl pH 6.8, 10% SDS (*w/v*) and 4% sucrose (*w/v*)) and electrophoresed, under nonreducing conditions, on 10% polyacrilamide gels containing 0.1% (*w/v*) gelatin or β-casein from bovine milk (Sigma-Aldrich, Darmstad, Germany). After electrophoresis, gels were washed twice, for 30 min, in 2% (*v/v*) Triton X-100 (Sigma-Aldrich, Darmstad, Germany) at room temperature, in order to remove SDS. Then they were incubated in a substrate reaction buffer for 20 h in the case of the gelatin gels (50 mM Tris-HCl, 5 mM $CaCl_2$, pH 7.5) or 72 h for β-casein gels (0.2M NaCl, 5 mM CaCl2, 1% (*v/v*) Triton X-100 in 50 mM Tris-HCl, pH 7.4) and finally stained with Coomassie Blue Staining Solution (0.1% (*w/v*) Coomassie Blue R250 in 10% (*v/v*) acetic acid and 40% (*v/v*) methanol) for 25 min. The gels' destaining was performed in a solution with 20% methanol and 10% acetic acid, until bands started to become visible. Enzymatic activity was visualized as a clear band against the blue background of stained casein gels, and matrix metalloproteases (MMPs) were identified by their molecular weight. Quantification of band density was carried out using the Quantity One software (version 4.0, BioRad, Hercules, CA, USA).

2.6. Mammosphere Assay

Cells were enzymatically harvested and manually disaggregated with a 25-gauge needle to form a single-cell suspension and resuspended in cold PBS. Cells were plated at 500 cm^2 in nonadherent culture conditions, in flasks coated with 1.2% poly-(2-hydroxyethylmethacrylate)/95% ethanol (Sigma-Aldrich, Darmstad, Germany), and allowed to grow for five days in DMEM/F12 containing B27 supplement, and 500 ng/mL hydrocortisone, 40 ng/mL insulin, 20 ng/mL epidermal growth factor (EGF) in a humidified incubator at 37 °C and 5% (*v/v*) CO2. Spheres' size was determined by a micrometer ruler used under the microscope optic. Mammospheres were considered when sphere size was superior to 60 μm of diameter. Mammosphere forming efficiency (MFE) was calculated as the number of mammospheres (≥60 μm) formed during five days divided by the original number of single cells seeded, being expressed as a percentage. Further, fold increase in mammospheres' formation was calculated performing the ratio of the % MFE for each condition when compared with the parental cell line (231) in each biological replicate. A minimum of five independent biological experiments was performed.

2.7. Chicken Embryo in Vivo Growth Assay

The chicken embryo chorioallantoic membrane (CAM) model was used to evaluate the growth potential of 231, 231.Br, and 231.Br.HER2 cells. Briefly, fertilized chick (*Gallus gallus*) eggs obtained from commercial sources were incubated horizontally at 37.8 °C in a humidified atmosphere and referred to embryonic day (E). On E3, a square window was opened in the shell upon removal of 1.5–2 mL of albumin to allow detachment of the developing CAM. Consecutive cell dilutions

were resuspended in 10 µL of complete medium and matrigel (1:1) (1×10^6—1M, 1×10^5—100K, 1×10^4—10K, and 1×10^3—1K cells per embryo) and placed on top of E10 growing CAM into a 3-mm silicon ring under sterile conditions (8–18 eggs per test condition/dilution). The eggs were sealed and returned to the incubator for an additional seven days. The embryos were euthanized by adding 2 mL of fixative on top of the CAM. After removing the ring, the CAM was excised from the embryos and photographed ex ovo under a stereoscope at 20× magnification (Olympus Iberia S.A.U., Barcelona, Spain, SZX16 coupled with a DP71 camera). To determine tumor area, Cells Sens software (version 1.14, Olympus Iberia S.A.U., Barcelona, Spain) was used to select and measure cell dense areas of the inoculum. According to European Directive 2010/63/EU and Portuguese law Decreto-Lei 113/2013, ethical approval is not required for experiments using embryonic chicken.

2.8. Limiting Dilution Assay in the in Vivo Mice Model

N:NIH(S)II-nu/nu mice strain produced at i3S, were housed, bred, and maintained at the i3S Animal House, in a pathogen-free environment, under controlled conditions of light and humidity. All the experiments were conducted with the application of the 3Rs (replacement, reduction, and refinement) (JP_2016_02 Project, animal ethics committee and animal welfare body of i3S). The groups of animals were established to use the minimal number of animals needed for a correct statistical analysis of the data.

The experiments consisted of the subcutaneous injection in the flank of female mice, with 6–8 weeks of age, with consecutive cell dilutions resuspended in matrigel (1:1) (1×10^6—1M, 1×10^5—100K, and 1×10^4—10K, per mice) from parental 231 and brain-tropic variant 231.Br, using a 25-G needle. Mice (3–4 per group and per condition) were weighed, and tumor width and length were measured with calipers, twice a week, for a total of three weeks. Tumor volume was estimated by using the equation, $V = 0.5 \times a \times b^2$, where V is the volume, a is the length of the major axis of the tumor, and b is the length of its minor axis.

2.9. Primary Breast Cancer Series

A series of 467 primary invasive breast carcinomas, diagnosed between 1978–1992, were retrieved from the Pathology Department, Hospital Xeral-Cíes, Vigo, Spain. Patient follow-up information was available for 454 cases, with a maximum follow-up of 120 months after diagnosis. The tumors were characterized for clinical and pathological features, as previously described [41]. The disease-free survival (DFS) interval was defined as the time from diagnosis to the date of breast cancer-derived relapse (DFS: mean with 95% confidence interval (CI) of 85.5 +/− 2.1 months), whereas overall survival (OS) was considered as the number of months from diagnosis to the disease-related death (OS: mean with 95% CI of 90.0 +/− 2.0 months) (Supplementary Materials Table S1). Breast cancer patients followed the adequate protocols for chemotherapy, radiotherapy, and hormone therapy given at that time. All patients were treated with adjuvant chemotherapy, which consisted of a protocol of six cycles of cyclophosphamide, methotrexate, and fluorouracil. Patients with ER-positive tumors were treated with hormonal therapy, which was carried out exclusively with tamoxifen. Patients with HER2-overexpressing carcinomas were not treated with specific targeted therapy (trastuzumab). No neo-adjuvant treatment was used in the patients included in this series. The present study was conducted under the national regulative law for the usage of biological specimens from tumor banks, where the samples are exclusively available for research purposes in the case of retrospective studies. All analyses were performed according to the REporting recommendations for tumor MARKer prognostic studies (REMARK) recommendations for prognostic and tumor marker studies.

2.10. Breast Cancer Brain Metastases Series

A total of 56 human brain metastases of breast cancer patients were collected in a retrospective manner from Centro Hospitalar de Lisboa Norte (CHLN), Portugal (n = 29), and from Barretos Cancer Hospital, Brazil (n = 27). Metastases present in the brain of breast cancer patients were collected after

surgical resection or postmortem, preserved and fixed in formalin, included in paraffin, and carefully evaluated by neuropathologists. Clinical and pathological features were retrieved for this study. At diagnosis, the majority of patients were stage IV (26.8%, 15/56), followed by stage III (19.6%, 11/56), stage II (26.7%, 15/56), stage I (14.3%, 8/56) and for 7 patients we did not have information on the stage. Information regarding prior metastatic dissemination to the brain was not complete and it was not used in the analysis. Whenever data were available, patients were grouped into intrinsic molecular subtypes: luminal (positive for estrogen receptor (ER) and/or progesterone receptor (PgR), HER2-negative), HER2-positive (HER2-positive/amplified, negative, or positive for ER and PgR), and triple negative (ER- and PgR-negative, HER-2-negative) (Supplementary Materials Table S2). Patient follow-up information was available for 60 patients, who were diagnosed between 2009–2013 (Centro Hospitalar de Lisboa Norte) and between 2007–2008 (Barretos Cancer Hospital), with a maximum follow-up of 223 months after diagnosis. These breast cancer patients followed the established protocols of chemotherapy, radiotherapy, and hormone therapy at that time. No neo-adjuvant treatment had been used in the patients included in this series. The brain metastases-free survival (BMFS) interval was defined as the time from diagnosis to the date of breast cancer-derived brain metastases' relapse, whereas OS was considered as the number of months from diagnosis to the disease-related death. BMFS ranged from 0–222 months (mean with 95% CI of 37.0 +/− 4.8 months and median of 25.0), whereas the OS ranged from 1–223 months (mean with 95% CI of 55.63 +/− 5.0 months and median of 42.0) (Supplementary Materials Table S2). These parameters are consistent with the biological and clinical behavior of such an aggressive disease condition. The present study was conducted with the approval of the Ethical Commission from both hospitals, under the national regulative law for the usage of biological specimens from tumor banks, where the samples are exclusively available for research purposes in retrospective studies (Ethical approvals: Barretos Cancer Hospital/Fundacao Pio XII (2-777-372) and CHLN/Nova Medical School (01/2017/CEFCM).

2.11. Immunohistochemistry

Immunohistochemistry for CD44, CD49f, P-cadherin, EpCAM, and ALDH1 was performed in 3-µm sections. Slides were placed in a Clear-Rite bath (Thermo Fisher Scientific, Waltham, MA, USA), rehydrated through a descending series of ethanol washes, and finally placed in distilled water. Epitope exposure was performed for 30 min at 95 °C with Tris/EDTA (Novocastra, Newcastle, UK) for CD49f and P-cadherin or citrate buffer (ThermoScientific, Freemont, CA, USA) for CD44, EpCAM, and ALDH1. Expression analyses were evaluated as follows: CD44 was detected using the antibody from Cell Signaling Technology (clone 156-3C11; Cell Signaling Technology, Danvers, MA, USA) (dilution 1:100); CD49f was assessed using the specific antibody from Sigma-Aldrich (HPA012696, Sigma-Aldrich, Darmstad, Germany) (dilution 1:50); P-cadherin expression was evaluated with the monoclonal antibody from BD Biosciences (clone 56, BD) (dilution 1:50); EpCAM was evaluated with the antibody from Santa Cruz Biotechnology (clone C-10, Santa Cruz Biotechnology, Dallas, TX, USA) (dilution 1:50); and ALDH1 was detected with an antibody from Abcam (clone EP1933Y, Abcam, Cambridge, UK) (dilution 1:100). Primary antibodies were detected using a secondary antibody with horseradish peroxidase polymer (Cytomation Envision System HRP; DAKO, Carpinteria, CA, USA) (CD49f, P-cadherin, EpCAM, ALDH1) or with the labeled biotin-streptavidin method (DAKO, Carpinteria, CA, USA) (CD44), according to the manufacturer's instructions. The detection method used diaminobenzidine (DAB) as chromogen. Of note, the BCSC markers CD44, CD49f, P-cadherin, and ALDH1 were previously characterized in the primary breast cancer series [34,41,42]; thus, only the EpCAM marker was performed in this specific series, as described. For breast cancer brain metastases, all BCSC markers were evaluated in the context of this work.

2.12. Immunohistochemical Evaluation

The expression of CD44, CD49f, P-cadherin, EpCAM, and ALDH1 was independently evaluated by one pathologist (F.S.) based on grading systems previously established [42–44]. Positive staining of

CD44, CD49f, and P-cadherin was considered when detected at the membrane of tumor cells and the extension of scoring was considered as follows: 0, 0–10% of positive tumor cells; 1+, 10–25% of positive tumor cells; 2+, 25–50% of positive tumor cells; 3+, more than 50% of positive tumor cells. For CD44, CD49f, and P-cadherin, the cases were classified as (0) when considered negative, whereas (1+), (2+), and (3+) were determined as positive cases. For EpCAM, only membranous staining intensity was considered, with strong and moderate expression being considered positive and low/absent expression being considered negative. Regarding ALDH1, it was classified as positive when more than 1% of tumor cells showed clear cytoplasmic positivity.

2.13. Statistical Analysis

Mammospheres' forming efficiency and tumor growth area in the CAM assay data were tested for significance using the Tukey's test and Mann–Whitney test, respectively. Flow cytometry experiments were carried out three times, with data pooled from all three. For the immunohistochemistry results, contingency tables and chi-square tests to estimate the relationship between staining patterns of each BCSC marker in both primary and metastasis series were performed. Survival analyses were estimated by the Kaplan–Meier method and compared using the log-rank test or with the Cox proportional hazards model. Statistical analyses were carried out using SPSS statistics V.17.0 software package for Windows (SPSS, Inc., Chicago, IL, USA) and Graph Pad Prism version 5.0c software (Graph Pad Software, San Diego, CA, USA), unless otherwise stated. *P* values lower than 0.05 were considered statistically significant. All statistical tests were two-sided.

3. Results

3.1. Brain-Tropic Metastatic Breast Cancer Cells Show Increased Stem Cell Activity and Tumorigenic Potential

A brain-tropic metastatic breast cancer model was used. In detail, it was developed by the intra-cardiac injection of human MDA-MB-231 (231) metastatic breast cancer cells into nude mice and by the subsequent isolation of metastases from the brain and their reculture in vitro and reinjection into mice. After multiple sequential rounds of selection, a brain-tropic clone was obtained (231.Br), where cancer cells acquired a higher ability to metastasize to this specific location compared to the original parental cell line, which showed a broader metastatic pattern [40]. Additionally, these brain-seeking breast cancer cells were transfected to overexpress HER2 (231.Br.HER2) [45]. We selected these two cell models, since HER-2 overexpression is enriched in breast cancer brain metastases and, importantly, this brain-tropic variant with Her-2 overexpression induces larger brain metastases than the brain-tropic variant without HER2. These data made us speculate if the CSC potential could be further enriched in 231.Br.HER2 cells.

Interestingly, we found that both brain-tropic cells were morphologically different from parental cells when grown in 2D, as well as when grown in suspension, indicating their putative enrichment in stem cell features (Figure 1A and Supplementary Materials Figure S1A).

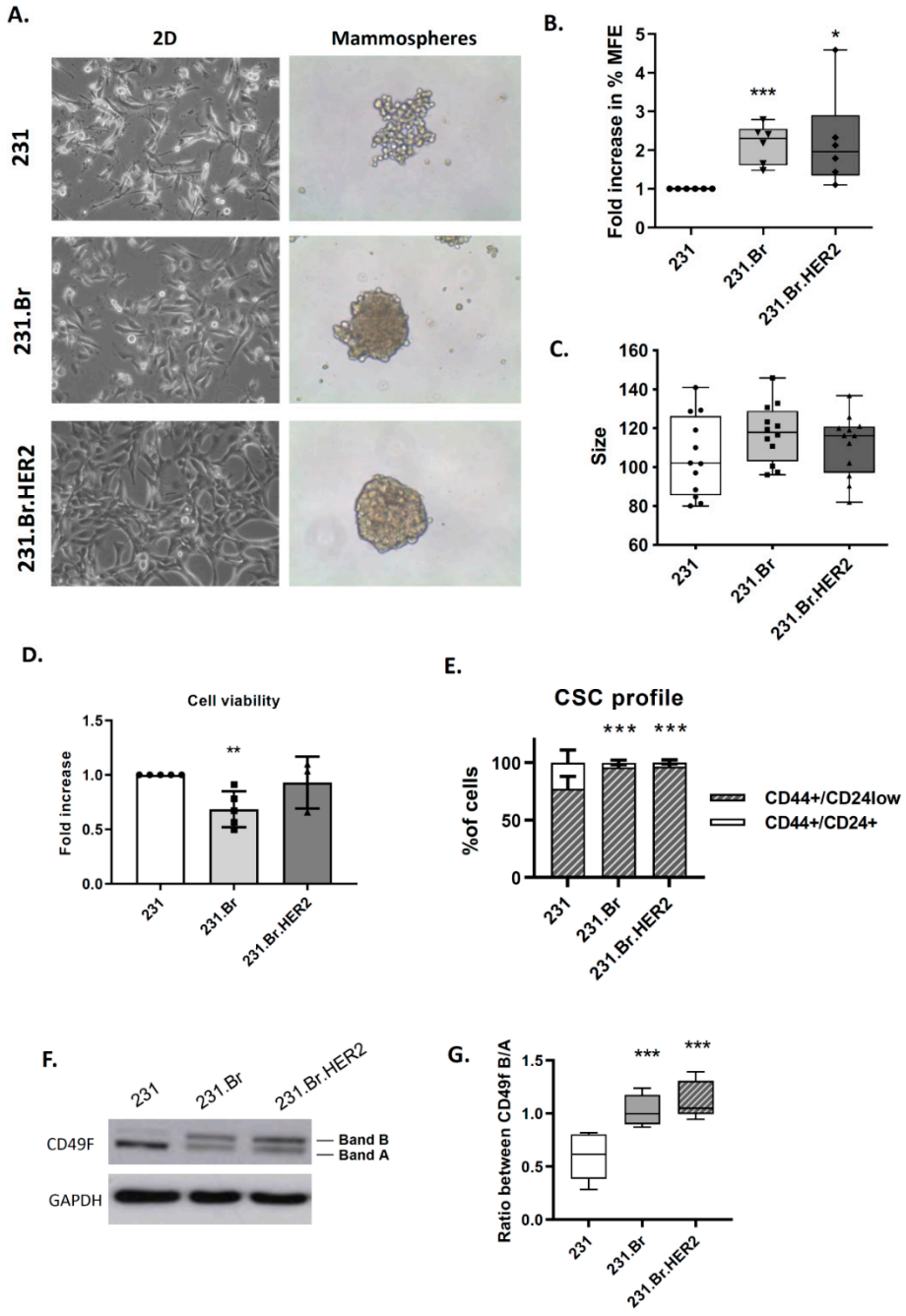


Figure 1. Brain-tropic metastatic breast cancer cells show increased stem cell activity. (**A**) Representative pictures of monolayer (2D) and mammospheres (20× magnification). (**B**) Fold increase in the % of mammospheres' formation efficiency (MFE) in brain-tropic cells (231.Br and 231.Br.HER2) compared with parental cells (231). Each dot in the graph represents an independent biological replicate. Both brain-tropic cells showed to have a significant increase in the stem cell activity. (**C**) Size of the mammospheres (spheres > 60 µm) at the end of the 5-day culture. (**D**) Fold change in cell viability and metabolic activity measured by the Presto blue assay, in brain-tropic cells (231.Br and 231.Br.HER2) compared with parental cells (231). Each dot in the graph represents an independent biological replicate. (**E**) Percentage of cells with the stem cell profile CD44+/CD24−, measured by flow cytometry. (**F**) Western blot for CD49f expression detecting two specific bands (**A** and **B**). (**G**) Ratio between the upper band (**B**)/lower band (**A**), using pixel density from each band. In all assays 4 to 6 biological replicas were performed. Statistical analysis * $p < 0.05$, ** $p < 0.01$, *** $p < 0.001$.

We performed the mammospheres' assay to measure their ability to grow in anchorage-independent conditions, which revealed that both cell lines with tropism to the brain yielded larger mammospheres with a compact and epithelial-like spherical structure, whereas the parental cell line exhibited mammospheres with a loose, grape-like and more mesenchymal-like structure and no central compact aggregate (Figure 1A). These morphological differences in cell phenotype were further confirmed by Western blot. Although no expression of E- and N-cadherin was detected in any cancer cell model, a decrease in vimentin expression was observed in the brain-tropic breast cancer cells (Supplementary Materials Figure S1B). Interestingly, we also found deregulation of MMPs activity when brain tropic cells were compared with the parental cell line (decrease in MMP9 and increase in MMP1 (Supplementary Materials Figure S1C). Aside from the morphological differences, the number and the percentage of mammospheres' forming efficiency (MFE) of brain-tropic cells showed to be significantly increased when compared to the parental cell line (Figure 1B and Supplementary Materials Figure S2A), while no differences were observed in the size of the mammospheres (Figure 1C) or on cell viability (Figure 1D). Interestingly, the stem-like phenotype was further confirmed by the enrichment in the $CD44^{+}CD24^{-/low}$ cell surface expression. All cell lines were constituted by a large subpopulation of $CD44^{+}/CD24^{-}$ cells; but a small, but very significant, enrichment in $CD44^{+}/CD24^{-}$ subpopulations was found in brain-tropic cells when compared with the parental cell line (with 76.9% in 231, 95.7% in 231.Br, and 96.4% in 231.Br.HER2 cells) (Figure 1E and Supplementary Materials Figure S3A,B). We also evaluated the expression of CD49f by Western blot, since two different isoforms with different functions in stemness have been reported [46]. Interestingly, we observed that the parental cell line and brain-tropic breast cancer cells displayed a different profile of these bands: a significant increase was observed in the ratio between high molecular weight (MW) band (band B) and low MW band (band A) (ratio B/A) in brain-tropic cells when compared with the parental cell line, which also supports that brain-tropic cells are enriched in stem cell activity [46] (Figure 1F,G).

Finally, we tested the ability of brain-tropic cells to grow and form in vivo tumors in the chick embryo chorioallantoic membrane (CAM) and in immunocompromised mice. All cell lines inoculated in the CAM were able to form tumors; however, brain-tropic variants formed significantly larger and more compact tumors than those formed by the parental cell line, which typically formed more disaggregated and diffuse tumors (Figure 2A,B).

Interestingly, an enrichment of CD44 expression was found in brain-tropic CAM tumors, whereas no significant differences were observed for CD49f expression (Figure 2C). Additionally, a limiting dilution assay was performed to evaluate the stem cell frequency of brain-tropic breast cancer cells. We evaluated not only the tumor size, but also the frequency of tumor formation. As shown in Figure 2D, both 231.Br and 231.Br.HER2 cells formed significantly bigger tumors when 1 M and 100K cells were inoculated in the CAM. Moreover, although tumor size differences were not maintained when 10K and 1K cells were inoculated, a significant impact was still observed in the frequency of tumor formation, as shown in Table 1. This same result was observed for the tumors formed in the immunocompromised animals (Supplementary Materials Figure S2B,C). In fact, statistical analysis, using the ELDA software [47], revealed a significant increase in the stem cell frequency of the brain-tropic breast cancer cells ($p < 0.0001$), although no significant differences were observed between 231.Br and 231.Br.HER2.

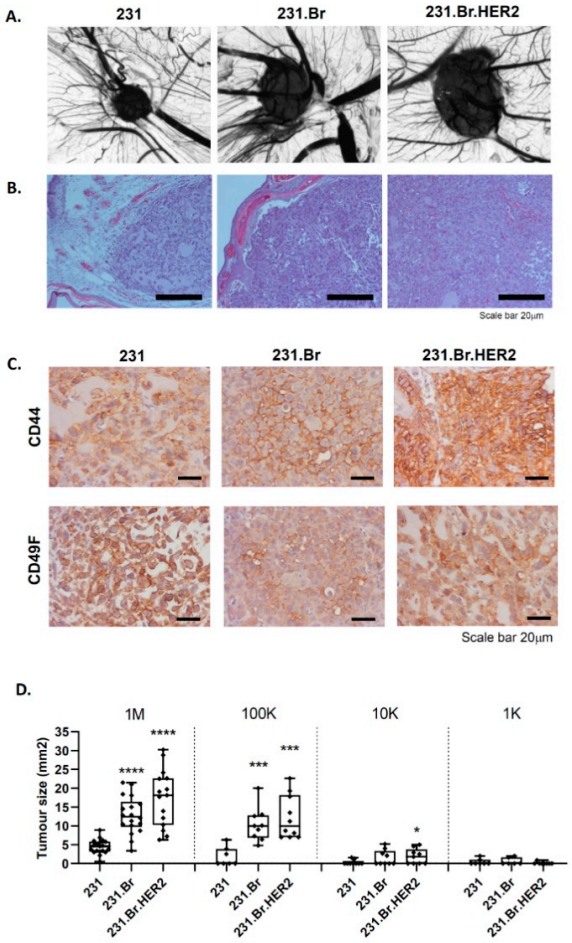


Figure 2. Brain-tropic metastatic breast cancer cells display an increased tumorigenic ability in the choriallantoic membrane of the chick embryo (CAM). (**A**) Representative pictures of tumors formed in the CAM, taken under a stereomicroscope (4× magnification). (**B**) Hematoxilin-eosin (HE) staining of the CAM tumors. Scale bar = 20 µm. (**C**) Illustrative representation of the immunohistochemical evaluation of the breast cancer stem cell markers CD44 and CD49f in CAM tumors. Scale = 20 µm. (**D**) Tumor size evaluation in a limiting dilution assay performed in the CAM, by inoculation of 1M, 100K, 10K, and 1K cell number per egg. Each dotted point corresponds to an independent biological replicate (1M: 18, 18, 15 eggs; 100K: 9, 10, 10 eggs; 10K: 10, 10, 10 eggs; and 1K: 8, 10, 9 eggs for 231, 231.Br, and 231.Br.HER2 respectively). Statistical analysis * $p < 0.05$, *** $p < 0.001$, **** $p < 0.001$).

Table 1. Number of tumors formed in the different cell lines using serial dilutions of inoculated cells (limiting dilution assays). 8–18 independent biological replicates have been performed in the different conditions (1M: 18, 18, 15 eggs; 100K: 9, 10, 10 eggs; 10K: 10, 10, 10 eggs and 1K: 8, 10, 9 eggs for 231, 231.Br and 231.Br.HER2 respectively). Using the ELDA software (http://bioinf.wehi.edu.au/software/elda/), a stem cell frequency was determined. A significant difference was obtained between the parental 231 and the brain-tropic variants (231.Br and 231.Br.HER2), however no significant enrichment is observed for 231.Br vs. 231.Br.HER2.

Cell Model	1M	100K	10K	1k	Stem Cell Frequency (ELDA)	*p*-Value (vs. 231) *	*p*-Value **
231	18/18 (100%)	5/9 (55.6%)	2/10 (20%)	3/8 (37.5%)	1/68769	-	
231.Br	18/18 (100%)	10/10 (100%)	4/10 (40%)	3/10 (30%)	1/12215	0.0007	7.31×10^{-5}
231.Br.HER2	15/15 (100%)	10/10 (100%)	6/10 (60%)	1/9 (11.1%)	1/10535	0.0003	

Multiple group statistical analysis: * Overall test for differences in stem cell frequencies between any of the groups; ** Pairwise tests for differences in stem cell frequencies.

3.2. Human Breast Cancer Brain Metastases Are Enriched in BCSC Markers

Based on our observations in brain-tropic breast cancer cell lines, as well as on literature that demonstrate that CSCs have a pivotal role in tumor growth and metastases [48], we decided to study the expression of five BCSC biomarkers in a series of human breast cancer brain metastases and compare it with the expression of these same proteins in a large series of primary breast cancers. Thus, we evaluated the expression of CD44 and CD49f, as well as P-cadherin, EpCAM, and ALDH1 [41–43]. CD44, CD49f, and P-cadherin expression were mainly membranous with some cytoplasmic staining. EpCAM expression was mainly membranous and ALDH1 expression was found essentially in the cytoplasm. A representative staining of the immunohistochemistry profile is shown in Figure 3A.

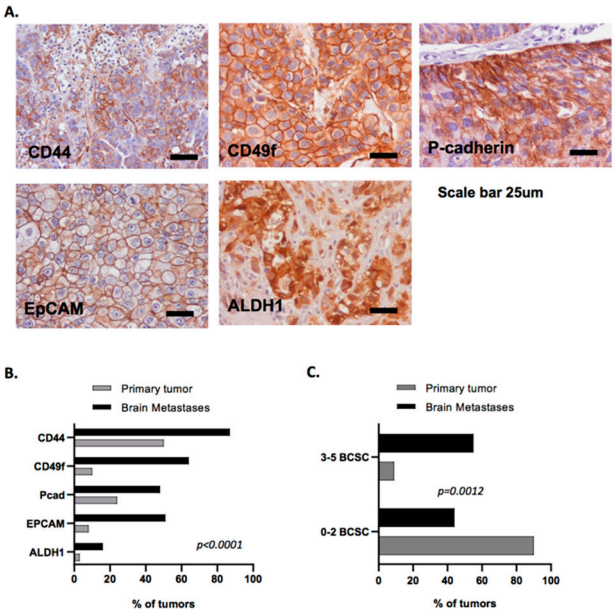


Figure 3. Human breast cancer brain metastases are enriched in breast cancer stem cell markers. (**A**) Illustrative representation of the immunohistochemical evaluation of the breast cancer stem cell markers CD44, CD49f, P-cadherin, EpCAM, and ALDH1 in human brain metastases. Scale = 25 µm. (**B**) Percentage of positive tumors with expression for each BCSC marker (CD44, CD49f, P-cadherin, EpCAM, and ALDH1) in the breast cancer brain metastases series vs. primary breast cancer patients. (**C**) Percentage of positive tumors with BR-BCSC signature (expression of any combination of 3–5 BCSC) in the breast cancer brain metastases series vs. primary breast cancer patients. Associations between the expression of the markers evaluated in primary tumors and breast cancer brain metastases were assessed by Pearson's $\chi 2$.

As shown in Figure 3B (and Supplementary Materials Tables S3 and S4), we compared the expression of each BCSC marker between unpaired primary breast carcinomas and breast cancer brain metastases. Interestingly, all BCSC markers showed to be significantly enriched in brain metastases when compared with primary tumors (Supplementary Materials Table S5). CD44, CD49f, P-cadherin, EpCAM, and ALDH1 were expressed in 87.7% vs. 51.2%, 66.7% vs. 11.5%, 50.9% vs. 24.5%, 52.6% vs. 9%, and 17% vs. 3% of brain metastases vs. primary tumors, respectively. In summary, we found an overall stem cell enrichment in human brain metastases, supporting the observations made in brain-tropic cell lines.

3.3. BCSC Signature Enriched in Brain Metastasis Is Significantly Associated with a Patient's Worse Prognosis

Numerous reports have shown the role of CSC markers in the maintenance of stem cell properties in tumor cells by their impact in cancer initiation and invasion. However, few studies evaluated the impact of a defined CSC enriched profile in breast cancer progression and metastases. Thus, we defined

a brain BCSC (BR-BCSC) signature, encompassing the expression of 3–5 of the previously evaluated BCSC markers in brain metastases, in order to explore its prognostic impact in terms of survival for breast cancer patients. Interestingly, and in accordance with the previously observed enrichment of the distinct BCSC markers in the brain metastases series, we found a very significant enrichment of the BR-BCSC signature in breast cancer brain metastases when compared with primary tumors (55.6% vs. 9.3% in primary tumors for 3–5 BCSC, Figure 3C).

After, we compared the impact of each BCSC marker alone with the BR-BCSC signature (0–2 BCSC vs. 3–5 BCSC markers) on patients' survival, when evaluated in both series of primary carcinomas and brain metastases. As previously reported, P-cadherin was the only marker that showed an impact on DFS and OS for breast cancer patients, when evaluated in the primary breast carcinomas (Supplementary Materials Table S6) [41]. Interestingly, CD44 was the only breast CSC marker with impact in brain metastases-free survival prognosis (BMFS), showing a decrease from 68.5 ± 21.8 months to 33.4 ± 4.5 months ($p = 0.029$) (Table 2) when its expression was evaluated in brain metastases.

Table 2. Survival for the individual breast cancer stem cell (BCSC) markers CD44, CD49f, P-cadherin, EPCAM, and ALDH1 and for the brain (BR) BCSC (BR-BCSC) signature. Survival means were estimated using the Kaplan–Meier method and compared using the log-rank (Mantel–Cox) test. A significant level of 5% was considered. Missing cases were not considered for statistical analysis. Mean survival are in bold as well as the significant *p*-values.

	Breast Cancer Brain Metastases									
	Brain Metastasis Free Survival					**Overall Survival**				
	10-Year BMFS					**10-Year OS**				
	Mean	**Std dev**	**95% CI**		***p*-Value**	**Mean**	**Std dev**	**95% CI**		***p*-Value**
			Inferior	**Superior**				**Inferior**	**Superior**	
CD44										
Negative (n = 7)	**68.5**	21.8	25.8	111.3	**0.029**	**81.5**	16.0	50.1	112.8	**0.045**
Positive (n = 49)	**33.4**	4.5	24.6	42.2		**53.4**	4.7	44.2	62.6	
CD49F										
Negative (n = 19)	**41.9**	10.5	21.2	62.6	0.552	**61.2**	8.7	44.2	78.1	0.488
Positive (n = 37)	**35.6**	5.2	25.4	45.9		**54.6**	5.6	43.7	65.6	
P-cadherin										
Negative (n = 27)	**41.6**	7.1	27.6	55.6	0.144	**64.7**	7.1	50.8	78.6	0.067
Positive (n = 27)	**30.5**	5.4	19.9	41.1		**47.9**	5.9	36.4	59.4	
EPCAM										
Negative (n = 27)	**46.8**	8.3	30.6	63.1	0.07	**65.0**	7.3	50.7	79.2	0.091
Positive (n = 29)	**29.3**	5.3	19.0	39.6		**49.5**	5.8	38.1	60.9	
ALDH1										
Negative (n = 57)	**33.8**	4.1	25.8	41.8	0.313	**53.8**	4.4	45.1	62.5	0.535
Positive (n = 9)	**53.4**	23.1	8.2	98.6		**55.7**	12.9	30.4	81.0	
BR-BCSC										
0–2 BCSS markers (n = 24)	**48.1**	8.1	32.1	64.0	**0.008**	**68.8**	7.6	54.0	83.7	**0.02**
3–5 BCSS markers (n = 29)	**26.7**	4.3	18.2	35.1		**46.2**	5.4	35.6	56.8	

None of the other BCSC markers evaluated had an impact on DFS, BMFS, or OS of breast cancer patients (Table 2 and Supplementary Materials Table S6). However, when we grouped the patients according to the defined BR-BCSC signature, we could observe a significant association with a decrease in both 5-year DFS (50.2 ± 0.9 months to 43.6 ± 3.3 months, $p = 0.018$) and 5-year OS (52.8 ± 0.8 months to 45.1 ± 3.2 months, $p = 0.004$) when evaluated in the primary breast cancer series (Supplementary Materials Table S6 and Figure 4A), as well as with a worse 10-year BMFS

(48.1 ± 8.1 months to 26.7 ± 4.3 months, $p = 0.008$) and OS (68.8 ± 7.6 months to 46.2 ± 5.4 months, $p = 0.02$) when evaluated in breast cancer brain metastases (Table 2 and Figure 4B).

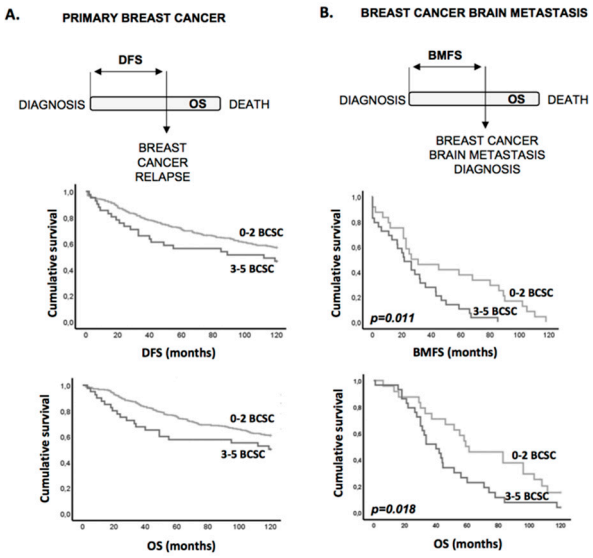


Figure 4. The BR-CSC signature associates with worse prognosis. (**A**) Kaplan–Meier analysis of disease-free survival (DFS) and overall survival (OS) using the BR-BCSC signature in the primary breast cancer series. Five-year DFS (50.2 ± 0.9 months to 43.6 ± 3.3 months, $p = 0.018$) and 5-year OS (52.8 ± 0.8 months to 45.1 ± 3.2 months, $p = 0.004$). (**B**) Kaplan–Meier analysis of brain metastases-free survival and overall survival using the SC enriched profile in the breast cancer brain metastases series. Ten-year brain metastasis free survival (BMFS) (48.1 ± 8.1 months to 26.7 ± 4.3 months, $p = 0.008$) and OS (68.8 ± 7.6 months to 46.2 ± 5.4 months, $p = 0.02$).

Interestingly, the BR-BCSC signature was associated with clinico-pathological features associated with poor prognosis, such as increased tumor size and high histological grade, but no association was found with regional lymph node involvement (Supplementary Materials Table S7). Furthermore, this BCSC enriched phenotype was inversely correlated with ER and PgR expression, but positively and significantly associated with Ki-67, EGFR, vimentin, CK5, CK14 and p63 (Supplementary Materials Table S8), as well as with the metabolic markers GLUT 1 and CAIX (Supplementary Materials Table S8).

Altogether, these results indicate that BCSC enriched tumors strongly associate with aggressive behavior features, such as high proliferation rates, poor differentiation, and basal-like and glycolytic profiles. Actually, univariate analysis showed that the BR-BCSC signature significantly impacts on the prognosis of breast cancer patients (5-year DFS: hazard ratio (HR) = 1.807, $p = 0.021$; 5-year OS: HR = 2.090, $p = 0.005$). However, this impact was lost in a multivariate Cox regression analysis, including the classical breast cancer prognostic factors (Supplementary Materials Table S9), showing that it is not an independent feature.

3.4. BR-BCSC Signature Strongly Predicts a Poor Overall Survival in Lymph Node-Positive Breast Cancer Patients

As the BR-BCSC signature was not associated with the lymph node (LN) involvement, which is one of the major prognostic factors in breast cancer, we decided to combine these two parameters in order to investigate whether the variation in BR-BCSC signature could allow the stratification of LN-positive patients regarding their clinical behavior. Remarkably, we found that breast cancer LN-positive cases with a BR-BCSC signature were from patients exhibiting the worst disease-free survival (59.8 ± 11.8 months vs. 79.0 ± 3.5 months in LN-positive cases with no BR-BCSC signature) and overall survival (60.4 ± 11.8 months vs. 86.2 ± 3.2 in LN-positive cases with no BR-BCSC signature) (Figure 5A,B and Supplementary Materials Table S6), in comparison with other combinatorial

possibilities. Accordingly, cases scored as harboring a BR-BCSC positive in the primary tumor, but for which lymph nodes were classified as negative, showed a better prognosis (Figure 5 and Supplementary Materials Table S6, $p < 0.001$ for DFS and OS).

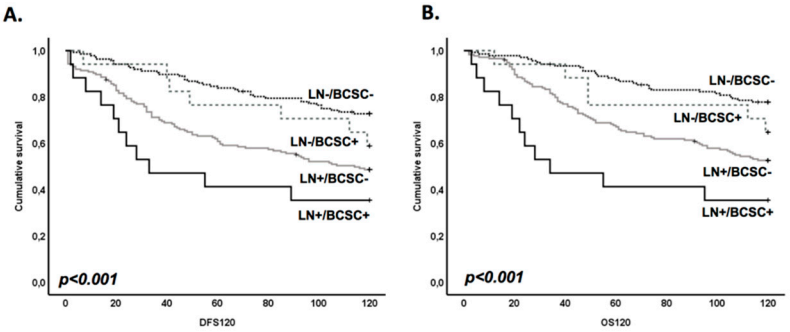


Figure 5. BR-BCSC signature strongly predicts a poor overall survival in lymph node-positive breast cancer patients. Kaplan–Meier analysis of DFS (**A**) and OS (**B**) using the BR-BCSC signature in both lymph node-positive and lymph node-negative breast cancer. LN-positive cases with a BR-BCSC signature were from patients who exhibited the worst DFS (59.8 ± 11.8 months vs. 79.0 ± 3.5 months in LN-positive cases with no BR-BCSC signature) and OS (60.4 ± 11.8 months vs. 86.2 ± 3.2 in LN-positive cases with no BR-BCSC signature).

Univariate Cox regression analysis showed that the BR-BCSC signature in the LN-positive patients was the most relevant factor in predicting poor prognosis, with a HR of 5.708 for 5-year DFS ($p < 0.001$) and a HR of 3.802 for 10-year DFS ($p < 0.001$), when compared with tumors remaining negative in the metastatic axillary site (Table 3). The same significant result was observed for OS (HR = 7.894, $p < 0.001$ at 5-year OS; HR = 5.101, $p < 0.001$ at 10-year OS) (Table 3). Importantly in this case, the multivariate analysis showed that the effect of the BR-BCSC signature was independent of primary tumor size and histological grade (HR = 3.490, $p = 0.002$ for 5-year DFS; HR = 4.133, $p = 0.001$ for 5-year OS; HR = 2.335, $p = 0.019$ for 10-year DFS; HR = 3.042, $p = 0.003$ for 10-year OS) (Table 3).

Therefore, for the first time, we have demonstrated that a BCSC signature, which is enriched in brain metastasis, strongly predicts a poor prognosis in lymph node-positive breast cancer patients.

Table 3. Univariate and multivariate Cox proportional hazard analysis for the lymph-node (LN) status and BR-BCSC signature in the primary carcinomas. This analysis allows risk prediction (hazard ratios and the corresponding 95% confidence interval) for DFS and OS of breast cancer patients, in the primary tumor series. A significant level of 5% was considered. Missing cases were not considered for statistical analysis. The multivariate Cox regression analysis included the effects of histological grade and tumor size.

		Disease-Free Survival								Overall Survival							
	Primary Tumor	5-Year Survival				10-Year Survival				5-Year Survival				10-Year Survival			
		HR	95% CI		*p*-Value	HR	95% CI		*p*-Value	HR	95% CI		*p*-Value	HR	95% CI		*p*-Value
			Inferior	Superior			Inferior	Superior			Inferior	Superior			Inferior	Superior	
Univariate analysis	LN/BR-BCSC																
	Negative/Negative (n = 136, ref.)	1.00			—	1.00			—	1.00			—	1.00			—
	Negative/Positive (n = 17)	1.62	0.55	4.75	0.38	1.57	0.70	3.52	0.27	2.08	0.69	6.21	0.19	1.68	0.70	4.04	0.25
	Positive/Negative (n = 174)	2.94	1.78	4.85	0.00	2.36	1.61	3.46	0.00	3.13	1.79	5.45	0.00	2.60	1.71	3.95	0.00
	Positive/Positive (n = 17)	5.71	2.67	12.21	0.00	3.80	1.94	7.46	0.00	7.89	3.58	17.42	0.00	5.10	2.55	10.19	0.00
Multivariate analysis	LN/BR-BCSC																
	Negative/Negative (n = 136, ref.)	1.00			—	1.00			—	1.00			—	1.00			—
	Negative/Positive (n = 17)	1.16	0.39	3.49	0.79	1.20	0.52	2.74	0.67	1.35	0.44	4.12	0.60	1.25	0.51	3.07	0.62
	Positive/Negative (n = 174)	2.33	1.35	4.02	0.00	1.89	1.25	2.85	0.00	2.15	1.19	3.88	0.01	1.98	1.27	3.10	0.00
	Positive/Positive (n = 17)	3.49	1.56	7.83	0.00	2.34	1.15	4.73	0.02	4.13	1.80	9.51	0.00	3.04	1.47	6.29	0.00
	Histological grade																
	Grade I (n = 54, ref.)	1.00			—	1.00			—	1.00			—	1.00			—
	Grade II (n = 94)	0.91	0.39	2.13	0.84	1.21	0.63	2.32	0.56	1.11	0.43	2.86	0.83	1.19	0.61	2.34	0.61
	Grade III (n = 175)	1.85	0.87	3.92	0.11	1.85	1.02	3.37	0.04	2.00	0.85	4.71	0.11	1.62	0.87	3.02	0.13
	Tumor size																
	T1: <2 cm (n = 82, ref.)	1.00			—	1.00			—	1.00			—	1.00			—
	T2: 2–5 cm (n = 189)	1.86	0.93	3.73	0.08	1.65	0.98	2.77	0.06	2.70	1.13	6.43	0.03	1.88	1.06	3.35	0.03
	T3: >5 cm (n = 52)	3.21	1.49	6.91	0.00	2.99	1.66	5.39	0.00	5.11	2.02	12.92	0.00	3.45	1.81	6.59	0.00

4. Discussion

Distant metastases' formation is a complex process, and the most limiting step is the outgrowth of tumor cells at distant sites [49]. According to the cancer stem cell theory, cancer cells are considered to exist in different populations, some of which may have stem cells' properties, such as self-renewal capacity, that may aid their adaptation to distant organs with distinct microenvironments. Although various CSC markers have been widely used to characterize stem properties of cancer cells and to predict patient prognosis, few studies investigate the dynamics of CSC markers' expression during the brain metastatic cascade.

In order to understand the role of CSCs in breast cancer brain metastases, we took advantage of the MDA-MB-231 breast cancer metastatic cell model in order to evaluate if there was an enrichment of stem-like properties in breast cancer cells with organotropism to the brain. In particular, we tested two brain-tropic variants, with and without HER-2 overexpression, previously established and characterized in terms of metastatic potential [45], since Her-2 overexpression may affect the natural history of breast cancer to accelerate brain progression.

Additionally, we also characterized the expression of five known BCSC markers, namely, CD44, CD49f, P-cadherin, EpCAM, and ALDH1 [24,34], in brain metastatic tumor samples in order to compare it with the expression found in primary tumors. Of note, Lawson and colleagues performed single-cell analysis of primary and metastatic tissues and found that brain metastatic cells show a distinct gene expression signature, with the highest levels of stem cell, quiescence, and anti-apoptosis genes found in brain metastases [35].

In this study, we found that brain-tropic breast cancer cells have an enrichment in their stem-like profile, since they display increased MFE, form larger tumors when inoculated in the CAM, and show a higher percentage of the $CD44^{+}/CD24^{-/low}$ population. In a study using the same cell model, McGowan and colleagues reported only a marginal difference between parental and brain-tropic cells regarding the in vitro $CD44^{+}/CD24^{-}$ phenotype [17], although they showed that this CSC population was enriched in metastases from mice. Furthermore, the authors also demonstrated that inhibition of a stem cell signaling pathway, specifically Notch signaling, in brain-tropic cells reduced the expression of the $CD44^{hi}/CD24^{low}$ phenotype and decreased metastases' formation [17].

Interestingly, we confirmed the increased stem cell potential of the brain-tropic cells by performing limiting dilution assays using the ex vivo CAM model. In fact, we observed a significant increase in the stem cell frequency of cells that show tropism to the brain when compared with the parental cells. These results corroborate a recent study where the authors show that targeting brain adaptive CSC signaling inhibits the brain metastatic colonization [50].

The brain-tropic breast cancer cells did not only show increased stem cell potential but also showed a striking difference in their phenotype, being more cohesive and exhibiting a more epithelial-like phenotype, in contrast to parental cells that displayed a mesenchymal morphology. Interestingly, we found an altered CD49f protein expression pattern between these cells, where brain-tropic cells yielded two bands, as detected by Western blot analysis, most probably corresponding to the two different isoforms previously reported to be associated with different stem cell-related functions. CD49f isoform B differs from isoform A due to the addition of a sequence of 18 amino acids to the cytoplasmic domain, promoting the regulation of stem cell responses to biochemical stimuli and/or biophysical cues in the stem cell niche, thus impacting the stem cell fate [46]. Interestingly, an increase was observed in the ratio of the stem cell-related isoform B with isoform A, suggesting an important role of this isoform on the stem ability of brain-tropic breast cancer cells.

In accordance, we also found a significant enrichment of the BCSC markers CD44, CD49f, P-cadherin, EpCAM, and ALDH1 in human breast cancer brain metastasis when compared with unmatched primary tumors previously analyzed by our group [34,41,42,51]. This clearly indicates that there is an imbalance of adhesion/stem cell molecules that lead to a modification in malignant and colonization properties in distant sites, such as the brain [18,52–57]. However, more importantly, our study revealed an enriched stem cell profile defined by the simultaneous expression of 3–5 of these

BCSC markers, which we defined as a BR-BCSC signature. Even though only 9.3% of the primary tumors display the BR-BCSC signature, these were found to be significantly associated with poor clinico-pathological features and with aggressive behavior properties, such as high proliferation rates, poor differentiation, basal-like features, and glycolytic profiles. These results are in accordance with data showing that predisposition or adaptation of the tumor cell energy metabolism is a key element in breast cancer brain metastases [58] and raises the possibility of targeting the functional differentiation of breast cancer brain metastases in therapeutic strategies.

Remarkably, patients with tumors enriched for the BR-BCSC signature exhibited a significant decrease in the 5-year DFS and OS when evaluated in primary breast cancer series, as well as in the 10-year BMFS and OS in the breast cancer brain metastases series, indicating that this profile would impact on the prognosis of breast cancer patients. Although not acting as an independent prognostic factor, our data disclose, for the first time, a signature of BCSC markers that significantly associates with poor prognostic tumors and that could probably help to identify tumors with potential to metastasize to the brain. Zhang and collaborators have already also suggested a four-protein signature (brain metastases selected markers (BMSM)) to identify CTCs with potential to metastasize to the brain, demonstrating that HER2+/EGFR+/HPSE+/Notch1+ circulating tumor cells (CTCs) displayed a significant propensity to metastasize to the brain in contrast to the parental CTC cells [59]. Although, targeting or isolating CTCs for clinical purposes still remains a challenge, it would be further interesting to test if our BR-BCSC signature would be able to isolate/identify CTCs that specifically metastasize to the brain.

Ultimately, the great novelty of our study was to demonstrate that we can use the BR-BCSC signature as an independent prognostic factor in LN-positive breast carcinomas. In this specific setting, we could observe that tumors harboring a BR-BCSC signature have a very significant and increased risk to recur after five years of the breast cancer diagnosis, as well as to die from this disease. These results are important to be clinically taken into account, since there are few biomarkers described until now that can be useful to stratify this group of high-risk breast cancer patients. In 2006, Brennan et al. also showed that CAIX expression did not correlate with lymph node status but was associated with a significantly worse prognosis in breast cancer patients harboring 1–3 positive lymph nodes. Cox multivariate analysis of the patients in the control arm of the trial revealed CAIX expression to be an independent prognostic factor of breast cancer-specific death in this subgroup [60]. This kind of knowledge is important to be acquired, since the involvement of lymph nodes is used to define patients who will require axillary radiotherapy and to determine the type and aggressiveness of adjuvant systemic therapy. Thus, the data presented in this study demonstrate that the BR-BCSC signature is a marker of poor prognosis in LN-positive patients, but probably can also be a marker of therapy resistance. However, to reliably measure its effect on therapy resistance, further studies are needed with cohorts specifically selected to address this question.

In summary, our data demonstrate that there is an enrichment of a stem-like profile in human brain metastasis, which is associated with a worse breast cancer prognosis. In particular, we found that this BR-BCSC signature is a prognostic factor for DFS and OS in patients with node-positive breast cancer. Thus, the characterization of this signature should be added as an independent prognostic variable and used to predict breast cancer patients at risk, helping in defining an improved and targeted therapy to this aggressive disease condition.

Supplementary Materials: The following are available online at http://www.mdpi.com/2073-4409/9/11/2442/s1. Supplementary Figure S1. Epithelial Mesenchymal phenotype. Supplementary Figure S2: CSC activity, Supplementary Figure S3: Representative flow cytometry analysis data, Supplementary Table S1: Characterization and clinico-pathological features of the primary breast cancer series, Supplementary Table S2: Characterization and clinico-pathological features of the two brain metastases series (from Portugal and Brazil), Supplementary Table S3: Frequency of expression of the BCSC markers CD44, CD49F, P-cadherin, EPCAM, and ALDH1 and the BR-BCSC signature in independent breast cancer brain metastases, Supplementary Table S4: Frequency of expression of the BCSC markers CD44, CD49F, P- cadherin, EPCAM and ALDH1 the BR-BCSC signature in primary carcinomas, Supplementary Table S5: Contingency table with the frequency of expression of the BCSC markers CD44, CD49F, P-cadherin, EPCAM, and ALDH1 the BR-BCSC signature in primary carcinomas vs. breast cancer brain metastases.

Chi-square tests were performed to estimate the relationship between staining patterns of each BCSC marker in both primary and metastases series, Supplementary Table S6: Survival for the individual BCSC markers (CD44, CD49f, P-cadherin, EPCAM, and ALDH1), BR-BCSC signature, lymph node invasion, and combined lymph node status with BR-BCSC profile, Supplementary Table S7: BR-BCSC signature in primary breast cancer associates with clinical poor prognostic factors, Supplementary Table S8: BR-BCSC signature in the primary carcinomas associates with poor prognostic, basal-like, and glycolytic markers, Supplementary Table S9: Univariate and multivariate Cox proportional hazard analysis for the BR-BCSC signature in the primary carcinomas.

Author Contributions: A.S.R., A.F.V., M.R.D., and J.P. conceived the structure of the work. M.R.D., R.C., and M.G. performed immunohistochemistry. I.C. and M.G. performed the mammosphere forming assay. A.S.R., A.F.V., and I.C. performed flow cytometry experiments. A.F.V., M.R.D., and M.O. performed cell culture experiments. M.R.D., P.P., and J.P. (José Pimentel) compiled patient data from Centro Hospitalar Lisboa Norte. C.S., A.B., and D.P. compiled patient data from Barretos Cancer Hospital. F.S., V.D.d.S., and J.F.C.-T. performed pathology analysis. M.G. and M.M.C.M. were involved in the tissue microarray construction. A.S.R. and M.T.P. performed and analyzed the in vivo CAM assay. M.R.D., A.F.V., and A.S.R. performed data analysis. A.F.V. and A.S.R. wrote the manuscript. J.P (Joana Paredes). conceived and supervised the work and final-edited the manuscript. All authors have read and agreed to the published version of the manuscript.

Funding: This work was funded by FEDER (Fundo Europeu de Desenvolvimento Regional) funds through the COMPETE 2020 Operacional Programme for Competitiveness and Internationalisation (POCI), Portugal 2020, and by FCT (Fundação para a Ciência e a Tecnologia) Ministério da Ciência, Tecnologia e Ensino Superior under the projects Pest-C/SAU/LA0003/2013, NORTE-01-0145-FEDER-000029, SAICTPAC/0022/2015 POCI—01-0145-FEDER-016390, and FCT/02/SAICT/2017/030625. A Novartis Oncology grant also funded part of the work, namely, the characterization of the Portuguese series of human brain metastases. FCT funded the research grant of R.C. (SFRH/BD/135831/2018). IPATIMUP integrates the i3S Research Unit, which is partially supported by FCT in the framework of the project "Institute for Research and Innovation in Health Sciences" (POCI-01-0145-FEDER-007274).

Acknowledgments: MDA-MB-231 brain-seeking cells were kindly provided by Patricia S. Steeg´s laboratory (Center for Cancer Research, National Cancer Institute, Bethesda, MD, USA).

Conflicts of Interest: The authors declare no conflict of interest.

Abbreviations

231.Br	MDA-MB-231.BR
231.Br.HER2	MB-231.BR.HER2 overexpressing cells
ALDH	Aldehyde dehydrogenase
BCSC	Breast cancer stem cells
BMFS	Brain metastases-free survival
BR-BCSC	Brain breast cancer stem cell signature
CAM	Chicken embryo chorioallantoic membrane model
CNS	Central nervous system
CSC	Cancer stem cells
DFS	Disease free survival
HER 2	Human epidermal growth factor receptor 2
MFE	Mammosphere forming efficiency
OS	Overall patient survival
REMARK	REporting recommendations for tumor MARKer prognostic studies
TNBC	Triple-negative breast cancer

References

1. Witzel, I.; Oliveira-Ferrer, L.; Pantel, K.; Müller, V.; Wikman, H. Breast cancer brain metastases: Biology and new clinical perspectives. *Breast Cancer Res.* **2016**, *18*, 1–9. [CrossRef] [PubMed]
2. Tabouret, E.; Chinot, O.; Metellus, P.; Tallet, A.; Viens, P.; Gonçalves, A. Recent trends in epidemiology of brain metastases: An overview. *Anticancer Res.* **2012**, *32*, 4655–4662. [PubMed]
3. Yau, T.; Swanton, C.; Chua, S.; Sue, A.; Walsh, G.; Rostom, A.; Johnston, S.R.; O'Brien, M.E.R.; Smith, I.E. Incidence, pattern and timing of brain metastases among patients with advanced breast cancer treated with trastuzumab. *Acta Oncol.* **2006**, *45*, 196–201. [CrossRef]

4. Witzel, I.; Kantelhardt, E.J.; Milde-Langosch, K.; Ihnen, M.; Zeitz, J.; Harbeck, N.; Jänicke, F.; Müller, V. Management of patients with brain metastases receiving trastuzumab treatment for metastatic breast cancer. *Onkologie* **2011**, *34*, 304–308. [CrossRef] [PubMed]
5. Kaplan, M.A.; Isikdogan, A.; Koca, D.; Kucukoner, M.; Gumussoy, O.; Yildiz, R.; Dayan, A.; Demir, L.; Geredeli, C.; Koçer, M.; et al. Biological subtypes and survival outcomes in breast cancer patients with brain metastases (study of the Anatolian Society of Medical Oncology). *Oncology* **2012**, *83*, 141–150. [CrossRef]
6. Quigley, M.R.; Fukui, O.; Chew, B.; Bhatia, S.; Karlovits, S. The shifting landscape of metastatic breast cancer to the CNS. *Neurosurg. Rev.* **2013**, *36*, 377–382. [CrossRef]
7. McPherson, C.M.; Suki, D.; Feiz-Erfan, I.; Mahajan, A.; Chang, E.; Sawaya, R.; Lang, F.F. Adjuvant whole-brain radiation therapy after surgical resection of single brain metastases. *Neuro Oncol.* **2010**, *12*, 711–719. [CrossRef]
8. Niwińska, A.; Murawska, M.; Pogoda, K. Breast cancer subtypes and response to systemic treatment after whole-brain radiotherapy in patients with brain metastases. *Cancer* **2010**, *116*, 4238–4247. [CrossRef] [PubMed]
9. Yuan, P.; Gao, S.L. Management of breast cancer brain metastases: Focus on human epidermal growth factor receptor 2-positive breast cancer. *Chronic Dis. Transl. Med.* **2017**, *3*, 21–32. [CrossRef] [PubMed]
10. Al-Hajj, M.; Wicha, M.S.; Benito-Hernandez, A.; Morrison, S.J.; Clarke, M.F. Prospective identification of tumorigenic breast cancer cells. *Proc. Natl. Acad. Sci. USA* **2003**, *100*, 3983–3988. [CrossRef] [PubMed]
11. Li, W.; Ma, H.; Zhang, J.; Zhu, L.; Wang, C.; Yang, Y. Unraveling the roles of Cd44/Cd24 and Aldh1 as cancer stem cell markers in tumorigenesis and metastasis. *Sci. Rep.* **2017**, *7*, 13856. [CrossRef]
12. Theodoropoulos, P.A.; Polioudaki, H.; Agelaki, S.; Kallergi, G.; Saridaki, Z.; Mavroudis, D.; Georgoulias, V. Circulating tumor cells with a putative stem cell phenotype in peripheral blood of patients with breast cancer. *Cancer Lett.* **2010**, *288*, 99–106. [CrossRef]
13. Wang, J.; Cao, M.G.; You, C.Z.; Wang, C.L.; Liu, S.L.; Kai, C.; Dou, J. A preliminary investigation of the relationship between circulating tumor cells and cancer stem cells in patients with breast cancer Cell. *Mol. Biol. (Noisy-le-grand)* **2012**, *58*, OL1641–OL1645.
14. Giordano, A.; Gao, H.; Cohen, E.N.; Anfossi, S.; Khoury, J.; Hess, K.; Krishnamurthy, S.; Tin, S.; Cristofanilli, M.; Hortobagyi, G.N.; et al. Clinical relevance of cancer stem cells in bone marrow of early breast cancer patients. *Ann. Oncol.* **2013**, *24*, 2515–2521. [CrossRef] [PubMed]
15. Sheridan, C.; Kishimoto, H.; Fuchs, R.K.; Mehrotra, S.; Bhat-Nakshatri, P.; Turner, C.H.; Goulet, R., Jr.; Badve, S.; Nakshatri, H. CD44+/CD24− Breast cancer cells exhibit enhanced invasive properties: An early step necessary for metastasis. *Breast Cancer Res.* **2006**, *8*, R59. [CrossRef] [PubMed]
16. Oskarsson, T.; Batlle, E.; Massagué, J. Metastatic stem cells: Sources, niches, and vital pathways. *Cell Stem Cell* **2014**, *14*, 306–321. [CrossRef]
17. McGowan, P.M.; Simedrea, C.; Ribot, E.J.; Foster, P.J.; Palmieri, D.; Steeg, P.S.; Allan, A.L.; Chambers, A.F. Notch1 inhibition alters the CD44hi/CD24lo population and reduces the formation of brain metastases from breast cancer. *Mol. Cancer Res.* **2011**, *9*, 834–844. [CrossRef]
18. Smid, M.; Wang, Y.; Zhang, Y.; Sieuwerts, A.M.; Yu, J.; Klijn, J.G.M.; Foekens, J.A.; Martens, J.W.M. Subtypes of breast cancer show preferential site of relapse. *Cancer Res.* **2008**, *68*, 3108–3114. [CrossRef]
19. Jhanwar-Uniyal, M.; Labagnara, M.; Friedman, M.; Kwasnicki, A.; Murali, R. Glioblastoma: Molecular pathways, stem cells and therapeutic targets. *Cancers* **2015**, *7*, 538–555. [CrossRef]
20. Sirkisoon, S.R.; Carpenter, R.L.; Rimkus, T.; Doheny, D.; Zhu, D.; Aguayo, N.R.; Xing, F.; Chan, M.; Ruiz, J.; Metheny-Barlow, L.J.; et al. TGLI1 transcription factor mediates breast cancer brain metastasis via activating metastasis-initiating cancer stem cells and astrocytes in the tumor microenvironment. *Oncogene* **2019**, *39*, 64–78. [CrossRef]
21. Stingl, J.; Eirew, P.; Ricketson, I.; Shackleton, M.; Vaillant, F.; Choi, D.; Li, H.I.; Eaves, C.J. Purification and unique properties of mammary epithelial stem cells. *Nat. Cell Biol.* **2006**, *439*, 993–997. [CrossRef] [PubMed]
22. Stingl, J.; Eaves, C.J.; Zandieh, I.; Emerman, J.T. Characterization of bipotent mammary epithelial progenitor cells in normal adult human breast tissue. *Breast Cancer Res. Treat.* **2001**, *67*, 93–109. [CrossRef]
23. Eirew, P.; Stingl, J.; Raouf, A.; Turashvili, G.; Aparicio, S.; Emerman, J.T.; Eaves, C.J. A method for quantifying normal human mammary epithelial stem cells with in vivo regenerative ability. *Nat. Med.* **2008**, *14*, 1384–1389. [CrossRef] [PubMed]

24. Vieira, A.F.; Ribeiro, A.S.; Dionisio, M.R.; Sousa, B.; Nobre, A.R.; Albergaria, A.; Santiago-Gomez, A.; Mendes, N.; Gerhard, R.; Schmitt, F.; et al. P-cadherin signals through the laminin receptor alpha6beta4 integrin to induce stem cell and invasive properties in basal-like breast cancer cells. *Oncotarget* **2014**, *5*, 679–692. [CrossRef] [PubMed]
25. Mercurio, A.M.; Bachelder, R.E.; Chung, J.; O'Connor, K.L.; Rabinovitz, I.; Shaw, L.M.; Tani, T. Integrin laminin receptors and breast carcinoma progression. *J. Mammary Gland. Biol. Neoplasia* **2001**, *6*, 299–309. [CrossRef] [PubMed]
26. Shaw, L.M.; Rabinovitz, I.; Wang, H.H.; Toker, A.; Mercurio, A.M. Activation of phosphoinositide 3-oh kinase by the alpha6beta4 integrin promotes carcinoma invasion. *Cell* **1997**, *91*, 949–960. [CrossRef]
27. Friedrichs, K.; Ruiz, P.; Franke, F.; Gille, I.; Terpe, H.J.; A Imhof, B. High expression level of alpha 6 integrin in human breast carcinoma is correlated with reduced survival. *Cancer Res.* **1995**, *55*, 901–906.
28. Cristofanilli, M.; Budd, G.T.; Ellis, M.J.; Stopeck, A.; Matera, J.; Miller, M.C.; Reuben, J.M.; Doyle, G.V.; Allard, W.J.; Terstappen, L.W.; et al. Circulating tumor cells, disease progression, and survival in metastatic breast cancer. *New Engl. J. Med.* **2004**, *351*, 781–791. [CrossRef]
29. Osta, W.A.; Chen, Y.; Mikhitarian, K.; Mitas, M.; Salem, M.; Hannun, Y.A.; Cole, D.J.; Gillanders, W.E. EpCAM is overexpressed in breast cancer and is a potential target for breast cancer gene therapy. *Cancer Res.* **2004**, *64*, 5818–5824. [CrossRef]
30. Hase, T.; Sato, M.; Yoshida, K.; Girard, L.; Takeyama, Y.; Horio, M.; Elshazley, M.; Oguri, T.; Sekido, Y.; Shames, D.S.; et al. Pivotal role of epithelial cell adhesion molecule in the survival of lung cancer cells. *Cancer Sci.* **2011**, *102*, 1493–1500. [CrossRef]
31. Hiraga, T.; Ito, S.; Nakamura, H. EpCAM expression in breast cancer cells is associated with enhanced bone metastasis formation. *Int. J. Cancer* **2015**, *138*, 1698–1708. [CrossRef]
32. Ginestier, C.; Hur, M.H.; Charafe-Jauffret, E.; Monville, F.; Dutcher, J.; Brown, M.; Jacquemier, J.; Viens, P.; Kleer, C.G.; Liu, S.; et al. ALDH1 is a marker of normal and malignant human mammary stem cells and a predictor of poor clinical outcome. *Cell Stem Cell* **2007**, *1*, 555–567. [CrossRef]
33. Croker, A.K.; Rodriguez-Torres, M.; Xia, Y.; Pardhan, S.; Leong, H.S.; Lewis, J.D.; Allan, A.L. Differential functional roles of ALDH1A1 and ALDH1A3 in mediating metastatic behavior and therapy resistance of human breast cancer cells. *Int. J. Mol. Sci.* **2017**, *18*, 2039. [CrossRef]
34. Vieira, A.F.; Ricardo, S.; Ablett, M.P.; Dionisio, M.R.; Mendes, N.; Albergaria, A.; Farnie, G.; Gerhard, R.; Cameselle-Teijeiro, J.F.; Seruca, R.; et al. P-cadherin is co-expressed with Cd44 and Cd49f and mediates stem cell properties in basal-like breast cancer. *Stem Cells* **2012**, *30*, 854–864. [CrossRef] [PubMed]
35. Lawson, D.A.; Bhakta, N.R.; Kessenbrock, K.; Prummel, K.D.; Yu, Y.; Takai, K.; Zhou, A.; Eyob, H.; Balakrishnan, S.; Wang, C.-Y.; et al. Single-cell analysis reveals a stem-cell program in human metastatic breast cancer cells. *Nature* **2015**, *526*, 131–135. [CrossRef]
36. Paredes, J.; Albergaria, A.; Oliveira, J.T.; Jerónimo, C.; Milanezi, F.; Schmitt, F.C. P-cadherin overexpression is an indicator of clinical outcome in invasive breast carcinomas and is associated with CDH3 promoter hypomethylation. *Clin. Cancer Res.* **2005**, *11*, 5869–5877. [CrossRef]
37. Paredes, J.; Lopes, N.; Milanezi, F.; Schmitt, F.C. P-cadherin and cytokeratin 5: Useful adjunct markers to distinguish basal-like ductal carcinomas in situ. *Virchows Arch.* **2007**, *450*, 73–80. [CrossRef]
38. Ribeiro, A.S.; Albergaria, A.; Sousa, B.; Correia, A.L.; Bracke, M.; Seruca, R.; Schmitt, F.C.; Paredes, J. Extracellular cleavage and shedding of P-cadherin: A mechanism underlying the invasive behaviour of breast cancer cells. *Oncogene* **2010**, *29*, 392–402. [CrossRef]
39. Vieira, A.F.; Paredes, J. P-cadherin and the journey to cancer metastasis. *Mol. Cancer* **2015**, *14*, 178. [CrossRef] [PubMed]
40. Yoneda, T.; Williams, P.J.; Hiraga, T.; Niewolna, M.; Nishimura, R. A bone-seeking clone exhibits different biological properties from the MDA-MB-231 parental human breast cancer cells and a brain-seeking clone in vivo and in vitro. *J. Bone Miner. Res.* **2001**, *16*, 1486–1495. [CrossRef]
41. Ribeiro, A.S.; Sousa, B.; Carreto, L.; Mendes, N.; Nobre, A.R.; Ricardo, S.; Albergaria, A.; Cameselle-Teijeiro, J.F.; Gerhard, R.; Söderberg, O.; et al. P-cadherin functional role is dependent on E-cadherin cellular context: A proof of concept using the breast cancer model. *J. Pathol.* **2013**, *229*, 705–718. [CrossRef] [PubMed]

42. Ricardo, S.; Vieira, A.F.; Gerhard, R.; Leitão, D.; Pinto, R.; Cameselle-Teijeiro, J.F.; Milanezi, F.; Schmitt, F.; Paredes, J. Breast cancer stem cell markers CD44, CD24 and ALDH1: Expression distribution within intrinsic molecular subtype. *J. Clin. Pathol.* **2011**, *64*, 937–946. [CrossRef]
43. Sousa, B.; Paredes, J.; Milanezi, F.; Lopes, N.; Martins, D.; Dufloth, R.; Vieira, D.; Albergaria, A.; Veronese, L.; Carneiro, V.; et al. P-cadherin, vimentin and CK14 for identification of basal-like phenotype in breast carcinomas: An immunohistochemical study. *Histol. Histopathol.* **2010**, *25*, 963–974.
44. Kamal, N.M.; Salem, H.M.; Dahmoush, H.M. Immunohistochemical expression of epithelial cell adhesion molecule (EpCAM) in mucoepidermoid carcinoma compared to normal salivary gland tissues. *Arch. Oral Biol.* **2017**, *79*, 87–94. [CrossRef]
45. Palmieri, D.; Bronder, J.L.; Herring, J.M.; Yoneda, T.; Weil, R.J.; Stark, A.M.; Kurek, R.; Vega-Valle, E.; Feigenbaum, L.; Halverson, D.; et al. Her-2 overexpression increases the metastatic outgrowth of breast cancer cells in the brain. *Cancer Res.* **2007**, *67*, 4190–4198. [CrossRef]
46. Zhou, Z.; Qu, J.; He, L.; Peng, H.; Chen, P.; Zhou, Y. Alpha 6-integrin alternative splicing: Distinct cytoplasmic variants in stem cell fate specification and niche interaction. *Stem Cell Res. Ther.* **2018**, *9*, 122–128. [CrossRef]
47. Hu, Y.; Smyth, G.K. ELDA: Extreme limiting dilution analysis for comparing depleted and enriched populations in stem cell and other assays. *J. Immunol. Methods* **2009**, *347*, 70–78. [CrossRef]
48. Li, F.; Tiede, B.; Massagué, J.; Kang, Y. Beyond tumorigenesis: Cancer stem cells in metastasis. *Cell Res.* **2006**, *17*, 3–14. [CrossRef]
49. Morris, V.L.; Koop, S.; Macdonald, I.C.; Schmidt, E.E.; Grattan, M.; Percy, D.; Chambers, A.F.; Groom, A.C. Mammary carcinoma cell lines of high and low metastatic potential differ not in extravasation but in subsequent migration and growth. *Clin. Exp. Metastasis* **1994**, *12*, 357–367. [CrossRef]
50. Ren, D.; Zhu, X.; Kong, R.; Zhao, Z.; Sheng, J.; Wang, J.; Xu, X.; Liu, J.; Cui, K.; Zhang, X.H.-F.; et al. Targeting brain-adaptive cancer stem cells prohibits brain metastatic colonization of triple-negative breast cancer. *Cancer Res.* **2018**, *78*, 2052–2064. [CrossRef]
51. Sousa, B.; Ribeiro, A.S.; Nobre, A.R.; Lopes, N.; Martins, D.; Pinheiro, C.; Vieira, A.F.; Albergaria, A.; Gerhard, R.; Schmitt, F.; et al. The basal epithelial marker P-cadherin associates with breast cancer cell populations harboring a glycolytic and acid-resistant phenotype. *BMC Cancer* **2014**, *14*, 734. [CrossRef]
52. Ribeiro, A.S.; Paredes, J. P-cadherin linking breast cancer stem cells and invasion: A promising marker to identify an "Intermediate/Metastable" EMT state. *Front. Oncol.* **2014**, *4*, 371. [CrossRef]
53. Jeevan, D.S.; Cooper, J.B.; Braun, A.; Murali, R.; Jhanwar-Uniyal, M. Molecular pathways mediating metastases to the brain via epithelial-to-mesenchymal transition: Genes, proteins, and functional analysis. *Anticancer Res.* **2016**, *36*, 523–532.
54. Auvinen, P.; Tammi, R.; Kosma, V.-M.; Sironen, R.; Soini, Y.; Mannermaa, A.; Tumelius, R.; Uljas, E.; Tammi, M. Increased hyaluronan content and stromal cell CD44 associate with HER2 positivity and poor prognosis in human breast cancer. *Int. J. Cancer* **2012**, *132*, 531–539. [CrossRef]
55. Narkhede, A.A.; Crenshaw, J.H.; Manning, R.M.; Rao, S.S. The influence of matrix stiffness on the behavior of brain metastatic breast cancer cells in a biomimetic hyaluronic acid hydrogel platform. *J. Biomed. Mater. Res. Part A* **2018**, *106*, 1832–1841. [CrossRef] [PubMed]
56. Schwertfeger, K.L.; Cowman, M.K.; Telmer, P.G.; Turley, E.A.; McCarthy, J.B. Hyaluronan, inflammation, and breast cancer progression. *Front. Immunol.* **2015**, *6*, 236. [CrossRef]
57. Soysal, S.D.; Muenst, S.; Barbie, T.; Fleming, T.; Gao, F.; Spizzo, G.; Oertli, D.; Viehl, C.T.; Obermann, E.C.; E Gillanders, W. EpCAM expression varies significantly and is differentially associated with prognosis in the luminal B HER2+, basal-like, and HER2 intrinsic subtypes of breast cancer. *Br. J. Cancer* **2013**, *108*, 1480–1487. [CrossRef]
58. Chen, E.I.; Hewel, J.; Krueger, J.S.; Tiraby, C.; Weber, M.R.; Kralli, A.; Becker, K.; Yates, J.R.; Felding-Habermann, B. Adaptation of energy metabolism in breast cancer brain metastases. *Cancer Res.* **2007**, *67*, 1472–1486. [CrossRef]

59. Zhang, L.; Ridgway, L.D.; Wetzel, M.D.; Ngo, J.; Yin, W.; Kumar, D.; Goodman, J.C.; Groves, M.D.; Marchetti, D. The identification and characterization of breast cancer CTCs competent for brain metastasis. *Sci. Transl. Med.* **2013**, *5*, 180ra48. [CrossRef]
60. Brennan, N.J.; Jirström, K.; Kronblad, Å.; Millikan, R.C.; Landberg, G.; Duffy, M.J.; Gallagher, W.M.; O'Brien, S.L.; Rydén, L. CA IX is an independent prognostic marker in premenopausal breast cancer patients with one to three positive lymph nodes and a putative marker of radiation resistance. *Clin. Cancer Res.* **2006**, *12*, 6421–6431. [CrossRef]

Publisher's Note: MDPI stays neutral with regard to jurisdictional claims in published maps and institutional affiliations.



© 2020 by the authors. Licensee MDPI, Basel, Switzerland. This article is an open access article distributed under the terms and conditions of the Creative Commons Attribution (CC BY) license (http://creativecommons.org/licenses/by/4.0/).